

***SEISMIC PERFORMANCE OF
REINFORCED CONCRETE
COUPLED WALLS***

RICHARD CLIVE MALCOLM

ID: 9298181

**SUPERVISED BY PROF. JASON INGHAM
(UNIVERSITY OF AUCKLAND)
AND ADJ. PROF. DES BULL
(UNIVERSITY OF CANTERBURY)**

A THESIS SUBMITTED IN FULFILLMENT OF THE
REQUIREMENTS FOR THE DEGREE OF MASTER OF
ENGINEERING IN CIVIL ENGINEERING, THE UNIVERSITY OF
AUCKLAND 2015

Abstract

Following the 2010/2011 Canterbury Earthquakes, an investigation by the Canterbury Earthquakes Royal Commission (CERC) considered the performance of a range of buildings in Christchurch. Several of the buildings investigated by the CERC included reinforced concrete coupled walls, which are comprised of two wall piers linked (or coupled) by a series of coupling beams at each floor level. Notably the coupled wall buildings investigated by the CERC were observed to have performed undesirably when compared to their design intent. It was found by the CERC that these coupled walls tended to display higher strengths and lower ductility capacity than was intended in design. The postulated reason for this behaviour was that interaction between structural components strengthened the coupling beams by restraining the tendency of the coupling beams to axially elongate. To better account for this interaction in design practice, it was recommended by the CERC that the behaviour of coupled walls be investigated further.

In this study, structural interaction between coupling beams and floors was first considered using finite element software VecTor2. It was found that the floors tended to restrain the elongation of coupling beams and to cause large coupling beam strength increases. The extent of floor that was activated to restrain coupling beam elongation being found to be dependent upon the arrangement of the floor. Existing provisions of NZS 3101:2006 for upper bounds on floor effective widths were found to be valid for assessment of the maximum coupling beam strength amplification caused by floor interaction.

Analysis of a series of seismically loaded coupled walls interacting with floors was undertaken using VecTor2 software. In agreement with the findings of the CERC, axial restraint of coupling beams was found to have a large impact on coupled wall performance. Coupling beam strengths were measured up to 300% of their design strength, which tended to change the strength hierarchy of the coupled wall. In particular it was found that many existing coupled walls would have behaved similarly to a single cantilever wall with penetrations because the coupling beams were too strong to yield. These coupled walls tended to display lower energy dissipation and higher wall pier damage than assumed in design.

The coupled wall provisions proposed (at the time of writing) in the 2014/2015 NZS 3101:2006 Amendment were found to over-estimate the impact of the floor systems on restraining coupling beam elongation. However these provisions did not include the effect of the wall piers restraining coupling beam elongation, so overall coupled wall overstrength capacities tended to be under-predicted. As an approximate method of accounting for axial restraint in design of coupled walls, it was recommended that redistribution of design demands be used to reduce the coupling beam design capacity and to achieve a more desirable coupled wall behaviour.

Acknowledgements

This research would not have been possible without the support of the University of Canterbury Quake Centre (UCQC). The support and coordination provided by UCQC is gratefully acknowledged. Special thanks also goes to Professor Richard Fenwick for his valuable input and insights into this project. To my supervisors, Des, Rick and Jason, thank-you for your valuable input into this research and for the generosity with which you gave your time.

To my family, thank-you for your support over the past 23 years and in particular over the past 12 months. To my grandparents Diane and Alan, thank-you for what you have done for me and for all the opportunities that you have given me. To my sister Laura, thank-you for always supporting me and providing good advice. To my partner Kristyn, thank-you for always keeping me positive and for giving me the motivation to succeed. Finally to my mother Linda, through your hard work you have made anything possible for me and I cannot thank-you enough for everything you have given for me over the past 23 years. Thank you.

Table of contents

Abstract.....	i
Acknowledgements	ii
Table of contents	iii
1 Introduction	1-1
1.1 Background.....	1-2
1.2 Research objectives	1-4
2 Literature Review.....	2-1
2.1 Coupling beam experimental research.....	2-1
2.2 Coupling beam computational modelling research	2-4
2.3 Coupled wall research	2-6
2.4 Axial elongation research	2-7
2.5 Floor and beam interaction research.....	2-9
2.6 Existing design standards.....	2-10
2.1 Summary	2-11
3 Floor Diaphragm Model Calibration.....	3-1
3.1 Experimental data used to calibrate floor models	3-1
3.2 Floor diaphragm axial restraint force generation.....	3-6
3.3 Floor diaphragm modelling	3-7
3.4 Comparison to experimental data.....	3-11
3.1 Conclusions	3-16
4 Floor Diaphragm Parametric Study	4-1
4.1 Base model layout and results	4-1
4.2 Parametric study results	4-5
4.3 Floor diaphragm model assumptions, exclusions and limitations	4-15
4.4 Conclusions	4-18
5 Floor Diaphragm Mechanical Models	5-1
5.1 Existing code provisions	5-1
5.2 Floor response to single elongating hinge.....	5-2
5.3 Floor response to multiple elongating hinges.....	5-14
5.4 Plastic hinge(s) in coupled wall applications	5-19

5.5	Discussion	5-22
5.6	Conclusions	5-25
6	Coupling Beam and Coupled Wall Model Calibration	6-1
6.1	Experimental data relevant to coupling beams	6-1
6.2	VecTor2 coupling beam model calibration	6-3
6.3	Two-dimensional coupling beam global response calibration	6-4
6.4	Calibration of three dimensional behaviour	6-7
6.5	Coupling beam calibration summary	6-12
6.6	Coupled wall model calibration	6-13
6.7	Modelling of coupled wall and floor interaction	6-20
6.8	Conclusions	6-20
7	Coupled Wall Modelling	7-1
7.1	Wall model design	7-1
7.2	Base wall model results	7-6
7.3	Wall model variations	7-15
7.4	Discussion	7-29
7.5	Conclusion	7-37
8	Conclusion	8-1
8.1	Floor diaphragm conclusions	8-1
8.2	Coupled wall conclusions	8-2
8.3	Recommendations for future work	8-4
9	References	9-1
10	Appendix A	10-1
11	Appendix B	11-1
12	Appendix C	12-1
13	Appendix D	13-1
14	Appendix E	14-1

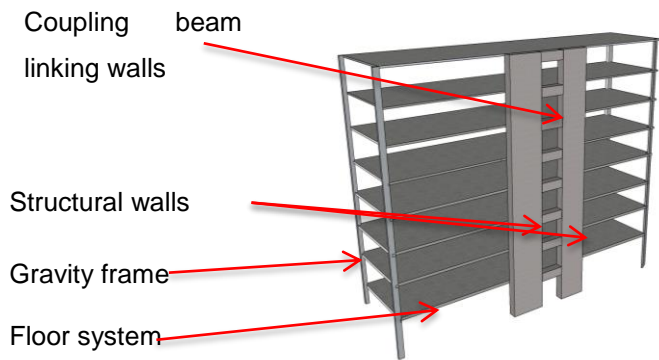
CHAPTER 1

1 Introduction

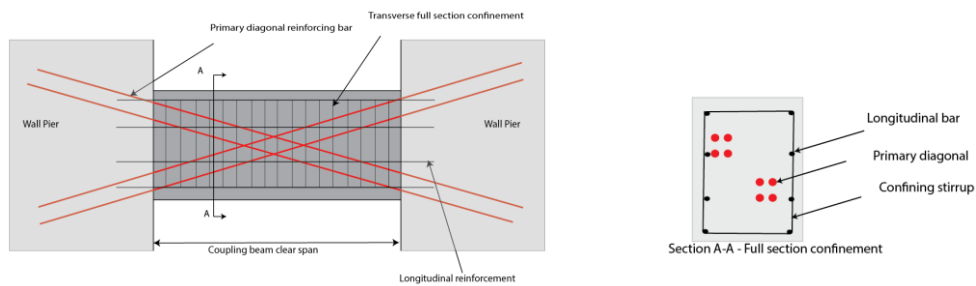
Following the 2010-2011 Canterbury earthquake sequence, the Canterbury Earthquakes Royal Commission (CERC) was established to report on “the causes of building failure” and “the legal and best practice requirements for buildings” (Canterbury Earthquakes Royal Commission 2012). The investigation undertaken by the CERC identified a series of issues with current practice based upon the observed behaviour of buildings in Christchurch. Despite generally being designed to modern seismic standards, many of the investigated buildings were observed to have performed undesirably when compared to their design intent, although catastrophic building collapses were relatively rare. Recommendations for improvements to design standards to mitigate the undesirable behaviour were then made by the CERC. In addition, the CERC also identified several areas where further research was required in order to account for the observed behaviour in modern seismic design.

Among the findings of the CERC, the behaviour of several buildings that incorporated reinforced concrete (RC) coupled walls were analysed and found to be unsatisfactory. RC coupled walls are an efficient lateral force resisting system, which comprise two structural walls linked with short coupling beams to act as a composite system, as shown in Figure 1-1 (a). The reinforcement of these coupling beams in New Zealand have typically been orientated diagonally, as shown in Figure 1-1 (b). Typically coupled walls are designed to resist a large proportion of the seismic demand of a building due to their high stiffness and ductility, and therefore it is critical that these systems perform well when subjected to seismic excitation.

Reference was made by the CERC to the Canterbury Television (CTV) building and the Inland Revenue Department (IRD) building, both of which included an RC coupled wall as part of their lateral force resistance systems. From analysis of the collapsed CTV building, the behaviour of the coupled wall was found to have not contributed to the collapse, although the performance of the coupled wall was considered to have differed markedly from the design intent. The coupled wall in the IRD building was also assessed as performing undesirably, contributing to major foundation damage. As a result of the observed performance of these RC coupled walls, it was recommended by the CERC that research be undertaken to better understand their performance in real structures.



(a) Coupled wall building typical layout



(b) Coupling beam typical diagonal reinforcement layout

Figure 1-1: Typical coupled wall building layout

1.1 Background

The CERC postulated that the undesirable RC coupled wall behaviour observed in Canterbury was due to coupling beam capacities being higher than predicted by existing design procedures. This increased capacity strengthened the coupled wall and invalidated the strength hierarchy intended in design. Consequently the coupled walls were found to have behaved more like a single cantilever wall with penetrations than as two wall piers, coupled by the coupling beams. The proposed reasoning for this increased coupling beam capacity related to the tendency for reinforced concrete members to increase in length when loaded, in a phenomenon known as axial elongation. It was proposed by the CERC that when the tendency for coupling beams to axially elongate was restricted, their capacity could have increased significantly. This restriction of the axial elongation was found to have occurred in the CTV and IRD buildings mentioned above, due to interaction with adjacent structural components which opposed the coupling beam elongation. In particular, the restraining effects of the adjacent floor system and the bounding wall piers were concluded to have impacted the coupling beam performance in these buildings.

The tendency of RC members to axially elongate occurred because of seismically induced damage in ductile RC buildings. This damage forms an inherent part of the ductile capacity design philosophy employed in RC buildings designed to modern design codes. By

concentrating damage into defined zones, known as plastic hinge zones, ductile RC buildings are able to sustain this damage without compromising the structures integrity. In this way, seismic demand is limited and energy dissipated. A consequence of this damage in the plastic hinge zones is that the RC members tend to axially elongate (Fenwick and Megget 1993). As such, plastic hinge formation, and its associated axial elongation, is fundamentally related to ductile capacity design of RC structures.

As realistic buildings comprise an array of structural components, in order for one component to elongate, compatibility strains are induced in adjacent building components which act to restrain this elongation. This restraint not only transfers damage from the plastic hinge region into adjacent members, but also results in the generation of an additional axial force on the plastic hinge to resist its tendency to elongate. The magnitude and effect of axial restraint forces on plastic hinges and adjacent structural members was typically not considered in design and hence may have led to undesirable behaviour.

Axial restraint of RC coupling beams has received limited research attention and consequently has been largely ignored in design. As highlighted by the CERC, potential coupling beam strength increases due to axial restraint could have impacted on the overall behaviour of coupled walls in Canterbury. Specifically, the increased coupling beam capacity could have invalidated the strength hierarchy of the coupled wall systems and caused increased damage in the walls. The CERC subsequently recommended that the axial restraint of coupling beams be investigated further to create more certainty around the performance of RC coupling beams. Design of coupled walls relies on isolating the plastic deformation to the coupling beams and to plastic hinges at the base of each wall to form a plastic sway mechanism, whilst the remainder of the structure is proportioned to remain essentially undamaged, as shown in Figure 1-2. In order to ensure this behaviour occurs, a greater understanding of coupled wall behaviour is required.

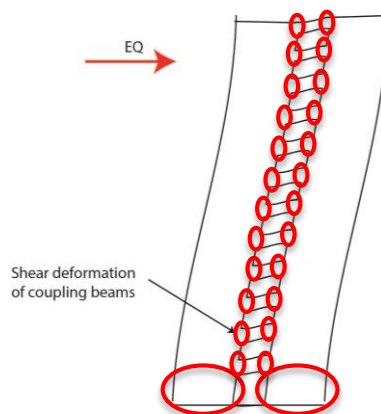


Figure 1-2: Deformed shape of coupled wall showing ideal plastic hinge locations

1.2 Research objectives

The objective of this research program was to analyse the origins and effects of axial restraint to plastic hinges in realistic RC coupled wall buildings. In particular, the adjacent floor system and bounding wall piers in coupled wall buildings were targeted to assess how they affected the behaviour of an elongating coupling beam. Finite element modelling was selected as the method of analysis due to its ability to assess a range of structural layouts.

This research project investigated:

- The level of axial restraint force generated by typical flooring systems and wall piers in New Zealand coupled wall buildings when the coupling beams were loaded inelastically;
- The effect of the axial restraint forces generated by both the floor and the walls on coupling beam sub-assembly performance;
- The effect of axial restraint on the global response of a coupled wall system when the coupled wall was seismically loaded;
- Comparison of the findings to NZS 3101:2006. At the time of writing a draft amendment to NZS 3101:2006 was available for public comment. Whilst the amendment was expected to be finalised in 2015, the findings of this study were compared to the 2014 draft amendment clauses;
- The development of further recommendations to allow the effect of realistic axial restraint on reinforced concrete coupling beams to be considered in future designs.

The research presented in this thesis was undertaken based upon the above requirements. As presented in Chapter 2, a literature review of existing research was first undertaken. As the research related to interactions between structural components, the behaviour of floors was first considered in Chapters 3, 4 and 5, before the behaviour of coupled walls interacting with these floors was considered in Chapters 6 and 7. For the analysis of floors, presented in Chapter 3 is the calibration process and modelling approach used for the analyses of floors subject to elongation strains. A parametric study of floors was then undertaken as presented in Chapter 4, upon which the behaviour of floor systems subjected to elongation compatibility strains was inferred in Chapter 5. For consideration of coupled walls, a further finite element model calibration process was then undertaken on coupled walls in Chapter 6 to ensure model accuracy. The modelling of coupled walls with floor systems was then undertaken as per Chapter 7 to analyse the behaviour of realistic coupled wall systems. Finally the research conclusions are reported in Chapter 8.

CHAPTER 2

2 Literature Review

Coupled walls have been considered in a wide range of research programs around the globe in order to achieve higher performance, specifically in seismically active regions. In particular, sub-assemblies of coupling beams, which connect the wall piers in a coupled wall system, have been extensively researched. A less extensive range of research programmes experimentally or analytically examining full coupled wall systems was also available in literature. Due to the size of coupled walls in real buildings making full system research difficult, the research available on full coupled wall super-assemblies was more limited. A review of this previous work relating to coupled walls, and aspects of reinforced concrete (RC) behaviour relevant to this study, are presented in this chapter. Due to the behaviour of realistic coupled walls being a structural interaction problem, other relevant research relating to floor systems and elongation mechanisms is also presented.

2.1 Coupling beam experimental research

A brief description of the existing experimental work related to coupling beam performance is discussed below. A summary list of the coupling beam experimental data is also provided in Appendix A.

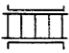




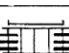
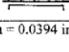

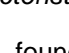
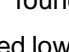
2.1.1 Paulay and Binney (1971 and 1974)

Researchers have experimented with the traditional ‘conventional’ reinforcement layouts of short coupling beams in order to improve their performance when subjected to high shear demands (Paulay 1971; Paulay and Binney 1974), where the term ‘conventional’ has been used here to refer to beams reinforced with bars placed horizontally as per a typical flexural beam. Paulay (1971) postulated that, based upon the diagonal strut and tie force resistance mechanism of shear dominated beams, a diagonal reinforcement layout would provide enhanced performance. Subsequent testing by Paulay and Binney (1974) confirmed that the performance of coupling beams was improved by adopting the diagonal reinforcement layout and resisting the shear demand axially with diagonally inclined reinforcement. Diagonally reinforced coupling beams were found to have improved energy dissipation and ductility capacity, with lower strength degradation observed. The resolution of shear forces into diagonal forces supported entirely by the diagonal reinforcement is the design method adopted in NZS 3101:2006 and ACI 318-11.

2.1.2 Tassios, Moretti and Bezas (1996)

Experiments were undertaken by Tassios et al. (1996) on 10 coupling beam specimens, in order to assess the performance of different coupling beam reinforcement layouts (Tassios et al. 1996). Diagonal reinforcement layouts were compared to variations of conventional reinforcement, including bent up bars (CB-3) and additional longitudinal dowels (CB-4 and CB-5), intended to improve sliding

shear resistance. The primary research objective was to evaluate alternative reinforcement layouts to achieve suitable strengths and ductility but with simpler reinforcement layouts, as shown in Figure 2-1.

	specimen	reinforcement layout	f'_c (MPa)	O_f (mm)	O_d (mm)	ρ_f (%) total	ρ_d (%) total
1	CB-1A		32.8	12	-	0.7	-
	CB-1B		33.0	12	-	1.1	-
2	CB-2A		28.5	6	10	-	1.0
	CB-2B		26.3	6	10	-	1.6
3	CB-3A		31.7	12	18	0.7	0.8
	CB-3B		33.8	12	14	1.1	0.8
4	CB-4A		29.8	6	4Ø20	-	1.9
	CB-4B		31.3	6	3Ø18	-	1.9
5	CB-5A		32.3	12	4Ø20	0.7	1.9
	CB-5B		33.1	12	3Ø18	1.1	1.9

1 Mpa = 145 psi, 1mm = 0.0394 in

Figure 2-1: Specimen experimental characteristics (Tassios et al. 1996)

From the experimental research it was found that the conventionally reinforced, and dowelled specimens (CB-1, CB-4 and CB-5), exhibited lower ductility and more brittle failures than the specimens with diagonal or bent up bars (CB-2 and CB-3). Reduced ductility was found to be particularly evident in the shorter, more shear dominated beams.

2.1.3 Galano and Vignoli (2000)

Galano and Vignoli (2000) investigated the performance of different reinforcement layouts in short coupling beams, by testing 15 specimens (Galano and Vignoli 2000). Primary test variables were reinforcement layout and loading history, with a range of monotonic and cyclic loading histories applied to the specimens. The reinforcement layouts included conventionally reinforced, diagonally reinforced and a rhombic (diamond) arrangement. An important feature of the test set up was that rollers were placed at the ends of the specimen which enforced full axial restraint of the specimen, preventing axial elongation but allowing end rotation, as shown in Figure 2-2. Analysis of the results showed that the rhombic reinforcement layout improved the rotational ductility capacity and strength degradation as compared to the conventionally reinforced coupling beam. It was also noted that the compressive strength of the concrete had a significant effect on the capacity of the diagonally reinforced specimens, with lower compressive strength specimens suffering compressive strut instability.

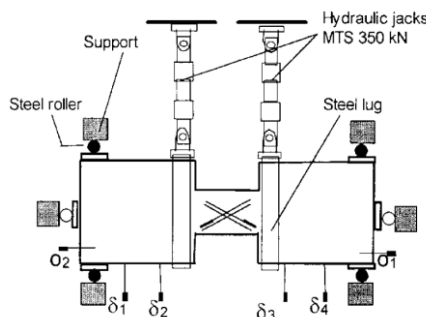


Figure 2-2: Experimental set up showing full axial restraint (Galano and Vignoli 2000)

2.1.4 Adebar et al. (2001)

Adebar et al. (2001) conducted a test on a single diagonally reinforced coupling beam (Adebar et al. 2001). The primary objective of the experiment was to understand the behaviour of the coupling beam when axially restrained by the wall piers that it was coupling. In order to simulate the effect of the axial restraint provided by the bounding walls, high strength steel 'Dywidag' bars were used to connect the ends of the coupling beam. Adebar et al. (2001) found that the compression forces in the coupling beams became very large and the failure mechanism under these conditions was found to be crushing of the concrete and subsequent buckling of the reinforcement, due to a loss of confinement. This compression failure suggested that the compressive force generated in a restrained beam altered the behaviour of the beam significantly.

2.1.5 Kwan and Zhao (2002)

Experimental testing by Kwan and Zhao (2002) was undertaken on six coupling beams of span/depth (aspect) ratios less than 2.0 in order to assess the effects of reinforcement layout and aspect ratio on coupling beam performance (Kwan and Zhao 2002). Five of the specimens were reinforced conventionally, with one specimen reinforced diagonally. A complex test setup was utilised in order to enforce equal end rotations on the coupling beam, to replicate the rotations enforced upon coupling beams in real coupled wall systems. As discussed by Kwan and Zhao (2002), the rotation of the walls tended to apply equal rotations into the ends of each coupling beam where the inelastic deformation was concentrated.

Analysis by Kwan and Zhao of their experimental results showed that the conventionally reinforced beams formed inclined shear cracks and exhibited tension in all of the longitudinal bars along the full length of the beam, confirming the work by Paulay (1971). Comparison of the reinforcing layouts showed that the diagonally reinforced beam provided much more stable hysteretic response, with improved energy dissipation and ductility than for the conventionally reinforced beams. The smaller aspect ratios were observed to generate more shear in the beams and resulted in a less ductile failure mode, dominated by shear. The beams were also observed to elongate significantly during inelastic load cycles which exceeded the maximum loading in the previous cycles. The measured elongation strain as a percentage of beam depth for the conventionally reinforced beams was in the order of 1.2-2.0% and approximately 2.5% for the diagonally reinforced beam.

2.1.6 Fortney et al. (2008)

The response of coupling beams with different arrangements of transverse reinforcement was experimentally analysed by Fortney et al. (2008). These tests were undertaken in order to determine whether the transverse reinforcement prescriptions of ACI 318-05 could be relaxed to improve the constructability of diagonally reinforced coupling beams (Fortney et al. 2008). A major complication of constructing diagonally reinforced coupling beams, in accordance with ACI 318-05, was transverse reinforcement congestion, particularly near mid-span where the primary diagonals intersected. ACI 318-05 required each 'bundle' of diagonal bars to be reinforced similarly to a column arrangement, with transverse bars around each diagonal bundle at close spacing, as shown in Figure 2-3 (a). This diagonal confinement detail was intended to provide buckling resistance to the diagonal bars and to

confine the concrete within the diagonal core but resulted in complex reinforcement arrangements. In order to overcome constructability issues, Fortney et al. (2008) tested two diagonally reinforced coupling beams without confining stirrups around each bundle at mid-span. Specimen DCB-1 included only nominal stirrups around the full section at mid-span. However specimen DCB-2 included confinement around the full diagonal bundle intersection zone sufficient to meet the shear requirements of ACI 318-05, as shown in Figure 2-3 (b) and (c).

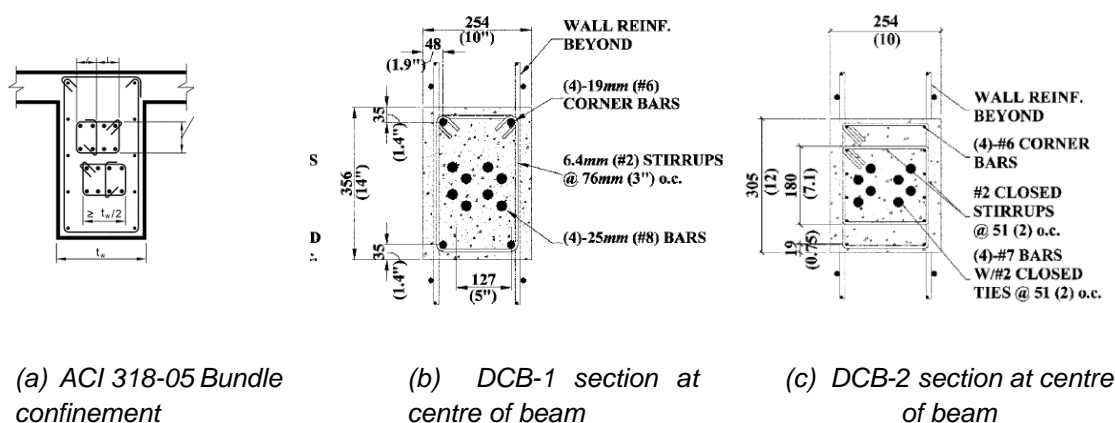


Figure 2-3: Test specimen sections showing stirrup arrangement (Fortney et al. 2008)

Fortney et al (2008) showed that the exclusion of confining reinforcement around the centre of the beam (DCB-1) led to a bar buckling failure at around 4% chord rotation. Specimen DCB-2 showed stable response up to 10% chord rotation and limited shear degradation because of the inclusion of closed stirrups around the intersecting diagonal groups. Ultimate failure was governed by diagonal bar rupture, suggesting that buckling failure was suppressed by the confining stirrups. The adequate performance of the full section confinement layout led to the use of full section confinement in ACI 318-08.

2.1.7 Naish et al. (2009)

An experimental research program was undertaken on diagonally reinforced concrete coupling beam sub-assemblages in order to assess the performance of the updated detailing options considered by Fortney et al. (2008) which were included in ACI 318-08 (Naish et al. 2009). The results from the Naish et al. (2009) tests were utilised to calibrate finite element models, and are discussed in detail in Chapter 3.

2.2 Coupling beam computational modelling research

In addition to the range of experimental research programmes undertaken to understand the performance of RC coupling beams, simulation by computer modelling has become increasingly common as a method of understanding coupling beam behaviour. The following is a summary of the most relevant modelling based research of RC coupling beams.

2.2.1 Mohr (2007)

Nonlinear analysis of RC coupled walls was undertaken by researchers in order to examine performance based design methods for coupled walls (Mohr 2007). Nonlinear analysis was performed using VecTor2, two-dimensional finite element software (VecTor Analysis Group 2011). A building

inventory was also undertaken in the Washington-California area, with drawings of four coupled shear wall buildings providing the basis of the analysis. Modelling was undertaken on coupling beam sub-assemblages to investigate the ACI 318-08 full section or diagonal bundle confinement options, including one coupling beam with additional steel included at the top of the beam to simulate the effect of the adjacent floor slab. The effect of the floor slab reinforcement was found to be an increased initial stiffness and decreased post-yield stiffness.

The finite element model was then extended to a 1/3 scale 10 storey coupled wall designed to the IBC Structural/Seismic Design Manual (2007). The coupled wall was modelled in VecTor2 software with three different coupling beam arrangements – diagonally confined, full section confinement and with coupling beam capacity reduced to 25% of the design value (to ensure that the full coupled wall plastic mechanism developed). Modelling results showed that the first two coupling beam arrangements (designed to the full recommended shear capacity) did not yield up the entire height of the building, and that the full ductile sway mechanism was not able to form. It was noted that due to the higher than predicted coupling effects of the strong coupling beams, the wall behaved more as a single wall than as coupled walls, relying on base plastic hinges for the majority of the energy dissipation. The model which included weak coupling beams (designed to 25% of the elastically derived shear demand), formed coupling beam plastic hinges up the entire height of the wall and allowed the coupled wall plastic mechanism to fully form. On the basis of the modelling, it was concluded that the ACI 318-05 code may have resulted in beams which were too strong to allow ductile sway mechanism formation.

2.2.2 Bower and Rassati (2008)

A study utilising ABAQUS non-linear analysis software, was undertaken to assess the effect of axial restraint on the stiffness and ductility of diagonally reinforced coupling beams (Bower and Rassati 2008; Dassault Systemes 2014). The considered axial restraint, originates in real buildings due to the presence of the floor and bounding walls restraining axial elongation.

The two-dimensional analysis undertaken by Bower and Rassati (2008) showed that the consideration of confinement around the main diagonal reinforcement bundles had a major impact on the model accuracy and the two dimensional model used could not adequately model the anti-buckling effect of diagonal confinement. To overcome the issues of the modelling, the analytical results were scaled to better match a set of the coupling beam experiments mentioned above. This scaled hysteretic response was input into a global wall model using CSI Perform software (Computers and Structures Inc 2014). The full axial restraint of the coupling beam was found to have reduced the inter-storey drift of the global structure due to the increased stiffness of the axially restrained coupling beams.

2.2.3 Barbachyn et al. (2012)

The effects of geometry, reinforcement layout and boundary conditions of coupling beams were considered analytically by developing a simplified two dimensional non-linear strut and tie coupling beam model (Barbachyn et al. 2012). This strut and tie model was input into the analysis software OpenSees (Pacific Earthquake Engineering Research Centre 2006) to compare to a set of the experimental data mentioned above for validation. The basis of the model was that force resistance in

a diagonally reinforced coupling beam was dominated by the diagonal reinforcement elements, which acted in tension and compression, with consideration of the confined concrete core within the diagonal reinforcement bundle acting in compression.

A parametric study was undertaken using a prototype 14 storey building with a coupled wall shear core as the basis for the analysis. The coupling beam axial restraint was found to vary over the height of the structure, with a much higher restraint observed near the base of the wall compared to near the top of the wall. It was found that the axial restraint had only a small effect on the capacity of the restrained coupling beams. As the restraint force was increased, it was noted that the axial elongation of the beam was effectively reduced to zero when the restraint force was approximately 8% of $f'_c A_{cw}$. The restraint force was also found to be more critical for deeper beams, resulting in more brittle failure modes.

2.3 Coupled wall research

In addition to the coupling beam sub-assembly analyses presented above, research has also been undertaken to examine the seismic behavior of coupled wall systems. A summary of this coupled wall research is presented below.

2.3.1 Shiu et al. (1981)

Early researchers experimented with two six storey coupled walls at 1/3 scale by varying the shear capacity of conventionally reinforced coupling beams (Shiu et al. 1981). A small area of floor slab was included in the tests in order to provide a platform for applying the cyclic pushover forces to the specimens. Shiu et al. (1981) suggested that the response of the system was strongly dependent upon the degree of coupling provided by the coupling beams. It was observed that when the wall coupling was weak, the walls behaved as two isolated walls after the formation of plastic hinges in the coupling beams. However the strongly coupled wall specimen deformed as expected in design for a coupled wall, with the wall piers deforming together.

2.3.2 Ozsalcuk (1989)

Two 4 storey coupled wall sub-assemblies were experimentally tested, based on the lower levels of a 15 storey prototype building. The experimental programme was undertaken in order to understand the shear demand in 'bar-bell' type walls, to investigate the capacity of edge columns in walls and to investigate the effects of coupling action on wall strength (Ozsalcuk 1989). Based upon the experimental data obtained, it was concluded that the axial force induced in each wall by the coupling beam shear force had a significant effect on the stiffness of the walls. In addition, it was observed that if the coupling beam strength was increased, then the damage in the wall piers was increased. On the basis of the research it was concluded that the coupling beam strength relative to the wall pier strength should be limited to ensure suitable ductility in the compression wall.

2.3.3 Harries (2001)

Existing experimental research of coupling beams was used by Harries (2001) in order to assess the ability of coupling beams to sustain ductility demands and to assess the degree of coupling achieved in coupled wall systems (Harries 2001). The degree of coupling (DOC) was defined as the ratio of the

total coupled wall overturning moment resisted by axial force in the wall piers, which was induced by the coupling beams in shear. The degree of coupling was a measure of the extent to which the wall acted as a coupled wall. The ductility capacities sustained in a range of coupling beam sub-assembly experiments were compared to analytically derived demands when included in coupled wall systems. Harries (2001) concluded that in many cases, the ductility demand on coupling beams in coupled wall systems exceeded the ductility capacity observed in experiments. When a coupled wall was designed to have a high DOC, it was modelled as having a very stiff response to lateral forces. Consequently the yield deformation was low and the ductility demand was high for stiff coupled walls. Coupled walls designed to have a low DOC were found to be flexible, which increased their yield deformation and reduced their ductility demands. To ensure the ductility demand was lower than the ductility capacity, it was proposed that the DOC be limited, as presented in Figure 2-4, to reduce the coupled wall stiffness. The recommendation for diagonally reinforced coupling beams was to limit the DOC to 55%.

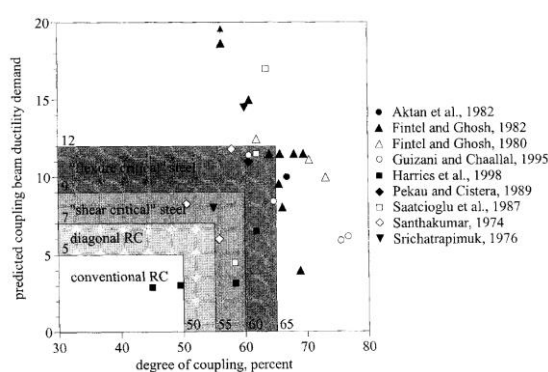


Figure 2-4: Coupling beam ductility demand versus analytically determined DOC (Harries 2001)

2.3.4 Lehman et al. (2013)

Testing of a 10 storey coupled wall prototype specimen was undertaken in order to investigate the seismic response of a coupled wall (Lehman et al. 2013). Only the lower three storeys of the prototype building were tested, with the demands from the upper storeys applied by means of loading devices applying shear, moment and axial forces or displacements. The specimen comprised diagonally reinforced coupling beams designed in accordance with ACI 318-08 and ASCE 7, with a span to depth ratio of 2.0. No floor slab was included in the specimen. The results of the experiment are discussed in detail in Chapter 6, where the results were used to calibrate computational models of coupled walls.

2.4 Axial elongation research

Presented in this section is a selection of the relevant research which contributed to the current understanding of axial elongation in RC members.

2.4.1 Fenwick et al. (1981) and Fenwick and Thom (1982)

Following a study by Fenwick and Fong (1979) a testing program was undertaken to investigate the inelastic deformation of RC beams (Fenwick et al. 1981; Fenwick and Thom 1982; Fenwick and Fong 1979). The experiment entailed cyclic loading of a moment frame sub-assembly and measurement of the components of deformation. Fenwick and Thom (1982) observed that the beams grew appreciably

in length (elongated) when plastic hinges formed, in addition to the beams growing in depth due to extension of the transverse stirrups. Based on these observations, Fenwick and Thom (1982) developed the understanding of axial elongation structural mechanics by proposing that the elongation of plastic hinges originated from three mechanisms:

1. Unequal tension and compression strains (Geometric elongation),
2. Prevention of crack closure due to dislodgement of aggregates (Contact stress effect),
3. Shear truss action (Truss action effect).

Geometric elongation is caused by the cracking of a concrete section under flexural actions. Flexural cracks develop because concrete has a low tension capacity and the flexural tension forces are resisted by reinforcement embedded in the concrete. Due to the presence of tension cracks, the point of zero flexural strain shifts away from the tension zone and the centroid of the concrete section is subjected to a tension strain. This tension strain at the centroid causes a net increase in length of the concrete member, referred to as geometric elongation.

The contact stress effect, as shown in Figure 2-5 (a), was found to occur due to the wedging action of aggregate particles which became dislodged from crack surfaces. Fenwick and Thom (1982) observed that as reinforcement was strained in flexural tension, lugs on the reinforcement were pulled through the concrete matrix on either side of the crack, which caused small aggregate particles to dislodge on the crack surface. During reversed cyclic loading, as opposite sides of an open crack translate relative to each other due to shear deformation, the crack surfaces no longer fit together due to the small dislodged aggregate particles. These aggregate particles effectively prop open the crack leading to an accumulation of tensile strain.

The truss action effect results from the mechanism of shear transfer in cyclically loaded plastic hinge regions, as shown in Figure 2-5 (b). Shear force in these plastic hinges is resisted by truss like action of inclined compression struts in the concrete, and vertical tension ties in the transverse reinforcement. As shown in Figure 2-5 (b), the inclination of these concrete compression struts results in a component of the strut force acting in the horizontal direction. Horizontal force equilibrium is satisfied if:

$$C = T - \frac{V}{\tan \theta} \quad (2-1)$$

Examination of equation 2-1 demonstrates that the flexural compression force is lower than the corresponding flexural tension force at any section. As a result, tensile strains in cyclically loaded plastic hinges tend not to be recovered after each cycle. Consequently the tensile strains accumulate leading to axial elongation of the member.

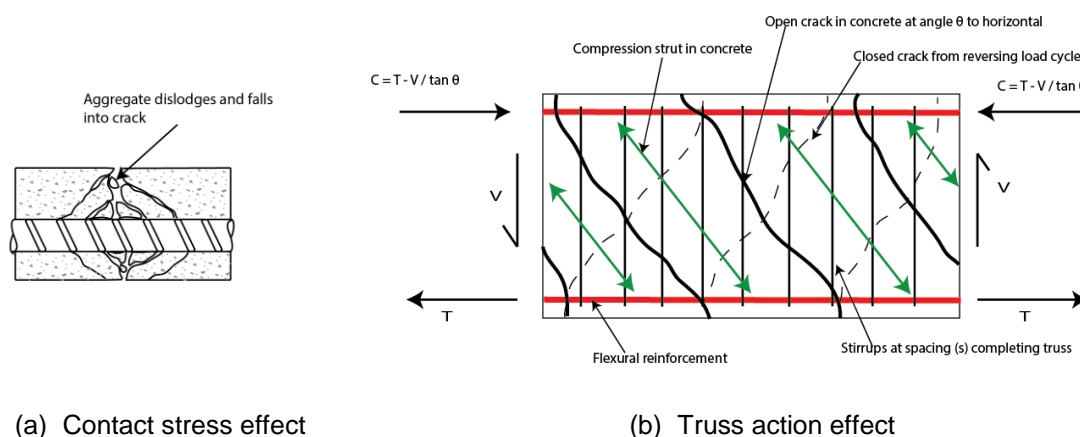


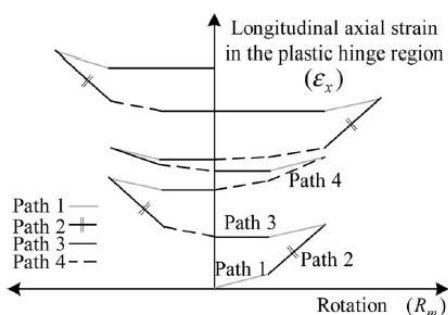
Figure 2-5: Axial elongation mechanisms adapted from Fenwick and Thom (1982)

2.4.2 Lee and Watanabe (2003)

A sectional based model of axial elongation in reversing plastic hinges of RC members was developed by (Lee and Watanabe 2003). Axial elongation was broken down by Lee and Watanabe (2003) into four paths, as shown in Figure 2-6. The majority of elongation occurs in the yielding region where the load is increased from previous cycles. This model allowed prediction of the axial elongation of RC plastic hinges with reasonable accuracy but it was noted by Lee and Watanabe (2003) to be too complex to apply to design problems. In order to overcome this complexity, a simplified envelope model was developed which excluded the small components of the axial elongation, and only considered elongation to have developed along path 2 as the plastic hinge yielded. This envelope was expressed by a simplified equation calculating the elongation due to flexural yielding:

$$\epsilon_x = \frac{(R_{mp} + R_{mn})jd}{2 l_h} \quad \text{(Lee and Watanabe 2003)} \quad (2-2)$$

where R_{mp} and R_{mn} are the positive and negative rotations of the beam, jd represents the internal moment lever arm and l_h is the length of the hinge. This envelope was found to have provided good correlation to experimental data.



- Path 1: Pre-flexural yielding or unloading region, small strain increase.
- Path 2: Flexural yielding, increasing demand from previous cycle.
- Path 3: Slip region, negligible strain change during unloading slip.
- Path 4: Repeat loading region, rate reduced with more cycles.

(a) Sectional path based model

(b) Path description

Figure 2-6: Sectional model components of axial elongation (Lee and Watanabe 2003)

2.5 Floor and beam interaction research

The interaction between floor diaphragms and their supporting beams has been considered in a range of research programs. The primary interaction relevant to this study is the interaction of floor

diaphragms with elongating plastic hinges in these supporting beams. A series of studies relevant to this topic are summarised below. A further series of experiments relating to floor and beam interaction are presented in Chapter 3, where they were used to calibrate finite element models of floor systems.

2.5.1 McBride (1995)

(McBride 1995) considered how floor slabs could affect the elongation of RC beams by undertaking experiments on beam-column sub-assemblies with and without floor slabs. The floor slab was reinforced with mild steel mesh, typical of design in that era. McBride (1995) showed that the floor slab reinforcing bars were strained to fracture because elongation of the beam caused strain transfer into the floor. This bar fracture occurred at low levels of elongation in the beam which meant that the tension capacity of the floor was compromised early in the experiment. Due to this loss of floor tension capacity, the magnitude of elongation was not observed to have been reduced appreciably by the floor slab as the capacity to restrain elongation was lost after fracture.

2.5.2 Fenwick, Bull and Gardiner (2010)

Fenwick, Gardiner and Bull (2010) reported a comprehensive study on the seismic performance of hollow-core precast prestressed floor units for practicing engineer's guidance (Fenwick et al. 2010). This report collates much of the existing frame-floor experimental findings, presented in this section and Chapter 3, to assist the engineering community in avoiding issues with precast floor units. Among the issues discussed in the research report, loss of floor unit seating is considered in the context of axially elongating frame beams. In addition, practical consideration of the axial restraint forces induced in the precast units is included in the report.

2.6 Existing design standards

Coupled walls are considered specifically in a number of design codes due to their behaviour differing somewhat from isolated cantilever walls. Presented in this section are a selection of existing design requirements for coupled walls in NZS 3101 and ACI 318, which include a number of similar clauses regarding coupled walls.

2.6.1 NZS 3101:2006

A draft amendment to NZS 3101:2006 was available for public comment at the time of writing which includes specific consideration for the design of coupled walls (Standards New Zealand 2014). At the time of writing in 2014, the amendment was expected to be finalised in 2015. As such, only the draft clauses were able to be compared to the findings of this research.

The draft 2014 NZS 3101:2006 Amendment include a range of new clauses, in response to the findings of the Canterbury Earthquakes Royal Commission (CERC) and to reconcile NZS 3101:2006 with other structural concrete codes. It is proposed in the amendment that the wall piers of a coupled wall system be designed to 1.2 times the over-strength of the coupling beams to ensure that inelastic deformation is restricted to the coupling beams and to the plastic hinges at the base of the wall piers. To account for the axial restraint of coupling beams it is proposed that the coupling beam over-strength be calculated on the basis of material over-strength stresses and an axial force applied to the coupling

beam. This axial force is included to account for the effect of the adjacent floor diaphragm in restraining elongation, which was found following the Canterbury earthquakes to have induced an axial force in coupling beams. The magnitude of this axial force is determined based upon the existing effective width considerations of NZS 3101:2006 in S9.4.1.6.2, where the reinforcement within the effective floor width is considered to impart an axial compression force on the elongating coupling beam. The basis of the assumed axial force generated by the floor system is that as the coupling beam elongates, the floor reinforcement is strained with the coupling beam and so resists any coupling beam elongation. The overstrength capacity of the coupling beam includes the effect of this axial force. The NZS 3101:2006 Amendment (2014) also proposes to remove the effect of the degree of coupling on the allowable ductility of coupled wall systems included in NZS 3101:2006, instead setting the maximum permissible ductility to 6.0.

2.6.2 ACI 318-11

ACI 318-11 contains a series of design requirements for coupled shear walls in Section 21.9.7 (ACI 318-11 2011). ACI 318-11 specified that if a coupling beam has an aspect ratio $l_n/h < 2.0$ and a shear demand $V_u > 4\lambda(f'_c)^{0.5}A_{cw}$, the beam must be reinforced with two groups of intersecting diagonal bars, positioned symmetrically about the mid-span of the beam, unless it can be shown that the loss of strength and stiffness would not impair vertical load carrying capacity or egress and integrity. Coupling beams with aspect ratios $l_n/h > 4.0$ can be designed based upon standard flexural beam theory, with beams having intermediate aspect ratios being designed by either method. The limit on the maximum aspect ratio represents the decreasing vertical load carrying efficiency of beams with lower diagonal reinforcement inclination. The diagonal bars must be embedded 1.25 times the development length of the bars into the walls to ensure that the high stress in the concrete around the bars does not initiate bond failure, similar to the requirement of NZS 3101:2006.

ACI 318-11 allows two options for transverse reinforcement, both of which are included in the NZS 3101:2006 proposed amendment (2014). The first transverse reinforcement option requires stirrups wrapped around each diagonal reinforcement bundle at spacings similar to that required in column members in order to provide anti-buckling restraint to the diagonal bars. The second option involves confinement of the entire beam section, similar to the level of confinement required for column sections. The two transverse reinforcement layouts are considered in a number of the experimental research programs outlined in section 2.1, with each layout found to have similar performance at up to large rotational ductility (Naish et al. 2009).

2.1 Summary

The existing literature presented above includes extensive research into the behaviour of a range of elements related to coupled walls and axial elongation. However the existing research available on the effects of this axial elongation in RC coupled walls has not been completed to date. The motivation for the research presented in this thesis is to improve upon the understanding of coupled wall systems, with emphasis on the effects of axial elongation in these systems. It is intended that this knowledge will be used to improve upon the design provisions for RC coupled walls in New Zealand and abroad.

CHAPTER 3

3 Floor Diaphragm Model Calibration

Research considering interaction between moment frames and reinforced concrete (RC) floor diaphragms subjected to earthquake loading has been undertaken in New Zealand over the past decade (Matthews 2005; Lindsay et al. 2004; MacPherson 2005; Fenwick et al. 2005; Peng et al. 2008; Matthews 2004; MacPherson et al. 2005; Lau et al. 2002). This research was undertaken to investigate how the performance of moment frames and floors were affected by interaction between these components during an earthquake. A particular emphasis of this research was to understand how the elongation of plastic hinges within these moment frames altered the seismic performance of the frame-floor sub-assembly.

Comparable experimental research of floor interaction with RC coupling beams had not been undertaken for comparison to the existing moment frame research. To assess the interaction of floor systems and elongating coupling beams, analysis of floor diaphragms was undertaken using finite element software VecTor2, as presented in Chapters 3, 4, and 5. The first stage of this analysis, as presented in this chapter, was model calibration. This model calibration utilised the existing experimental data related to moment frame-floor systems to calibrate a series of finite element models of floor diaphragms. These calibrated floor diaphragm models were used to investigate how interaction between elongating RC coupling beams and an adjacent floor system altered the seismic performance of both components. The results of the subsequent analysis using calibrated floor models are presented in Chapters 4 and 5.

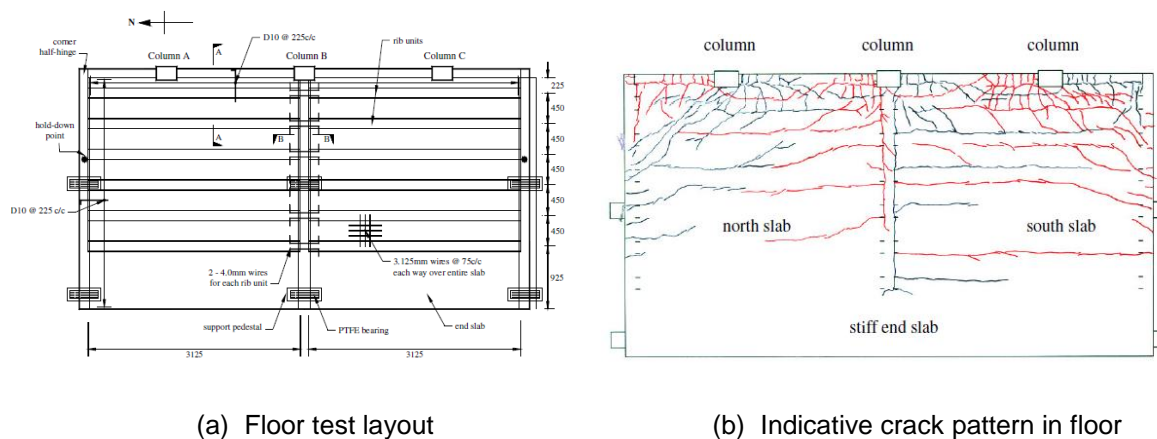
3.1 Experimental data used to calibrate floor models

A range of experiments have been undertaken in New Zealand to examine the interaction between moment resisting frames and floor systems. Floors which comprised precast prestressed units were tested because these precast floor units were most commonly used in New Zealand construction. When subject to lateral seismic forces, the beams of these moment frames were observed to have developed plastic hinges which tended to axially elongate. In response, the floor systems were observed to have resisted the propensity of the beams to elongate. The general findings of these tests are presented below because the results of these experiments were used to calibrate the computational models of floor diaphragms presented in this chapter.

3.1.1 Lau et al. (2002)

A frame-floor assembly which included a precast prestressed floor system supported by a perimeter frame was tested as shown in Figure 3-1 (Fenwick et al. 2005; Lau et al. 2002). In addition, two frame only specimens (excluding the floor system) were also tested. The Lau et al. (2002) tests were the first in a series of tests of this type undertaken in New Zealand. As shown in Figure 3-1, the frame assembly

test included three columns, with precast floor units orientated parallel to the frame span. Two columns had precast floor units positioned to span parallel past the beam column joint, while the internal column supported a transverse beam upon which the floor units were supported. The frame was loaded cyclically to simulate seismic excitation.



(a) Floor test layout (b) Indicative crack pattern in floor
 Figure 3-1: Experimental floor-frame test setup (Fenwick et al. 2005)

As the floor acted to axially restrain the plastic hinges, the measured plastic hinge elongation at columns A and C was approximately halved as compared to the corresponding elongation measured in the specimen excluding the floor. This axial restraint was found to have generated an inclined crack pattern directed away from the plastic hinges at columns A and C, in accordance with the principal compression stresses which developed in the floor to restrain plastic hinge elongation. A marked increase in the frame beam plastic hinge capacity was observed, particularly in plastic hinges located at columns A and C due to interaction with the floor system. Floor interaction effects were less pronounced at column B, as the transverse beam support provided a weak zone over which the floor restraint was reduced. In this case, the plastic hinge axial restraint was found to have originated from a combination of floor reinforcement acting in tension, and additional deep beam action derived from crack pattern analysis, as shown in Figure 3-2 (Fenwick et al. 2005). Deep beam action was found to have occurred where large cracks opened up due to a transverse beam weakness. Bending in the horizontal plane of the floor occurred as diagonal compression struts ‘clamped’ the beam plastic hinge. These diagonal compression struts were associated with crack development and aligned with principal compression stresses. In addition, cracks parallel to the moment frame tended to develop in the floor as tension was induced between the floor and frame. This tension force developed to balance the deep beam compression strut component oriented perpendicular to the frame. Deep beam action was found to contribute to approximately 75% of the total restraint force for the plastic hinge at column B (Fenwick et al. 2005).

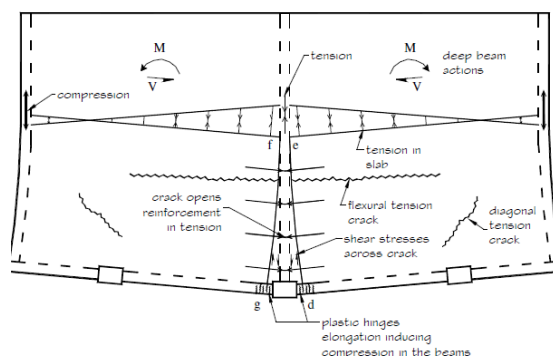


Figure 3-2: Deep beam action bending in floor (Fenwick et al. 2005)

3.1.2 Matthews (2005) and Lindsay et al. (2004)

Researchers have also examined alternative arrangements of precast prestressed floor units in a moment frame sub-assembly when subjected to seismic excitation (Matthews 2005; Lindsay et al. 2004). The primary focus of this testing was on the performance of precast prestressed hollow-core floor units which spanned parallel to moment frames. Hollow-core floors were tested because they were among the most common flooring types used in New Zealand construction. The specimen comprised a two bay moment frame supporting floor units which spanned past an internal column. Floor specimen details were based upon design practice in New Zealand at the time, as presented in Figure 3-3. The floor included an insitu topping reinforced with cold-formed non-ductile mesh.

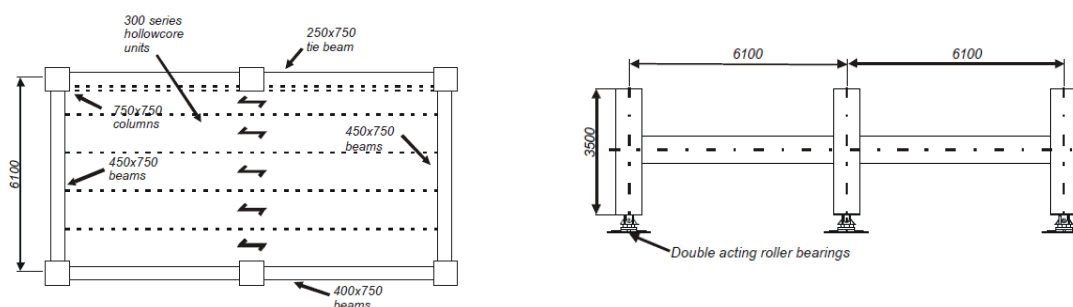


Figure 3-3: Frame floor sub-assembly test arrangement (Matthews 2005)

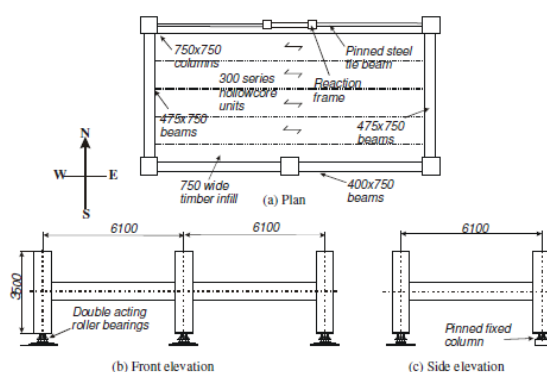
Observations made during the experiment showed that the floor units were significantly damaged as drift was applied to the frame, whilst the frames exhibited only minor damage. Significant cracks were observed in the topping and in the precast unit webs, with eventual loss of seating and floor unit web failures observed. A large crack at the interface of the first and second floor units was observed due to out-of-plane movement of the central column. This column became unrestrained out-of-plane once the topping reinforcement was fractured, suggesting that the column was not adequately tied into the floor diaphragm. The use of non-ductile topping reinforcement was therefore found to have led to unacceptable floor damage. A recommendation that flexible link slabs be placed between the frame and first floor unit, to prevent frame deformation from damaging the floor units, was made based upon these damage observations. Detailing recommendations were also made to prevent loss of floor

seating or positive moment failures in the floor units due to displacement compatibility with elongating plastic hinges.

Based upon the findings of Matthews (2005), two subsequent experimental programmes were undertaken. These subsequent tests were undertaken to develop the recommendations made by Matthews (2005) and to confirm the improvements to floor diaphragm performance. The Lindsay et al. (2004) experiment tested a similar frame floor sub-assembly as Matthews (2005) but with improved details, which showed significantly improved performance. Issues with the use of ductile topping reinforcement meant that a further experiment (MacPherson (2005)) was required to confirm the effect of improved detailing as discussed subsequently. Whilst the earlier testing provided the foundation for the MacPherson (2005) test, the data collected during the preceding experiments was found to be less useful for finite element model calibration as presented in this chapter due to the undesirable failures of hollow-core floor units without improved detailing. Therefore the MacPherson (2005) test was the primary data from this series of tests used for calibrating finite element models.

3.1.3 MacPherson (2005)

Tests by MacPherson (2005), as shown in Figure 3-4, followed on from the series of tests discussed above by incorporating the recommended detailing improvements. As shown in Figure 3-4(a), the test setup was a two bay perimeter frame with precast hollow-core floor units as per the preceding experiments. The floor diaphragm exhibited only minor damage and the specimen achieved improved levels of displacement ductility with reduced strength degradation compared to earlier testing. Confirmation of the improved floor performance led to the improved detailing being incorporated into NZS 3101:2006.



(a) Floor test layout



(b) Indicative floor crack pattern

Figure 3-4: Experimental test setup - (MacPherson 2005)

Similar to the findings of the Lau et al. (2002) tests, the internal plastic hinges were found to be more restrained against axial elongation than the outer plastic hinges. These outer plastic hinges exhibited greater elongation and less strength increase due to the presence of weak zones in the floor at the transverse support beam which reduced the restraining effect of the floor. The pattern of diagonal cracks in the floor that was directed away from the central elongating hinges, as shown in Figure 3-4(b), supported the concept of deep beam action suggested by Fenwick et al. (2005). Cracks in the floor running perpendicular to the perimeter frame were observed over the transverse support beams on the exterior of the specimen, similar to the cracks observed in the Lau et al. (2002) tests. The central column, which did not support a transverse beam, did not exhibit these major cracks. Instead distributed cracks that angled towards the central column were observed. Consequently the axial restraint force calculated for the internal plastic hinges significantly exceeded that of the external plastic hinges. The use of high strength drag bars to prevent column-floor disconnection by tying the column into the floor was found to be successful. The use of ductile deformed bars in the insitu topping was also found to provide significantly improved performance and prevented the fracture of topping bars observed in previous testing.

3.1.4 Peng et al. (2008)

Further experimental research has focused on the behaviour of a precast prestressed floor, as shown in Figure 3-5, which differed from the previous tests as the precast units did not span past the internal columns, but were supported on transverse beams at each column (Peng et al. 2008). The focus of the study was to assess frame seismic performance, with particular reference to frame strength enhancement and plastic hinge behaviour changes due to floor interaction.

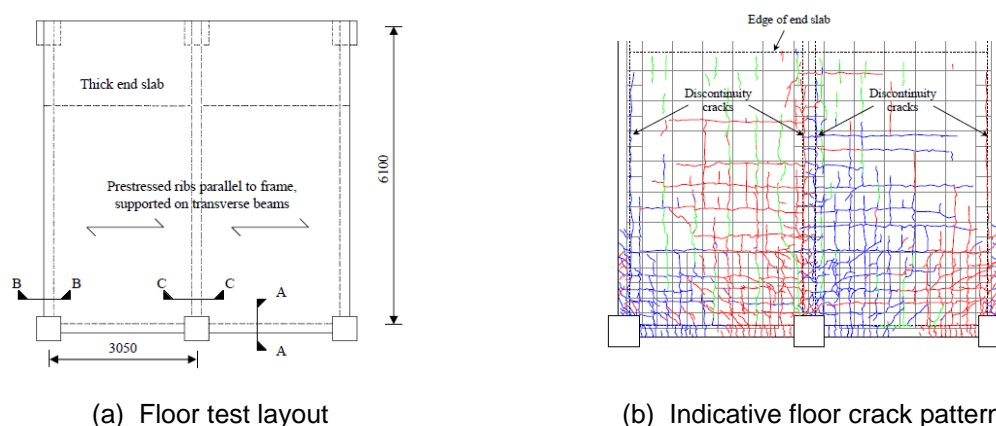


Figure 3-5: Experimental Test Setup - (Peng et al. 2008)

The Peng et al. (2008) results supported those presented previously, with cracks concentrated at weak transverse beam zones as shown in Figure 3-5(b). Observations of diagonal floor cracks also confirmed that the mechanism of deep beam action was valid (Peng et al. 2008). Analysis demonstrated that the magnitude of elongation in beam plastic hinges located at internal column faces was approximately half that measured in beam hinges located at exterior column faces because of the restraint provided by the floor acting in deep beam bending. Analysis of these results also showed that both theoretical and over-strength beam flexural capacities were significantly under-estimated when using NZS 3101:2006

(S9.3.1.2, S9.3.1.4 and S9.4.1.6.2). Measured strength increases and reduction in hinge elongations were again most significant at internal plastic hinge zones around the central column. Peng et al. (2008) also demonstrated that lightly reinforced floors had larger widths activated in restraint of elongating hinges than for heavily reinforced floors. The experimental data obtained was subsequently used by Peng et al. (2008) to generate computational models of the plastic hinges and floor restraining behaviour (Peng et al. 2011a; Peng et al. 2011b).

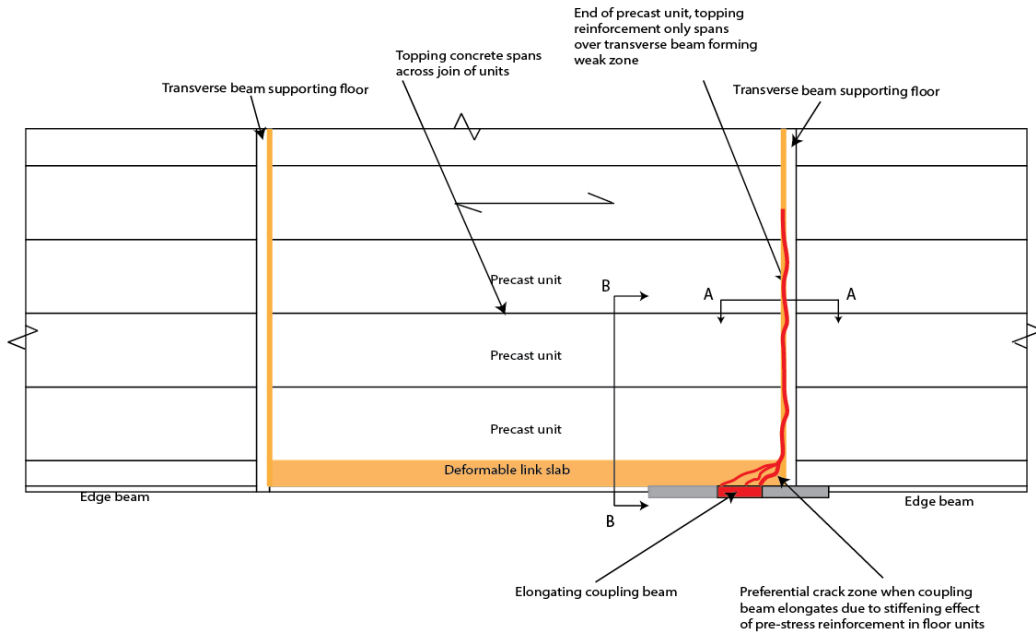
3.2 Floor diaphragm axial restraint force generation

Based upon the experimental testing discussed in section 3.1, the proximity of plastic hinges to weak zones within a floor diaphragm has been found to influence the way in which floors and plastic hinges interact. The influence of weak zones was evident in the experiments on precast floor systems which typically included weak zones around the edges of the precast floor units where large cracks were observed. These weak zones limited the axial restraint force provided by the floor diaphragm to the elongating plastic hinges. Consequently the floor crack patterns and the behaviour of plastic hinges was found to differ markedly based upon the floor arrangement.

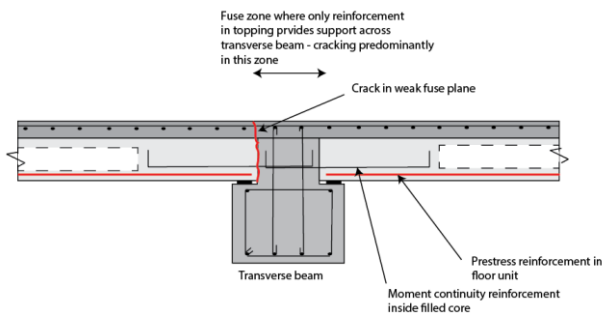
Previously discussed experimental crack patterns and measured strength increases have led to the concept of potential ‘fuses’ acting within a floor. A potential fuse is defined as a relatively low strength region of the floor, with the potential to limit a floor’s axial restraint capacity and concentrate deformations. Given that by definition the capacity of a fuse is lower than that of the surrounding floor, plastic deformation tends to concentrate at these fuse locations and prevents excess damage from developing elsewhere in the floor. A precast floor system typically includes a large number of these potential fuses, as the precast floor units represent high strength and high stiffness regions relative to locations where only the insitu topping is present. These weaknesses occur primarily at the interface of precast floor units. A typical precast floor, showing a common layout of weak zones representing potential fuses is presented in Figure 3-6 (a). Sections through typical fuses in precast flooring systems are also shown in Figure 3-6 (b) and (c). These fuses are generally present in typical New Zealand precast flooring systems and hence relate to a variety of different floor arrangements. Insitu concrete floors tend to be less governed by fuses as the floor diaphragm is more homogeneous.

Where the floor units are supported on transverse beams, the termination of stiff precast pre-stressed units causes any axial tension force in the floor units to be resisted by topping reinforcement and any continuity reinforcement across the transverse beam, as shown in Figure 3-6 (b). As the mild steel topping reinforcement and continuity reinforcement typically have a lower capacity than the high strength floor unit prestress strands, transverse beam supports provide a weak zone over which the tension force in the floor could be limited and deformation concentrated. These weak transverse beam fuse zones were observed in the experiments outlined in section 3.1, in which wide cracks were observed to occur in the floor parallel to transverse beams. Expanding the fuse concept to consider additional weak zones suggests that the interfaces where floor units are placed against each-other also represents a weak zone limited by topping reinforcement capacity. Another weak zone is the flexible link slab which is typically reinforced with starter bars similar to the topping reinforcement. As the floor

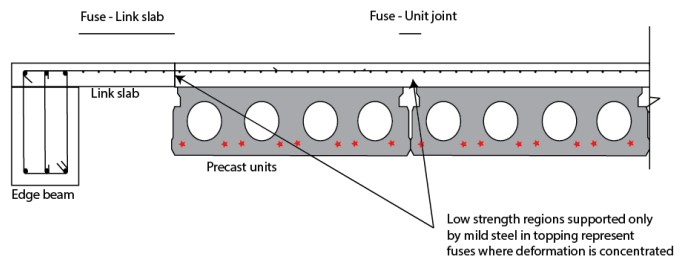
restraint force must be transferred through this zone, the strength of the link slab may also limit the restraint capacity of the floor units.



(a) Floor plan indicative fuse layout of typical precast floor system



(b) Section A-A through transverse beam fuse



(c) Section B-B through typical link slab and hollow-core floor units

Figure 3-6: Floor fuse concept – Based on typical detailing recommended in (Fenwick et al. 2010)

As observed in the previous experiments, the arrangement of floors with respect to the plastic hinges had a significant effect on the axial restraint force generated. Due to the small number of existing experiments, the existing body of experimental data was insufficient to characterise the wide variety of floor arrangements possible. As such, a range of finite element models with a variety of floor arrangements and strength hierarchies were analysed to better characterise the interaction of floor systems with elongating plastic hinges. These models are presented in Chapters 4 and 5, with the model calibration presented below.

3.3 Floor diaphragm modelling

The selected modelling software to analyse floor diaphragms was VecTor2, a two-dimensional finite element analysis software which has been under ongoing development at the University of Toronto

since 1990 (VecTor Analysis Group 2011). VecTor2 software has been specifically developed for two-dimensional reinforced concrete membrane structures based upon the Modified Compression Field Theory (MCFT) (Vecchio and Collins 1986) and the Disturbed Stress Field Model (DSFM) (Vecchio 2000). The MCFT and DSFM are analytical models for reinforced concrete elements subject to normal and shear stresses in the plane of the concrete membrane.

VecTor2 utilises an orthotropic concrete material with rotating smeared cracks to model concrete membranes. Iterative secant stiffness is used to capture non-linear cracking of reinforced concrete. VecTor2 incorporates constitutive models to represent complex stress-strain behaviour of cracked concrete including compression softening, tension stiffening, tension softening and tension splitting. The software relies upon a fine mesh of low powered elements for numerical stability and to capture local cracking. Concrete is modelled with a range of three planar elements to create the element mesh. Reinforcement is modelled as smeared throughout the concrete section or modelled discretely using truss bar elements and connected to concrete elements using either link or contact bond elements. The suite of software available includes a pre-processor FormWorks © which utilises a graphic user interface (GUI). Augustus © is the VecTor2 graphic post-processor which allows visualisation of modelling results and incorporates a number of data analysis functions. A comprehensive explanation of VecTor2 modelling can be found in (Wong et al. 2013).

To ensure that the finite element models accurately reflected realistic floor diaphragm behaviour, test data on floor-frame interaction was compared to modelled results. Frame-floor test data from the experimental programmes outlined in section 3.1 was used for the model calibration as these test setups provided reasonable experimental data on the floor response to an elongating plastic hinge. The primary output of interest was the magnitude of axial restraint force generated by the floor. It was also important to ensure that the floor damage pattern matched experimental observations well because the damage pattern provided information regarding the activation of weak zones in the floor. The correlation to experimental data was important to ensure that the models represented realistic behaviour suitably so that analyses could be undertaken on a range of floors with confidence.

3.3.1 Floor model basic inputs

The first stage of the calibration process involved iterating on model inputs until the models of floors were found to be numerically stable and could be analysed in a computationally efficient manner. Such inputs as loading increment and mesh size were first compared to ensure that the floor models were numerically stable and computationally efficient. This initial convergence assessment, presented in Appendix B, was used to develop a method of idealising the floor diaphragms in a two dimensional plane in a computationally efficient manner. This method of idealisation is presented below.

The behaviour of floors in response to elongating plastic hinges was analysed by considering the floor in two dimensions in the horizontal plane of the floor, as shown in Figure 3-7. Elongation strain was applied along the edge of the floor diaphragm with displacement control and the response of the floor was monitored. The resulting stress field and deformation pattern were then used to analyse the floor response induced by an axially elongating plastic hinge. Although the experimental data contained

more than one plastic hinge elongating simultaneously, the finite element models considered only the central plastic hinge elongating independent of the other hinges to simplify the analyses. The elongations applied at the internal column were intended to represent the cumulative elongation at the central location due to a combination of positive and negative bending hinges. The layout of the initial floor models in VecTor2 are shown in Figure 3-8.

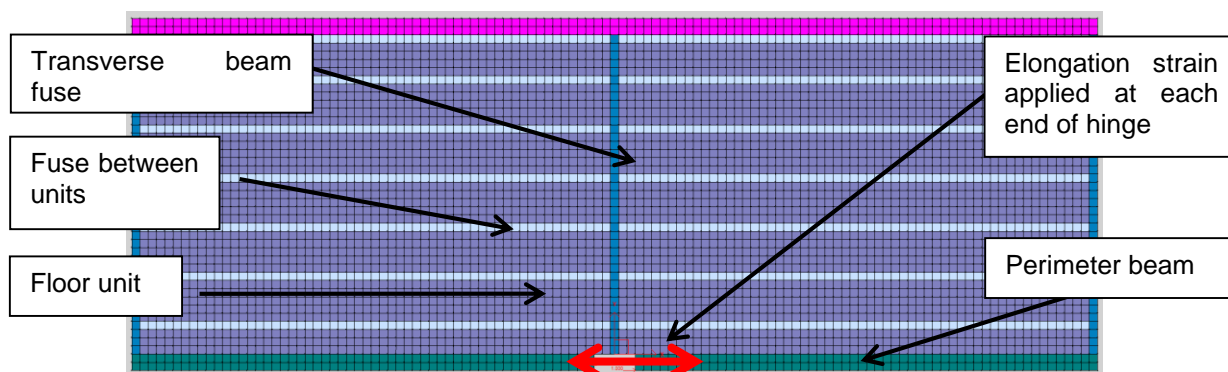
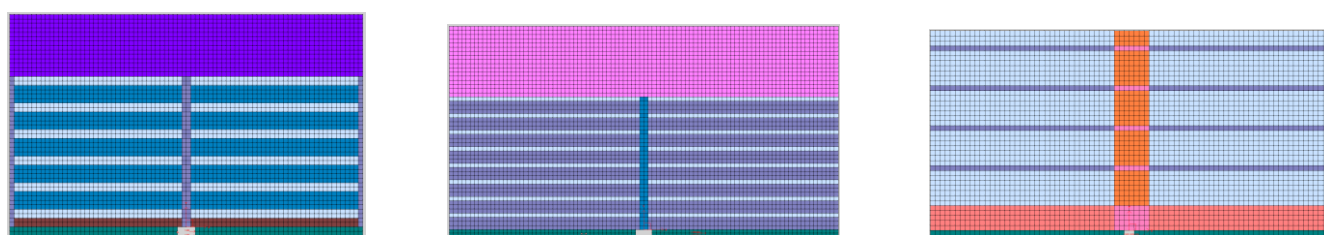


Figure 3-7: Typical plan of 2D VecTor2 floor model – colours represent different material properties



(a) Lau et al. (2002) floor model

(b) Peng et al. (2008) floor model

(c) MacPherson (2005) floor model

Figure 3-8: General layout of VecTor2 floor models for calibration -colours represent material properties

As VecTor2 is a two dimensional simulation tool designed to capture the in-plane response of concrete members, out-of-plane effects were not considered in the model. While the important behaviour occurred primarily in the horizontal plane of the floor, it was important to first consider the actions which were not captured in the simplified in-plane model. These included:

- Floor bending deformation out of the horizontal floor plane near plastic hinges due to rotation about a horizontal axis;
- Combination of diaphragm transfer forces with axial restraint forces;
- Vertical loads on the floor diaphragm due to gravity and/or vertical ground acceleration;
- Torsional response of transverse beams framing into the columns.

The bending of the floor diaphragm out of the horizontal plane was largely localised to the flexible link slab (where present). Bending in the link slab reduced the concrete shear capacity, which resulted in a localised reduction of shear transfer capacity across the interface of the perimeter frame and floor. However this out-of-plane bending was assessed as not having a significant effect.

Diaphragm force transfer was a transient force which depended on ground motion and modal effects, as seismic demand was distributed between lateral force resistance systems by the floor diaphragm. In contrast the floor axial restraint force was induced by a stable, generally increasing strain which depended on axial elongation and did not typically reverse. Peak transfer force demand and axial elongation restraint demand in the floor diaphragm were therefore not simultaneous and it was more conservative to consider the maximum restraint force generated independent of any diaphragm transfer demand. However transfer forces may have reduced the measured floor restraint capacity.

Vertical loads on the floor diaphragm could not be incorporated into the two dimensional model as they acted normal to the floor. This lack of consideration was an issue because of the way in which precast floor units in New Zealand supported tension forces associated with axial elongation (Fenwick et al. 2006). Consideration of a hollow-core floor section shown in Figure 3-6 (c) suggests that at this section of the floor, elongation strain was introduced to the floor units through the topping. Consequently the applied strain was eccentric to the centroid of the floor units and so applied a hogging (negative) bending moment which caused an upwards deflection of the floor units. However precast floor units in New Zealand are typically unreinforced at the top of the section so have a low negative moment capacity. As discussed by Fenwick et al. (2006), the negative moment applied by an elongating plastic hinge does not result in a direct tension in the top of the floor units (because the tension capacity here is low), but instead reduces the compression stress associated with positive (sagging) moments already applied to the section. Therefore the tension capacity of precast floor units without reinforcement at the top of their section (as are typically used in New Zealand) can be defined based upon the magnitude of positive (sagging) moments applied to the section. The tension capacity of the floor units can therefore be determined according to equation 3-1, where z represents the lever arm of the section.

$$T_{Floor\ Units} = \frac{M_V}{z} \quad (3-1)$$

The moment demand M_V includes the gravity moment acting on the floor, in addition to the positive moment capacity at the end of the section and the moment induced by the link slab shear capacity acting downwards on the floor units. As the tension capacity of the floor units was dependent upon three-dimensional behaviour, it was logical to use this floor tension capacity for the two-dimensional modelling. Therefore in order to account for three-dimensional behaviour in these simplified two-dimensional models, the floor units were input into the modelling using this equivalent tension capacity. This capacity was additive to the tension capacity of the topping reinforcement based upon the analysis conducted by Fenwick et al. (2006).

Torsion of transverse beams was considered by Peng et al. (2008) who found that the torsional resistance of the transverse beam significantly increased the column shear force sustained by the sub-assembly. In addition, it was found that the torsional response of the transverse beam altered the penetration of elongation strains into the floor. The effect of the transverse beams acting in torsion was not considered in the two-dimensional floor models.

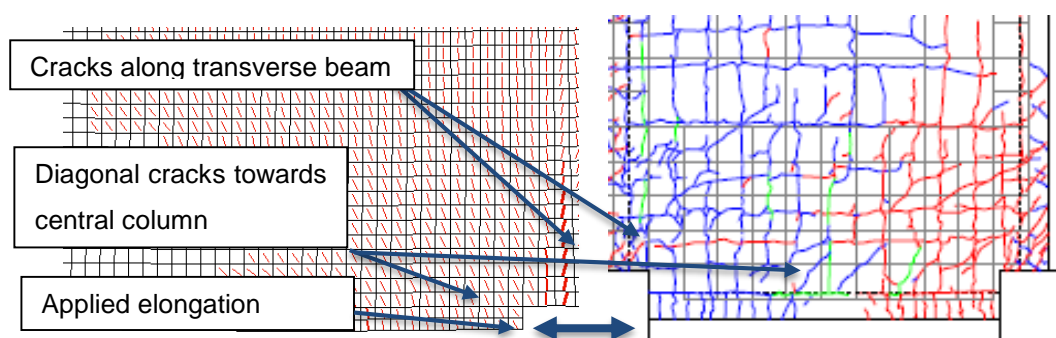
3.4 Comparison to experimental data

Using the modelling approach presented above, the experimental floors previously discussed were computationally modelled to ensure that confidence could be placed in the results. Material properties and section dimensions were set in the models to match the measured properties from the experiments, as detailed in Appendix B. In this way the models were intended to replicate as closely as practical the experimental setup. Basic VecTor2 constitutive models were applied to the computational models, as outlined in Appendix B. Each of the previously discussed experimental floors were modelled, subject to elongation strains at a single hinge location as per Figure 3-7 and Figure 3-8.

Two general floor layout cases were considered, which differed markedly in their behaviour. The first case was related to situations where a transverse beam weakness governed the floor behaviour, as per the Peng et al. (2008) test and the internal hinge of the Lau et al. (2002) test. These weakness governed cases were considered in section 3.4.1. The second case to consider was when the floor behaviour was not governed by a transverse beam weakness, as was the case in the internal hinge of the MacPherson (2005) test. The case where transverse beam weaknesses did not govern the floor response was considered in section 3.4.2.

3.4.1 Floor axial restraint behaviour where transverse beam weaknesses were present

Where a transverse beam, as shown in Figure 3-6 (b), was located adjacent to an elongating hinge, the experimental data showed floor deformation tended to be concentrated at this weak zone. Consequently the floor axial restraint force applied to the elongating hinge was limited by the tension capacity across the transverse beam. This floor deformation type was observed to have occurred in both the Peng et al. (2008) floor and the Lau et al. (2002) floor. A comparison of crack patterns from the Peng et al. (2008) tests to their corresponding VecTor2 model results are presented in Figure 3-9 to demonstrate the accuracy of the models in predicting this floor deformation pattern. Although it was difficult to visualise the crack patterns because the simulations used rotating crack assumptions, it was observed that the crack orientation tended to match that from the experiment reasonably well. In accordance with the principal compression stresses, the diagonal cracks oriented towards the central column were well approximated. Additionally, the cracking oriented perpendicular to the frame elongation along the central transverse beam could be seen in the modelled results.



(a) Modelled crack pattern

(b) Experimental crack pattern

Figure 3-9: Half section of Peng et al. (2008) floor showing crack pattern comparison between computational model and experiment

The total restraint forces generated from the models are compared to the experimentally derived restraint forces in Figure 3-10 and Figure 3-11. The experimental restraint forces were typically determined at a single point rather than throughout the development of elongation. As a result, the figures also indicated an approximate elongation at which the experimental restraint forces were derived in order to compare the restraint force more accurately at the corresponding elongation magnitude.

Analysis of Figure 3-10 and Figure 3-11 showed that the modelled restraint force was over-predicted by approximately 20% in the Peng et al. (2008) tests and under-predicted by approximately 15% in the Lau et al. (2002) tests. Given that the two-dimensional model excluded out-of-plane deformation and cyclic loading effects, and hence under-predicted floor damage, it was expected that the models would have over-predicted the floor restraint force slightly as seen in the Peng et al. (2008) comparison. However the Lau et al. (2002) results were slightly under-predicted, an error attributed to the effect of the end slab used in the experiment. The experimental end slab, as shown in Figure 3-1, was heavily reinforced to replicate a larger floor area and was erroneously predicted to influence the behaviour in the model. An additional source of the anticipated over-prediction related to the lack of bond assumed in smeared reinforcement, which tended to concentrate the modelled strains and over-predict the floor effective width. As a result, the modelled reinforcement tended to be activated over a wider floor extent.

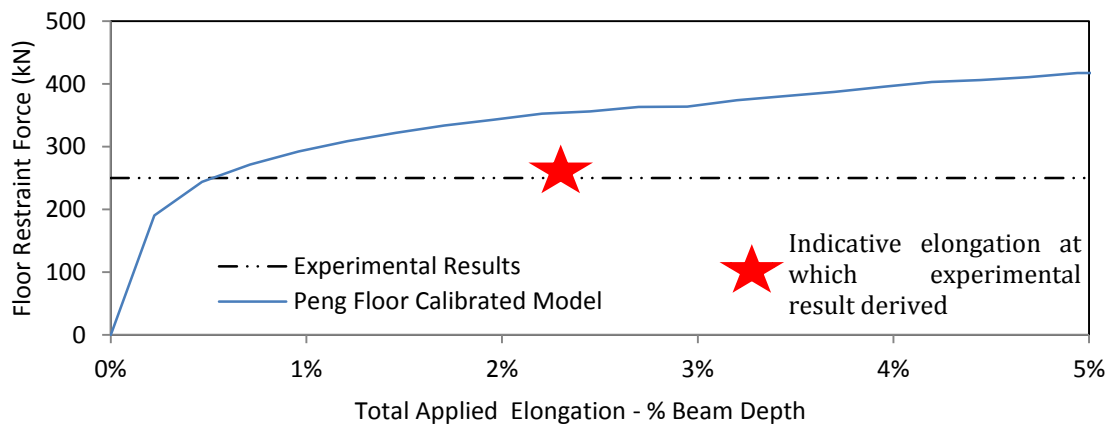


Figure 3-10: Comparison of floor restraint forces for Peng et al. (2008) specimen

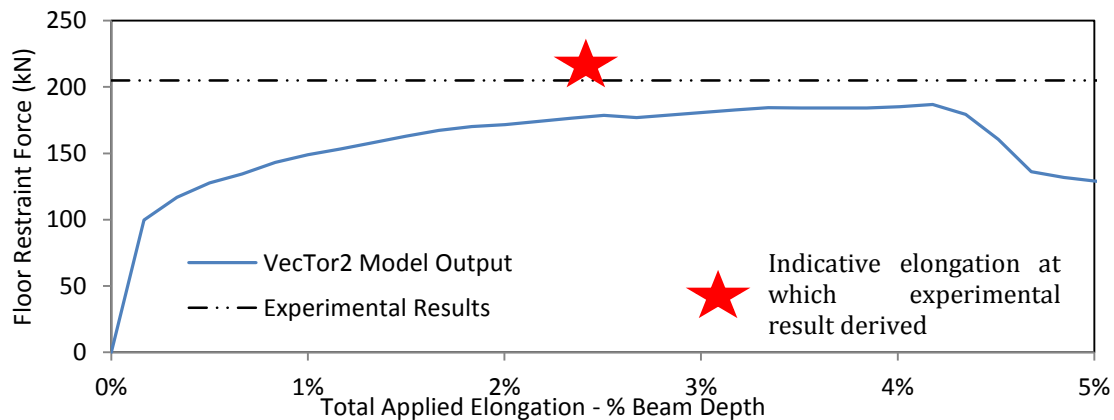


Figure 3-11: Comparison of floor restraint forces for Lau et al. (2002) specimen

The models presented above predicted restraint force degradation in the Lau et al. (2002) test due to first fracture of the bars at approximately 4-5% elongation. Onset of bar fracture could not be compared to the experimental data as elongation in the internal hinges did not exceed the predicted fracture magnitude. In order to demonstrate the effect of the transverse beam weakness, an indicative floor reinforcement stress field is presented in Figure 3-12, showing a general concentration of stresses along the transverse beam and at the end of the plastic hinge zone.

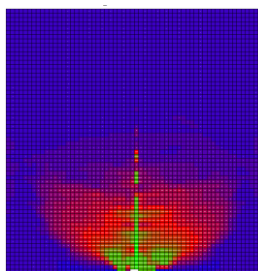


Figure 3-12: General floor reinforcement stress field for Peng et al. (2008) floor (stress parallel to elongation, green represents high levels of tension stress)

Computational models of the Lau et al. (2002) floor tended to provide reasonable correlations with the experimental data from the outset and were only improved marginally by the model calibration. However as shown in Figure 3-10, despite the model calibration process, the Peng et al. (2008) floor model still showed a significant over-estimate of the floor restraint force generated, although the correlation was improved from the initial models. It was inconclusive exactly why the model over-predicted the response particularly for the Peng et al. (2008) test. Among the possible reasons for the error were that the damage associated with realistic three-dimensional behaviour was more severe for this case, which reduced the ability of the floor to resist perimeter frame elongation and this was not captured in two-dimensional modelling. Torsional damage in the transverse beam was an alternative reason for the behaviour which was not captured in two-dimensions. Another possible explanation was that the damage induced in the floor by the exterior hinges not considered in the finite element model interacted with the damage related to the interior plastic hinge and reduced the floor restraint capacity.

Comparison of the VecTor2 models to experimental data shown in Figure 3-10 and Figure 3-11 suggested that the models provided a reasonable approximation of the activated floor restraint, provided the behaviour relevant to the analysis occurred prior to strength degradation of the floor. A slight restraint force underestimate was observed in the Lau et al. (2002) specimen model (likely due to the effect of the end slab), and a significant over-estimate observed in the Peng et al. (2008) specimen model. In general a slight over-prediction of the restraint force would be expected in the models due to a lack of out-of-plane effect and early strain hardening due to mesh strain concentration.

3.4.2 Floor axial restraint behaviour where transverse beam weaknesses were not present

When transverse beams were not located adjacent to an elongating plastic hinge, the floor restraint behaviour differed markedly from that discussed above. Analysis conducted by MacPherson (2005) and subsequently by Fenwick et al (2006) suggested that the restraint force generated when precast units spanned past an elongating hinge could significantly exceed that generated when a weakness

across a transverse beam was activated (Fenwick et al. 2006). The MacPherson (2005) experimental data was used to confirm confidence in the computational models in absence of a transverse beam weakness, with a typical model layout shown in Figure 3-13.

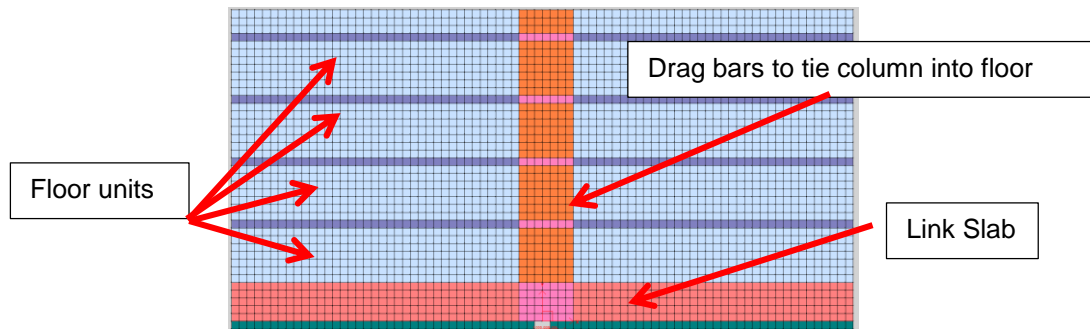


Figure 3-13: VecTor2 representation of MacPherson (2005) floor where colours represent different material properties

Based upon the previously discussed method of idealising the floor tension capacity (as a function of the floor moment demand) the MacPherson (2005) floors were modelled using equivalent tension properties. The resulting floor restraint force generated with an equivalent tension model is presented in Figure 3-14. The modelled restraint force of the floor was compared to that derived by Fenwick et al. (2006) based upon the equivalent tension method which showed good agreement with the experimental data. As can be seen in Figure 3-14, the restraint force was slightly underestimated by the model as compared to the maximum floor restraint capacity derived by Fenwick et al. (2006). The reinforcement stress parallel to the elongation direction predicted by VecTor2 is shown in Figure 3-15, giving an indication of the floor extent participating in the restraint response.

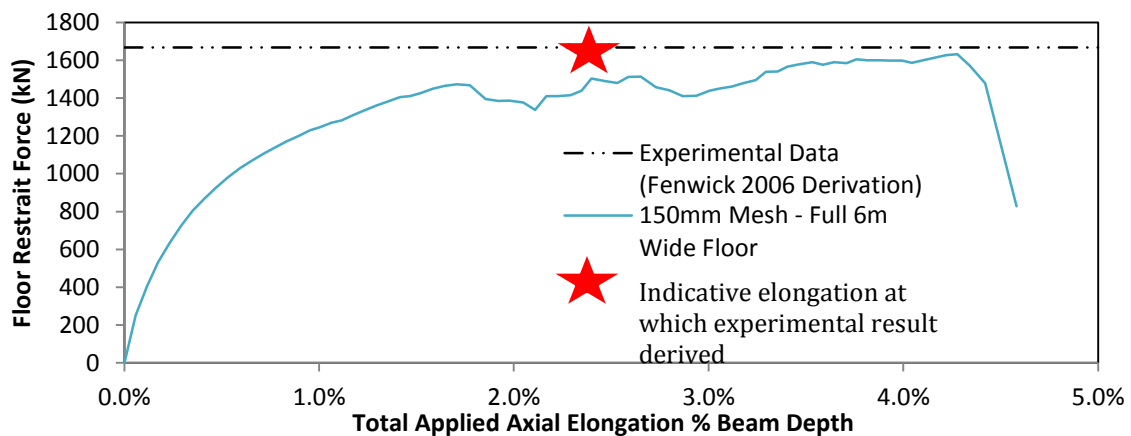


Figure 3-14: Floor restraint force generated in VecTor2 model based upon MacPherson (2005) test with equivalent floor tension properties

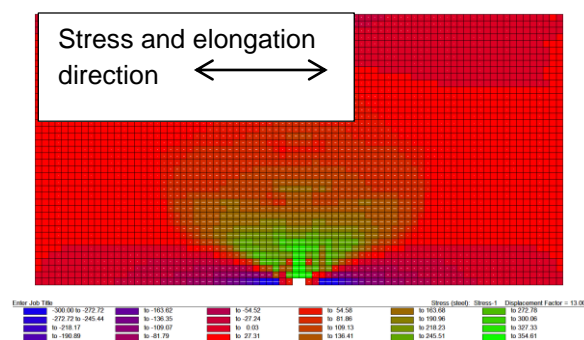
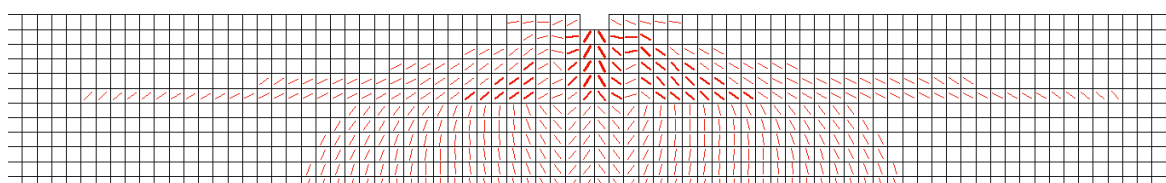


Figure 3-15: Plan view of reinforcement stress field in floor due to elongation for MacPherson (2005) floor (reinforcement stresses shown in MPa – positive in tension)

The crack pattern derived from the VecTor2 data is compared to the experimental crack pattern in Figure 3-16 with the crack directions from the model showing good agreement with the experimental crack pattern. A predominance of cracks angling towards the central column, particularly in the link slab can be observed in Figure 3-16. Note that the model only considered the internal plastic hinges, so the crack pattern at the exterior transverse beams was not considered in the model.



(a) VecTor2 crack pattern output



(b) Experimental crack pattern (MacPherson 2005)

Figure 3-16: Crack pattern comparison of effective floor model

The model outputs presented showed reasonable agreement with the experimental data, with a slight underestimate of the total restraint force. The postulated reason for the slight restraint force underestimate related to the shear transfer and shear deformation at the beam-floor interface. This shear deformation was inherently difficult to model and inaccuracy at high strain levels was to be expected with computational models due to numerical convergence issues with highly damaged concrete elements. Variability in the modelled restraint force at large applied strain was due to the onset of large shear distortions in the link slab which was observed to have begun failing in shear. Consequently the shear slip along cracks inhibited complete numerical convergence of the model, which was manifested as the peaks and troughs in the modelled restraint force.

Examination of Figure 3-15 also showed that a compression zone was present at the furthest extent of floor from the elongating hinge due to deep beam action. This deep beam action compression zone

was observed to have acted parallel to the elongation strain and hence reduced the tension capacity available for the restraint of beam elongation. In a real floor, if the floor area considered was wider, the compression stress would have been reduced and hence the restraint force increased.

The model calibrations presented generally showed reasonable agreement with the experimental data for the case where transverse beam weaknesses were absent. This good correlation was despite simplifications required to analyse floors in two dimensions and the relatively large mesh sizes required to consider large areas of floor. In particular, the use of an equivalent floor unit tension capacity, based upon the bending moment in the floor, was found to be valid. The cracking behaviour also appeared to be reasonably well represented in the computational model suggesting that the mechanisms of floor axial restraint were representative of realistic behaviour.

3.1 Conclusions

Comparison of computational floor models to the available experimental data has led to a modelling technique which provided reasonable results of floor system response to axial elongation strains applied at the edge of the floor. In general, good correlation has been found between the models and the experimental data. The primary discrepancy between the model and the experimental data was found to be related to the case that was governed by the weakness of the transverse beam for the Peng et al. (2008) floor. The over-prediction in the model was found to be the result of strain concentration in the weak zones of the floor which was not representative of the experimental data. The error associated with the Peng et al. (2008) floor was reduced significantly by the model calibration process. However the comparison showed a 20% over-prediction of the floor restraint force.

Although the experimental data used for model validation did not include detailed information about the development of axial restraint forces as elongation developed, the approximate comparisons made in this chapter have demonstrated that the models were generally of reasonable accuracy to extend to further models. The calibrated models were used to undertake a parametric study of floors, as presented in Chapter 4. The VecTor2 model data developed from the experimental programmes was explored further when the inferred mechanics of floor restraint is discussed in Chapter 5.

CHAPTER 4

4 Floor Diaphragm Parametric Study

Floors in multi-storey buildings have traditionally been designed to support gravity loads such as people and objects within a building. During an earthquake, floors are also required to act as diaphragms by transferring force between a building's structural elements such as frames and walls. Floor diaphragms have typically been designed to remain elastic under these demands and tended not to be designed to sustain inelastic deformations. An adequate understanding of the demands imposed upon the floor is required to enforce this elastic floor response. One aspect of the floor demand that has been ignored in many design codes is the response of floors to axial elongation in supporting beams as these elongating beams have been shown in the studies presented in Chapter 3 to interact with the floor system. The characterisation of the floor response when subjected to beam axial elongation compatibility strains is the subject of Chapters 4 and 5.

A parametric study of the wide variety of floor diaphragm arrangements, support conditions and detailing that is possible in multi-storey buildings is presented in this chapter. The objective of this study was to assess the importance of the floor arrangement and support conditions on the response of a floor diaphragm when subjected to applied elongation strains. Particular emphasis was placed on the performance of precast prestressed floor units as the detailing of these floors could have had a major impact on their response to axial elongation strain. Two-dimensional finite element modelling software VecTor2 was used to characterise the behaviour of a wide variety of floors and to assess the importance of floor detailing. The parametric study of floor diaphragms was undertaken on the basis that the floor response was dependent only upon the elongation progression on the edge of the floor. In this way, the study was independent of whether the elongation occurred in a coupled wall system, or a moment frame system. The results of the study were therefore intended to be applicable to a generalised floor system response to any plastic hinge.

The results of the parametric study of floor detailing are presented in this chapter based upon the model calibration presented in Chapter 3. A series of base models were first simulated. These base model results were used as a base case for comparison against a series of parametric variations of floor detailing presented in this chapter. A discussion of the mechanics of floor systems subject to axial elongation strains is presented in Chapter 5, based in part upon these results.

4.1 Base model layout and results

A series of base models were first run in VecTor2 to provide base cases for the parametric study comparisons. A base model of each floor arrangement listed below was analysed prior to the parametric study, with typical detailing in accordance with NZS 3101:2006. The layout of these base

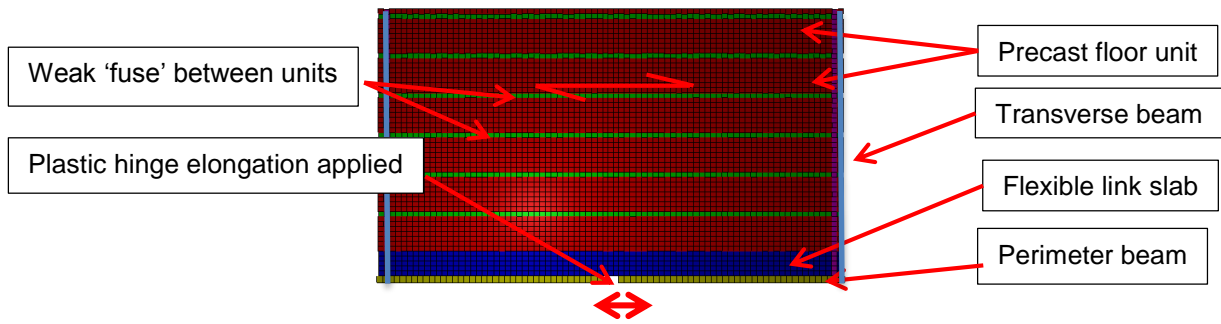
models is briefly presented in this section. As the base models were used for comparison to parametric variations in section 4.2, a summary of the base models results is presented in Appendix C.

The base models were analysed as per the technique outlined in Chapter 3. This technique involved modelling in the horizontal plane of the floor, where the floors were subjected to displacement controlled elongation strains of a plastic hinge on the floor edge. The assumptions, exclusions and limitations of this modelling technique are presented in section 4.3. An indicative layout of the two-dimensional VecTor2 floor idealisation is presented in Figure 4-1. Four different floor arrangements were considered in the base models and parametric study. As shown in Figure 4-3, reference was made to orientations with respect to the applied elongation direction. Parallel or perpendicular references related to orientations relative to the applied elongation direction in the models. The floor arrangements considered were referred to as arrangements 1 – 4:

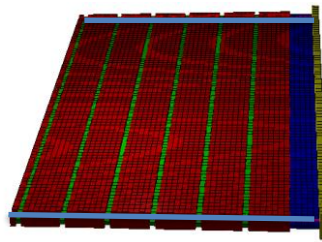
- Precast prestressed floor units:
 - **Arrangement 1 (A1)** - Spanning perpendicular to applied elongation (Figure 4-1 (c)),
 - **Arrangement 2 (A2)** - Spanning parallel to applied elongation, supported on a transverse beam adjacent to elongating hinge (Figure 4-1 (d)),
 - **Arrangement 3 (A3)** - Spanning parallel to applied elongation, spanning past elongating hinge (Figure 4-1 (a) and (b)).
- **Arrangement 4 (A4)** - Cast insitu floor reinforced with mild steel (Figure 4-1 (e)).

As floors have been shown in Chapter 3 to include weak 'fuse' zones, the two dimensional models were developed to include the relative strengths within the floor. These weak zones are shown in Figure 4-1 (b) for a precast floor system, represented by thinner concrete sections and reduced reinforcement contents. As shown in Figure 4-2, the weak zones represented a deformable link slab as per MacPherson (2005), topping reinforcement between floor units and low strength regions over transverse beams.

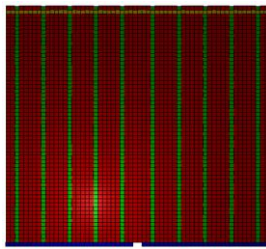
A suitable floor width (see Figure 4-3) to consider in the models was determined by comparing the results of models with different widths, until consideration of additional width did not change the measured response. Thus the behaviour of a floor with large plan area was considered in this modelling. A suitable length (see Figure 4-3) to consider in the models was less easily defined. As the building system would in reality have included multiple hinges elongating simultaneously, the length of floor activated in axial restraint of a single elongating hinge was dependent upon hinge spacing rather than absolute floor dimensions. To account for multiple hinges elongating simultaneously, a tributary area basis was adopted. Based on tributary areas of each elongating hinge, the dimensions L1 and L2 in Figure 4-3 referred to half the spacing to the next plastic hinge zone. In the case of arrangement 2, L1 and L2 refer to half the span of the precast floor units to prevent the overlap of stress fields associated with different hinges occurring. The limitation of considering this approach is discussed in section 4.3. On the basis of these requirements, the base models were 12m long in the direction of the floor span, with floor widths measured away from the plastic hinge of either 8m or 12m depending upon the floor being considered, as shown in Figure 4-3.



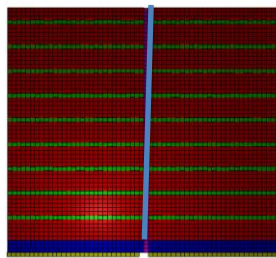
(a) VecTor2 plan view of A3 - floor system spanning parallel to applied elongation, spanning past elongating hinge (Arrangement 3)



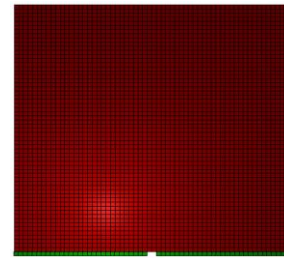
(b) VecTor2 typical three dimensional floor visualisation



(c) A1 - Precast floor spanning perpendicular to elongation (Arrangement 1)

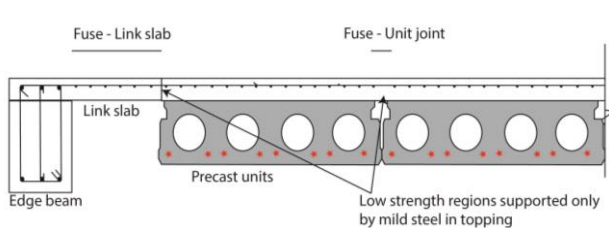


(d) A2 - Precast floor spanning parallel to elongation – supported on transverse beam (Arrangement 2)

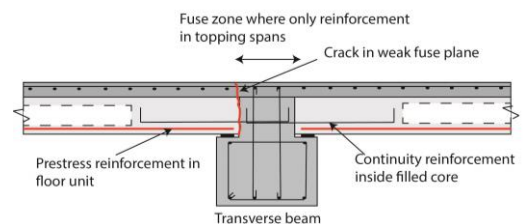


(e) A4 - Cast insitu mild steel reinforced floor (Arrangement 4)

Figure 4-1: VecTor2 floor model typical layouts. Colours represent different material properties.



(a) Section through mid-span of floor units



(b) Section through floor at transverse beam

Figure 4-2: Typical sections through precast floor diaphragm showing weak zones

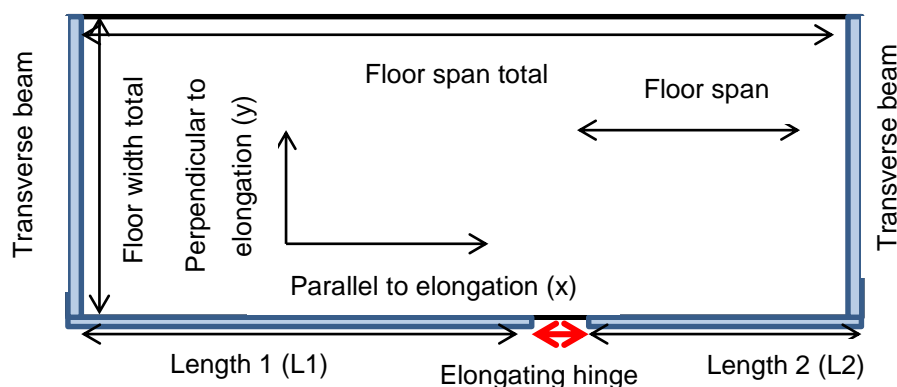


Figure 4-3: General floor plan layout showing relevant dimensions

Typical details of the base floor models are presented in Table 4-1. The precast floor base models represented the 300 Hollowcore floor (300mm deep) used in the MacPherson (2005) experiment including the detailing recommended from these experiments. This detailing included a 750 mm wide deformable link slab, ductile topping reinforcement and continuity reinforcement across the transverse beam (MacPherson 2005). Variations of precast floor unit orientation were run in order to assess the effect of floor layout on the model behaviour. Material properties were based upon specified properties of the experiments discussed in Chapter 3, as these values replicated typical design details. The properties of the grade 300 mild steel were based upon the material tests undertaken by MacPherson (2005), as shown in Table 4-2. The concrete strength used in the two-dimensional modelling was based upon a weighted average of the insitu topping and the hollowcore units. To idealise the floor in two-dimensions, an equivalent floor thickness of 245 mm was used based upon 75 mm topping, and the average floor unit thickness (less the hollow cores) of 170 mm. More information about the layout and results of the base models used for parametric comparison is presented in Appendix C.

Table 4-1: Typical precast floor base model details

Floor unit span	12 m		Topping Reinforcement	D12's @ 300 mm centres each way
Floor width	12 m			
FEM mesh size	200 mm			
Unit type	300 Hollowcore		Topping Thickness	75 mm
Equivalent floor unit tension capacity used (Based upon Fenwick et al. (2006))				937 kN/m

Table 4-2: Base model general material properties

Grade 300 Steel		Floor Concrete (weighted average)	
Yield Strength	300 MPa	Compressive Strength	41 MPa
Ultimate Strength	450 MPa	Elastic Modulus	25,000 MPa
Elastic Stiffness	200,000 MPa	Prestress Strands	
Ultimate Strain	200 me	Yield Strength	1,860 MPa

4.2 Parametric study results

A series of floor diaphragm arrangements were modelled and assessed as part of the parametric study. These models were analysed in the horizontal plane of the floor and were subjected to elongation strains as per Chapter 3. Each model in the parametric study represented identical details to the base models, with one aspect of the floor detailing varied each time. The effect of each detailing variation was assessed by comparison against the base models for each of the different floor arrangements (A1-A4). The significant results from the parametric study are presented in section 4.2.1. Where the findings were related to specific floor arrangements, the results are presented in section 4.2.2. The parameters found to have a significant effect on floor diaphragm behaviour are summarised in in Table 4-3. Additional parameters which were found to not have a significant effect on floor behaviour are summarised in Table 4-4 and discussed in Appendix C.

Table 4-3: Parametric study variables (Observed to have significant effect)

		Base case	Var 1	Var 2	Var 3
1	Topping Reinforcement	D12's @ 300 EW	D16's @ 300 EW	D10's @ 300 EW	D10's perp, D12's parallel
2	Starter Bars	None	D12's @ 150	-	-
3	Drag Bars	None	2-H16's	2-H20's	4-H20's
4	Precast Unit Equivalent Strength Ratio	1.0	1.5	0.5	-
Specific variables to a floor layout					
		Base case	Var 1	Var 2	Arrangement
5	Floor Unit Span	12 m	8 m	15 m	A3 - PT Span Past Elong
6	Fuse Offset	0 m	2 m	3 m	A2 - PT Span to T Beam
7	Continuity Reinforcement	2-D16's	None	4-D16's	

Table 4-4: Parametric study variables (Observed to have insignificant effect) - Presented in Appendix C

		Base case	Var 1	Var 2	Var 3
8	Floor Width	12 m	16 m	8 m	-
9	Topping Thickness	75 mm	65 mm	100 mm	
10	Fuse Strain Width	200 mm	400 mm	600 mm	100 mm
11	Link Slab Length	750 mm	450 mm	1050 mm	-
12	Concrete Properties	$f_c=35$ MPa	$f_c=50$ MPa	$f_c=20$ MPa	$f_t=0$ MPa
13	Precast Unit Depth	300 mm	200 mm	400 mm	-
14	Load Application	PHZ Ends	Centre	-	

4.2.1 General parametric study results

A summary of the general parametric study results is presented below for the key variables (1-7) found to have a significant impact on the floor behaviour. Additional parameters found to have a limited impact on the response of the floor (8-14) are presented in Appendix C. The primary variables used to infer the effects of each parameter were:

- The magnitude of axial restraint force resisting beam elongation generated by the floor system,
- The effective width of floor activated in response to the applied elongation – defined as width of floor yielded in tension (fully activated) in restraint of an elongating hinge,
- The proportion of shear transfer capacity between the perimeter beam and floor activated to transfer force between the elongating beam and floor system.

1. Topping reinforcement

The effect of topping reinforcement content was analysed first. Presented in Figure 4-4 is the measured response of arrangement 1 (precast floor units spanning perpendicular to the applied elongation) with varying topping reinforcement contents. With the floor units in this perpendicular orientation, the axial restraint force generated in the floor was observed to increase in proportion to the topping reinforcement content. In response to the elongating hinge, cracks developed in the topping between floor units which caused the floor units to have separated. The effective width measurement confirmed this separation behaviour, as the floor units tended to separate over the majority of their 12 m span by rotating at their supports. It was also observed that the effective width of floor activated was reduced with a higher topping reinforcement content.

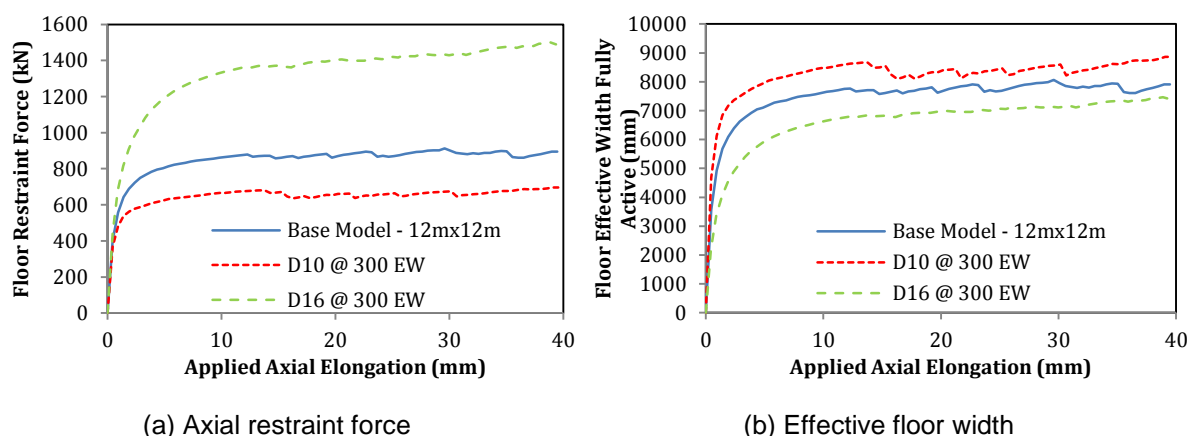


Figure 4-4: Topping reinforcement effects – Arrangement 1 (Precast units perpendicular to elongation). Base model D12's each way at 300mm centres.

The effect of topping reinforcement on the modelled response of arrangements 2 and 3 (precast units spanning parallel to elongation) is presented in Figure 4-5 and Figure 4-6 respectively. In the case of arrangement 2, a large increase in restraint force was measured when the topping reinforcement was increased. This increase in axial restraint capacity was due to an increased area of reinforcement

across the transverse beam weakness, which was found to have limited the restraint force generated in the floor. However the effective floor width was observed to be approximately unaffected.

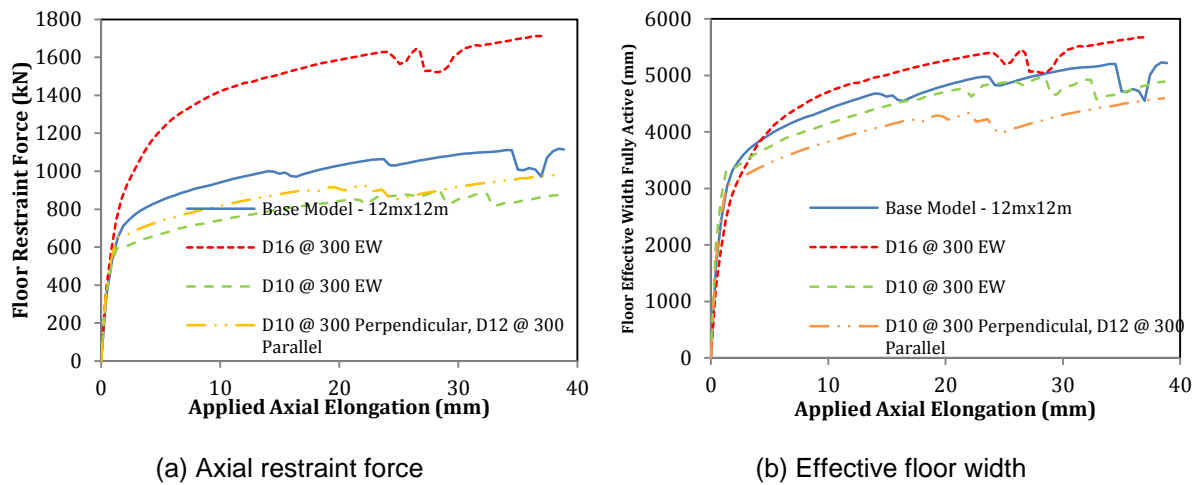


Figure 4-5: Topping reinforcement effects – Arrangement 2 (Precast units parallel to elongation, supported on transverse beam). Base model D12’s each way at 300mm centres.

Modelled results of arrangement 3 (precast units spanning parallel past the hinge) are presented in Figure 4-6. These results demonstrated that the magnitude of axial restraint force was dependent upon the topping reinforcement content. Comparison between the topping reinforcement details of D10’s each way, and D10’s perpendicular only (with parallel reinforcement unchanged as D12’s), indicated near identical behaviour. The result suggested that it was the change in reinforcement orientated perpendicular to elongation which caused the measured response changes, not the reinforcement orientated parallel as per the previous models.

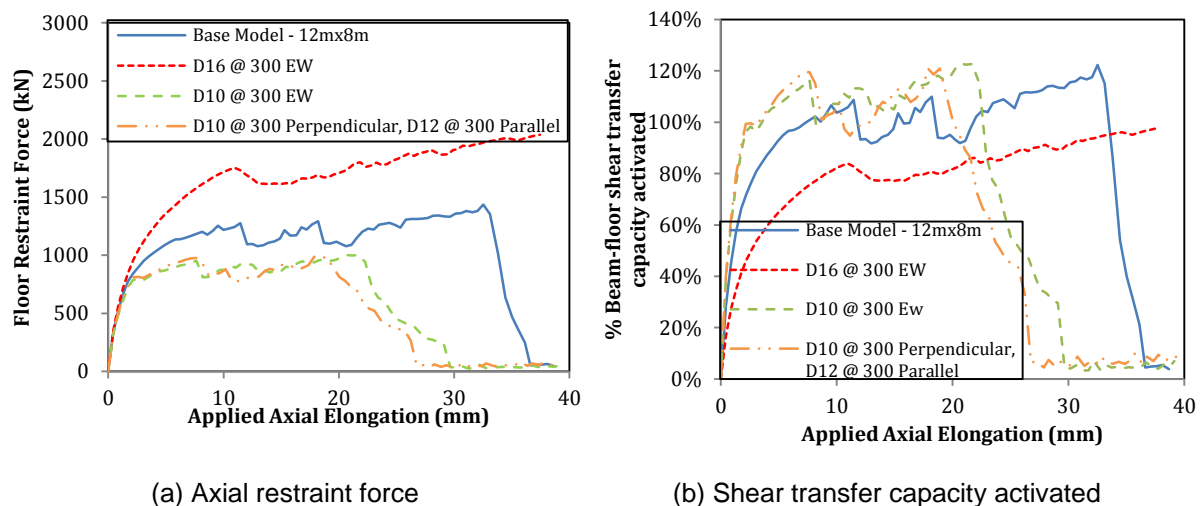


Figure 4-6: Topping reinforcement effects – Arrangement 3 (Precast units parallel to elongation, spanning past hinge). Base model D12’s each way at 300mm centres.

The effect of the reinforcement orientated perpendicular to applied elongation is presented in Figure 4-6 (b), which shows the proportion of shear transfer capacity activated. This shear transfer capacity was defined as the capacity of the beam-floor connection to transfer force between these elements. As

discussed by Fenwick et al. (2005) (see Chapter 3), the floor response to elongating hinges generated inclined floor compression struts in deep beam bending, as shown in Figure 4-7. The beam-floor connection was required to prevent separation of the beam and floor by restraining these inclined struts, with an assumed strut angle of 30° to the horizontal (Fenwick et al. 2005). These inclined compression struts therefore activated the floor in tension, in the direction perpendicular to applied elongation. The tension capacity of the floor in this perpendicular direction was fully activated in the majority of the models shown in Figure 4-6 (b). When the reinforcement perpendicular to the elongation was reduced, the full shear capacity was activated at yield, causing eventual link slab shear failure. As a result, the floor restraint capacity was limited by the link slab shear capacity. However when the perpendicular orientated topping reinforcement was increased, the shear demand took much longer to exceed the shear capacity, allowing a larger floor restraint to be generated. Therefore where the precast units spanned past the elongating hinge, a shear failure in the link slab became the limiting capacity as the tension capacity of the floor units oriented parallel to applied elongation was high.

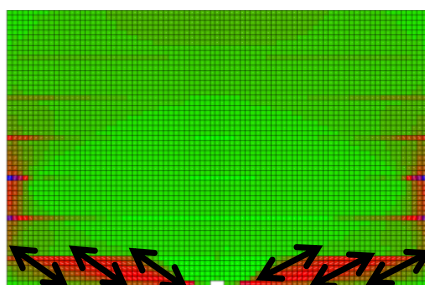


Figure 4-7: Principal compression stress field for arrangement 3 (red indicates compressive stress)

The results of the topping reinforcement comparisons have been used to show that the effect on the floor response was significant. For arrangements 1 and 2, when weaknesses between units or over transverse beams were activated, topping reinforcement content directly affected the floor restraint capacity by changing the tension capacity of these weak zones. For arrangement 3, the floor restraint capacity was found to be limited by shear transfer through the link slab. Topping reinforcement provided the majority of the shear transfer capacity through the link slab and was therefore found to have had a significant effect on the behaviour of floors in arrangement 3.

2. Starter bars

As a subset of the variations in topping reinforcement, the inclusion of starter bars was also considered. As indicated in Figure 4-8, starter bars were included as an additional set of D12 bars at 300 mm centres which connected the perimeter frame to the floor. The starter bars were placed over the link slab and half the first floor unit to ensure suitable development length.

Presented in Figure 4-9 (a) is the effective width derived for arrangement 2, demonstrating that the starter bars had negligible effect on the floor response. In contrast, Figure 4-9 (b) presents the derived effective width for arrangement 3. Analysis of this result demonstrated that the inclusion of starter bars increased the floor effective width. The reason for the difference related to the observation discussed above, of a shear failure in the link slab limiting the restraint capacity of arrangement 3 (precast units

spanned past the hinge). The starter bars acted to increase the shear transfer capacity between the floor and perimeter beam, thus allowing a larger restraint force to be generated. This restraint force was also more stable due to less shear dominated deformation causing convergence issues with the modelling software.

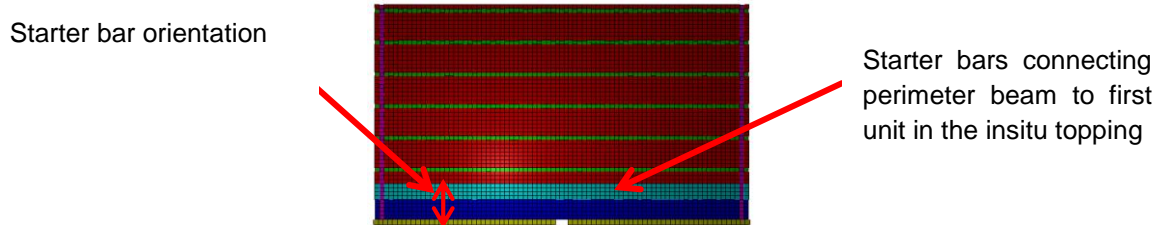


Figure 4-8: Starter bar typical model layout (arrangement 3 shown)

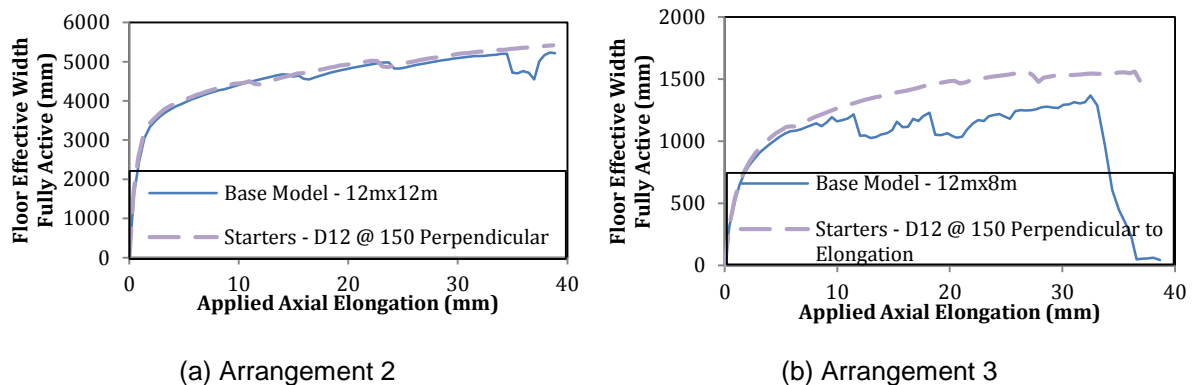


Figure 4-9: Modelled effective floor width with starter bars -Precast units oriented parallel to elongation

3. Drag bars (to tie column to floor)

The inclusion of drag bars in the topping concrete, oriented perpendicular to the elongation direction, was examined as per the typical layout shown in Figure 4-10. The drag bar detail was similar to that considered by (MacPherson 2005) in order to prevent the supporting column and floor disconnecting in response to deep beam action compression struts (discussed above). As the base models did not include these drag bars, the parametric study considered the inclusion of drag bars ranging from 2-H 16 bars to 4-H 20 bars which were anchored in the beam adjacent to the elongating hinge.

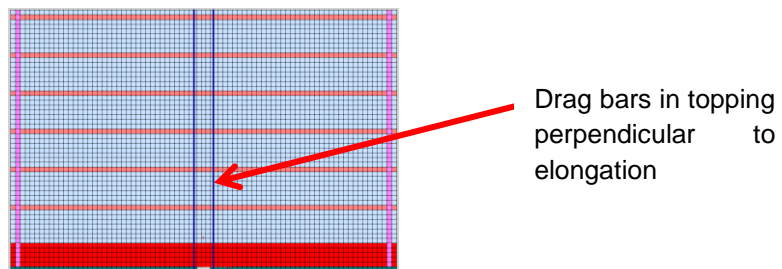


Figure 4-10: Typical floor model layout with drag bars in topping (arrangement 3 shown)

The modelled results for arrangements 2 and 3 are presented in Figure 4-11 and Figure 4-12 respectively. Analysis of the results in Figure 4-11 demonstrated that the drag bars caused only a slight

increase in the measured restraint force. The proportion of the shear transfer capacity was also slightly reduced because of the contribution of drag bars to the link slab shear capacity.

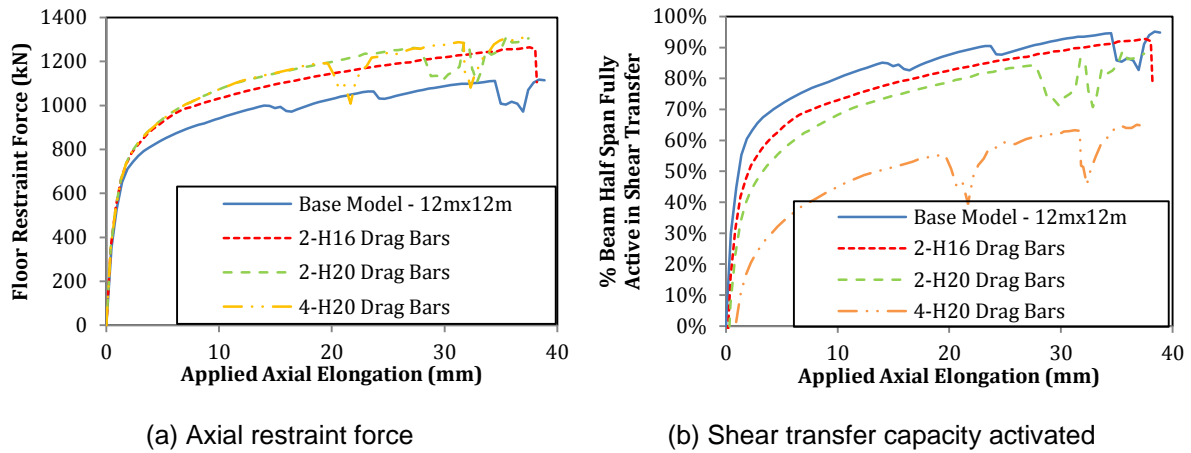


Figure 4-11: Modelled drag bar effect for arrangement 2 (precast units oriented parallel to elongating hinge supported on transverse beam)

As presented in Figure 4-12, the drag bar inclusion notably increased the measured restraint force of the floor in arrangement 3. The result was consistent with the previous findings that the shear transfer capacity tended to govern the behaviour of floor systems which included precast floor units spanning parallel past an elongating hinge. As the drag bars prevented disconnection of the perimeter beam from the floor, they increased the shear transfer capacity and the floor restraint capacity was increased accordingly. This finding suggested that where the tension capacity of the floor in the direction parallel to the hinge elongation was high (arrangement 3), a shear failure in the link slab tended to govern the floor response. However when this tension capacity was low, such as when a weakness over a transverse beam was located adjacent to the elongating hinge (arrangement 2), shear failures were not observed and the capacity of this weakness tended to govern the floor response.

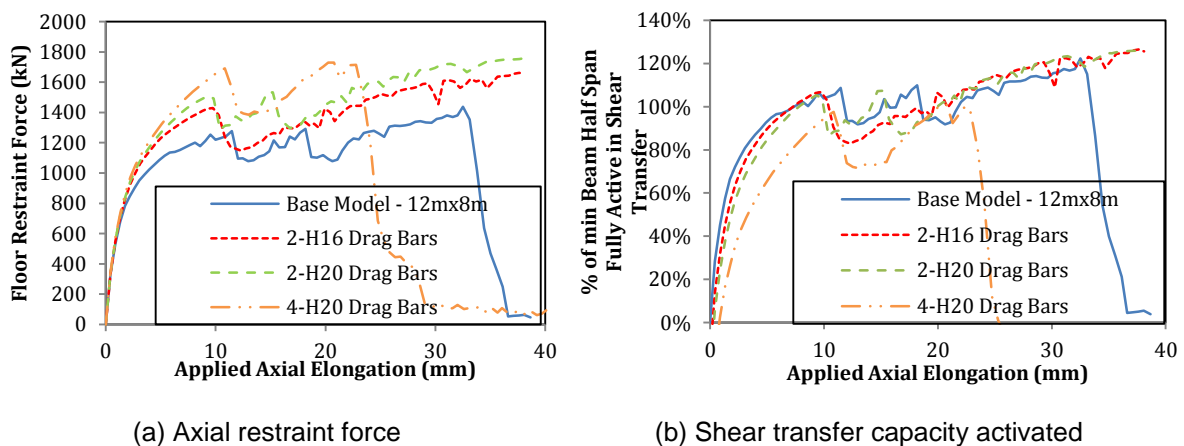


Figure 4-12: Modelled drag bar effect for arrangement 3 (precast units spanning parallel to elongation past hinge)

4. Precast unit equivalent strength

As discussed in Chapter 3, the tension capacity of precast floor units when strained by an elongating hinge was defined based upon their applied bending moment (Fenwick et al. 2006). Given this dependence on applied load, model variations were run in order to assess how the floor behaviour changes under different loading conditions. Models with either 150% or 50% of the base model floor unit tension strength were considered to simulate changes in the vertical loading applied to the floor units. The resulting axial restraint force generated for the arrangement 3 is presented in Figure 4-13 (a), with the corresponding effective floor width presented in Figure 4-13 (b). Analysis of the results showed that the axial restraint force was not dependent on the floor unit strength. Only a slight decrease in the floor restraint response was observed when the precast floor unit equivalent tension capacity was halved.

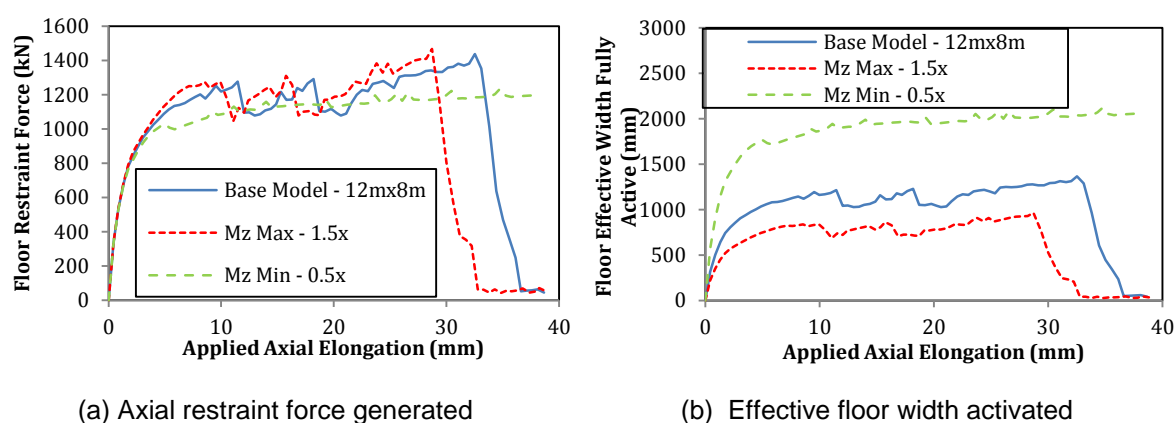


Figure 4-13: Floor unit equivalent tension strength effect for arrangement 3 (precast floor spanning parallel past elongating hinge)

A similar result to that described above was observed for arrangement 2, as shown in Figure 4-14, except that lower strength precast floor units were observed to result in a much larger effective widths, as shown in Figure 4-13 (b). This increase in effective width was observed to be inversely proportional to the strength change in the floor units because the floor response was not limited by the capacity of the units themselves, but instead by activation of a fuse. In the case of arrangement 3, which was governed by shear failure in the link slab, a reduction in the capacity of each unit simply resulted in more units being activated until the shear capacity of the link slab was exceeded. The result confirmed the previous discussion that the shear transfer capacity limited the restraint response for floor units which spanned past the elongating hinge.

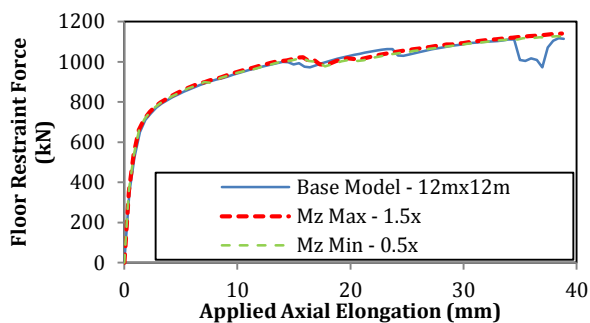


Figure 4-14: Floor unit equivalent tension strength effect for arrangement 2 (precast floor spanning parallel to elongating hinge, supported on transverse beam)

4.2.2 Parametric results specific to a floor arrangement

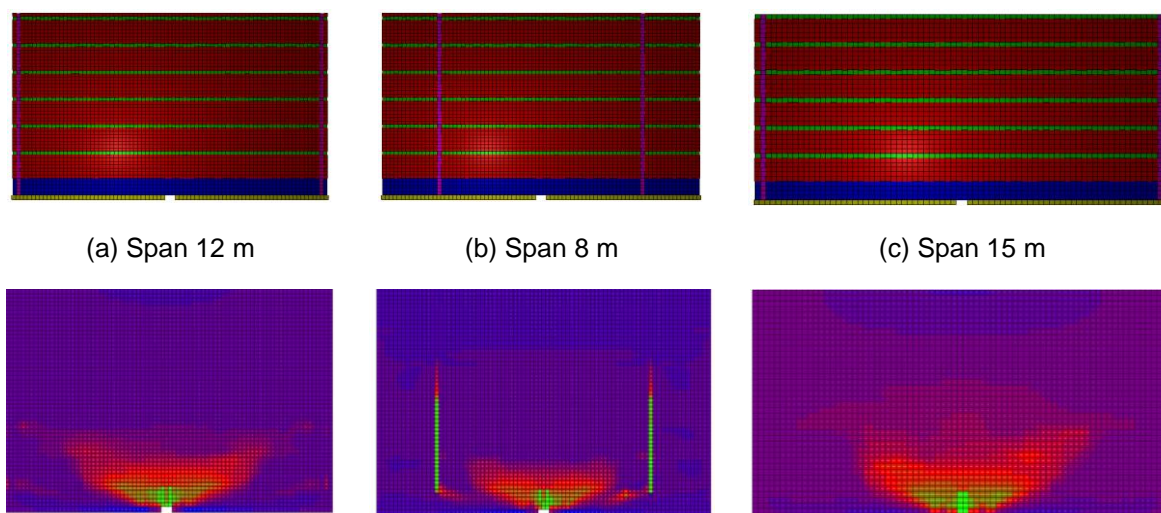
The parametric results specific to a floor arrangement are discussed in this section as a supplement to the previously discussed parametric study findings.

4.2.2.1 Arrangement 3

The findings of the parametric study relevant to floors where the precast units spanned parallel past the elongating hinge (arrangement 3) are discussed below.

5. Floor unit span

The effect of precast floor unit spans on the response of a floor system was explored by considering the range of floor spans shown in Figure 4-15. The stress field results presented in Figure 4-15 were used to indicate whether or not the transverse beam weaknesses were located close enough to the elongating hinge to activate and limit the restraint force generated.



Floor stress field parallel to elongation direction -- green = tension stress, purple = low stress

Figure 4-15: VecTor2 model of arrangement 3 (precast floor unit spanning past elongating hinge) with varied floor span

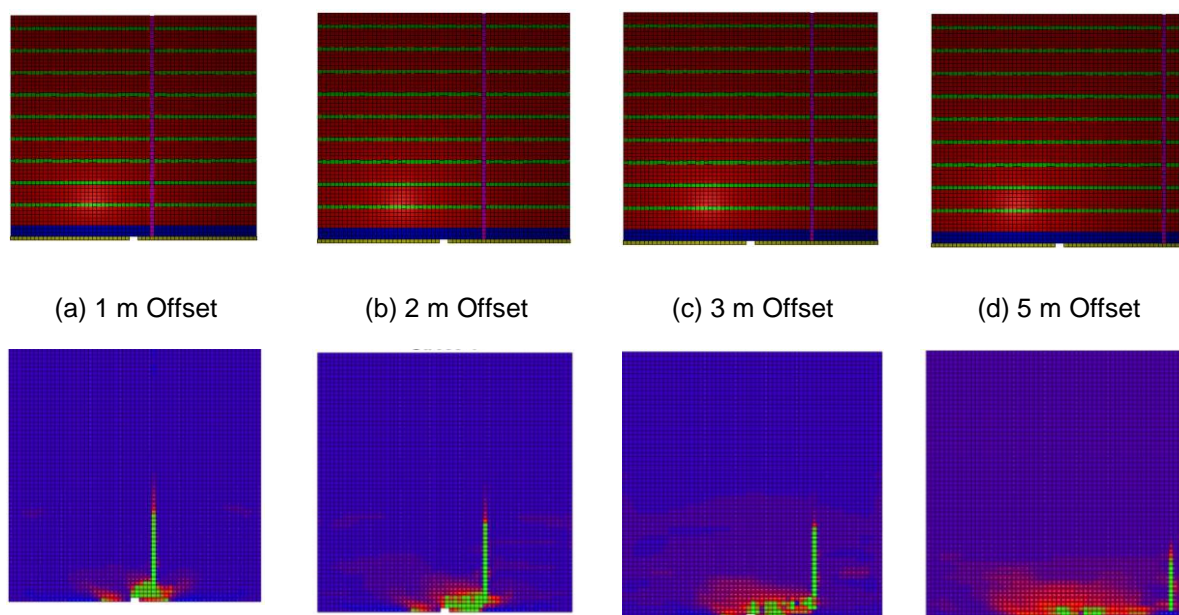
Analysis of Figure 4-15 indicated that when the floor span was reduced to 8m the areas of high stress were observed to penetrate into the transverse beam weakness. However for the remaining cases of a 12 m and 15 m span, the transverse beam weaknesses were not subjected to sufficiently high demand to activate and had no effect on the behaviour. The result indicated that even if transverse beams were not co-located with the elongating hinge, when the floor span was suitably short the weakness in this region could still activate and limit the restraint capacity of the floor system.

4.2.2.2 Arrangement 2

Parametric study findings relevant to floors where the precast units spanned parallel to the elongation, but were supported on a transverse beam (arrangement 2) are discussed below.

6. Fuse offset

Following the analysis outlined in section 4.2.2.1, the effect of offsetting a transverse beam from the applied elongation position was explored as shown in Figure 4-16. Such an offset was unlikely to occur in a moment frame as most transverse beams were supported on columns. This offset situation could arise in a coupled wall system where the transverse beam would not be supported on the elongating coupling beam, but instead by load bearing wall piers. The offset of a transverse beam weakness could influence the way in which beam elongation deformations were transferred into a floor system.



Stress field parallel to elongation – green = tension stress, purple = low stress

Figure 4-16: VecTor2 model output of arrangement 2 (precast floor units spanning parallel to elongation supported on a transverse beam offset from hinge location)

Analysis of the stress fields shown in Figure 4-16 indicated that in all cases the transverse beam weakness tended to activate. High stress was observed to have penetrated to all transverse beam locations. Analysis of the diagrams also indicated that as the offset increased, the width over which this high stress penetrated was reduced. In particular, when a 5m offset was used, the stress field

tended to distribute much more into the floor, with a lower penetration of stress along the transverse beam. The analysis indicated that for offsets below 5 m, the transverse beam weakness became important, and for offsets larger than 5 m, the floor behaved as though the floor unit was spanning past the elongating hinge (arrangement 2). This finding was in agreement with analysis of Figure 4-15, which showed that when the floor span was 8 m (an offset of $8 \text{ m}/2 = 4 \text{ m}$), the transverse beam weakness governed. However, when the floor span was 12 m (a fuse offset of $12 \text{ m}/2 = 6 \text{ m}$), the floor behaved as though the transverse beams were not present.

7. Continuity reinforcement

Continuity reinforcement refers to the additional reinforcement placed near the ends of precast floor units to tie into supporting transverse beams. The effect of the continuity reinforcement quantity was examined by varying the reinforcement placed across the transverse beams. The base model included 2-D16 bars at the base of each unit, anchored in filled cores within the hollowcore unit as recommended by (MacPherson 2005). The effect of excluding the continuity bars, and of doubling them, was assessed with the modelled results presented in Figure 4-17.

The restraint force generated was observed to increase in proportion to the amount of continuity reinforcement placed across the transverse beam. The result was unsurprising given that the tension strength across the transverse beam was directly related to the quantity of reinforcement which spanned across it. The effective floor width activated in response to the elongating hinge was observed to be suppressed as the capacity over the transverse beam was increased. Analysis of this result indicated that with a stronger fuse, the strains were less prone to spreading into the floor system. The result implied that when the strength of a fuse was increased, the corresponding increase in the floor restraint response was not directly proportional, as a smaller effective width was observed.

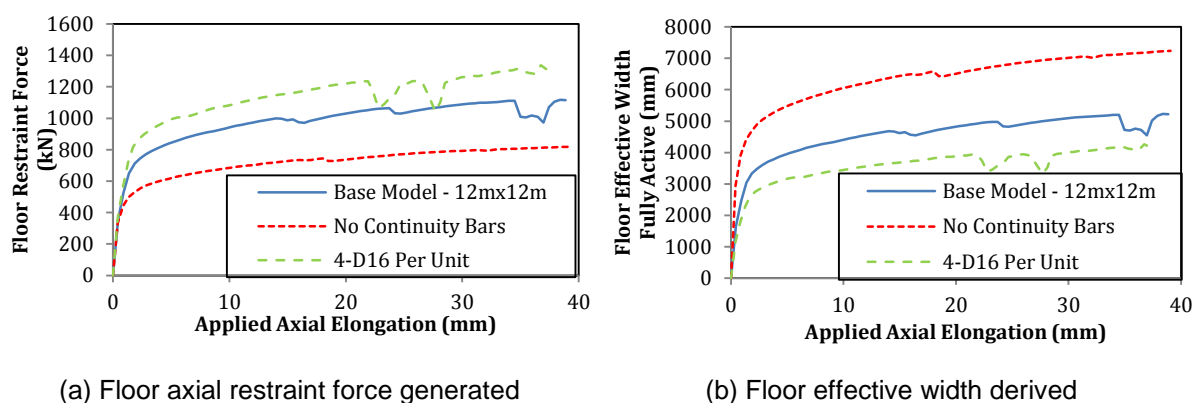


Figure 4-17: Continuity bar effect on modelled response of arrangement 2 (precast units spanning parallel to elongation, supported on a transverse beam)

4.2.3 Parametric study summary

From the parametric study on the behaviour of floors it was found that the arrangement and detailing of floor systems has a significant effect on the floor response to elongation compatibility strains. The reinforcement content and the orientation of the precast units have been observed to influence the

magnitude of restraint force generated and the effective width of floor activated by the elongation strains applied. The underlying reasons for the effects of the parametric variations are discussed further in Chapter 5 where the mechanics of floor diaphragms are discussed.

4.3 Floor diaphragm model assumptions, exclusions and limitations

As with any computational modelling idealisation, there were a number of assumptions and exclusions which were employed to simplify the analyses. These assumptions and/or exclusions are presented below with the corresponding limitations that these assumptions and exclusions placed on the model results also discussed.

4.3.1 Load application

For the floor parametric study, as per the model calibration outlined in Chapter 3, elongation strains were applied to the floor diaphragm at the edge of the floor. The elongation was applied using displacement controlled, monotonic displacement of a section of beam, as presented in Figure 4-1 (a). Typical axial elongation development as a function of plastic hinge rotation is presented schematically in Figure 4-18.

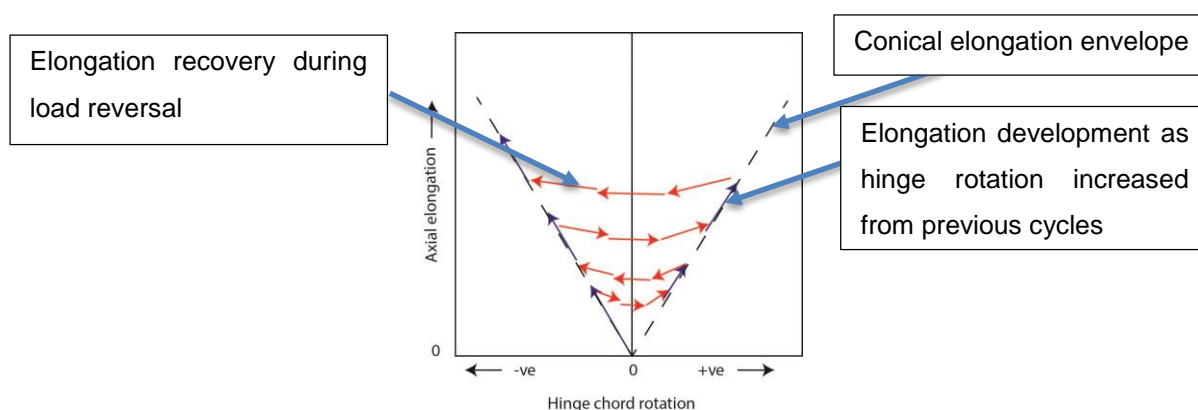


Figure 4-18: Typical plastic hinge axial elongation development

As shown in Figure 4-18, elongation tends to develop predominantly in load cycles which exceed previous maximum rotations, with only a small amount of elongation recovery during rotation reversal (Lee and Watanabe 2003). The trend presented in Figure 4-18 indicates that while beam elongation develops cyclically with applied hinge rotation, it does not fully recover as the hinge rotation is reversed. To represent this steady development of beam elongation in computational floor models, monotonically increasing displacements were applied at the edge of the floor. The effect of using monotonic displacement application in the floor models was that the floor was not subjected to compression during the small recovery of elongation presented in Figure 4-18. As the reinforcement spanning across the floor cracks has been shown in previous research to prop open the floor cracks (Wuu 1996), applying compression to the floor as a reversing load was assessed to have not had a significant effect on the floor response.

For the parametric analysis of floor diaphragms presented above, elongation was applied to the floor at a single plastic hinge only, despite recognising that in a real building multiple plastic hinges were likely to have been elongating simultaneously along the length of the perimeter beam. To account for simultaneously elongating hinges in a real building, the area of floor considered was based upon the tributary area of each hinge, as shown in Figure 4-19. The potential that the floor stress fields associated with nearby plastic hinges may have overlapped was not considered in this modelling and may have increased the effective floor widths measured in the parametric study.

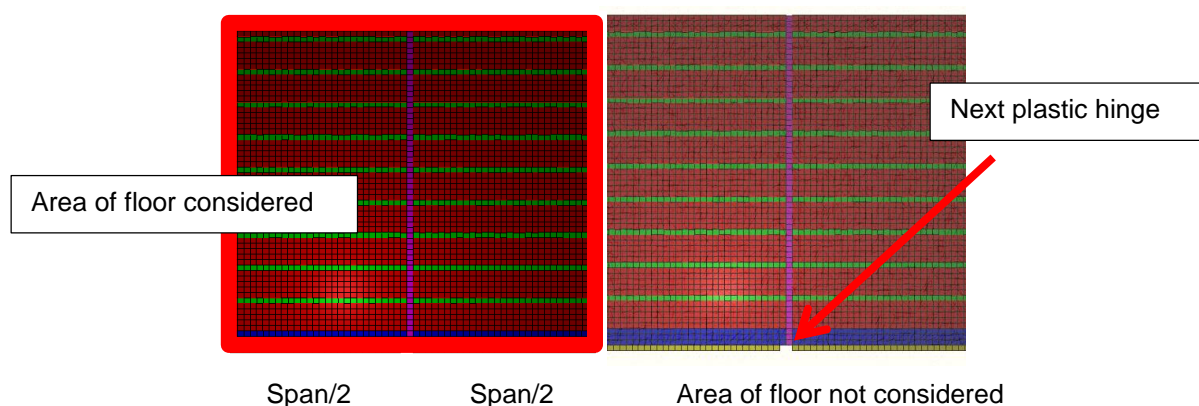


Figure 4-19: Width of floor considered in transverse beam fuse governed floors (arrangement 2)

4.3.2 Two-dimensional modelling

The primary limitation of the floor modelling technique was the application of two-dimensional software to model inherently three-dimensional problems. For this study it was deemed more appropriate to use a two-dimensional program designed for the analysis of reinforced concrete, to capture complex non-linear concrete behaviour, rather than use a less specific three-dimensional software which was not designed for reinforced concrete analysis. VecTor2 software was selected for its specificity to reinforced concrete and its ability to capture complex behaviour in reinforced concrete (VecTor Analysis Group 2011). However there were some inaccuracies in applying such a simplification, as discussed subsequently.

Variations through floor section depth

As presented in Figure 4-2, the layout of the floor through its depth is not uniform because floor units are typically designed to incorporate the majority of their reinforcement near the bottom of the units in order to support gravity loads. This reinforcement layout led to some important considerations for two-dimensional modelling in the plane of the floor. As presented in Chapter 3, the modelled response was found to accurately represent the experimentally derived floor response where precast floor units spanned parallel past an elongating hinge (as per arrangement 3 and the MacPherson (2005) floor). This result confirmed that three-dimensional effects in floor diaphragms of this arrangement were adequately accounted for in two-dimensional modelling. The case of arrangement 2, where the precast floor units were supported on transverse beams adjacent to an elongating hinge, was not as accurately

accounted for in two-dimensions. As presented in Chapter 3, the correlation of the model to experimental data was less accurate for this type of floor arrangement which suggested that the full behaviour of the floor was not captured in two-dimensions. The reason for this inaccuracy, as shown in Figure 4-2, related to the floor section changes which occurred around the edges of the precast floor units where the stiff prestressed floor units were terminated. These section changes were accounted for in VecTor2 by changing the material properties at the edge of the floor units. The use of smeared, perfectly bonded reinforcement in the models meant that development lengths were not accounted for and the full section capacity was assumed to have been developed at the interface of these section changes. Consequently at the interface of the precast floor unit and transverse beam, it was assumed in VecTor2 that the precast floor unit tension capacity was fully developed. In real floor units, the development of this tension capacity occurred towards the mid-span of the floor. Thus the real floor unit capacity was lower in the vicinity of the transverse beam than assumed in the modelling.

A consequence of the lack of modelled development length discussed above was that modelled cracks were less able to spread into the floor units because they had developed their full strength adjacent to the weak zones in the floor. Consequently the model tended to over-predict the strain concentration into these weak zones. Recent experimental observations showed that elongation induced deformation in precast floor systems tends to result in the opening of a single crack over the transverse beam (Corney et al. 2014). However the errors discussed above were deemed to have over-estimated this tendency to generate only a single crack in precast floor systems. When a transverse beam fuse was activated, the modelled response tended to concentrate the deformations at this weak interface zone and little deformation was spread outside of this zone. The demands placed upon these weak 'fuse' zones, and the effective widths measured, were therefore over-estimated. Conversely the demands placed on the floor units themselves were underestimated. The abrupt change in the floor unit capacity at the ends of the floor units was the primary limitation of the floor two-dimensional modelling and it introduced significant uncertainty into the results relating to where transverse beam fuses governed floor behaviour.

Based upon the assumptions and exclusions discussed above, the primary limitation of the models related to the strength differences between components at the edges of the floor units. The model results could therefore be used with confidence when the ends of floor units had no effect on the behaviour (ie arrangement 2 where the floor units spanned past the hinge) because the two-dimensional modelling accounted for the three-dimensional behaviour well. The accuracy of the modelling approach was supported in this case by the calibration undertaken in Chapter 3 on the MacPherson (2005) floor. In this case the correlation to the measured restraint force generated in the floor was very good. On this basis, a high level of confidence has been placed in the modelling results of floor systems which were not affected by transverse beam weaknesses. Less confidence was able to be placed in the modelled results of floors found to be governed by the activation of transverse beam weaknesses, such as arrangement 2. Where these weaknesses were critical in the behaviour of the floor, the correlation to experimental data presented in Chapter 3 (Lau et al. (2002) and Peng et al. (2008) floors) was found to have significant uncertainty. This uncertainty was found to have arisen primarily due to the inability

to model in two dimensions the gradual strength changes near the ends of the precast floor units. Additionally, the effective floor widths predicted for the cases where transverse beam weaknesses governed were significantly larger than what would have been derived based upon NZS 3101:2006. Although these effective widths were noted in the NZS 3101:2006 Commentary to have been a subject requiring further research, the lack of correlation indicated that two-dimensional modelling may have not captured all of the important behaviour. Consequently less confidence could be placed in the model results for floors whose behaviour was governed by transverse beam weaknesses, and in general the effective widths were deemed to have been over-estimated. However the limited floor size and number of experiments upon which the prescriptions of NZS 3101:2006 were based may have resulted in the effective floor width provisions being under-estimated.

It is recommended that further research be undertaken on this subject in order to better quantify the effective floor widths along transverse beams in response to elongating plastic hinges. In particular, a method of calculating the effective width based upon floor capacities rather than geometric assumptions is likely to provide more realistic effective floor widths. It would be preferable if this research is undertaken using large scale experimental testing of floor systems subject to elongation compatibility strains.

4.4 Conclusions

The parametric study of floor diaphragms has led to an improved understanding of how floor detailing affects the response of a floor to elongation strain. The important findings of the parametric study have helped to form the basis for the understanding of the mechanics of floor diaphragms subject to compatibility elongation strains, which is discussed further in Chapter 5. The primary findings of the parametric study were:

- Increased topping reinforcement increases the ability of the floor to restrain elongation, and suppresses the effective width of floor activated in restraint of an elongating hinge.
- When precast units span parallel past a hinge, and a transverse beam weakness is not activated, the restraint force is limited by the shear capacity of the link slab to prevent separation of the perimeter beam from the floor.
- If a transverse beam is located closer than 5-6m to the elongating hinge, the weakness in this region was observed to govern the behaviour. If the transverse beam weakness is located greater than 5-6m from the elongating hinge, then the floor behaves as though there were no transverse beam weaknesses.

As part of the parametric study, the accuracy of the modelling to capture general floor behaviour was found to be good for the majority of floor arrangements. Where precast units spanned parallel to an elongating hinge and were supported on a transverse beam (as per arrangement 2), the model results were concluded to be less reliable. As a result, the response of floor diaphragms governed by a transverse beam weakness was identified as a topic for future research. The results of the parametric study of floors were used to infer the underlying mechanics of floor behaviour in Chapter 5.

CHAPTER 5

5 Floor Diaphragm Mechanical Models

In Chapters 3 and 4, floor diaphragms were modelled and shown to deform in response to the axial elongation of plastic hinges in adjacent beams. This elongation was found to be partially restrained by the floor diaphragm which resulted in floor diaphragm damage and plastic hinge strength increases. The parametric study presented in Chapter 4 was used to demonstrate that this floor behaviour was dependent upon the floor layout with respect to an elongating beam. In order to improve the understanding of floor diaphragm behaviour and its effect on elongating plastic hinges, the underlying in-plane mechanics of the floor diaphragm responding to an elongating hinge was explored as presented in this chapter. This analysis was undertaken using results from the modelling presented in Chapters 3 and 4.

The research presented in this chapter focused upon the behaviour of precast prestressed floor systems, as these are the most common floor systems used in New Zealand construction. In particular, the research focused upon precast hollowcore floors that account for a large proportion of all floors in New Zealand multi-storey buildings. Analysis of the previously modelled floor diaphragms led to the development of a series of mechanical models to represent the behaviour of these floors when strained by an elongating plastic hinge. These mechanical models were used to derive expressions to estimate the effective width of floors activated when restraining elongating hinges.

The behaviour of a floor diaphragm subjected to a single elongating plastic hinge was first examined as a generalised case, before consideration was given specifically to a floor in a coupled wall system. The behaviour was extended further to floor systems where multiple hinges were elongating simultaneously, as is expected to occur in moment frame applications. Finally discussion is provided on the implications of the inferred floor diaphragm behaviour for buildings in general, and specifically for buildings with coupled wall systems.

5.1 Existing code provisions

As defined in NZS 3101:2006, an 'effective floor width' represents a nominal width over which a floor is assumed to contribute to the bending capacity of a beam (Standards New Zealand 2006). The tension force generated in an effective floor width which contributes to the beam bending capacity is balanced by a corresponding compression force in the beam. As this compression force reduces axial elongation and thus acts as a restraint force, the effective width of floor may also be thought of as the width of floor that contributes to restraining plastic hinge axial elongation. NZS 3101:2006 approximations for effective width are based upon shear lag in simply supported beams and take no account of axial restraint due to floor interaction. These shear lag effects rely on geometric relationships to approximate

the extent of floor which interacts with a beam in bending. These approximations, although not directly related to axial restraint, provide the existing means of estimating the amount of restraint force generated in a floor system because there was no accepted method of analytically defining an effective floor width. As presented below, a series of computational models of floors were analysed to assess the activation of effective floor widths in response to an elongating hinge.

5.2 Floor response to single elongating hinge

The analysis described in this section was based upon the parametric study data presented in Chapter 4, which was analysed in more detail to better understand the floor behaviour. The first and simplest case considered was the behaviour of floor diaphragms with a single plastic hinge elongating on one edge of the floor. As presented in Chapter 4, the floor diaphragm models were loaded in the horizontal plane of the floor by simulating the elongation of a plastic hinge in a perimeter beam. Each of the four floor arrangements, as defined in Chapter 4 and discussed below, were considered in the analysis of these floors:

- Precast floor units:
 - **Arrangement 1 (A1)** - Spanning perpendicular to applied elongation (Figure 4-1(c)),
 - **Arrangement 2 (A2)** - Spanning parallel to applied elongation, supported on a transverse beam (Figure 4-1 (d)),
 - **Arrangement 3 (A3)** - Spanning parallel to applied elongation, spanning past elongating hinge (Figure 4-1 (a) and (b)).
- **Arrangement 4 (A4)** - Cast insitu floor reinforced with mild steel (Figure 4-1 (e)).

5.2.1 Arrangement 1 - Precast floors spanning perpendicular to elongation

The behaviour of arrangement 1 was considered by more detailed analysis of the models presented in Chapter 4, with analysis outputs reproduced in Figure 5-1. As per Chapter 4, the floor diaphragm was subjected to elongation deformation at the edge of the floor. The resulting stress field parallel to elongation, shown in Figure 5-1 (b), demonstrated that the floor stress was concentrated at the weak joints between precast floor units. The deformation pattern typical of these models, presented in Figure 5-1 (d), indicated that large cracks opened up between the floor units as the elongation was applied.

As presented in Figure 5-2, the restraint force activated in the floor model was a function of floor unit span (denoted floor width in figure). When elongation was applied at one edge of a floor model with floor units spanning perpendicular to the elongation direction, the floor units were observed to separate by rotating on their supports. Consequently cracks developed in the topping along the edges of the floor units. When considering longer span floor units, these cracks tended to penetrate further into the floor which activated more of the topping bars in tension and resulted in a larger restraint force. A logical upper bound for this restraint force was to have assumed the topping reinforcement over the full floor unit span was strained to yield (as little strain hardening was observed in the models). However elongation tends to occur in the frames at each end of the floor unit span in a real building. In such buildings only the topping reinforcement (oriented in the direction parallel to applied elongation) over

half the floor unit span can contribute to the restraint of an elongating hinge based upon tributary area. Therefore in this arrangement it was found that a maximum floor effective width of half the floor unit span was appropriate, in agreement with the NZS 3101:2006 upper bound recommendation.

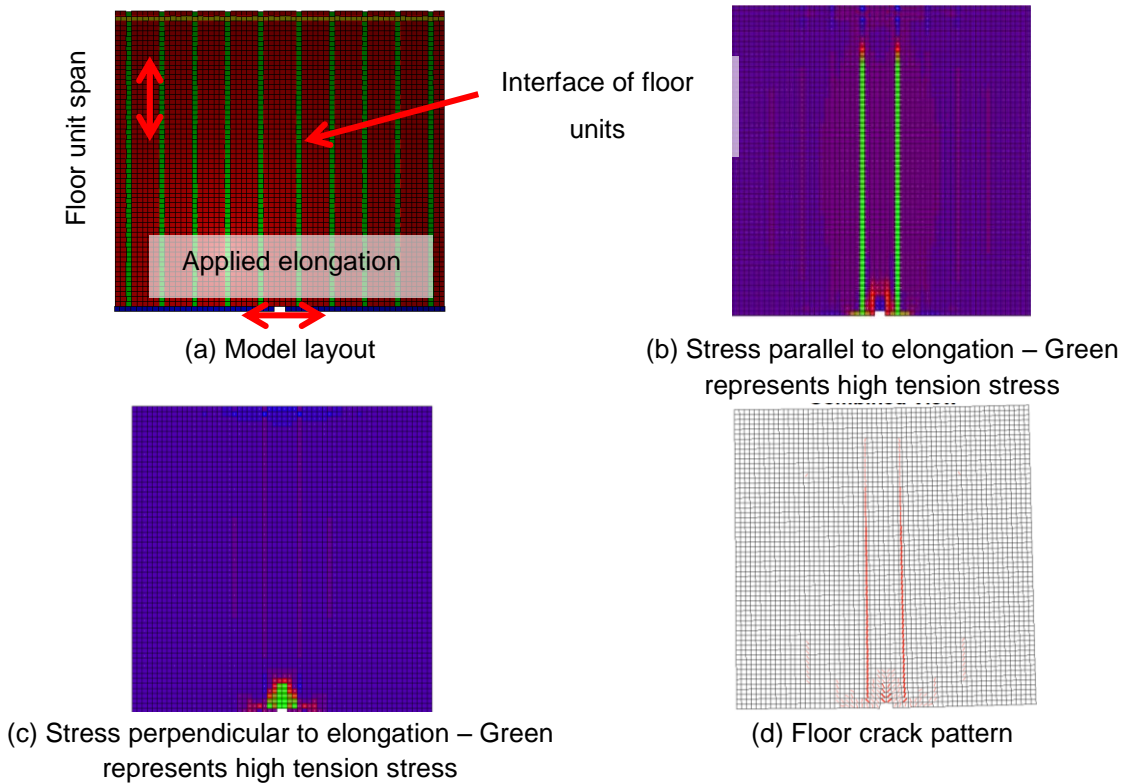


Figure 5-1: VecTor2 visual outputs at 10 mm applied elongation for arrangement 1 (Precast floor spanning perpendicular to elongation)

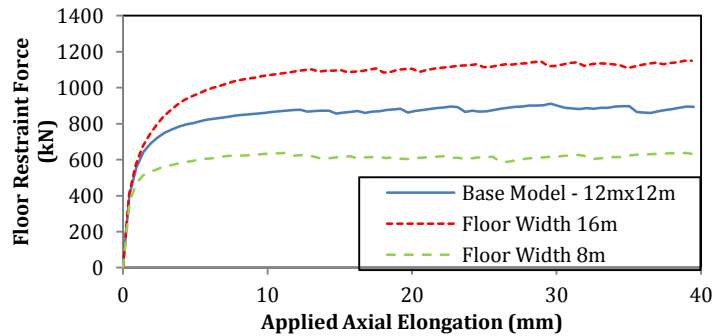


Figure 5-2: Modelled axial restraint force for units spanning perpendicular to elongation with different floor widths considered – reproduced from Chapter 4.

5.2.2 Arrangement 2- Precast floors spanning parallel to elongation – supported on transverse beam

Arrangement 2 with precast floor units spanning parallel to the applied elongation was considered as shown in Figure 5-3. This model arrangement included a central weak zone over the transverse beam, as shown in Figure 5-3, where the precast floor units were supported. As discussed in Chapter 4, only half the floor span was considered to prevent the interaction of other plastic hinges from influencing the

behaviour on a tributary area basis. The consideration of multiple hinges elongating simultaneously is discussed in section 5.3.

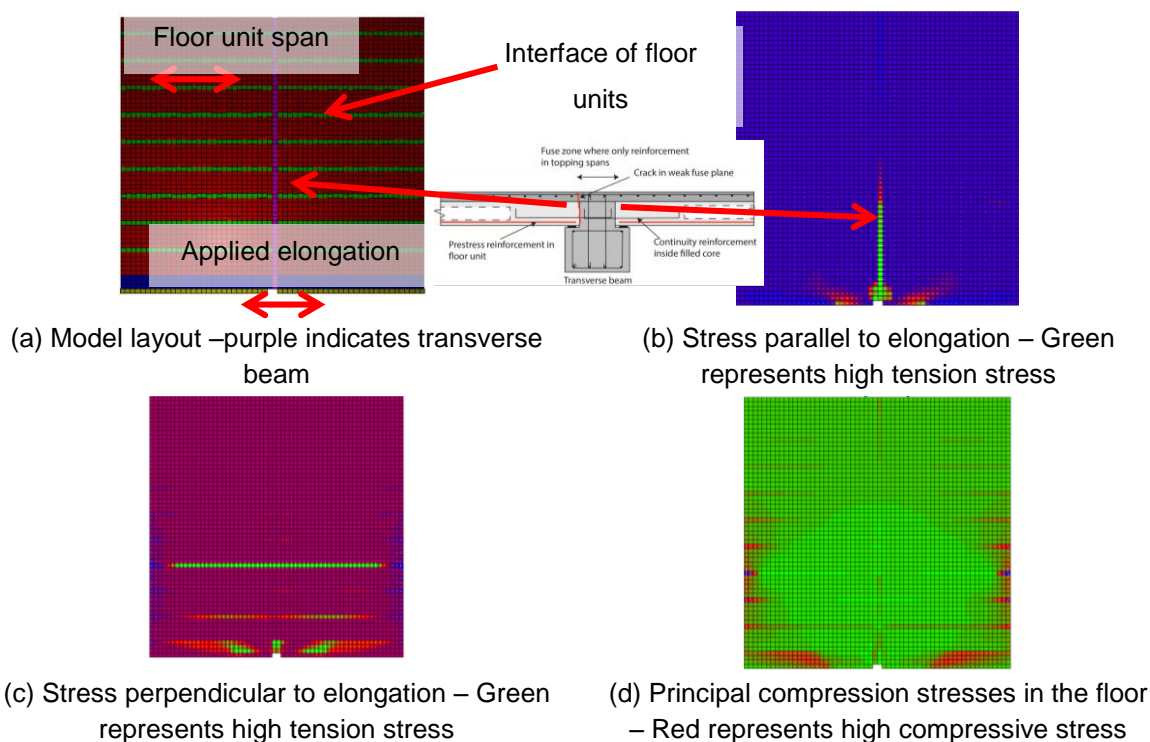


Figure 5-3: VecTor2 visual outputs at 10 mm applied elongation for a precast floor spanning parallel to elongation, supported on a transverse beam

In the model of arrangement 2, weak zones associated with the transverse beam and between floor units (parallel to the floor span) were observed to be subjected to high stress. As presented in Figure 5-3 (b) and (c), deformations and stresses were found to have concentrated into these weak zones. The principal compression stress field, presented in Figure 5-3 (d), indicated that high compression stress occurred primarily in the link slab as a shear force. The deformation pattern was in agreement with the crack patterns presented in Figure 5-4, with cracks opening up at weak zones between the floor units and at the transverse beam.

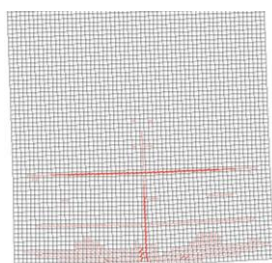


Figure 5-4: Crack pattern at 10 mm applied elongation for a precast floor spanning parallel to elongation supported on transverse beam

Presented in Figure 5-5 are the stress distributions in the reinforcement measured across the transverse beam. The transverse beam represented a weakness in the floor which acted as a fuse, to concentrate deformations away from the precast floor units. These transverse beam weaknesses tended to be

subject to high stress over larger effective widths when less continuity reinforcement was included. Additionally, a compression zone was observed in the floor at the furthest extent from the elongating hinge, as shown by the negative reinforcement stress. Similar deformation patterns were observed in the testing of frame floor systems (Fenwick et al. 2005) where a deep beam bending of the floor was inferred to have restricted the elongation of a plastic hinge at a transverse beam weakness, as shown in Figure 5-6. The bending induced in the floor system was observed to have generated a moment couple in the floor as the plastic hinge was clamped by the floor system.

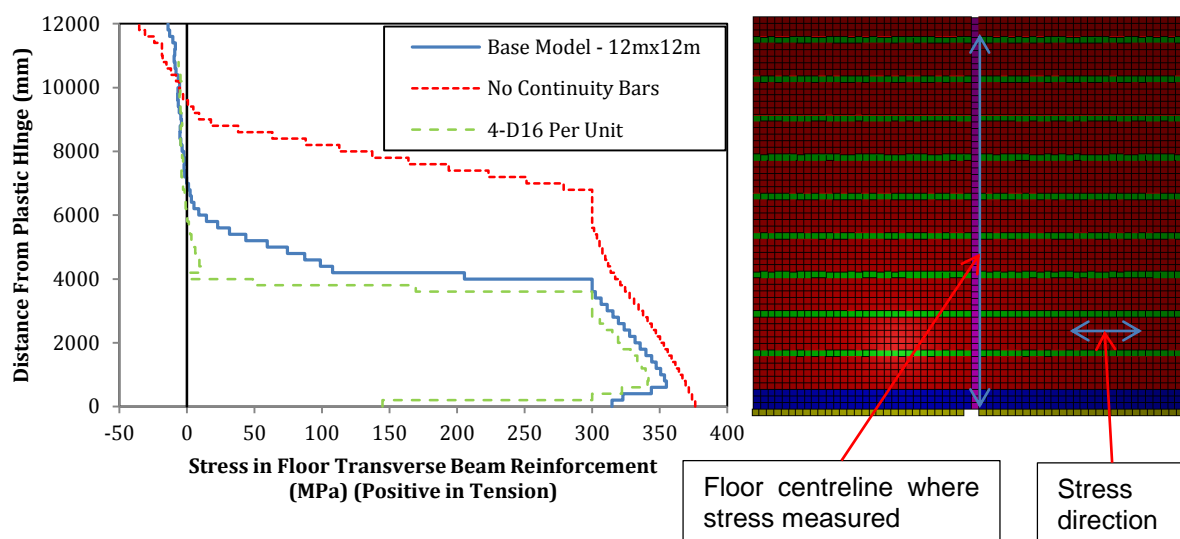


Figure 5-5: Stress in reinforcement over transverse beam fuse for a precast floor spanning parallel to elongation, supported on transverse beam

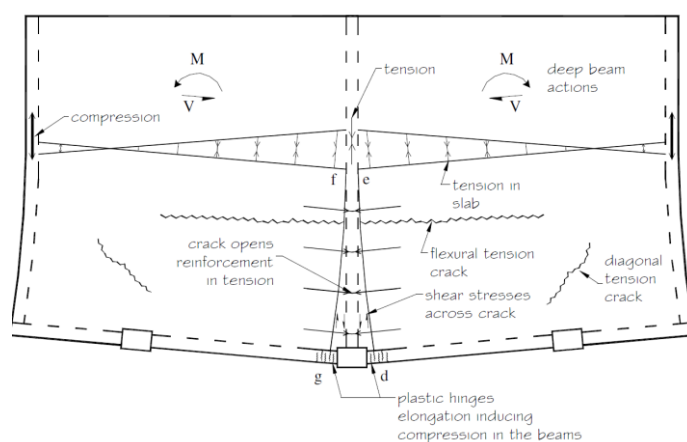


Figure 5-6: Inferred floor deep beam bending (Fenwick et al. 2005)

The deep beam action observed in previous floor testing was used as the basis for development of a mechanical model for floor diaphragms with transverse beam weaknesses (arrangement 2). Based upon deep beam bending, a cantilever beam analogy was used to infer the maximum restraint force that can be generated by a floor when a transverse beam fuse is activated, as shown in Figure 5-7. A similar approach was used by (Peng et al. 2008) to characterise the behaviour of the floor system providing axial restraint.

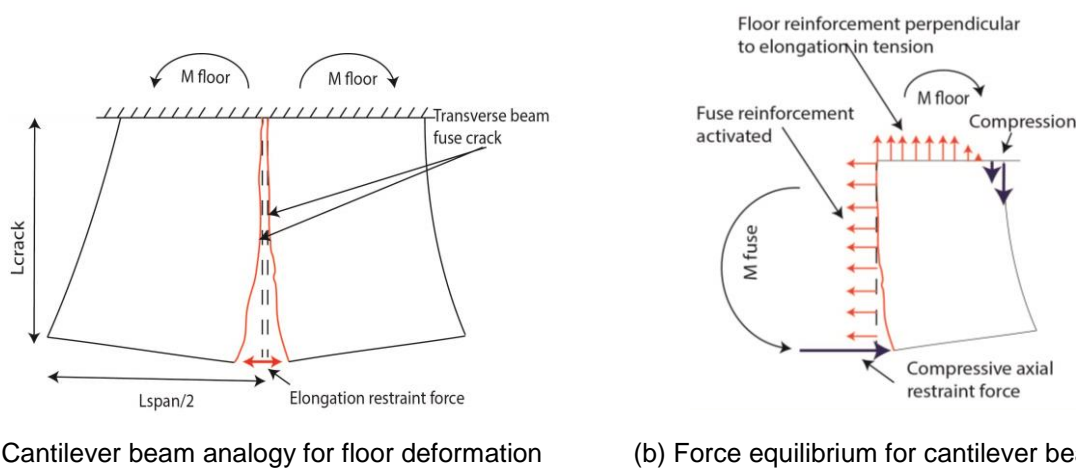


Figure 5-7: Cantilever beam analogy as limiting floor capacity when transverse beam fuse opens

Crack opening along a transverse beam was observed to have caused the floor models to bend as two cantilevers. These cantilevers were assumed to be fixed about the end of the cracks by the internal undamaged floor system. As shown in Figure 5-7 (b), crack opening induced a tension force across the transverse beam which was offset from the corresponding compression restraint force in the elongating hinge and created a moment couple. This moment couple was balanced by a corresponding moment in the floor at the end of the crack to enforce the cantilever beam analogy. The basic premise of the cantilever beam analogy is that the extent of floor reinforcement activation cannot result in a greater moment than can be resisted by the floor in bending. Therefore if the moment capacity of the floor is known, moment equilibrium can be used to determine the maximum extent of floor reinforcement that can be activated to restrain the plastic hinge, which provides an upper bound on the floor restraint capacity.

The derivation of the floor effective width in restraint of axial elongation, when a transverse beam fuse was activated, is presented below based upon the diagram shown in Figure 5-7 (b). The variables are presented in Table 5-1. For moment equilibrium:

$$M_{Floor} = M_{Fuse} \tag{5-1}$$

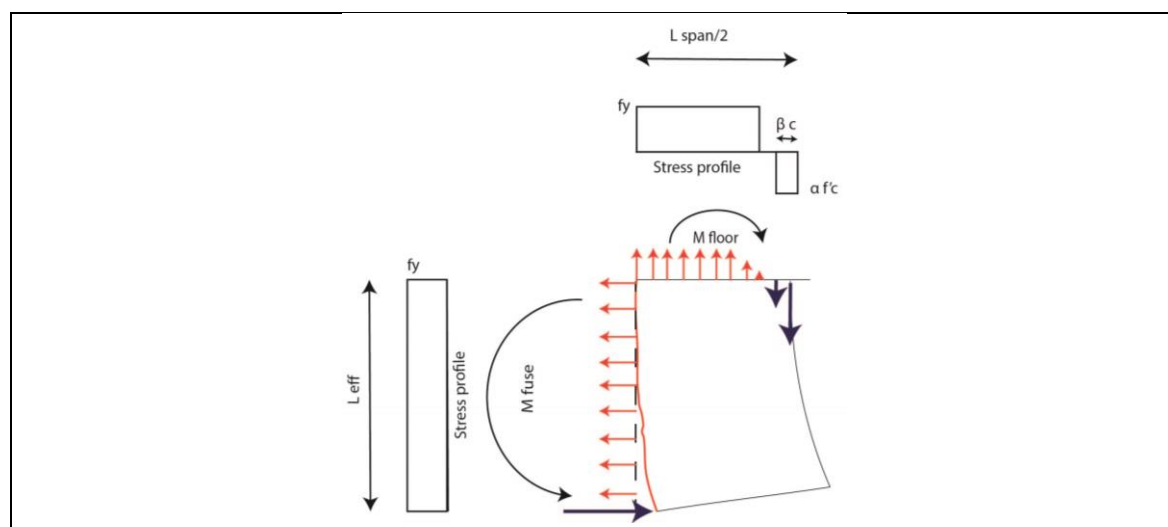
The moment capacity of the fuse is defined assuming that all the reinforcement over the cracked width is yielded, and that the centroid of the compression force occurs in the plastic hinge. Note that as little strain hardening was observed in the models, only nominal yield stress f_y was used.

$$M_{Fuse} = A_{Fuse} f_y \frac{l_{eff}^2}{2} \tag{5-2}$$

The moment capacity of the floor was also derived on the basis that the reinforcement engaged in tension is at yield. Using an equivalent compression block, equilibrium is satisfied if:

$$A_{Floor} f_y \left(\frac{L_{Span}}{2} - \beta c \right) = \alpha f'_c \beta c t_{Top} \tag{5-3}$$

Table 5-1: Variables for derivation of cantilever analogy equations



M_{Fuse}	Moment capacity of fuse (Nmm)
M_{Floor}	Moment capacity of floor (Nmm)
A_{Fuse}	Area of reinforcement across transverse beam fuse per mm length (mm^2/mm)
A_{Floor}	Area of reinforcement in floor topping perpendicular to elongation direction per mm length (mm^2/mm)
f_y	Yield capacity of topping reinforcement (MPa)
L_{eff}	Effective length of activated transverse beam fuse (mm)
$L_{span/2}$	Length of floor active in bending per hinge (mm)
f'_c	Compressive strength of concrete (MPa)
α, β	Coefficients for moment capacity of concrete (0.85)
c	Depth of neutral axis in bending plane (mm)
T_{Top}	Floor topping thickness (mm)
j	Proportion of floor $L_{span/2}$ in compression (10%)

The derived moment capacity of the floor was found to be:

$$M_{Floor} = A_{Floor} f_y \left[L_{\frac{span}{2}} - \frac{1}{2} \left(\frac{A_{Floor} f_y L_{\frac{span}{2}}}{\alpha f'_c t_{Top} + A_{Floor} f_y} \right) \right] \left[\frac{1}{2} L_{\frac{span}{2}} - \frac{1}{2} \left(\frac{A_{Floor} f_y L_{\frac{span}{2}}}{\alpha f'_c t_{Top} + A_{Floor} f_y} \right) \right] \quad (5-4)$$

Alternatively, a simple assumption to describe the length of the lever arm was made by assuming that the floor compression zone is relatively small:

$$Lever\ arm = \frac{(1-j)L_{span/2}}{2} \quad (5-5)$$

And the corresponding moment capacity is:

$$M_{Floor} = A_{Floor} f_y \frac{(1-j)^2 L_{span/2}^2}{2} \quad (5-6)$$

By equating M_{Floor} to M_{Fuse} :

$$A_{Fuse} f_y \frac{L_{eff}^2}{2} = A_{Floor} f_y \frac{(1-j)^2 L_{span}^2}{2} \quad (5-7)$$

And by rearranging Eq. 5-7, the effective floor width is expressed as:

$$L_{eff} = \sqrt{\frac{A_{Floor} (1-j)^2 L_{span}^2}{A_{Fuse}}} \quad (5-8)$$

The validity of the analogy was confirmed by comparison to three modelled floors (which were governed by transverse beam fuses with different continuity reinforcement contents) from Chapter 4. The results from both computational model and simplified analyses were based upon the section and material properties presented in Chapter 4. A comparison of the effective widths is presented in Figure 5-8, which indicated reasonable correlation between the computational models and simplified analytical equations. As the simplified analysis provided only a maximum restraint force generated, comparison was made between peak values only. In general, the effective width was under-predicted by the analysis. This under-estimate was attributed to a lack of consideration of strain hardening in the simplified analysis which reduced the effective width predicted. Only small extents of strain hardened reinforcement were observed in the modelled responses presented in Chapter 4. As a result, and to prevent the derivation being strain dependent, nominal yield was used with an understanding that at large applied elongation, the restraint force may be slightly under-estimated.

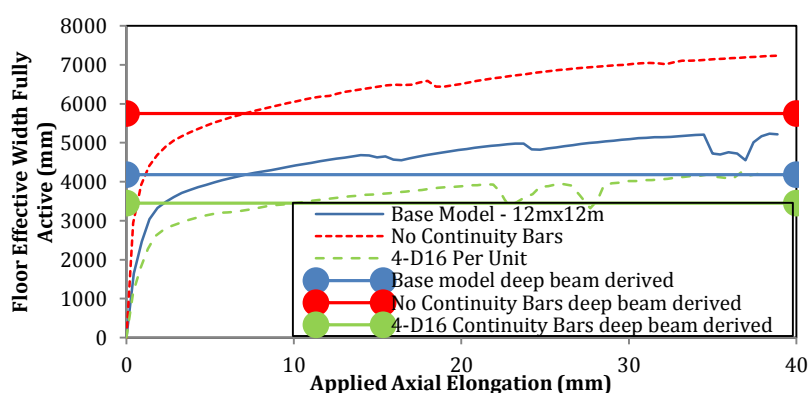


Figure 5-8: Arrangement 2 modelled effective floor width - Values derived from bending of floor plotted with solid lines dotted at ends

Comparison was also made to the experimental data used for model calibration in Chapter 3, as presented in Figure 5-9. Both the computational models and simplified analyses used material properties and section dimensions to match the experiments (see Appendix B). Analysis of Figure 5-9 indicated that in both cases the cantilever analogy and the VecTor2 results were correlated well, suggesting that the behaviour in the computational model was well captured by the simplified analysis method. However the error between analysis and experimental data was significant in both cases, where the error was in the same direction as the errors associated with the computational models (an over-prediction of the Peng et al. (2008) test and an under-prediction of the Lau et al. (2002) test).

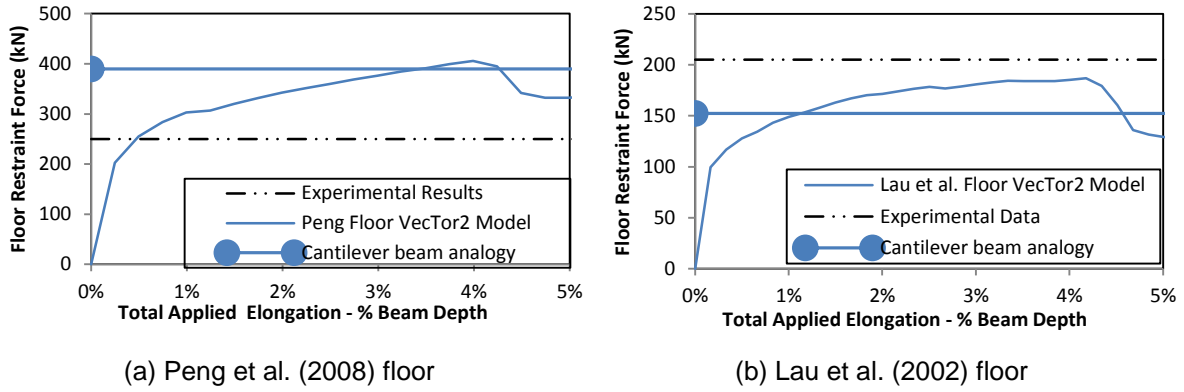


Figure 5-9: Floor restraint forces generated in experimental tests as compared to model and cantilever beam analogy

Ratios of analytical effective floor width predictions (based upon the cantilever analogy) to the model and experimental results are presented in Figure 5-10. The data points plotted are only for floors whose behavior was observed to be governed by a transverse beam fuse. In general the cantilever beam analogy tended to under-predict the effective width from the models by approximately 20%. The result was similar to the model under-prediction of 20% for the Lau et al. (2002) floor. The Peng et al. (2008) floor was a major outlier in this comparison, with the cantilever beam analogy over-predicting the effective width by 60%. The error associated with the prediction was deemed to be related to the errors which were encountered throughout the entire research project when modelling the Peng et al. (2008) floor (see Chapter 3).

A lack of consideration of material strain hardening was the reason for the general under-predictions of the analytical results as compared to the modelled results. The analytical results were not extended to include strain hardening because, as presented in section 5.3, the cantilever beam analogy was subsequently found to be invalid for realistically sized floor systems.

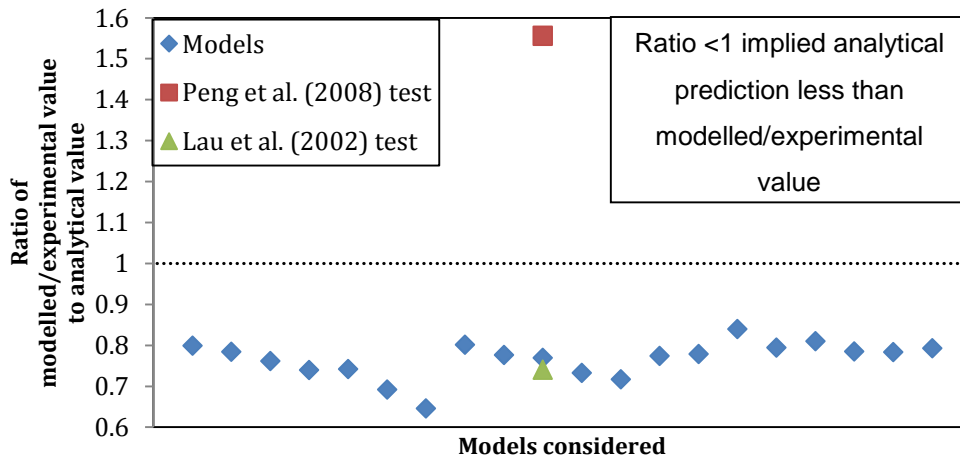


Figure 5-10: Ratio of analytically derived effective widths to modelled or experimental effective widths when transverse beam fuse governed the floor behaviour

5.2.3 Arrangement 3 - Precast floors spanning parallel past elongating hinge

Arrangement 3, where precast floor units span parallel past the elongating plastic hinge, was examined by further analysis of the models reproduced in Figure 5-11. Analysis of the floor stress field, presented in Figure 5-11 (b), indicated a well-defined effective width of high tension stress in the floor in response to the elongating hinge. The transverse beam weaknesses were not highly strained so the behaviour differed significantly from arrangement 2 due to the location of these transverse beams. Presented in Figure 5-11 (c) is the stress field perpendicular to elongation which showed that the link slab and weak interfaces between floor units were highly stressed in restraining the elongation of the perimeter frame. This high stress perpendicular to the applied elongation was confirmed by analysis of principal compression stresses, shown in Figure 5-11 (d), where compression struts in the link slab tended to push the perimeter frame and floor apart. As presented in Figure 5-12, the cracks in the link slab and weak joints between floor units also confirmed that the perimeter frame tended to be pushed outwards by compression struts in the floor. Consequently the link slab and interfaces between units were highly stressed in the direction perpendicular to the applied elongation as they resisted the separation of the perimeter frame and floor.

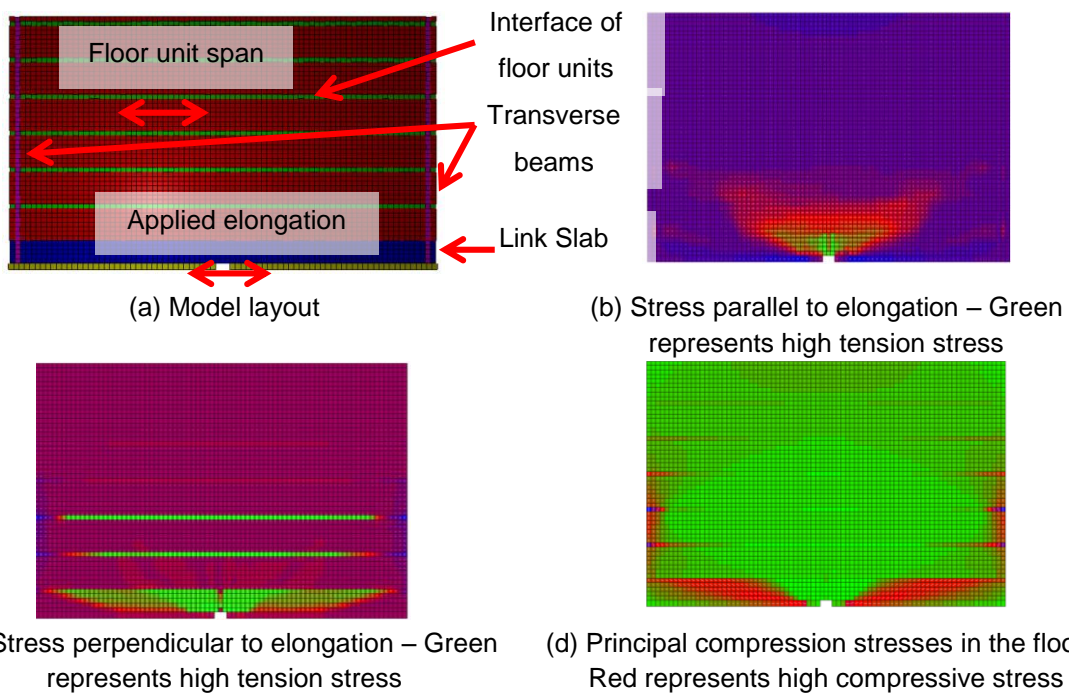


Figure 5-11: VecTor2 visual outputs at 10 mm applied elongation for arrangement 3 (Precast floor units spanning parallel past elongating hinge)

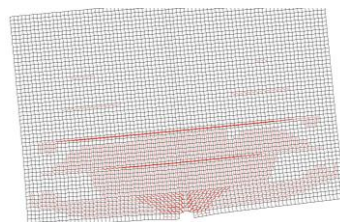


Figure 5-12: Crack pattern at 10 mm applied elongation for a precast floor spanning parallel past elongating hinge

Modelled stresses in the link slab reinforcement, orientated perpendicular to the applied elongation direction, were compared in Figure 5-13. These models included drag bars which were also oriented perpendicular to the applied elongation to tie the floor and frame together as per recommendations by MacPherson (2005). Analysis of Figure 5-13 indicates that the link slab reinforcement in the direction perpendicular to applied elongation tended to be yielded over nearly the full beam span irrespective of the drag bar content.

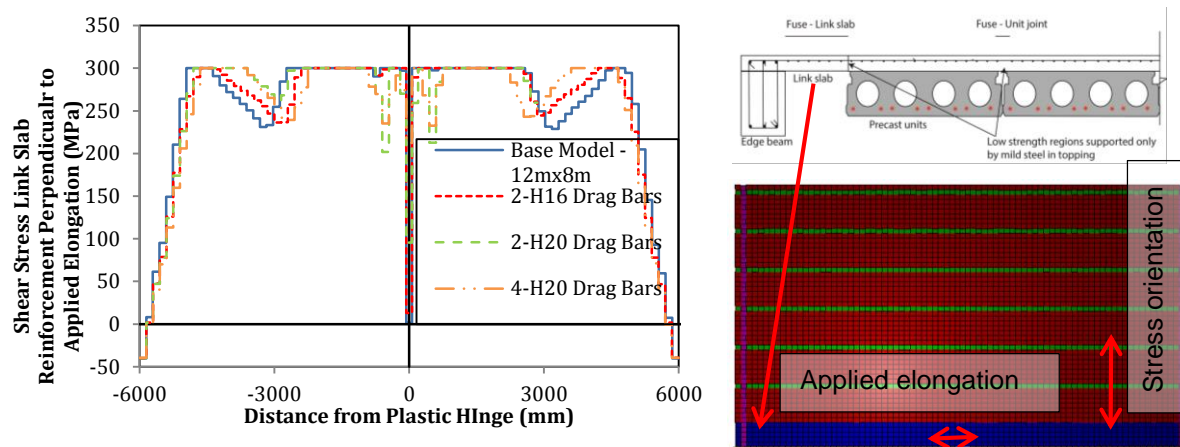


Figure 5-13: Stress in link slab reinforcement at 10 mm applied elongation for arrangement 3 (Precast floor units spanning parallel past elongating hinge)

A mechanical model was developed for floors which comprised precast floor units spanning parallel past an elongating hinge using the high floor stresses observed in the direction perpendicular to the applied elongation. This mechanical model was based upon an existing provision in NZS 3101:2006 (eq 9-17) which provided an upper bound on the effective width that could be generated in a floor diaphragm (Standards New Zealand 2006). This existing upper bound was based upon the ability of the link slab to enforce displacement compatibility between the beam and the floor by transmitting a shear force between these elements. Shear transfer through the link slab relies upon the formation of diagonal compression struts in the floor which tend to push the beam and floor apart in accordance with deep beam bending. Consequently this shear transfer capacity is limited by the ability of the link slab reinforcement (orientated perpendicular to the applied elongation) to restrain these struts and prevent separation of the beam from the floor, as shown in Figure 5-14. Therefore with this mechanical model, the magnitude of axial restraint which can be generated in a floor diaphragm is limited by the link slab reinforcement's capacity to restrain these compression struts. The failure mechanism when the maximum axial restraint force in the plastic hinge is reached is essentially a shear failure in the link slab as the floor disconnects from the perimeter frame. The onset of this shear failure is shown in Figure 5-12, where cracks in the modelled floors were beginning to open in the link slab at the peak floor restraint force generated. The opening of these cracks tended to reduce the aggregate interlock shear capacity in the link slab as the link slab began to slide in shear as the floor and beam began to disconnect.

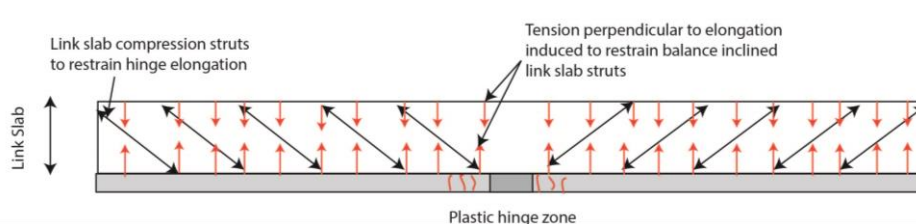


Figure 5-14: Link slab shear capacity defined by reinforcement perpendicular to elongation

The reinforcement content of the link slab was used to define the magnitude of restraint force sustained by a floor with precast units arranged to span parallel past an elongating plastic hinge. The resultant outwards force generated by the floor diagonal compression struts is balanced by the link slab reinforcement (in the direction perpendicular to applied elongation). As per the existing NZS 3101:2006 upper bound provision, the derived model equation which limited the floor restraint capacity is:

$$Floor\ Restraint\ Force = \frac{A_{TP}f_y + A_{Drag}f_y}{\tan \theta} \quad (5-9)$$

Where A_{Drag} = area of drag bars orientated perpendicular to applied elongation direction each side of the elongating hinge. f_y = yield stress of reinforcement and θ = assumed strut angle from beam span direction (noted to be 30° or less in tests by (Lau et al. 2003; MacPherson 2005)). A_{TP} is the area of topping reinforcement orientated perpendicular to the applied elongation. Only the reinforcement within half the floor unit span of the elongating hinge is considered in A_{TP} because the reinforcement outside this range is expected to have been restraining the elongation associated with another hinge.

To confirm that the floor behavior was governed by shear in the link slab, quantitative model results (from Chapter 4) with and without drag bars are presented in Figure 5-15. Analysis of the modelled results indicated that with larger drag bar capacities, the restraint force generated in the floor system increased. Presented in Figure 5-15 (b) is the proportion of link slab shear capacity activated, as defined by the ability of the floor reinforcement (including drag bars) to restrain compression struts in the floor at an assumed angle of 30° to the horizontal. Analysis of the results indicated that despite the inclusion of different drag bar contents, the floor response was limited when the full shear capacity was reached. Maximum plastic hinge restraint force was measured at the onset of failure in the link slab, as the link slab reinforcement yielded and cracks in the link slab opened.

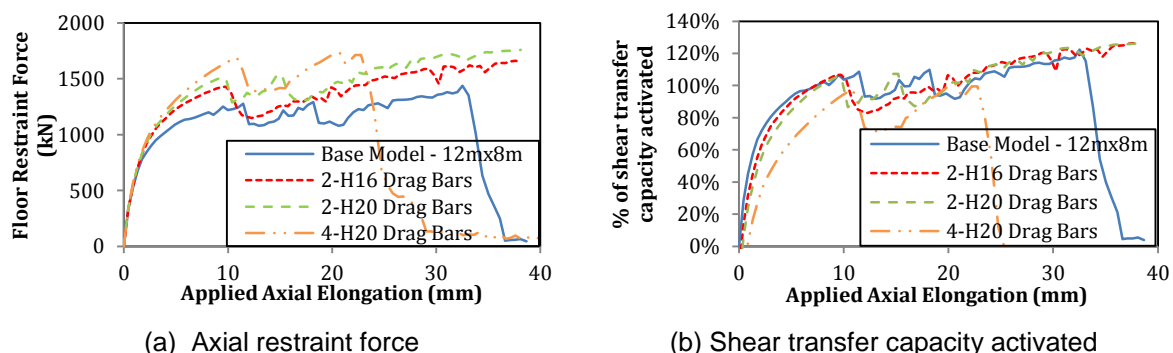


Figure 5-15: Modelled outputs with and without drag bars for arrangement 3 (Precast floor spanning parallel past elongating hinge)

A comparison of the shear transfer capacities that were activated in the floor models for the scenario when the precast floor units spanned parallel past an elongating hinge is presented in Figure 5-16. In general, the modelled values were well correlated to the 100% value predicted by equation 5-9, with a general over-estimate due in part to an assumed strut angle of 30° . In general the peak axial restraint force generated in the modelled floors was well predicted by equation 5-9. The MacPherson (2005) experimental data is also presented which indicated good correlation to equation 5-9, with some small spread based upon the assumed angle of the compression strut θ . The result confirmed the applicability of the shear transfer analogy, and the general validity of the existing NZS 3101:2006 upper bound effective width for this type of floor arrangement.

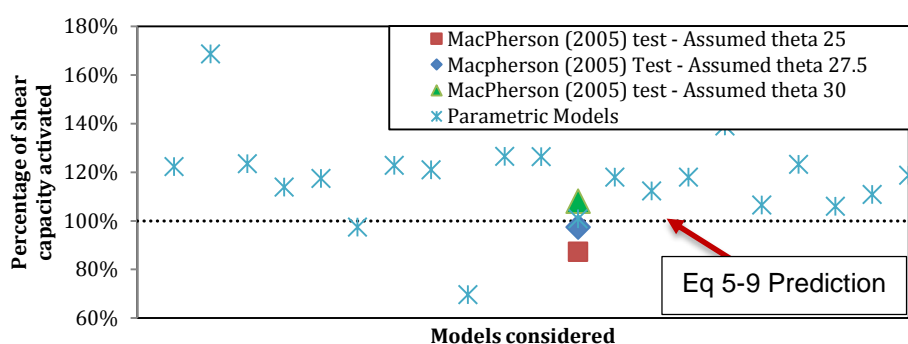


Figure 5-16: Proportion of derived shear capacity activated in models and experiments for arrangement 3 – model values assumed 30° strut angle

5.2.4 Arrangement 4 - Insitu mild steel reinforced floors

Although the focus of the research has been on the behaviour of precast floor systems, cast insitu mild steel reinforced floors have also been considered as part of the analysis. A model layout of this floor type is shown in Figure 5-17 (a). The floor stress fields parallel and perpendicular to the applied elongation which were induced by the elongation strain are shown in Figure 5-17 (b) and (c) respectively. These stress fields indicated a relatively well defined area of high stress adjacent to the elongating hinge. Presented in Figure 5-17 (d) is the principal compression stress field which shows a similar pattern to the deep beam action presented earlier, with compression zones at the edges of the floor due to the bending of the floor in its own plane.

To explain the behaviour of cast insitu floors responding to an elongating plastic hinge, the cantilever beam analogy outlined in section 5.2.2 for precast floor units supported on transverse beam fuses was compared to the insitu floor model results. Comparison between the modelled restraint forces and the values derived from the cantilever beam analogy is presented in Figure 5-18. The correlation presented can be seen to be reasonably good between the model and the analysis, which suggested that the restraint force in the floor was limited by the bending capacity of the floor system. Therefore the mechanical model developed in section 5.2.2 (using the cantilever beam analogy) was found to be applicable to cast insitu floors.

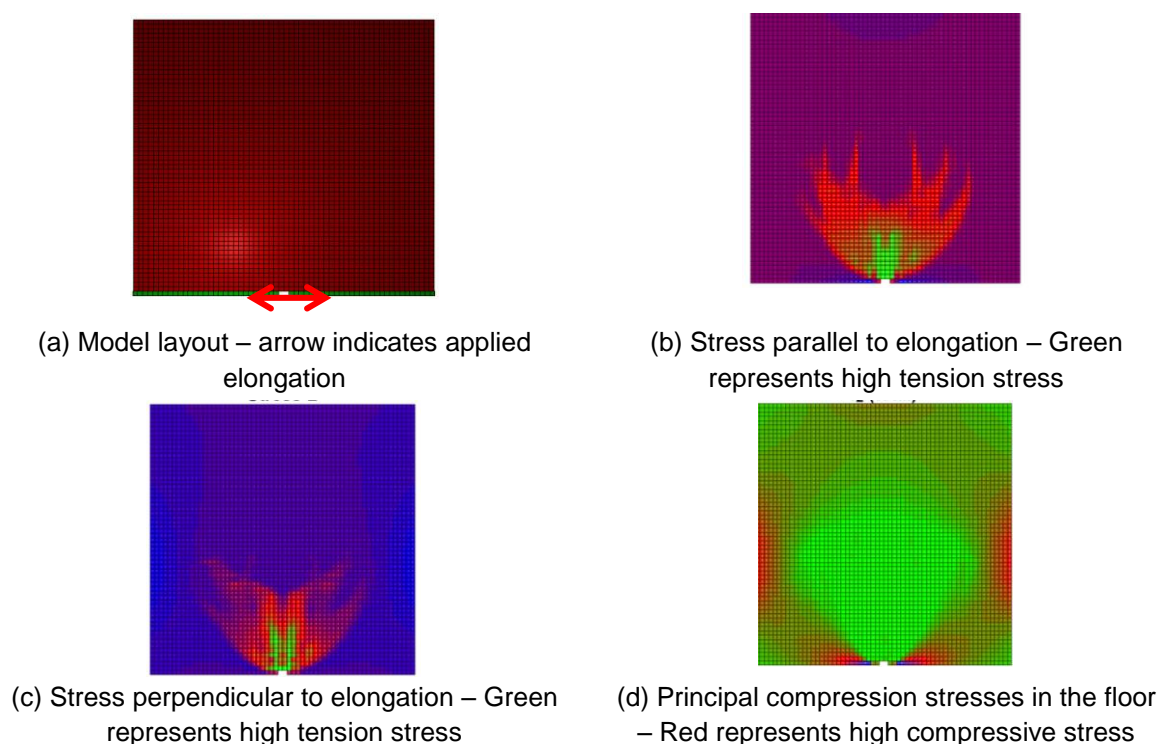


Figure 5-17: VecTor2 visual outputs at 10 mm applied elongation for an insitu floor

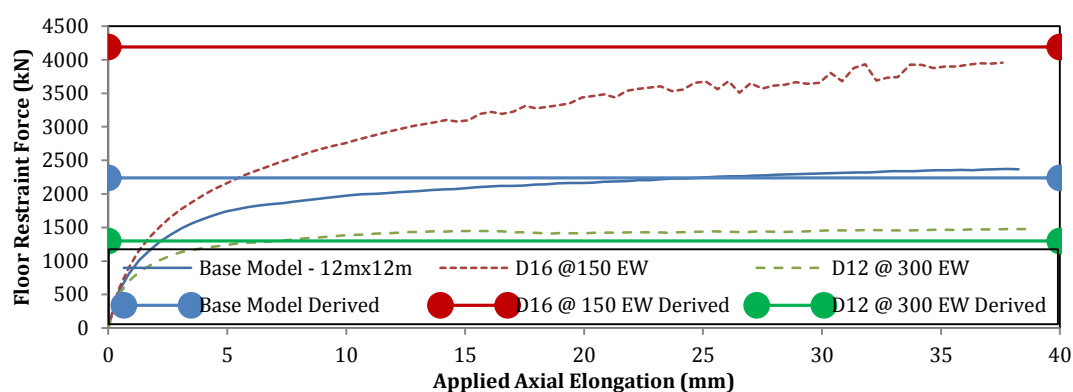


Figure 5-18: Modelled restraint capacity for arrangement 4 (Insitu floor) - Values derived from bending of floor plotted with solid lines dotted at ends

5.3 Floor response to multiple elongating hinges

The previous analyses have focused upon a small section of a floor diaphragm responding to a single plastic hinge. However in realistic buildings with either moment resisting frames or coupled wall systems, multiple plastic hinges are likely to develop simultaneously when the building is subjected to seismic actions. As presented in Figure 5-19 (b) and (c), each of the supporting frame systems is required to undergo seismically induced deformation, regardless of whether or not the frame was designed to form part of the lateral force resisting system. The deformation induced in these supporting frames would typically enforce plastic hinges to form in all of the supporting beams. An example of multiple elongating hinges affecting a floors response is shown in Figure 5-19 (a), where deformation associated with plastic hinge axial elongation occurs in the frames supporting each end of the floor units. To prevent an overlap of stress fields associated with different hinges in the case of Figure 5-19

(a), half the beam spacing represented a logical upper bound to the effective floor width activated in axial restraint of each of the hinges shown. Such an upper bound on the effective width is included in NZS 3101:2006, scaled in proportion to the relative depth of the two elongating beams. In order to account for these more realistic situations of multiple elongating plastic hinges in realistic buildings, the models considered previously were updated to include more than one hinge elongating simultaneously.

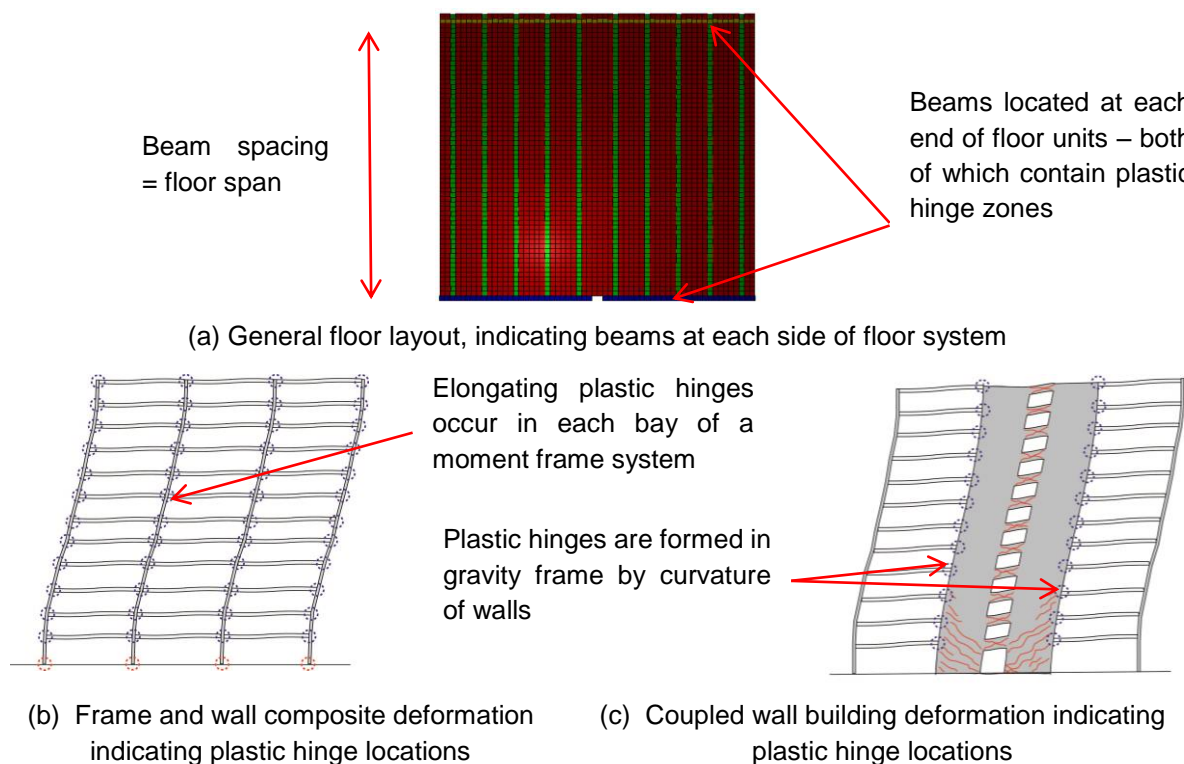
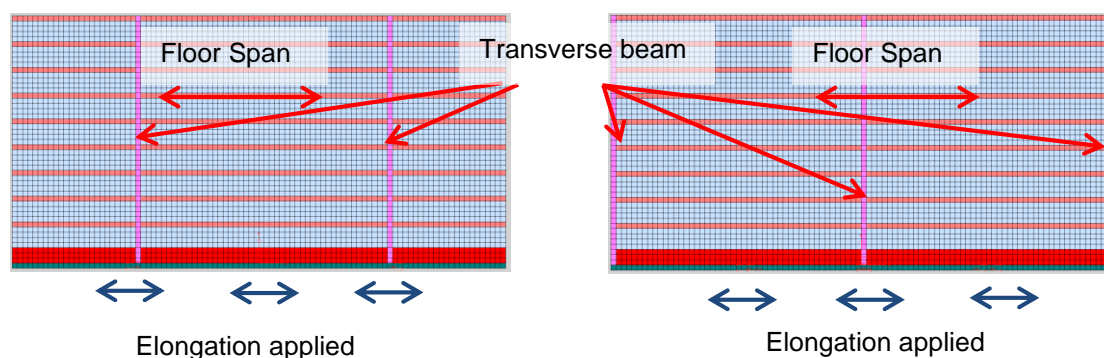


Figure 5-19: Indicative location of additional plastic hinges zones in typical building

The floor models considered were subjected to displacement controlled deformation at multiple plastic hinge zones, as presented in Figure 5-20. Experimental testing by Peng et al. (2008) indicated that the elongation of a plastic hinge was a function of the restraint force applied. To avoid an iterative modelling approach the elongation strains were applied equally to allow qualitative comparison of the deformation patterns. The floor details used matched that considered in Chapter 4, based upon a 300 hollowcore precast prestressed floor, with 75 mm insitu topping and spanning 12 m. See Chapter 4 for more information on the material or section properties of the base models.

The outputs from the modelling of floors subjected to elongation strains of multiple hinges are presented below. The results presented were generally related to the qualitative behaviour of the floor diaphragms so that comparison could be made to the previous models with only single elongating hinges. Instead of a rigorous quantitative comparison, the qualitative comparisons below were used to confirm whether the previously derived mechanical models applied to more realistic situations where floors were responding to multiple elongating hinges.

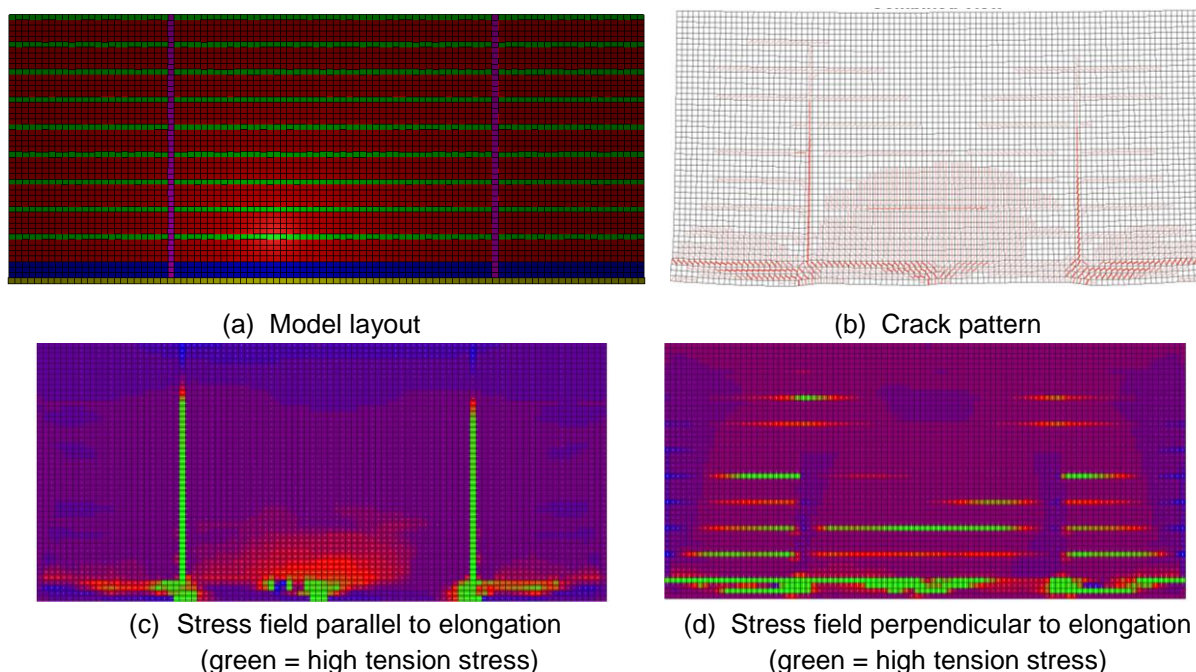


(a) Single frame bay of elongation applied

(b) Two bays of elongation applied

Figure 5-20: Floor model layouts for multiple elongating hinge application

The outputs for the modelling of a single frame bay with multiple hinges, shown in Figure 5-20 (a), are presented in Figure 5-21. As the outputs included multiple hinges, the deformation and stress patterns were less clearly defined due to the overlap of stress fields.



(a) Model layout

(b) Crack pattern

(c) Stress field parallel to elongation
(green = high tension stress)

(d) Stress field perpendicular to elongation
(green = high tension stress)

Figure 5-21: Visual outputs for multiple hinge model of single frame bay at 10 mm elongation per hinge

The salient features of these visual outputs are presented below.

- Deformation was largely concentrated into the link slab and weak zones over the transverse beams, as indicated by the crack patterns shown in Figure 5-21 (b),
- The extent of activated floor width for the central hinge (with the floor units spanning past the hinge) was equivalent to the previous isolated hinge results. The central hinge elongation activated the full shear transfer capacity of the link slab, as indicated by the high tension stress perpendicular to elongation shown in Figure 5-21 (d),
- The activated floor width for the hinges located at a transverse beam weakness, as indicated by the lines of high tension stress in Figure 5-21 (c), was much larger than for the previous isolated hinge results and extended almost the full width of the 12 m wide floor. The larger

activated floor width resulted in the restraint force also being observed to be larger than the previously modelled single hinge cases.

The visual outputs for the floor with multiple hinges across two frame bays, shown in Figure 5-20 (b), are presented in Figure 5-22. The salient features of these results were:

- Deformation was again concentrated into the link slab and the weakness over the transverse beam, as indicated by the crack patterns shown in Figure 5-22 (b),
- The activated floor width, for the hinges where precast units spanned past the elongating hinges, were equivalent to previous isolated hinges, and were again limited by the fully activated shear transfer capacity. The activation of the full shear transfer capacity was indicated by the extent of high stress perpendicular to elongation, shown in Figure 5-22 (d), and was found to be similar in magnitude to the single elongating hinge cases,
- The activated floor width, for hinges located adjacent to the central transverse beam, was again significantly larger than the measured values for isolated hinges, as denoted by the extent of high stress parallel to elongation along the transverse beam weakness. Again the effective width extended almost to the edge of the 12m wide floor. This large activated floor width gave a much larger axial restraint force than for the previously presented single elongating hinges.

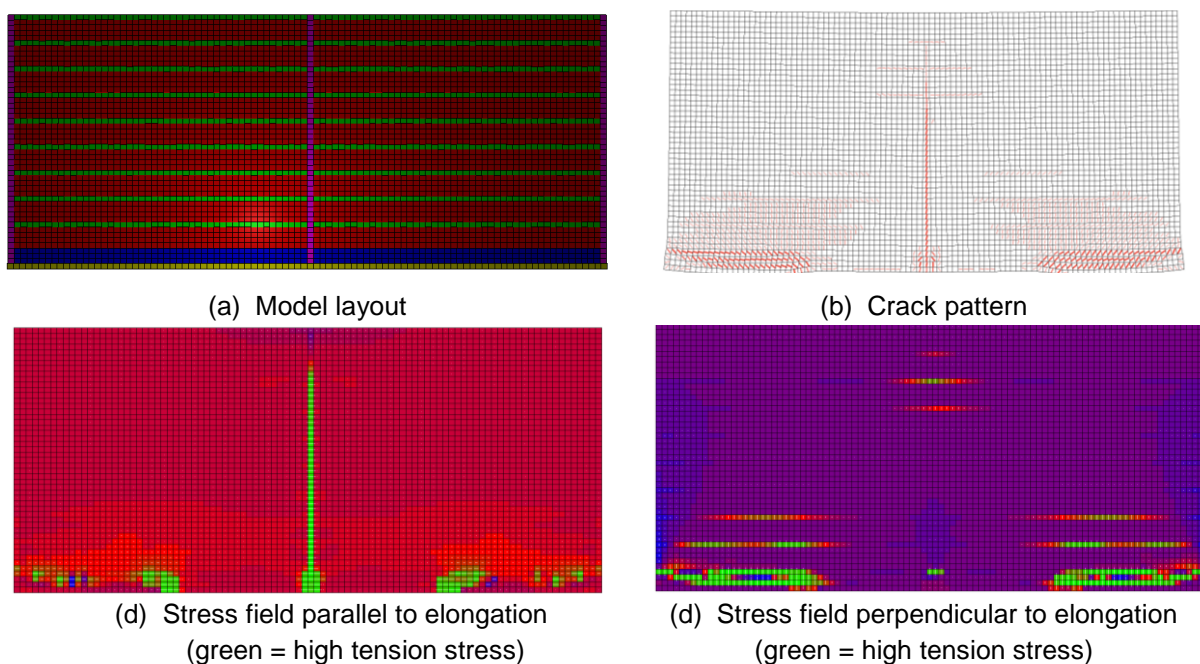


Figure 5-22: Visual output for multiple hinge model of two floor bays at 10 mm elongation per hinge

The model results presented above have led to two key conclusions regarding the behaviour of a floor system with multiple elongating hinges. Firstly the mechanism presented in section 5.2.3 has been found to be valid even when multiple hinges interact with the floor system. This mechanism was based upon the shear capacity of the link slab and was used to derive the effective widths of floors with precast floor units arranged to span parallel past an elongating hinge. Validation of this shear transfer mechanism was based upon the model results indicated that as elongation strain was applied to the floor, the topping reinforcement oriented perpendicular to elongation yielded over the full length of the

beam spans, as shown by the areas of high stress in Figure 5-21 (d) and Figure 5-22 (d). The full yield of this perpendicular reinforcement was caused by shear transfer through the link slab so full yield of this reinforcement indicated that the shear capacity of the link slab limited the restraint force applied to the plastic hinge. The extent of the fully yielded reinforcement zone was found to be equal to the tributary area of each of these hinges. This result confirmed the applicability of the upper bound limit provided in NZS 3101:2006 (eq 9-17) which is based upon the shear capacity of the link slab.

The second conclusion that was made based upon the analysis of floors with multiple elongating hinges was that the mechanism presented in section 5.2.2 was found to be invalid when multiple hinges occurred simultaneously. This invalid mechanism is referred to as the cantilever beam analogy and is based upon the effective width of floor along a transverse beam weakness being limited by the floor bending capacity. Analysis of the results presented above indicated that the effective widths along a transverse beam increased when a greater extent of floor and multiple hinges were considered. When multiple hinges were considered, the modelled and analytically predicted effective widths were found to be so large that more than 75% of the floor unit span was activated in restraint of any given hinge. This increase in effective floor width is because with a larger floor area, the strength of the floor in deep beam bending is larger and consequently the restraint applied by the floor to the plastic hinge is increased. As previously discussed, realistic floors include hinges elongating at each end of the floor units. A realistic floor system cannot activate an effective width more than half the transverse beam span for any given hinge on a tributary area basis. When considering realistically sized floor plates, this geometric tributary width requirement tends to be reached before the floor capacity in deep beam bending is exceeded. Therefore the cantilever beam analogy, presented in section 5.2.2, was found to not be valid for realistic floors subjected to multiple elongating hinges. This analogy was found to be invalid in realistic floor plans despite the reasonably good prediction of the experimental effective widths discussed above. As a result, the experimental floors discussed above may have not captured the full behaviour of a floor diaphragm due to the test specimens representing only part of a floor diaphragm.

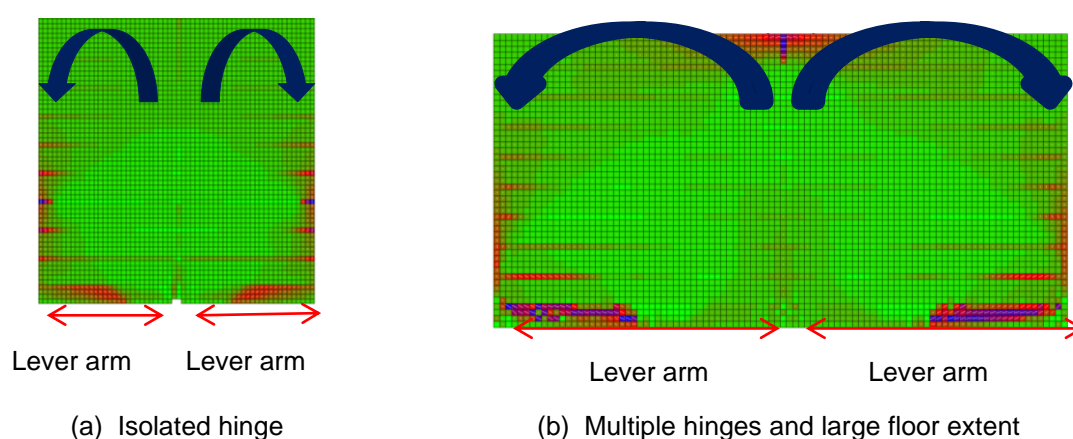


Figure 5-23: Principal compression stress fields in floor showing cantilever beam analogy moment arm

On the basis of the comparisons made above, two upper bounds were concluded to exist for the effective floor widths which can be activated in a realistic floor diaphragm due to the elongation of a plastic hinge. These upper bounds placed limits on the axial restraint that could be imposed upon a

plastic hinge due to floor diaphragm interaction. The first limit was based upon the shear transfer capacity of the link slab, as discussed in section 5.2.3 and included in NZS 3101:2006. The link slab failing in shear was confirmed to limit the force transfer between the floor and elongating hinge when the tension capacity of the floor was high and so placed an upper limit on the restraining effect of the floor diaphragm. This limiting shear failure was typically observed in floor diaphragms where the precast floor units spanned parallel past the elongating hinge (such as arrangement 3 and the MacPherson (2005) floor) because of the high tension capacity of precast floor units.

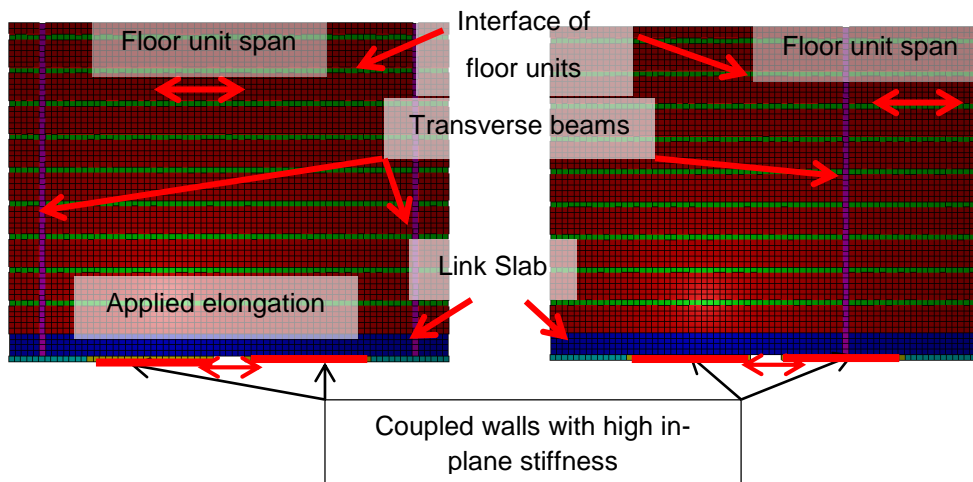
The shear transfer capacity limit in the computational models was not found to have been activated when the floor arrangement resulted in a low tension capacity. In such cases, the modelled effective widths were observed to have been large and tended to exceed the provisions of NZS 3101:2006. A low floor tension capacity was generally caused by the presence of weak zones in the floor, such as those at a transverse beam location or along the interface of precast floor units. In realistic buildings these effective widths activated for a particular hinge cannot exceed half the distance to the next elongating hinge. Therefore when the tension capacity of the floor was low, a geometric limit based on tributary widths of each hinge was found to limit the restraint provided by the floor diaphragm. This geometric effective width limit was found to be relevant to arrangements 1 and 2 which included weak zones between floor units or over transverse beam weaknesses. Both of the above upper bounds are included in NZS 3101:2006 and so the modelling presented above has confirmed that the existing effective width upper bounds are valid.

5.4 Plastic hinge(s) in coupled wall applications

Consideration was given to a specific case when elongation deformation in a floor system was induced by an elongating coupling beam. The model layouts analysed, shown in Figure 5-24, included a wall pier element with high in plane stiffness to replicate the high stiffness of the wall piers in resisting in-plane shear. The basis of this modelling was that the findings of a previous study showed that floors tended to act as large external 'stirrups' when interacting with a wall system (Mercer 2012). As the floors acted as horizontal stirrups with the walls, they restricted the in-plane deformation of the walls when subjected to shear. Modelling of layouts as per Figure 5-24 was undertaken in order to assess whether the opposite effect also occurred, where the stiffness of the wall piers reduced the deformation induced in the floor system. When coupled walls with high in-plane stiffness were considered, the potential for the walls to prevent the deformation of the link slab or activation of weak zones in the floor was important to consider. As per section 5.3, a qualitative comparison was undertaken to observe if the floor diaphragm behaviour was altered by the presence of these wall piers.

The modelled outputs, presented for the case shown in Figure 5-25 where precast floor units spanned past the elongating coupling beam indicated that the effect of the wall stiffness was negligible. Based on the crack patterns presented in Figure 5-25 (b), it was found that the link slab deformed as per the previous models and that the axial restraint force generated was unchanged by inclusion of the stiff wall piers and matched the models previously presented. The primary effect of inclusion of the stiff wall

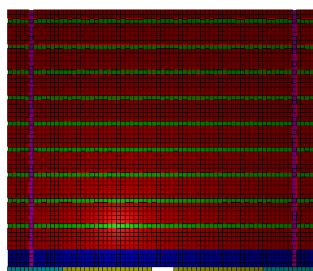
piers was to force the majority of the deformation a single mesh block further into the link slab by restraining the ability of the link slab immediately adjacent to the wall piers from deforming.



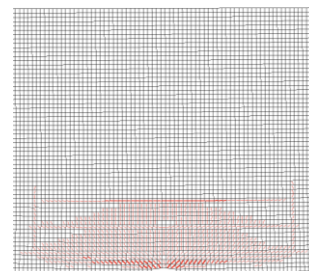
(a) Precast floor units spanning past coupled wall

(b) Precast units spanning to transverse beam on load bearing wall

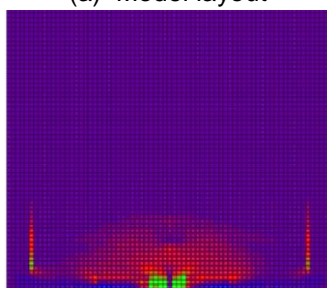
Figure 5-24: Floor model layouts specific to coupled wall with elongation occurring only in coupling beam. Colours represent different material properties.



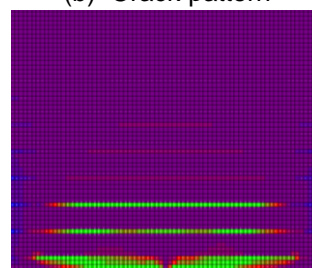
(a) Model layout



(b) Crack pattern



(c) Stress parallel to elongation.
Green = tension stress



(d) Stress perpendicular to elongation.
Green = tension stress

Figure 5-25: Visual outputs for precast units spanning past elongating coupling beam

The model results for the case where the precast floor units spanned to a transverse beam supported on a load bearing coupled wall, as shown in Figure 5-24 (b), are presented in Figure 5-26. The crack pattern, presented in Figure 5-26 (b), showed that the transverse beam fuse was heavily cracked which demonstrated that the wall stiffness did not prevent the activation of cracks along the transverse beam. Again the restraint force was found to be unchanged by the inclusion of stiff wall piers. The stress parallel and perpendicular to elongation, presented in Figure 5-26 (c) and (d) respectively, matched similar stress field plots without the inclusion of the stiff wall piers. The results for floor models including

stiff wall pier components, presented in Figure 5-25 and Figure 5-26, were used to conclude that the effect of the wall pier stiffness on preventing floor deformation from spreading was negligible.

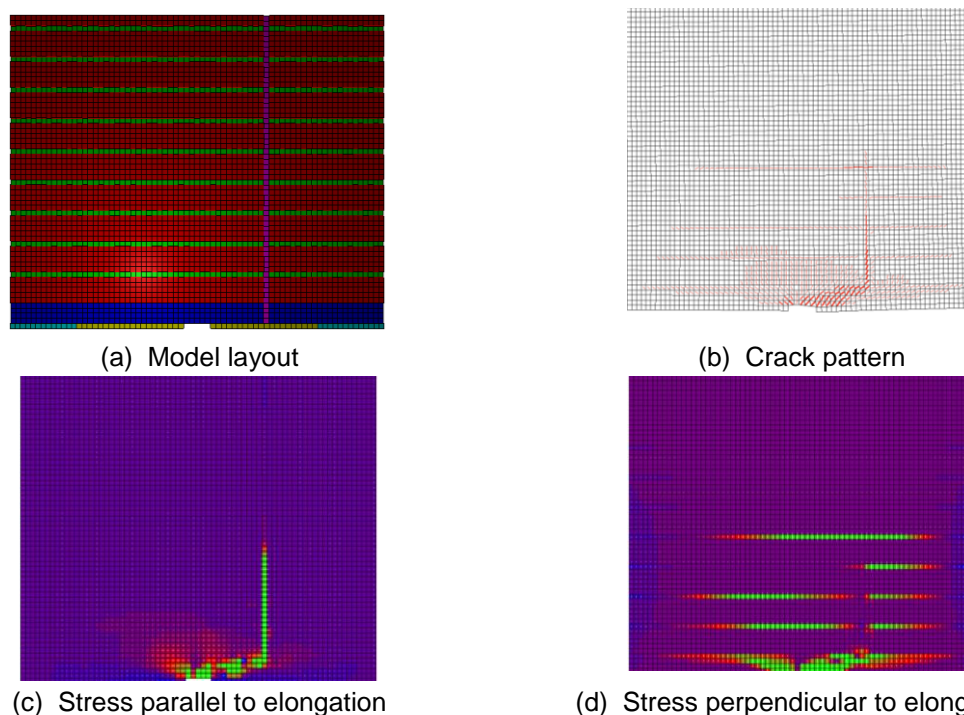


Figure 5-26: Visual outputs for precast units spanning to transverse beam supported on coupled wall with an elongating coupling beam (green represents high tension stress in stress fields)

A final floor model was run to assess the effect of elongation distribution in the coupling beams. During previous experimental tests, the primary coupling beam reinforcement has been observed to yield over the full span of the beam (Paulay 1971). To better match this realistic elongation, an option to apply the elongation as distributed over the length of the beam, as shown in Figure 5-27, was undertaken to compare to the previous models with elongation applied only at each end of the coupling beams. The modelled crack patterns which used distributed elongation indicated that the floor deformation was unchanged as compared to previous models, as presented in Figure 5-28. Therefore the elongation distribution was concluded to have had no significant effect on the behaviour of the floor systems in the model.

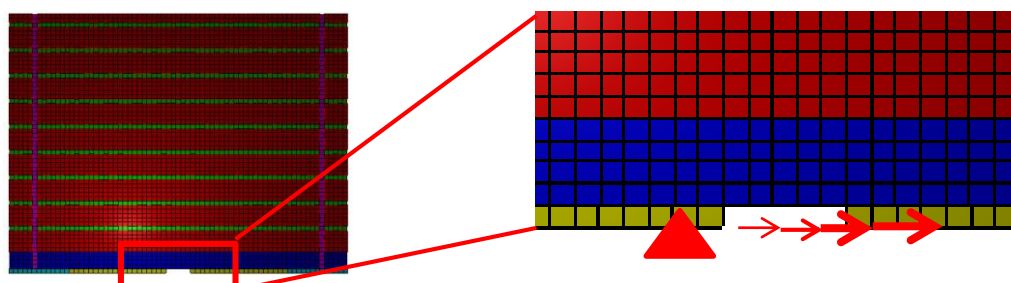


Figure 5-27: Coupling beam distributed elongation application

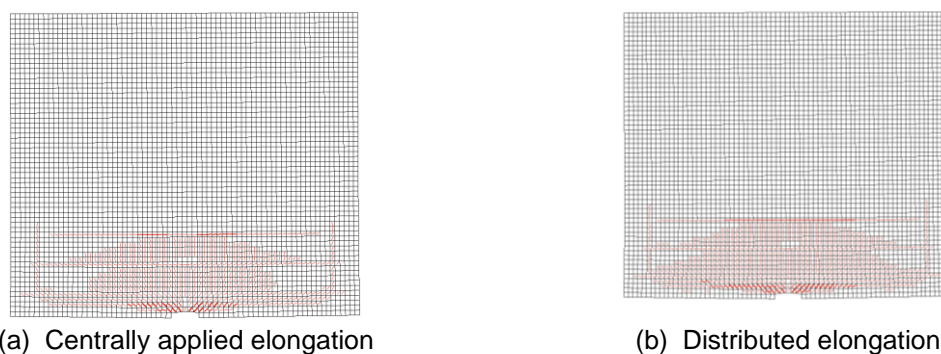


Figure 5-28: Crack patterns of floor with coupled wall elements

5.5 Discussion

The floor mechanical models outlined in this chapter have led to a greater understanding of the behaviour of floor diaphragms when subjected to axial elongation strains. As discussed in section 5.2, the analysis has primarily led to the development of mechanical models for the floor behaviour based upon the floor arrangement considered. These mechanical models have been used to infer how floor diaphragms tended to deform in response to an elongating hinge. More significantly for design, analysis of these mechanical models has led to an improved understanding of upper bound floor effective widths which could interact with an elongating plastic hinge.

Two mechanical models were developed in section 5.2 to explain the behaviour of floor diaphragms when subjected to elongation strains. The cantilever beam analogy, presented in section 5.2.2, was developed to explain the behaviour of floor diaphragms made up of precast units which included weak zones in the floor, particularly over transverse beams and at the interface of precast floor units. Floor models which included these weak zones adjacent to a plastic hinge were observed to have developed large cracks when the plastic hinge elongated and these cracked zones limited the capacity of the floor to restrain an elongating plastic hinge. Whilst the cantilever beam analogy provided good correlation to modelled floor responses, it was found to have been invalid when the floor plans of realistically sized buildings were considered. Despite the shortcomings of the cantilever beam analogy, an upper bound of the effective width in such floors was confirmed to be geometric in nature, based upon the tributary floor area for any given plastic hinge. This existing effective width upper bound provision based upon the tributary area of each plastic hinge zone is included in NZS 3101:2006. Therefore the modelling results presented above confirmed the validity of this existing upper bound. It is recommended that further research be undertaken on precast floor systems spanning parallel to the elongation direction and supported on transverse beams, to better quantify the width of floor activated in axial restraint of a plastic hinge. In particular it is recommended that larger floor extents than previously analysed be considered, with allowance for multiple frame bays in the research.

The second mechanical model developed was based upon the deep beam action observed in previous frame-floor experiments by Fenwick et al. (2005). Using the deep beam action analogy, the maximum restraint force which could be activated in a floor diaphragm was found to be limited by the shear transfer capacity of the link slab, as presented in section 5.2.3. Again such an upper bound provision addressing the extent of floor interaction with a beam plastic hinge is included in NZS 3101:2006 (eq 9-17) and this

provision was confirmed to be valid based upon the modelling results. This upper bound was found to govern where the tension capacity of precast floor units was high, as the link slab was subjected to large shear demands to ensure the integrity of the beam-floor connection. Such a situation arises where precast prestressed floor units are arranged to span parallel past an elongating hinge. In such cases, weaknesses in the floor (such as over a transverse beam) are located too far away from the hinge to activate and consequently a large axial restraint force is generated in the plastic hinge.

5.5.1 Impact of damage patterns

An implication of the concept of weak zones in the floor acting as fuses is that when a plastic hinge elongates, damage tends to be concentrated at defined regions in the floor diaphragm. This damage was observed in the models to be concentrated in the flexible link slab and at the transverse beam support. These damage patterns indicated that the precast floor units themselves were subject to low damage which allowed the floor system to retain its gravity load supporting integrity. However a detrimental effect of these damage patterns was the deterioration of diaphragm load paths, such as at the flexible link slab or at the interface between precast floor units.

Flexible link slabs were recommended to be used between precast floor units and highly deformable locations, such as frame or coupled wall plastic hinges following the work of Matthews (2005). The link slabs were intended to reduce the seismic damage transferred into less resilient floor systems from the ductile lateral force resisting system. While these link slabs were designed to be flexible, the transfer of diaphragm forces into the lateral force resisting system was still a primary requirement. The flexible link slabs were observed to have been heavily damaged in the floor models which may have led to a breakdown of the diaphragm transfer capacity through the link slab and a loss of diaphragm stiffness. Even with the inclusion of drag bars to tie the floor and perimeter beam together, shear failures in the link slab were observed in several of the floor models as elongation was simulated at the edge of the floor. Although the failure of the link slab in these floor models was manifested as a shear failure, the loss of load capacity associated with shear failures was not observed. This lack of load carrying capacity failure was because the link slab failure developed initially as yielding of the floor topping reinforcement in a ductile manner. The opening of large cracks because of this yielding eventually resulted in a loss of aggregate interlock and eventual sliding along the interface of the perimeter beam and floor system. However this sliding and degradation of the shear transfer capacity occurred only after a large elongation was applied. This ductile shear failure suggested that while the damage was significant, diaphragm transfer integrity may have been retained up to high levels of elongation because of ductility in the link slab behaviour.

Despite the ductile behaviour of the link slab as discussed above, it was likely that the capacity of the link slab was reduced in the highly damaged zone immediately adjacent to the elongating plastic hinge. In this region the floor strains are the highest as the plastic hinge transfers strain into the immediately adjacent floor slab. This damage induced immediately adjacent to the elongating hinge is difficult to prevent due to the high strains in this region and it may be preferable for designers to allow the link slab to be heavily damaged adjacent to the plastic hinge and to ensure diaphragm force transfer by the

placement of additional starter bars outside of this damaged zone to tie the floor into the perimeter beam. The diaphragm forces can then be transferred into the frame or coupled wall system through the surrounding beams. To provide more confidence in the integrity of diaphragm transfer forces between a floor and lateral force resisting system, it is recommended that more research be undertaken on the transfer capacity of the link slab when plastic hinge elongation induces large damage in the link slab.

5.5.2 Effect of floor on plastic hinge hysteretic response

As previously discussed, the elongation of a plastic hinge was observed to be resisted by the deformation of floor diaphragms. As a result, a compressive force was induced in the modelled plastic hinges which opposed the elongation of the hinges. In an earthquake this compressive force would not be applied as a constant force but instead would incrementally increase as the plastic hinge elongates due to cyclic loading. The effect of this varying axial restraint on the plastic hinge hysteretic response has been qualitatively considered in this section. There are two cases to consider which differ based upon whether or not the floor diaphragm is responding in the elastic or inelastic range. When the axial restraint is generated by the undamaged elastically responding floor, the restraint applied to the plastic hinge is simply a function of the plastic hinge elongation because a larger plastic hinge elongation induces more strain in the floor and hence a higher axial restraint force is generated. The inferred effect of such an elastic restraint response on a plastic hinge is presented qualitatively in Figure 5-29 (a). As the restraint applied to a plastic hinge in this scenario is only a function of the plastic hinge elongation, the capacity of the plastic hinge tends to increase by the same amount during each cycle of loading because the plastic hinge is subjected to the same axial restraint force.

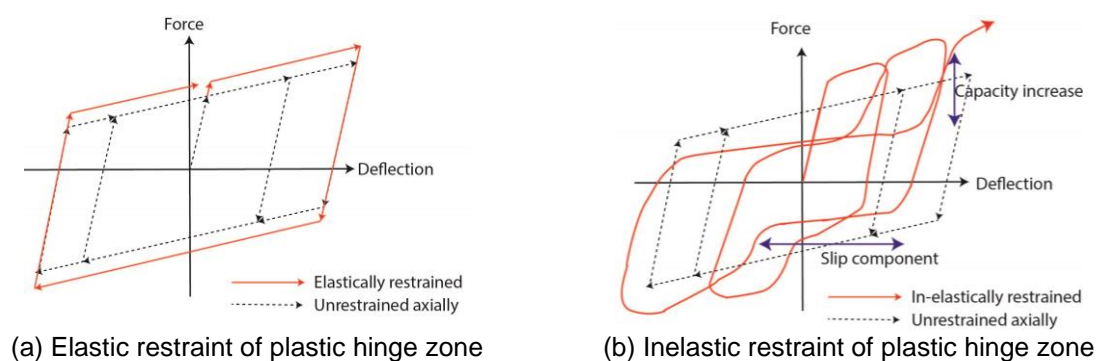


Figure 5-29: Qualitative hysteretic response of axially restrained plastic hinges

An elastic restraint force in a plastic hinge can be generated by a floor at low levels of plastic hinge elongation where the floor is uncracked. A more common case of elastic restraint is inferred to be where precast floor units span parallel past an elongating hinge, as per arrangement 3. The response in this case is inferred to be only partially elastic because the deformation in the precast floor units themselves is elastically recoverable, while the deformation in the floor topping induces inelastic cracking and yielding. The precast floor unit deformation is recoverable because as discussed in Chapter 3 based on the work by Fenwick et al. (2006), the tension capacity of a precast floor unit is derived from the vertical load applied rather than from the direct tension capacity of the floor unit. These

vertical loads induce a positive bending moment in the precast floor units and a corresponding compression at the top of the floor units. In response to the elongating plastic hinge, the tension strain induced in the precast floor units is manifested as a decompression rather than an applied tension, so the precast floor units are not subjected to cracking or reinforcement yielding and instead respond elastically. As a result, the restraint force generated in the precast floor units is recoverable and is dependent only upon the applied elongation strain, giving rise to a stable increase in the capacity of the plastic hinge.

The second case where the axial restraint is generated in the floor diaphragm due to inelastic deformation is different to that discussed above. (Wuu 1996) found that the cracks which developed in a mild steel reinforced floor due to elongation of a frame plastic hinge tended to be propped open by the floor reinforcement. During cyclic loading, this propping of cracks reduces the magnitude of axial restraint force applied to the plastic hinge. The full axial restraint capacity of the floor is not recovered until the strain applied to the floor exceeds the previous maximum values, such that the floor cracks begin to open further. The effect of this type of behaviour on the plastic hinge is shown schematically in Figure 5-29 (b). The full capacity of the plastic hinge is not developed until the applied plastic hinge rotation exceeds previous maximum values and consequently a slip component is observed where the axial restraint applied to the plastic hinge is relaxed due to floor damage. As a result, the hysteretic response of these plastic hinges is pinched. This inelastic deformation tended to occur primarily in the floor models presented above which included weak zones over the transverse beams as these zones were subjected to high levels of damage when elongation was applied. Consequently when a plastic hinge is restrained by a floor whose behaviour is governed by weak zones over a transverse beam, the hysteretic responses of these plastic hinges was inferred to have been more pinched and the resultant damping in such buildings was inferred to have been reduced.

5.6 Conclusions

The behaviour of floor diaphragms when subjected to axial elongation strains has been analysed by use of a series of parametric models of floor arrangements in an attempt to better characterise the behaviour of floor diaphragms in restraining elongation. The analysis has led to the following conclusions:

- Floor system arrangement has a significant impact on the restraint force generated by a floor diaphragm to restrain elongating plastic hinges.
- The findings of this research confirmed the accuracy of existing NZS 3101:2006 effective width upper bound recommendations on the extent of floor activated in response to a flexural plastic hinge. These effective width upper bounds place limits on the restraint force induced in an elongating plastic hinge due to interaction with an adjacent floor system:
 - Where precast floor units span perpendicular to elongation, the restraint force is limited by the topping reinforcement oriented parallel to elongation direction, within an effective width of half the floor span of the elongating hinge,

- Where precast units span parallel to elongation, and are supported on a transverse beam, the logical upper bound for the restraint force is determined by the topping and continuity reinforcement across the transverse beam, within an effective width of half the transverse beam span of the elongating hinge,
- Where precast units span parallel past the elongating hinge, the floor response was found to be governed by the shear capacity of the link slab,
- Where insitu mild steel reinforced floors are considered, the logical upper bound of axial restraint force generated is limited by the reinforcement in the floor within an effective width of half the transverse beam span of the plastic hinge.
- The uncertainty in the floor behaviour led to the recommendation that further research be undertaken for floor systems interacting with elongating plastic hinges, particularly when floor units are supported on transverse beams at the plastic hinge location. Consideration of larger extents of floor with multiple frame bays is recommended,
- The capacity of the flexible link slab to transfer diaphragm forces into and between lateral force resisting systems is also recommended to be investigated when elongation of plastic hinges has damaged the link slab,
- The hysteretic response of the plastic hinge was qualitatively identified as being dependent upon the floor arrangement considered. In particular, where the damage induced in the floor to restrain elongation is in the inelastic regime, the response of the plastic hinge tends to be pinched, with increased peak capacity only when the elongation exceeds previous maximum values.

CHAPTER 6

6 Coupling Beam and Coupled Wall Model Calibration

Unlike the flexural plastic hinges at the base of the wall piers, coupling beams are deformed predominantly in shear when a coupled wall system is loaded laterally. This large inelastic shear deformation in the coupling beams added complexity to computational modelling of coupled wall systems because inelastic shear behaviour was particularly difficult to assess. Calibration of finite element software VecTor2 was undertaken in order to ensure that the coupling beam and coupled wall computational model results were representative of realistic coupled walls, particularly related to complex shear deformation. In order to achieve suitable accuracy in the computational models, existing experimental data was used for comparison against modelled results to improve the accuracy of the finite element models.

Calibration of isolated coupling beam finite element models was first undertaken. The calibrated finite element models of coupling beams were then extended to consider full coupled wall specimens in order to verify the accuracy of overall coupled wall models. The process of coupling beam and coupled wall model calibration involved numerous iterations based upon comparisons to the available experimental data. An outline of the process is presented in this chapter, with supplemental details provided in Appendix D.

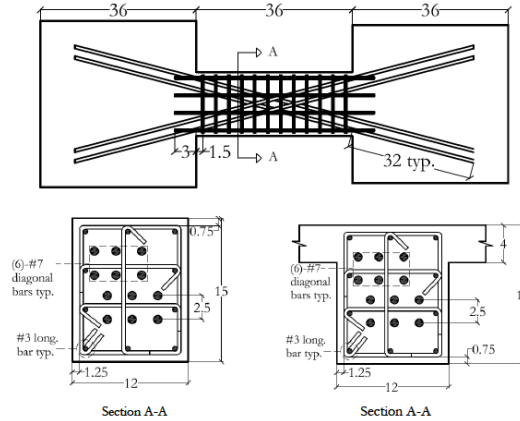
6.1 Experimental data relevant to coupling beams

Conventionally reinforced coupling beams (using horizontal reinforcement) were assessed by Paulay (1971) as being unable to attain high ductility, who instead proposed a diagonally inclined reinforcement layout. Subsequent testing by (Paulay and Binney 1974) confirmed the adequacy of this diagonal reinforcement. These early studies were eventually followed by a range of coupling beam tests around the world, as outlined in Chapter 2, which confirmed this behaviour. The most relevant of the coupling beam experiments to this study, undertaken by Naish et al. (2009), is presented below because data from this experiment was used to calibrate the finite element models presented below.

6.1.1 Testing by Naish et al. (2009)

A range of test specimens were analysed by Naish et al. (2009), with the primary objective of the research to assess the two options allowed by ACI 318-08 for transverse reinforcement of coupling beams. Transverse reinforcement options considered in ACI 318-08 include confinement around each diagonal bundle, similar to a column cage (diagonally confined), and full confinement around the entire coupling beam section (full section confinement) as set out in ACI 318-08 S 21 and subsequent revisions (ACI 318-11 2011). A full section confinement option is presented Figure 6-1. The primary advantage of including the full section confinement option was to ease constructability issues with the

traditional diagonally confined option. Specimens with aspect ratios of 2.5-3.33, relevant to modern commercial and residential tall buildings, were analysed. Half-scale coupling beam specimens were constructed, giving specimen dimensions of 12" x 15" and 12" x 18", reinforced with two bundles of 6 - No.7 diagonal bars.



(a) No floor included (b) Floor included

Figure 6-1: Full section confinement layout of specimen CB24F (Naish et al. 2009) – Dimensions in inches.

Tests by (Naish et al. 2009) went some way to address a lack of consideration of coupling beam interaction with adjacent structural components in the previously discussed experiments. This interaction was considered by including floors in several coupling beam sub-assembly experiments as shown in Figure 6-2. These specimens were tested cyclically as shown in Figure 6-3. The experimental data was accessed from the Network for Earthquake Engineering Simulation (NEES) Project Warehouse <https://nees.org/warehouse/project/1100/> as publically accessible data for the earthquake engineering research community (NEEShub 2014).

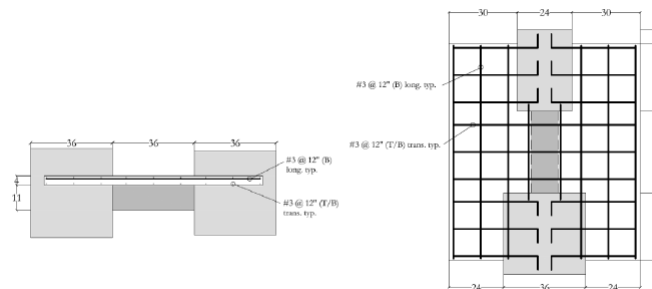


Figure 6-2: Floor slab reinforcement layout (typical) (Naish et al. 2009) – Dimensions in inches.

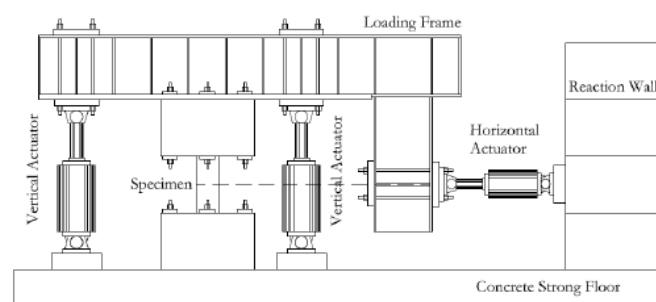


Figure 6-3: Experimental test setup (Naish et al. 2009)

Naish et al. (2009) showed that the force-deformation response of the full section confinement option (CB24F) and the diagonally confined option (CB24D) were similar, both achieving chord rotations of approximately 8% with stable hysteretic responses and only minor strength degradation. Beyond 8% chord rotation, the strength of the fully confined section specimen was observed to degrade less rapidly than the diagonally confined specimen. The full section confinement option in ACI 318-08 was concluded to provide equivalent, if not improved, performance to the traditional diagonal confinement of each bundle required in ACI 318-05.

The impact of the floor slab was found to be dependent upon the type of slab included. Specimen CB24F-RC included a mild steel reinforced concrete floor slab on each side of the beam. The inclusion of the floor slab in specimen CB24F-RC was found to increase the capacity of the specimen by 17%, corresponding to the additional shear capacity provided by the contribution of the slab to the section moment capacity. The inclusion of the mild steel reinforced floor slab was found to have no significant impact on the axial elongation of the coupling beam, with the beams elongating approximately 25mm (6.5% beam depth). Specimen CB24F-PT included a post-tensioned floor slab built integrally with the coupling beam. Similar to CB24F-RC, the inclusion of the post-tensioned floor slab increased the coupling beam shear capacity due to the increase in nominal moment capacity, provided by the slab reinforcement and the applied axial force of the post-tensioning in the floor slab. The axial elongation of CB24F-PT was found to be reduced due to the effect of the post-tensioning axial force restraining growth. The reduction in axial elongation due to the post-tensioning force was found to be in the order of 30-40% of the unrestrained coupling beam elongation.

6.2 VecTor2 coupling beam model calibration

Before the models were extended to full coupled walls in section 6.6, the ability of computational models to capture coupling beam behaviour was first verified. As per the analysis of floors presented in Chapters 3-5, VecTor2 finite element software was selected due to its ability to accurately capture in-plane behaviour of reinforced concrete. Data collected by (Naish et al. 2009) on isolated coupling beam specimens (some including floor slabs) was used to verify finite element models of coupling beam sub-assemblies. The Naish et al. (2009) data was selected for the calibration due to the high levels of detail obtained from the experiment, the range of coupling beams considered and the inclusion of floors in several of the specimens.

The approach taken to calibrate the computational models of coupling beams was undertaken in three steps. General convergence criteria were first compared by simulating a Naish et al. (2009) test specimen to a single cycle of loading. The cyclic behaviour of the specimen, in two dimensions (excluding floors), was then explored and the models updated to achieve suitable agreement with the experimental data. Finally, the three dimensional behaviour was considered due to the influence of floor slabs. As this process involved a number of iterations, a summary of the considerations and findings of the process is presented below. The calibration of the initial model inputs such as mesh size and load increment is supplemented by iterations presented in Appendix D.

6.2.1 Model setup

The first model was developed in VecTor2 to geometrically represent, as closely as practical, the detail used in the Naish et al. (2009) CB24D coupling beam specimen. This specimen was the basis for the first series of calibrations on generic parameters such as mesh density and load increment. The measured material properties from the experiment were used in the modelling. These properties included a concrete compressive strength of 6850 psi (47.22 MPa) and steel strengths of 70000 psi (482.6 MPa) and 90000 psi (620.5 MPa) for yield and ultimate respectively.

Smear reinforcement was used for the idealisation of the coupling beam transverse reinforcement. As discussed in Appendix D, smeared reinforcement was found to represent the tri-axial stirrup confinement well at low computational expense and was implemented for the confining stirrup cage. Given the criticality of the diagonal reinforcement in the overall coupling beam behaviour, it was important to gain detailed response information about the diagonal bars. It was also important to model the bond slippage components of deformation as the beam became highly damaged. To achieve a high level of detail in the diagonal reinforcement, discrete reinforcing bars were used to model the diagonal bars in the coupling beam, with an allowance for bond slippage.

6.3 Two-dimensional coupling beam global response calibration

The numerically stable model developed in Appendix D was extended to consider the cyclic inelastic behaviour of coupling beams observed by Naish et al. (2009). A series of VecTor2 simulations were run, with varying input parameters to verify the accuracy of the simulation with respect to the experimental data. The CB24D specimen from the Naish et al. (2009) tests was once again used as the basis for the calibration. A summary of the considerations and results are presented in this section, with a supplemental explanation of the iterations undertaken presented in Appendix D.

A two-dimensional numerical representation of the coupling beam specimen was input into VecTor2 software based upon the convergence criteria outlined in Appendix D, as shown in Figure 6-4. The model was based upon the conditions specified in the test and based upon the material properties measured by Naish et al. (2009). Constitutive models used for the initial analysis were the default advanced models provided by VecTor2 software. Enforcement of support constraints and displacements replicated the fixed end conditions specified in the experiments. The simulated and experimental global force-displacement responses from the initial model are presented in Figure 6-5.

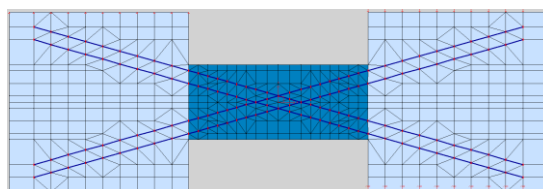


Figure 6-4: VecTor2 model of CB24D including components used in testing

As shown in Figure 6-5, the force-displacement comparison between the experiment and the initial simulation showed significant discrepancy. The features of this plot included:

1. Early bar fracture predicted in the model during beam re-loading at 6% chord rotation,
2. Over-prediction of the shear capacity of the coupling beam by approximately 25% as the beam became inelastic,
3. Computed stiffness of the simulation was significantly higher than the experimental values in both elastic and inelastic range.

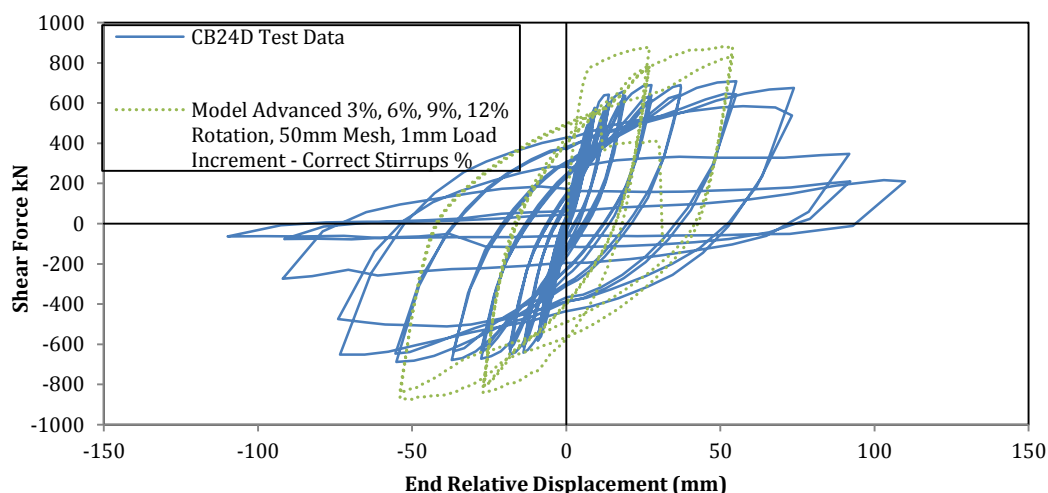


Figure 6-5: Global response of CB24D (Experimental and modelled values) (Naish et al. (2009))

As discussed in Appendix D, a series of models were run in order to improve the accuracy of the modelled response with respect to the experimental data. Based upon this study, the features mentioned above were improved as discussed below:

1. The early fracture of the diagonal bar specimens was found to be the result of mesh complications at the ends of the coupling beam. Enforcement of nodes around the member ends resulted in irregular mesh spacing and concentration of strain in the primary diagonal reinforcement. The fracture was found to be avoided if the wall piers were simulated as a single concrete type.
2. The shear capacity was found to be over-predicted because the contribution of the transverse confining stirrups to the beam shear capacity was over-estimated in the model. Perfect bond assumptions in VecTor2 resulted in the modelling output over-predicting the shear capacity

provided by the stirrups. By reducing stirrups to nominal confinement levels, the model provided a much more accurate representation of the experimental results.

3. The stiffness over-estimate was found to be the result of boundary condition enforcement. Perfectly rigid supports imposed in VecTor2 were found to result in an under-estimate of flexural deformations as compared to the experimental data, thus over-predicting the stiffness. The modelled stiffness was improved by reducing the number of support locations in VecTor2 to allow flexural deformations to occur.

The improvements outlined above were incorporated into the cyclic modelling presented in section 6.3.1 and compared to experimental data to prove their relevance.

6.3.1 Global two dimensional cyclic response

Based upon calibrations against the experimental data, the global response of CB24D was cyclically loaded using the updated models, to simulate the hysteretic response of the coupling beam. The hysteretic response of the experimental specimen and the VecTor2 model are compared in Figure 6-6. The plotted hysteretic response showed a much improved correlation to the experimental data compared to the first iteration of two-dimensional cyclic modelling. The peak capacity was predicted accurately by the updated computational model in both the positive and negative loading directions. The onset of strength degradation and eventual specimen failure was also predicted accurately by the modelling software.

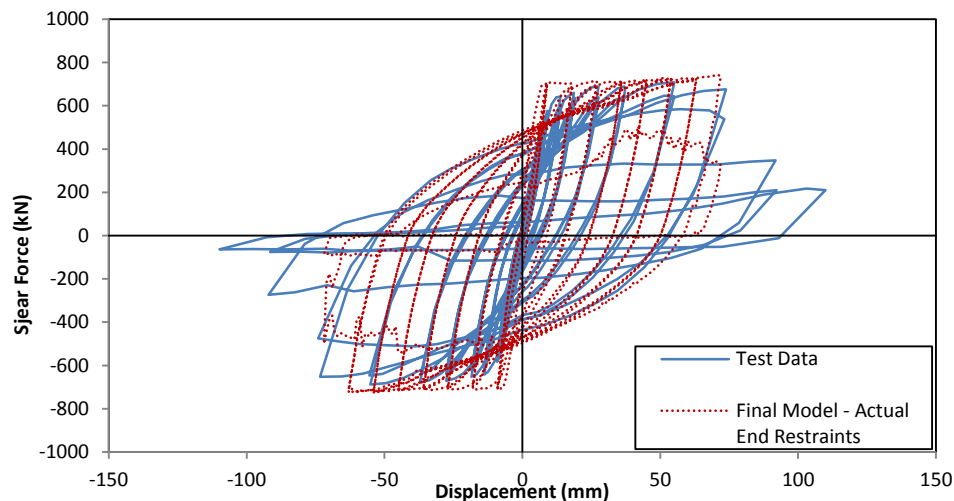


Figure 6-6: CB24D Global hysteretic response of final VecTor2 model with actual end restraints and experimental data

A key feature of the coupling beam response which was not modelled accurately was the elastic stiffness, which was observed to be over-predicted by the model. The stiffness of the specimen was over-estimated due to enforcement of unrealistically rigid boundary conditions in the modelling software. A method of avoiding this over-estimate was developed by relocating the supports, to allow flexural deformations, which were not fully considered in the model due to the perfect support rigidity. However as discussed in Appendix D, this support relocation resulted in poor elongation prediction accuracy as

the specimen became too flexible when highly damaged. Consequently the stiffness over-estimate was unable to be avoided.

The average axial elongation of the member over the full load cycles is presented in Figure 6-7 (a), showing good correlation between the experimental and modelled data when the actual end restraints were included in the model. As the member elongation tended to become unstable at the onset of strength degradation, due to the spalling of concrete, the member elongation up to the onset of strength degradation is also compared in Figure 6-7 (b). The VecTor2 model provided good agreement with experimental axial elongation at vertical displacements of less than 55mm (chord rotation 6%). Beyond 6% chord rotation, the VecTor2 model tended to under-predict member axial elongation, predicting that the elongation rate reduced and the member began to axially shorten under further loading cycles. This error was due to inherent inaccuracies in modelling of highly non-linear damaged concrete behaviour. Although the models presented herein showed good correlation to the experimental data, the models used for the VecTor2 analysis were further refined as presented in section 6.4, based upon the findings of the three dimensional behaviour.

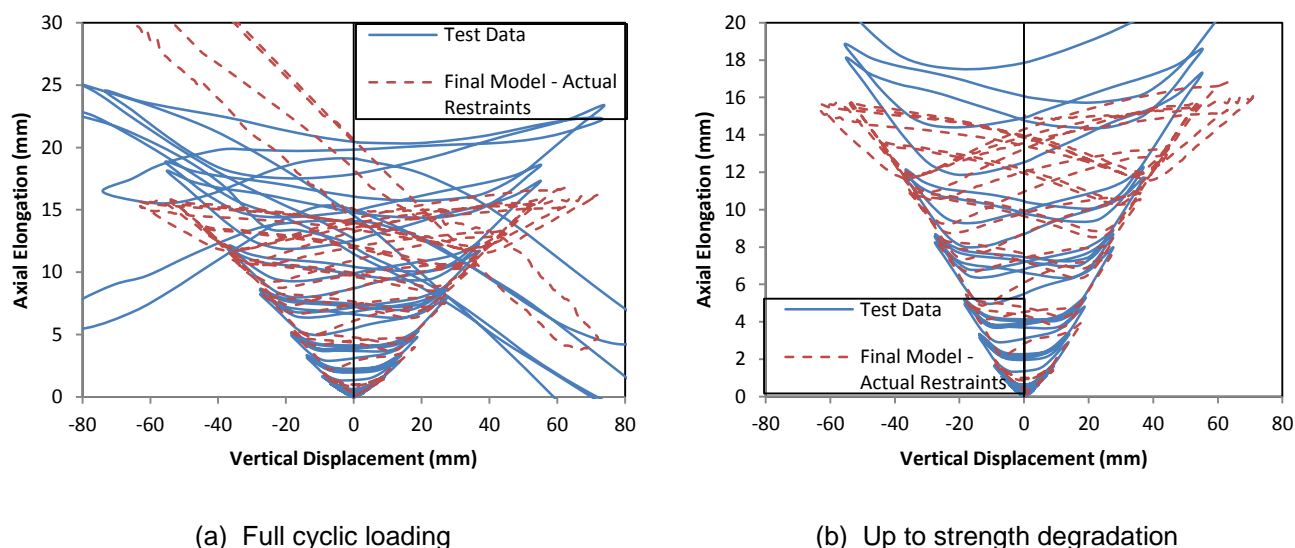


Figure 6-7: Axial elongation of CB24D specimen

6.4 Calibration of three dimensional behaviour

In order to apply two-dimensional software to realistic problems, simplifications were required to approximate three-dimensional behaviour. A further calibration process was undertaken to ensure that the simplifications necessary to use two-dimensional software provided realistic results. Experimental results of coupling beam specimens from the Naish et al. (2009) experiments were again used for this comparison. In the case of three-dimensional behaviour, the experimental specimens which included floor components were modelled in VecTor2 (CB24F-RC and CB24F-PT). An outline of the three dimensional model calibration is presented in this section. Presented in Appendix D is a supplement this process which elaborates on the iterations required to develop the selected modelling technique and confirm the model accuracy.

The primary assumption in analysing three-dimensional behaviour in two dimensions was that the behaviour in the analysis plane was constant throughout the third (depth) dimension not considered in the analysis. The approach adopted to model a three-dimensional system, such as the Naish et al. (2009) coupling beam experiments which included floor systems, was to analyse the floor in its own plane, subject to the elongation strains of the coupling beam (as per the modelling in Chapters 3-5). The response of the floor could then be incorporated into a two-dimensional coupling beam model by representing the floor as an equivalent tension tie restraining the coupling beam growth based upon the restraint force generated in the isolated floor models. In this way, the three-dimensional effects of coupling beam-floor interaction could be considered in a two-dimensional model. To confirm the validity of this approach, the Naish et al. (2009) experimental coupling beams with floors were modelled. Comparison was then made to the experimental data to ensure that the modelling approach represented these experiments well. This approach also provided a method of analysing floor-wall interaction in two dimensions, by considering the wall and floor to represent two interacting planar elements.

6.4.1 Combined coupling beam and floor modelling

Isolated models of the floor components used in the Naish et al. (2009) experiments were first run by subjecting the floors to elongation strains as per the approach used in Chapter 3. The results of this floor modelling are presented in Appendix D. Based upon the findings of these floor models, equivalent floor components were developed to represent these floors in the two-dimensional modelling of the Naish et al. (2009) coupling beams. The equivalent floor properties were idealised as a reinforcement tie which linked the ends of the coupling beam and provided axial restraint to simulate the effect of floor interaction, as shown in Figure 6-8. The strength of these tension ties was based upon the modelled restraint force generated in the isolated floor models, presented in Appendix D.

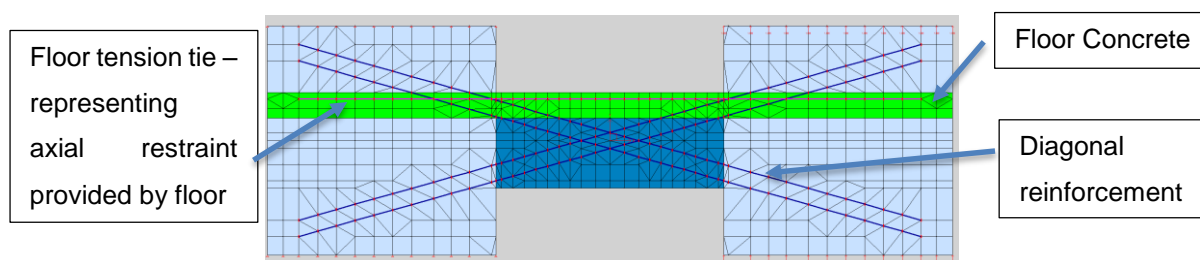


Figure 6-8: CB24F-RC and CB24F-PT indicative model elevation in VecTor2 including width of floor effective in axial restraint of the coupling beam

As per NZS 3101:2006, where the increased flexural capacity of a composite beam-floor section in bending differed based upon positive or negative bending, the effective width of the floor in flexural compression was found to be less than the corresponding tension width. NZS 3101:2006 recommends that the width of the floor effective flange when the top of the section was in flexural compression (positive bending) is related to four times the slab thickness. For the models produced as part of this research, the effective width of the floor concrete which acted in compression was based upon the

depth of the beam each side of the beam, or four times the slab thickness each side of the beam, whichever was greater.

With the inclusion of a floor axial restraint component, the coupling beam response was subjected to a higher compression demand than previous models. Under these increased compression demands, the behaviour was found to be dependent upon the constitutive models used. A process of updating the constitutive models was undertaken in order to ensure the behaviour was being suitably well captured under such demands. Default constitutive models utilised in VecTor2 for the response of RC were the parabolic Hognestad (pre-peak response), and the Modified Park-Kent (post peak response) (Wong et al. 2013). The experimental data indicated little softening of the concrete post peak, however the default models tended to predict significant concrete softening as the coupling beams were loaded. In order to improve the post-peak concrete performance in the model to more accurately represent the experimental data, alternative constitutive models were analysed. Studies by (Mohr 2007) found that the default models used by VecTor2 tended to over-predict the softening response of the concrete beyond the peak strain, and hence alternative models were recommended. Mohr (2007) found that the Popovics pre-peak model for normal strength concrete provided improved pre-peak concrete stiffness. In addition, the Popovic/Mander model, for the post peak concrete modelling, provided a lower reduction in the capacity of the concrete once the peak stress was exceeded. The default compression softening model used in VecTor2 was the Vecchio A model. It was also found that the Vecchio B model provided a reduced level of softening which more accurately represented the experimental results. More information on the models used in VecTor2 can be found in the user manual (Wong et al. 2013).

VecTor2 also included a default crack width check which was designed to reduce the compressive stress capacity in concrete elements adjacent to large cracks, in addition to the compression softening modelled separately. As noted by Wong et al. (2013), the crack width check was included for shear critical members where little or no shear reinforcement caused large shear slip distortions which were not modelled (Wong et al. 2013). The crack width check effectively applied additional softening to the surrounding concrete once crack widths exceeded a specified value, as a function of aggregate size. This defined the crack width at which aggregate interlock was lost. Although a coupling beam by definition was a shear critical member, the coupling beams were well confined and the shear response was dominated by diagonal reinforcement, so the crack width check was found not to be applicable to well detailed coupling beams. It was noted by Wong et al. (2013) that it may have been preferable to neglect the crack width check and instead to explicitly account for shear slip distortions. This was the approach taken in the final three-dimensional model, with the crack width check neglected and the shear slip accounted for using the Hybrid Walraven model. More information about the models can be found in (Wong et al. 2013). The advantage of replacing the crack width check with explicit shear slip analysis was that the compression softening around large cracks, which tended to form in coupling beams, was not considered so the concrete was less prone to crushing failure and strength degradation. Shear slip distortion was still considered by inclusion of a shear slip model in place of the crack width check. If the coupling beam was not designed to be well confined, the crack width check would need to be included to account for the large cracks which could occur leading to loss of capacity. Final

models input into VecTor2 are given in Table 6-1, with the models which differ from default basic models highlighted.

Table 6-1: Final VecTor2 constitutive models based upon three-dimensional calibration

Concrete Models		Reinforcement Models	
Compression Pre-Peak	Popovics (NSC)	Hysteretic Response	Baushinger (Seckin)
Compression Post Peak	Popovics/Mander	Dowel Action	Tassios (Crack Slip)
Compression Softening	Vecchio B (ϵ_1/ϵ_0)	Buckling	Refind Dhakal-Maekawa
Confined Strength	Kupfer/Richart		
Dilation	Variable - Kupfer	Analysis Models	
Cracking Criterion	Mohr-Coulomb (Stress)	Strain History	Previous Considered
Crack Stress Calculation	Basic (DSFM/MCFT)	Strain Rate Effects	Not Considered
Crack Width Check	Omitted	Structural Damping	Not Considered
Crack Slip Calculation	Hybird 1 (Walraven)	Geometric Nonlinearity	Considered
Creep and Relaxation	NA	Crack Process	Uniform
Hysteretic Response	Nonlinear w Plastic Offsets		
Tension Stiffening	Modified Bentz 2003		
Tension Softening	Linear		
FRC Tension	SDEM Mono		

Modelling outputs for the specimen CB24F-RC (including a mild steel reinforced floor slab) with final constitutive models are presented in Figure 6-9 and Figure 6-10. Examination of the plots showed a good representation of the experimental data, with accurate model predictions of the ultimate displacement and axial elongation. Analysis of Figure 6-9 showed that the model over predicted the initial stiffness and also over predicted the ultimate strength of the specimen slightly. The over-prediction of the initial stiffness, as discussed in section 6.3, was due to the assumed perfectly rigid end connections in the model when in reality there was some inherent flexibility in the end restraints of the experiment. The over-estimate of strength was attributed to the contribution of the nominal confinement reinforcing in the coupling beam. The errors observed in the model results were observed to be small which suggested that the model was representing the important behaviour in the experiment. It also indicated that out-of-plane floors were well accounted for in the two-dimensional model using the equivalent floor tie approach.

Axial elongation of the beam was under-predicted at large rotations, as presented in Figure 6-10. Concrete crushing and a reduction in the development of axial elongation beyond 70mm deflection were observed in the model results. The reason for the underestimate of axial elongation at large rotation was because the concrete was in a highly damaged state at the onset of crushing. The modelling software did not accurately model the redistribution of stresses away from the crushed concrete as this process occurred very quickly in reality and so the concrete was predicted to undergo more rapid crushing and strength degradation than was realistic.

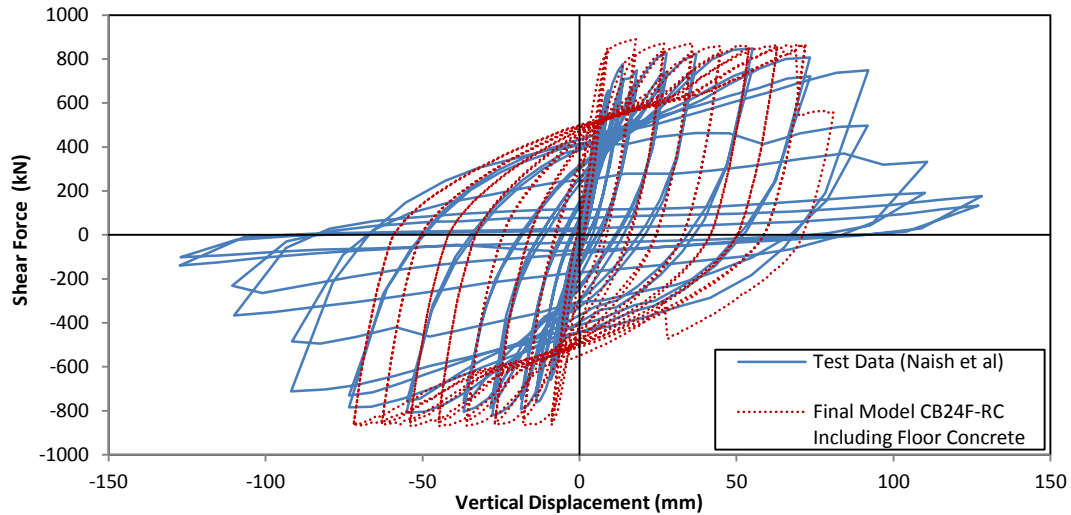


Figure 6-9: VecTor2 final model global hysteresis output for CB24F-RC including full floor area

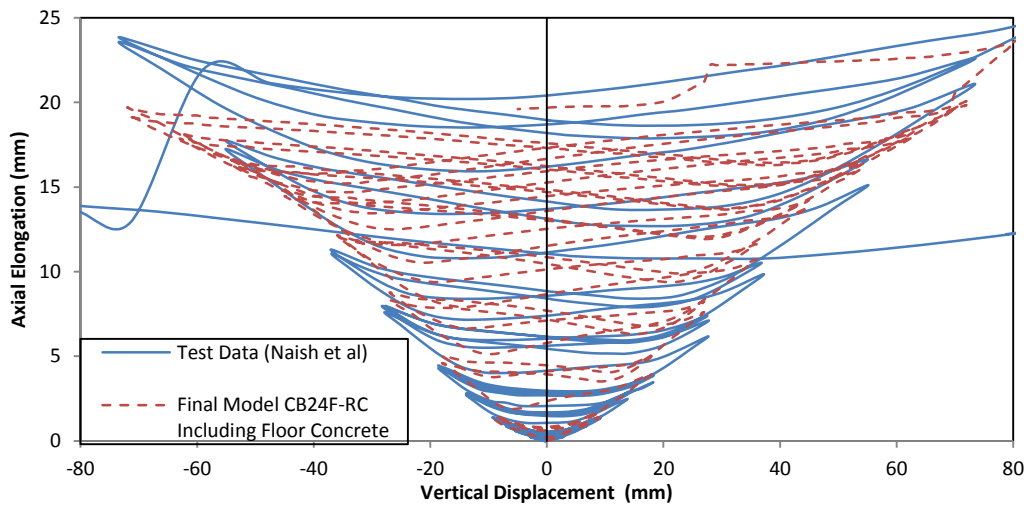


Figure 6-10: VecTor2 final model axial elongation output for CB24F-RC including full floor area

The updated VecTor2 models were extended to consider the specimen tested by Naish et al. (2009) which included a post-tensioned floor area (CB24F-PT). Isolated floor modelling, as presented in Appendix D, showed that the experimental mild steel floor (from specimen CB24D) activated the full floor tension capacity to restrain the elongating coupling beam, thus its equivalent floor tie included the full floor reinforcement content. In contrast, the response of the post-tensioned steel reinforced floor specimen CB24F-PT activated only 42% of the nominal yield capacity of the floor reinforcement based upon the VecTor2 model. Consequently the CB24F-PT equivalent floor tie was based upon 42% of the total floor tension capacity. The results of the modelling of CB24F-PT with the equivalent tension tie included are presented in Figure 6-11 and Figure 6-12.

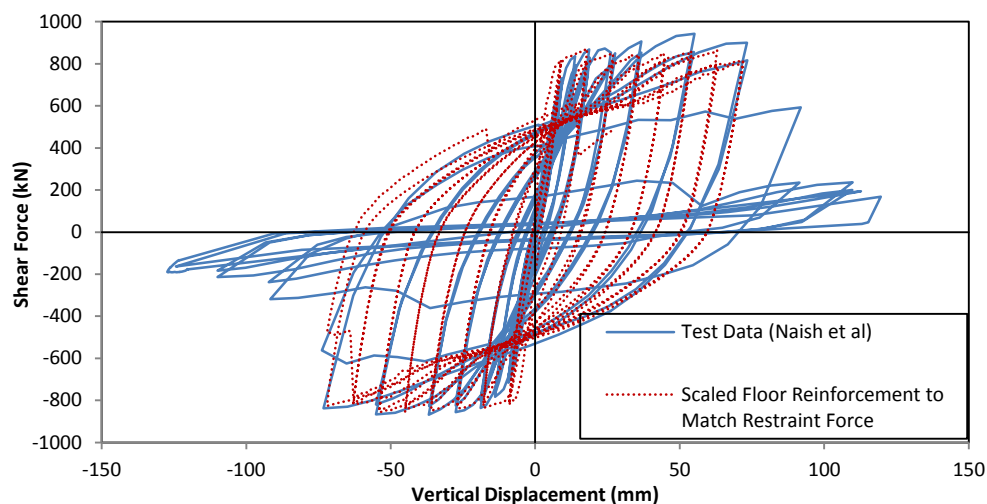


Figure 6-11: Equivalent reduced floor reinforcement global hysteretic response for CB24F-PT

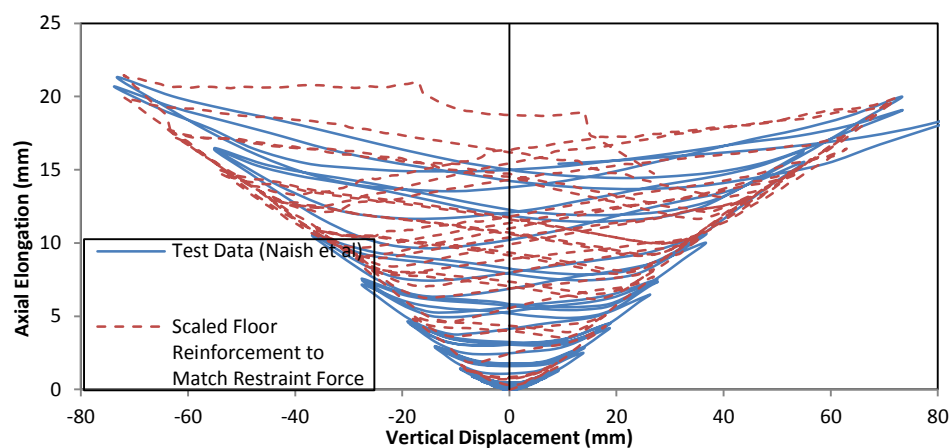


Figure 6-12: Equivalent reduced floor reinforcement axial elongation for CB24F-PT

Analysis of the model which included equivalent floor reinforcement showed good agreement with the experimental data, particularly with reference to the ultimate displacement capacity and axial elongation of the beam. The primary shortfall of the approach was that the shear capacity of the section was under-predicted by approximately 11% in the positive shear force direction, whilst the error was approximately 2% in the negative shear force direction. Despite this underestimate, the scaled floor effective width provided a robust method for representing the floor effects out-of-plane in a two-dimensional model.

6.5 Coupling beam calibration summary

As discussed in this chapter, the modelling of coupling beams with and without floors has been calibrated to provide good representation of experimental data. The constitutive models chosen have been selected based upon the accuracy required for reliable results and the level of damage expected. It is worth noting that the proposed models in VecTor2 were calibrated with the expectation that high levels of damage will be sustained in well confined regions of plastic hinges in coupling beams and at the base of walls. Care must be taken when extending these models to applications which exhibit different expected behaviour, such as shear sliding, and as such the models proposed should only be

applied to well detailed sections. The most suitable method of analysing the three-dimensional problem in a simplified two-dimensional plane has been found to be based upon the following procedure:

- Model the full floor in horizontal floor plane, subjected to the anticipated magnitude of axial elongation in an unrestrained coupling beam;
- Calculate the floor restraint force generated and effective floor width activated to restrain the coupling beam elongation;
- In the two-dimensional model of the coupling beam, include only the floor reinforcement within this effective floor width;
- Model the two dimensional beam model in-plane including the effective area of floor reinforcement. Include in the beam-floor model an effective flange of floor concrete based upon the beam depth each side of the beam to consider composite bending action.

6.6 Coupled wall model calibration

In addition to considering coupling beams in isolation, the accuracy of the finite element models in replicating the realistic behaviour of coupled walls was also confirmed via a process of model calibration against experimental data. The developments made above relating specifically to coupling beams were used as the starting point of the model calibration and extended to coupled wall systems.

6.6.1 Coupled wall experimental data

Experimental analysis of coupled walls has historically been a difficult undertaking given the indeterminate nature of a coupled wall system and the large experimental facilities required to experimentally analyse full coupled wall behaviour. A number of these coupled wall experimental programs have been outlined in Chapter 2. These experimental specimens generally only considered parts of the coupled wall structure. In particular, there was a notable lack of experimental data regarding coupled wall systems supporting floor systems.

A recent experimental program conducted jointly between the University of Washington and University of Illinois, Urbana-Champaign, investigated the behaviour of a coupled wall system as part of a wider RC wall research programme and provided the most relevant experimental data for comparison (Lehman et al. 2013; Turgeon 2011). The intent of this research was to assess the performance of a coupled wall system designed to current design codes. The 1/3 scale test specimen did not include floors, and was analysed based upon the loading of ASCE 7, with the specimen designed to the requirements of ACI 318-08. The experimental setup, shown in Figure 6-13, tested the bottom three storeys of a ten storey coupled wall. The test setup simulated the higher level storeys by applying boundary condition force at the third floor level. Based upon analysis of the full coupled wall, conducted in VecTor2 finite element software, boundary conditions were enforced at the third storey of the specimen by application of shear, moment, axial force and displacements intended to simulate the full wall behaviour. An important aspect of the boundary conditions was that the setup allowed the coupled wall piers to displace independently. The independent movement of the walls allowed elongation of the coupling beams above the third floor to be accommodated, making the data useful for analysis of

elongating coupling beams. The experimental data was accessed from the Network for Earthquake Engineering Simulation (NEES) Project Warehouse <https://nees.org/warehouse/project/104/> as publically accessible data for the earthquake engineering research community (NEEShub 2014).

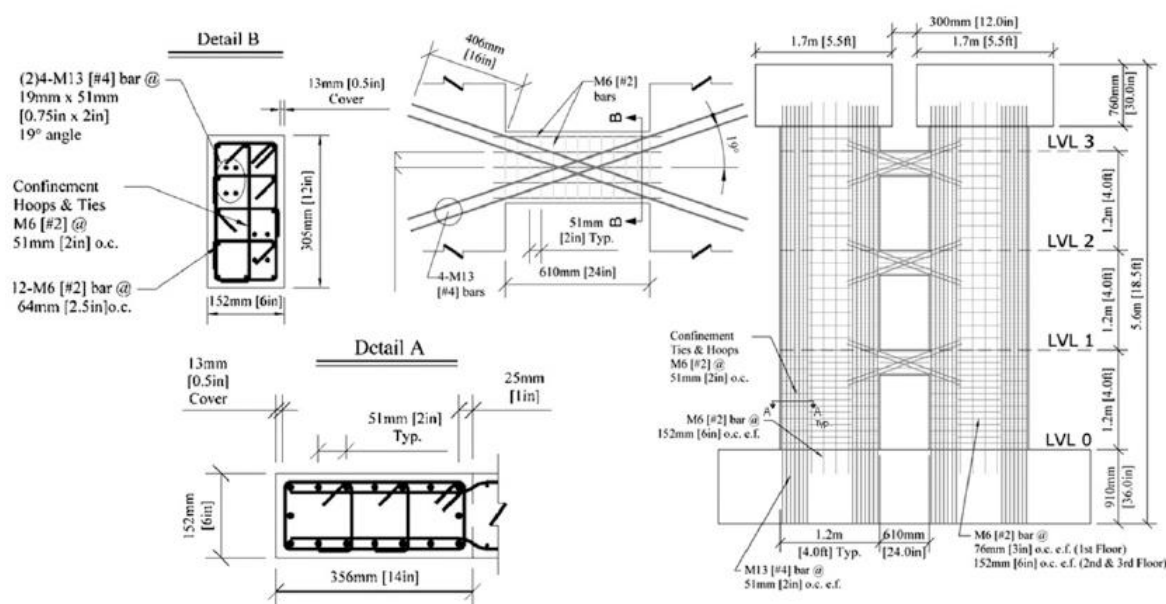


Figure 6-13: Coupled wall experimental program specimen (Lehman et al. 2013)

The specimen was cyclically loaded to 2.27% drift, before a sudden compression failure occurred in the compression wall pier, resulting in significant strength degradation, as shown in Figure 6-14. The coupling beams were observed to reach yield at between 0.36% and 0.67% drift, whilst the wall piers yielded at approximately 0.5% drift. The maximum base shear was measured as 778kN. The coupled wall specimen achieved an ultimate drift capacity in excess of comparable planar wall specimens tested as part of the research programme. The coupled wall specimen was then subjected to an axial compression test, in which the axial compression capacity was measured to be 42% of the gross section compressive capacity.

Among the findings of the experiment related to coupling beams, it was found that the coupling beams sustained shear stresses in excess of the ACI 318-08 nominal strengths, but were measured to be less than the upper limit specified by ACI 318-08. Minor spalling was observed to occur at the corners of the coupling beams from 1% wall drift onwards. The coupling beams sustained end plastic rotations of between 4-5%. The third and second storey coupling beams were observed to yield first while the coupling beam at the first floor yielded after the onset of yield of the wall longitudinal reinforcement.

The primary findings of the test, related to the overall coupled wall behaviour, were that the progression of damage prior to failure was moderate in nature, with spalling of the cover concrete in the wall pier boundary elements in accordance with expectations. Significant force redistribution from the tension wall pier to the compression wall pier was measured as part of the experiment. However the sudden loss of strength at 2.27% drift was somewhat unexpected. At 2.27% drift, the compression wall was observed to undergo concrete crushing and buckling of the primary longitudinal reinforcement in the

boundary element. Reloading in the opposite direction following the buckling caused the other wall pier to undergo similar failure. The postulated reasoning for the failure was that a shear-moment-axial force interaction occurred as the compression wall pier compression capacity was exceeded due to larger than predicted force redistribution between wall piers. As a result, it was found that the ductility and drift capacity of the coupled wall system were limited solely by the compression wall pier. The experimental results suggested the compression demand may have been underestimated at the ultimate capacity by existing code recommendations.

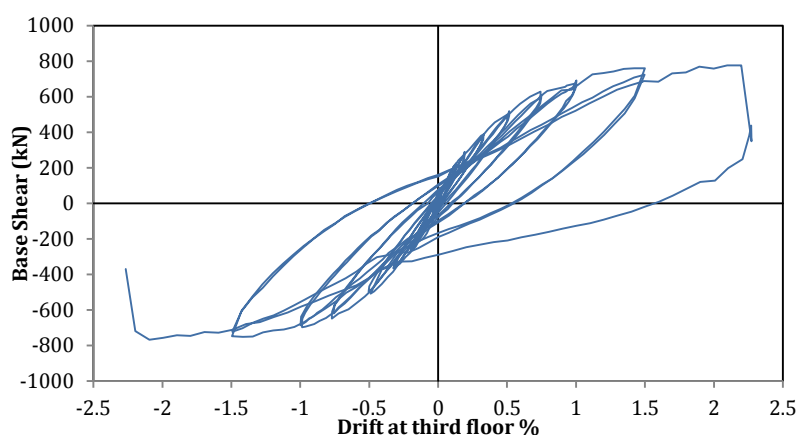


Figure 6-14: Experimental results for coupled wall lower three stories (NEES Project Warehouse)

6.6.2 Coupled wall finite element model calibration

As per the coupling beam computational modelling, the finite element program VecTor2 was used for analysis of coupled walls. VecTor2 allowed only one set of constitutive models to be input in a single model and it was important that the constitutive models were selected carefully to capture the important behaviour. In the case of a full coupled wall, the most critical and complex behaviour related to the plastic hinge zones in the coupling beams and at the base of the walls. As the wall pier plastic hinge zones were typically well confined and highly strained, the constitutive models and mesh sizes selected previously to capture coupling beams were considered appropriate to accurately model the behaviour of the wall pier plastic hinges. The remainder of the coupled wall system was predominantly in the elastic range and subject to low levels of damage, so it was recommended that the constitutive models be set to best capture the highly damaged regions of the coupling beams and wall pier plastic hinges. The constitutive models proposed for coupling beams in section 6.4 were therefore used to capture the global coupled wall behaviour.

The primary variables for ensuring the global coupled wall behaviour was captured in VecTor2 were the input method of the specimen and the load application. Lehman et al. (2013) imposed boundary conditions to a three storey wall sub-assembly based upon the behaviour expected when the full wall was subjected to ASCE 7 equivalent static loading. Given the complexity and inherent assumptions of these boundary conditions, greater accuracy was achieved with VecTor2 by analysing the full wall subject to the ASCE 7 loading, rather than considering only the lower three storeys and employing boundary condition assumptions. The full wall, at 1/3 scale as per the experiment, was input into

VecTor2 for analysis. The model layout is shown in Figure 6-15, where the colours represent different material properties. In particular, the presence of heavily reinforced boundary elements required different material properties in the ends of the walls. Wall reinforcement was input as smeared to avoid the computation size limitations of VecTor2, with the diagonal bars of the coupling beams input as discrete truss bars. As per the coupling beam convergence testing, the mesh sizes were set based upon expected damage. In particular, the coupling beams and wall bases were set to 50mm mesh size, with the mesh size of the remaining predominantly linear elastic zones set to 100mm.

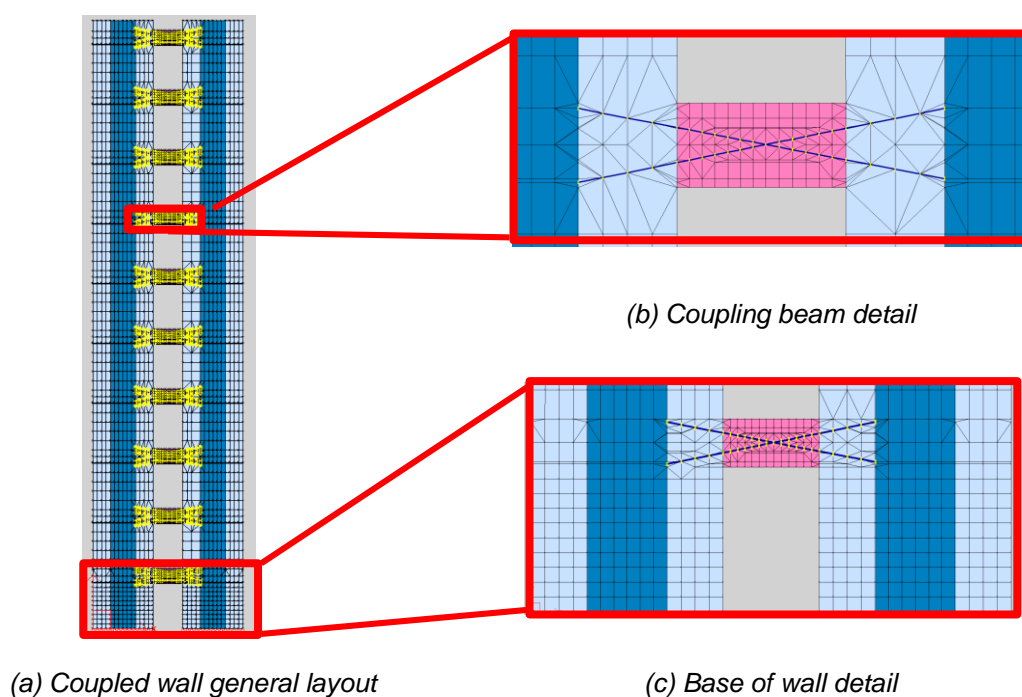


Figure 6-15: VecTor2 representation of Lehman et al. (2013) coupled wall

The other primary variable in ensuring the coupled wall was adequately captured in the model was the application of lateral force. There were two lateral force application alternatives considered, namely force controlled and displacement controlled. The force based application tended to provide good numerical stability on the ascending branch of the force displacement plot. As the specimen began to yield, the numerical stability was compromised as the stiffness reduced and eventually decayed. Displacement controlled force application remained stable regardless of stiffness reduction. However, the imposition of a displacement enforced a displaced shape which was not representative of how the specimen may deform in an earthquake due to inertial effects. More critically, enforcement of displacement in each wall constrained the wall piers to deform identically, which prevented development of elongation in the coupling beams. Elongation could be allowed for if the displacement was applied to a single wall pier only. However this method induced axial forces in the coupling beams, in either tension or compression depending upon loading direction, in order transfer force between the walls. Displacement controlled force application was therefore found to be unfeasible for the assessment of coupled walls where elongation was significant.

Force controlled application was found to be the only appropriate method available for lateral force application in VecTor2. However the use of force controlled loading was limited by the numerical instability beyond peak wall capacity, and an inability to capture strength degradation and ultimate failure. The method of force based loading was only able to capture behaviour up to peak wall capacity. In order to reduce the limitations of the loading protocol, a spring system was used to provide positive stiffness to the coupled wall at or just past peak load, as shown in Figure 6-16. This spring could only allow a small amount of post peak behaviour to be analysed as the degradation of the coupled wall at failure was very rapid. Capturing the full failure mechanism of the system would have required the springs to be very stiff, which changed the overall behaviour up to peak loading. To avoid the overall behaviour of the system changing due to spring inclusion, the tie capacity was limited to 25% of the maximum base shear (200kN total = approx. 25% of the maximum expected base shear). Once the model was analysed, the force supported by the springs was subtracted from total applied shear to assess the overall force supported by the coupled wall.

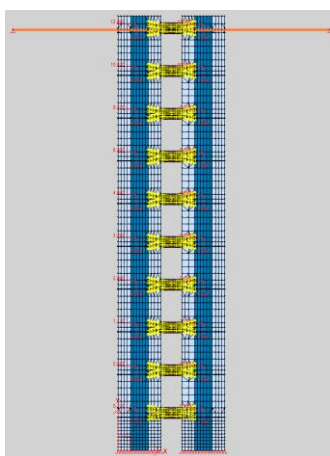


Figure 6-16: Lehman et al. 2013 wall with tie near top to enforce positive stiffness

As the Lehman et al. (2013) coupled wall was subjected to ASCE 7 equivalent static loading, force based loading was undertaken based upon an equivalent static distribution. The magnitude of the inverted triangular force distribution was incrementally increased in cycles until the model became numerically unstable. It is worth noting that force based application became unstable at or near zero stiffness because the coupled wall could not support further load. However this point did not necessarily mark the onset of failure and may have represented only the full yield plateau of the specimen.

The modelled force-deformation response, measured at the third floor, is compared to the experimental data in Figure 6-17. The force displacement response showed good agreement between the model and experimental data. The primary shortfall of the model was an over-prediction of the elastic stiffness. As has been demonstrated previously, the stiffness over-estimate was a function of the fully fixed boundary conditions imposed by the model. These boundary conditions did not match the finite stiffness of the experimental setup and inaccuracies in modelling elastic shear deformations resulted. However in general, the model provided a good representation of the behaviour prior to yield.

The model predicted the measured capacity of the coupled wall well in the positive direction. However an underestimate of the capacity was observed through the middle range of applied negative wall drift. Additionally, due to model numerical instability, the model was unable to capture the failure of the wall. However comparison of the modelled results to experimental results found that the onset of strength degradation was predicted to occur slightly earlier in the model than in the experiment. As discussed previously, this was due to inaccuracies in computational modelling techniques, which did not accurately capture the rapid redistribution of stresses which can occur as concrete softens.

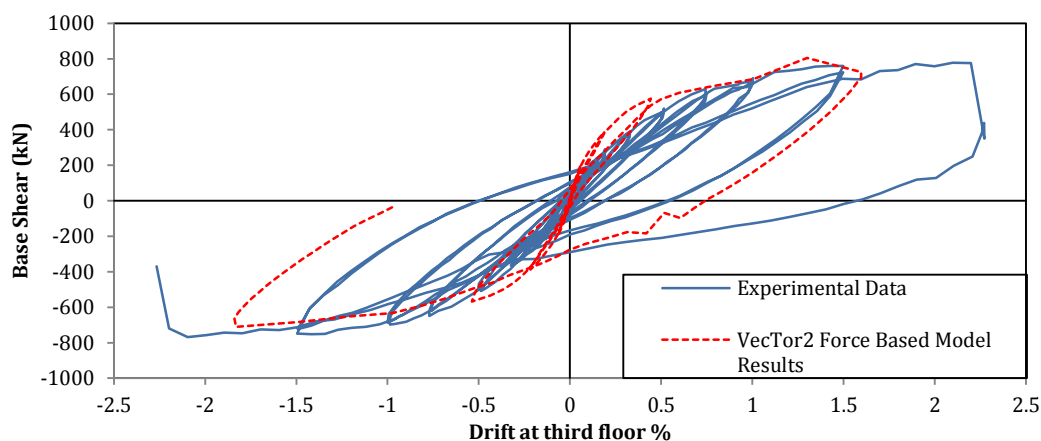


Figure 6-17: Lehman et al. (2013) coupled wall model results using force based loading

The displaced shape profiles of the wall, based on measurements at each storey height, are compared in Figure 6-18. The dashed line represents the experimental data demonstrating that in general the VecTor2 analysis tended to under-predict the displacement induced at each floor level for a given level of drift. In particular, analysis of Figure 6-18 showed that the displacements were under-predicted significantly at low levels of base shear, with the accuracy of the models improving at higher magnitudes of base shear. It was apparent that the VecTor2 models resulted in inaccuracy related to the elastic shear deformations near the base of the wall. As the coupled wall behaved inelastically, the error was reduced for two reasons. Firstly, the relative contribution of the shear deformation reduced as first mode flexure began to dominate the response. Flexure was more accurately modelled in VecTor2 as it was a simpler form of deformation. Secondly, the non-linear shear behaviour was accounted for with the crack slip approximations of the Disturbed Stress Field Model (DSFM) utilised by VecTor2. The inaccuracy in floor displacements at low levels of base shear was related to the over-prediction of stiffness in the elastic range which did not account for the elastic deformation as accurately, as presented in Figure 6-17.

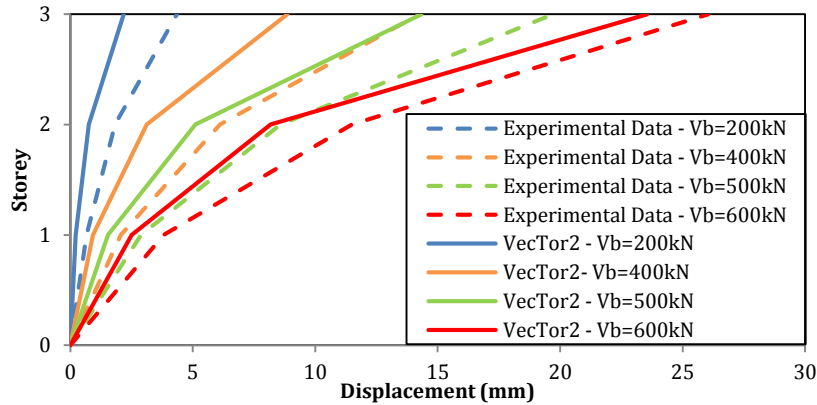


Figure 6-18: Displaced shape profiles of coupled wall (averaged coupled wall value) at varying base shear demands for Lehman et al. (2013) coupled wall

The approximate elongations of the coupling beams are compared at the first and second floor level to the modelled values in Figure 6-19 and Figure 6-20 respectively. As can be seen, the model provided good correlation with the axial elongation experimental data, with a slight tendency to under-predict the magnitude of elongation. This under-prediction was due to not all shear components of wall deformation being included in the model simplification. In general, the elongation results showed good correlation to the experimental data, despite the slight under-prediction of axial elongation magnitude. As anticipated, the elongation in the second floor coupling beam was significantly larger than the elongation in the first floor coupling beam in both the experiment and the model.

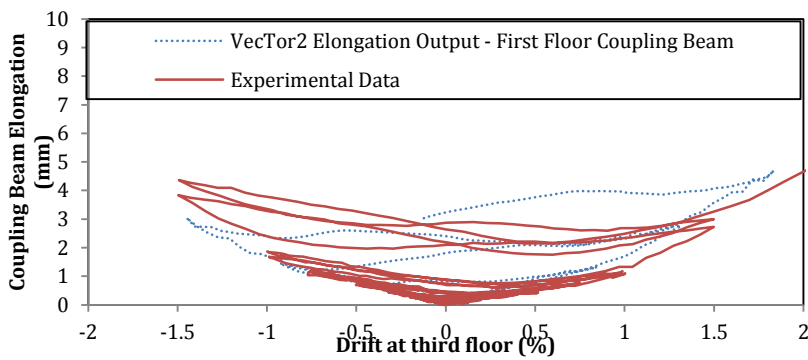


Figure 6-19: Elongation in first floor coupling beam of Lehman et al. (2013) coupled wall

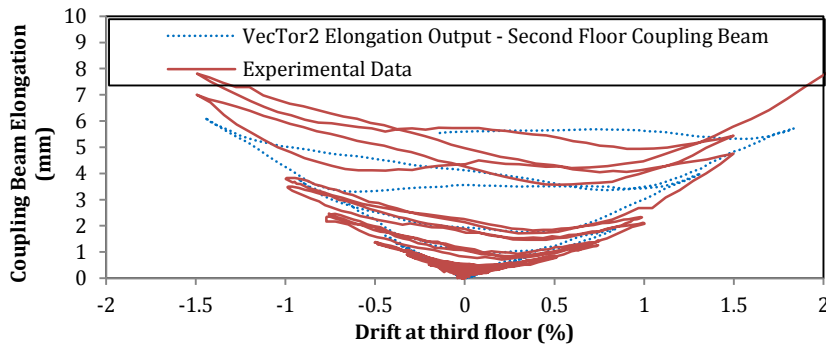


Figure 6-20: Elongation in the second floor coupling beam of Lehman et al. (2013) coupled wall

In general the coupled wall behaviour has been found to be well captured by the two-dimensional coupled wall modelling which provided confidence in the modelling technique of coupled walls subject to in-plane loading. The comparison also confirmed that the calibration undertaken on isolated coupling beams also provided suitable results when the coupling beams were part of a coupled wall system.

6.7 Modelling of coupled wall and floor interaction

The approach taken to model coupled wall systems interacting with floors was developed based upon the three-dimensional model calibration of coupling beams presented in section 6.4. The approach taken was to represent the floor diaphragm as an equivalent tension tie. The application of these floor ties as reinforcement truss bars in a coupled wall model is presented in Figure 6-21. The properties of this tension tie were based upon the modelled floor responses, presented in Chapters 3-5 for a range of different floor layouts. The strength of each equivalent tension tie was determined based upon the maximum effective width measured in the floor models for each floor arrangement considered. The strength of these equivalent floor ties was therefore set to match the tension capacity of the floor within the modelled effective width, such that the floor effects were able to be considered in a two-dimensional coupled wall model. In this way, the effect of weak zones in the floor was inherently accounted for in the modelling of coupled walls. An area of concrete, equal to two times the depth of the coupling beam as developed in section 6.4, was also included to represent the floor concrete in compression.

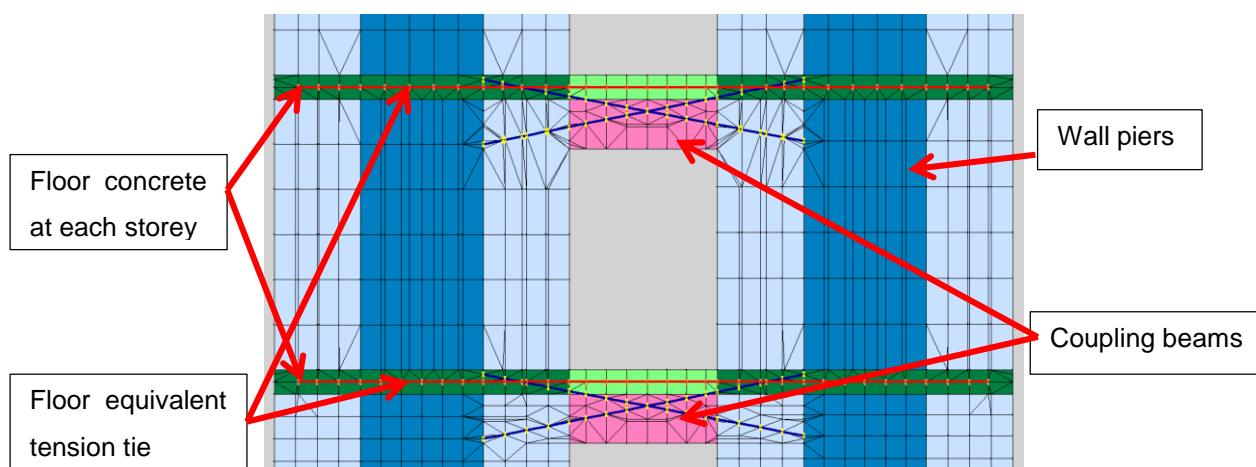


Figure 6-21: Two-dimensional coupled wall and floor model with equivalent floor included – colours represent different material properties, thickness, and/or reinforcement contents

6.8 Conclusions

A series of relevant coupling beam and coupled wall experimental data have been used to compare the results of VecTor2 finite element modelling software in two dimensions. On the basis of the data comparison, VecTor2 has been found to provide a good representation of realistic reinforced concrete coupling beams in isolation, with and without floor systems, and of full coupled wall systems. The calibration process led to the use of more advanced concrete constitutive models which provided enhanced post-peak concrete performance due to the initial over-prediction of concrete compression

softening. The primary update to the default constitutive models was replacement of the crack width check softening approach with the 'Hybrid Walraven I' crack slip model,

A methodology for analysis of three-dimensional coupling beam and floor interaction was developed which provided suitable representation of reality, as shown below:

- Model the full floor in the horizontal floor plane, subjected to the anticipated magnitude of axial elongation in an unrestrained coupling beam;
- Calculate the floor restraint force generated and effective floor width to restrain the coupling beam elongation;
- In the two-dimensional model of the coupling beam, include the floor reinforcement only within this effective floor width;
- Model the two dimensional beam model in-plane including the effective area of floor reinforcement. Include in the beam-floor model an effective flange of floor concrete based upon the beam depth each side of the beam to consider composite bending action.

The approach to model coupled wall systems was based upon comparison to available experimental data. A force based load application, incorporating a positive stiffness spring, was found to be the most accurate method of capturing behaviour of the coupled wall up to peak capacity. On the basis of the findings presented in section 6.6, the most appropriate loading protocol for coupled wall analysis was:

- Apply force based equivalent static analysis pushover forces equally to each wall pier,
- Use a spring with <25% total base shear capacity to provide positive stiffness to the wall up to and just past peak capacity,
- Analyse the wall up to the onset of numerical instability, related to the point of strength degradation in the coupled wall.

Based upon comparison to experimental data of coupling beams and coupled walls, VecTor2 has been validated as an acceptable computational modelling tool for analysing coupled wall systems.

CHAPTER 7

7 Coupled Wall Modelling

Observations made following the 2010/2011 Canterbury earthquakes showed that the coupled walls of several buildings performed undesirably when compared to their design intent (Canterbury Earthquakes Royal Commission 2012) (CERC). The proposed reasoning given by the CERC for this undesirable behaviour was that the coupling beams were subjected to axial restraint forces which were not considered in design. The origin of this axial restraint was found to have been the interaction between coupling beams with adjacent wall piers and floor systems, which resisted the tendency of the coupling beams to elongate. Consequently, the axially restrained coupling beams were stronger than their unrestrained capacity assumed in design, which led to the design strength hierarchy of the coupled walls being invalidated. The lack of consideration of axial restraint in the design of coupled walls was proposed to have caused the undesirable behaviour of coupled wall buildings in Canterbury.

Analysis of coupled wall systems has been undertaken in several experimental programmes, as outlined in Chapter 2. However the effects of axial restraint may have been not fully captured in these experiments due to the size and static indeterminacy of coupled walls, which prevented analysis of full wall systems. Additionally there was little consideration of the effect of floors in these experiments. Based upon the findings from Canterbury, further research was required into coupled wall behaviour to improve design procedures, and in particular to better understand the effects of axial restraint in coupled walls. Due to the limitations of experimental procedures, the analysis of such large scale coupled walls was well suited to computational modelling that allowed large scale wall-floor systems to be analysed.

Presented in this chapter is a summary of the analyses undertaken on coupled wall systems, including floor components. The analyses were undertaken using VecTor2 finite element software (VecTor Analysis Group 2011), where model inputs were based upon the model calibration processes presented in Chapters 3 and 6. A series of coupled walls were designed according to NZS 3101:2006, including the proposed 2014 amendments, which were available for public submission at the time of writing (Standards New Zealand 2014). Seismic loading was simulated on the walls in order to analyse the behaviour of realistic coupled walls when subjected to earthquake induced actions. The behaviour of these wall systems has been compared to existing design assumptions in order to draw conclusions on the realistic behaviour of such coupled wall systems.

7.1 Wall model design

A series of coupled walls was first designed according to NZS 3101:2006 (including the proposed 2014 amendment) for the purposes of analysis. These designs included allowance for the specific clauses for coupled walls, in particular related to coupling beam overstrength due to floor interaction, included

in the proposed amendment. Allowance was also made for the proposed increased minimum vertical reinforcement requirements for walls. These coupled wall designs were intended to replicate a range of coupled walls which could realistically be designed in a New Zealand context. A prototype building was used to replicate realistic wall designs based upon the 10 storey prototype building used in the 1998 Red Book wall design (CCANZ 1998). Accordingly, this prototype office building was assumed to consist of a square floor plan, and to be braced independently in each direction, as shown in Figure 7-1. 300 mm deep Hollow-core (300HC) precast prestressed floor units were assumed for the building, which were supported on a gravity frame. The building was designed to be in Christchurch ($Z=0.3$) for a standard earthquake return period of 500 years ($R=1$). The geometry of the coupled walls varied for each of the wall designs. As presented below, a base model that used the geometry shown in Figure 7-1 (b) was first designed. This base coupled wall model was subsequently used for comparison to a series of coupled wall variations also presented below. The geometry of the coupling beams was based upon recent research undertaken in the United States which found that tall buildings frequently required less squat coupling beams than had been traditionally used (aspect ratios of 1.5-3) (Naish et al. 2009). However the effect of more squat coupling beams as has traditionally been employed in New Zealand was also considered in the design variations presented below.

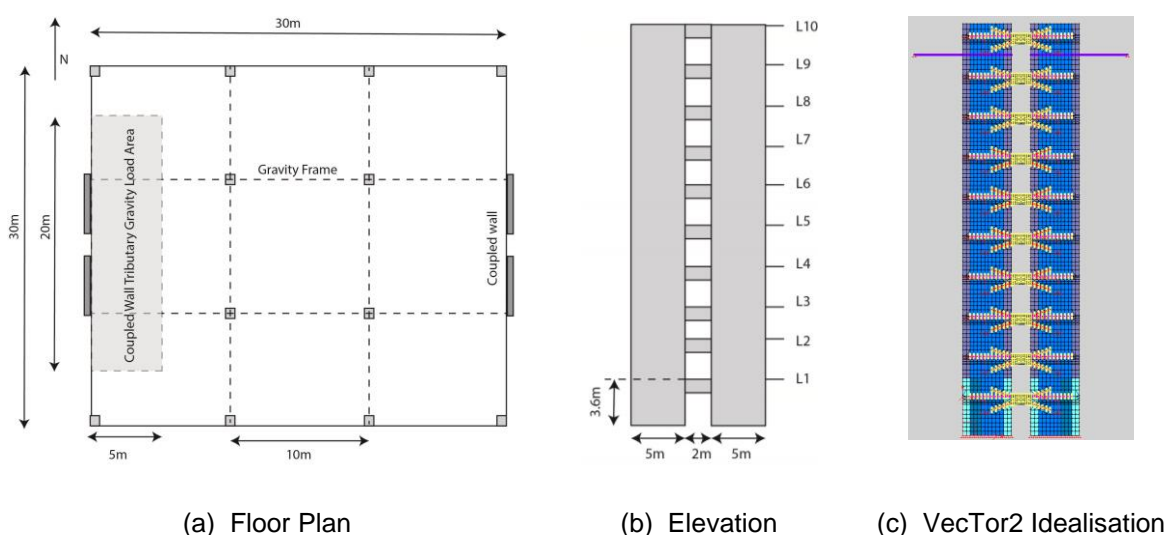


Figure 7-1: Prototype building and base model coupled wall layout

7.1.1 Base coupled wall design

Modal analysis of the assumed geometry, shown in Figure 7-1, was first used to design a base coupled wall, as shown in Figure 7-2. Design gravity loads in the wall piers were based upon the tributary floor area shown above. The base design resulted in a lightly reinforced wall with heavily reinforced boundary elements. These boundary elements, referred to throughout this chapter as the heavily reinforced regions at the edges of the walls, were designed with a concentration of longitudinal (vertical) reinforcement to support wall bending moments more effectively than walls designed with evenly distributed reinforcement. As presented in Figure 7-2 (b), the wall shear reinforcement varied dependent upon the assumed floor type because the floor type influenced overstrength wall shear demands.

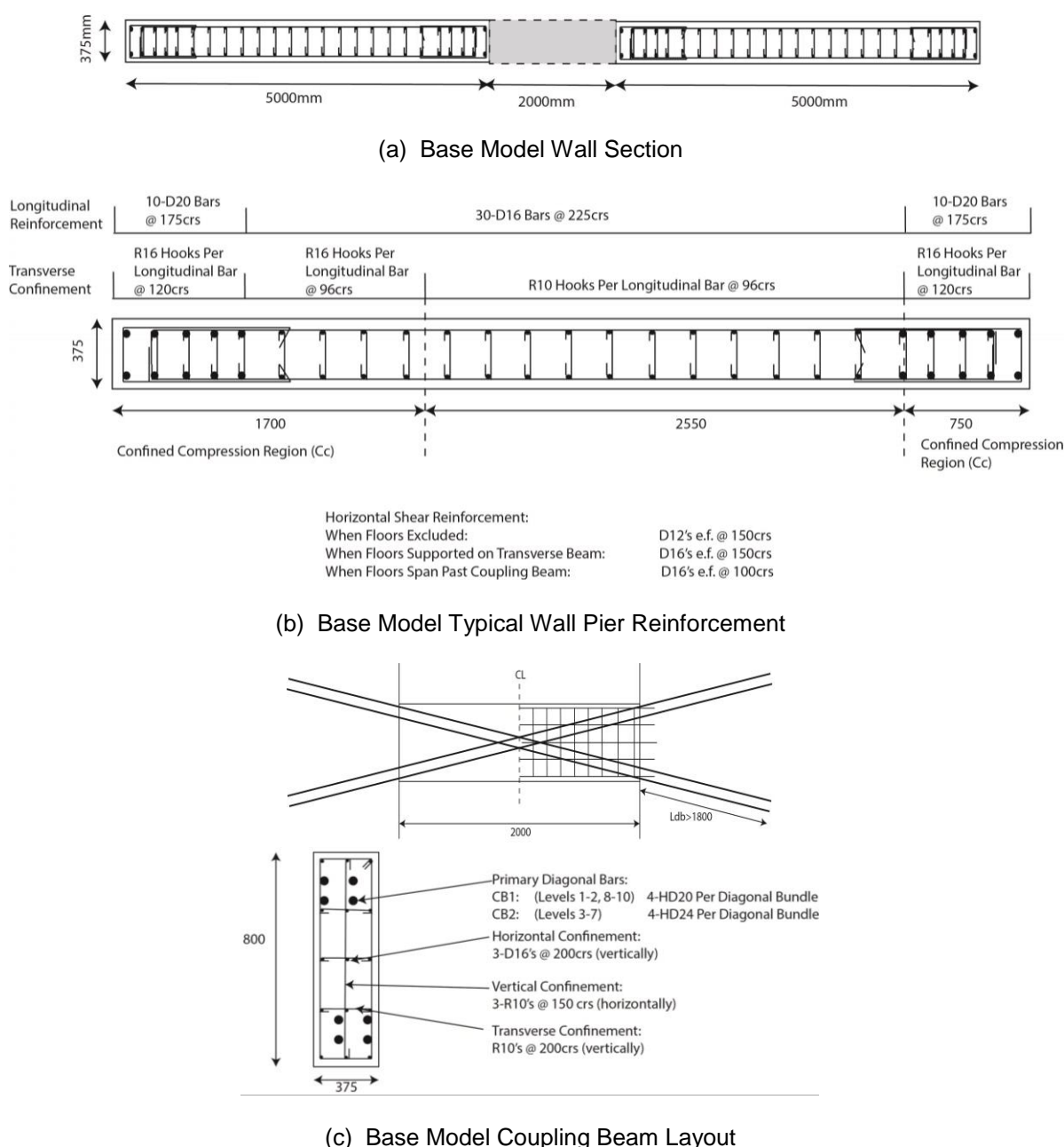


Figure 7-2: Base coupled wall model design details

7.1.2 Coupled wall design variations

A further series of walls was designed using modal analyses, which each differed from the base model in one key aspect as presented in Table 7-1. The consideration of designs referred to as 0.5x Base and 1.5x Base was to assess the effect of changes in coupling beam strength, whilst retaining the same wall pier details as the base model. These models therefore varied the coupling beam capacity by the multiplier value shown (0.5x and 1.5x respectively). CW2 and CW3 differed from the base model in the initial geometry used for modal analysis, to replicate changes in architectural requirements. In CW2 it was assumed that the gap between wall piers was shortened to 1 m, resulting in an identical wall pier design to the base model but different coupling beam designs, as presented in Figure 7-3. CW3 was designed assuming that the wall pier length was shortened to 3 m, with the same coupling beam

dimensions as the base model. Analysis of the prototype building braced by the shortened CW3 wall piers showed the building to be excessively flexible. To reduce interstorey drifts, the design of CW3 was undertaken assuming that two coupled walls were present in each direction (four total). The layout of CW3 wall piers is presented in Figure 7-4. The coupling beam designs for CW3 used the same layout as the base model, with the reinforcement as presented in Table 7-1. The final design, CW3x2, was assessed to determine if a heavily reinforced wall pier changed the behaviour of the system appreciably. CW3x2 was identical to CW3 presented in Figure 7-4, except that the vertical wall pier reinforcement was doubled (with a corresponding increase in the shear reinforcement provided). More information on the coupled wall design properties is presented in Appendix E.

Table 7-1: Coupled wall design variations from base model design

Design	Abbrev.	Distinctive properties from base design
1a. Base Wall	(Base)	NA
1b. Base Wall 0.5x Coupling Beam	(0.5x Base)	Base Model as shown above, except area of coupling beam diagonal reinforcement decreased by 50%.
1c. Base Wall 1.5x Coupling Beam	(1.5x Base)	Base Model as shown above, except area of coupling beam diagonal reinforcement increased by 50%.
2. Wall 2	(CW2)	Coupling Beam span reduced to 1000mm. Wall pier geometry and design unchanged.
3a. Wall 3	(CW3)	Wall Pier length reduced to 3000mm, lightly reinforced similar to base model. Coupling beam diagonal reinforcement altered to D24's (Levels 1-4, 10), D28's (Levels 5-9).
3b. Wall 3 x2	(CW3 x2)	As for 3a but with wall vertical reinforcement increased by 100% to simulate heavily reinforced wall piers.

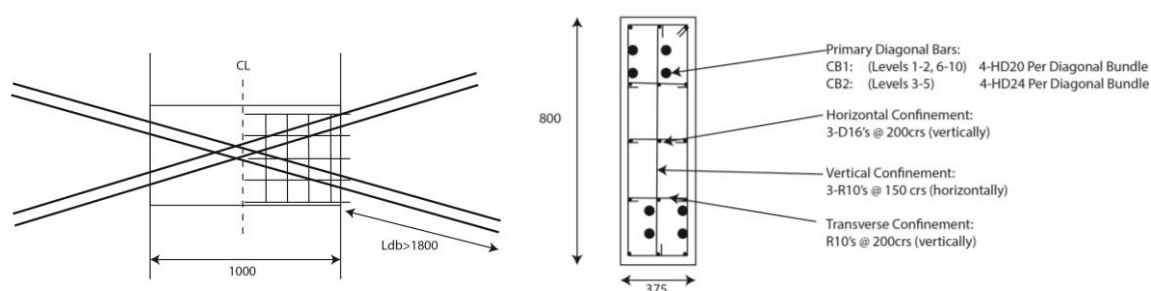


Figure 7-3: Coupled Wall 2 (CW2) coupling beam design (wall piers match base model)

Three types of floor systems were assumed in the design and analysis of the coupled wall variations, as shown in Table 7-2. These floors represented a spectrum of the measured floor responses from Chapters 3-5. The first case assumed that the floor and coupled wall were isolated, such that no floor interaction occurred with the coupled wall. The second and third cases were based upon typical precast prestressed floor systems used in New Zealand buildings. Both of these floor systems assumed that the precast floor units spanned parallel to the coupling beam span. However the 'fused' floor represented the case where precast floor units were supported by a transverse beam at the coupled wall location. This transverse beam support represented a weak zone in the floor system (a fuse) which

limited the capacity of the floor to restrain elongation. In contrast, the non-fused floor represented the case where the precast units spanned past the coupling beam such that the weak zone in the floor was absent. As per the approach developed in Chapter 6, the floors were approximated as equivalent ties in two-dimensional coupled wall models, where the effective width and tie strength were based upon modelling undertaken in Chapters 3 and 4. Each of the coupled walls was designed and modelled with each of these three floor systems.

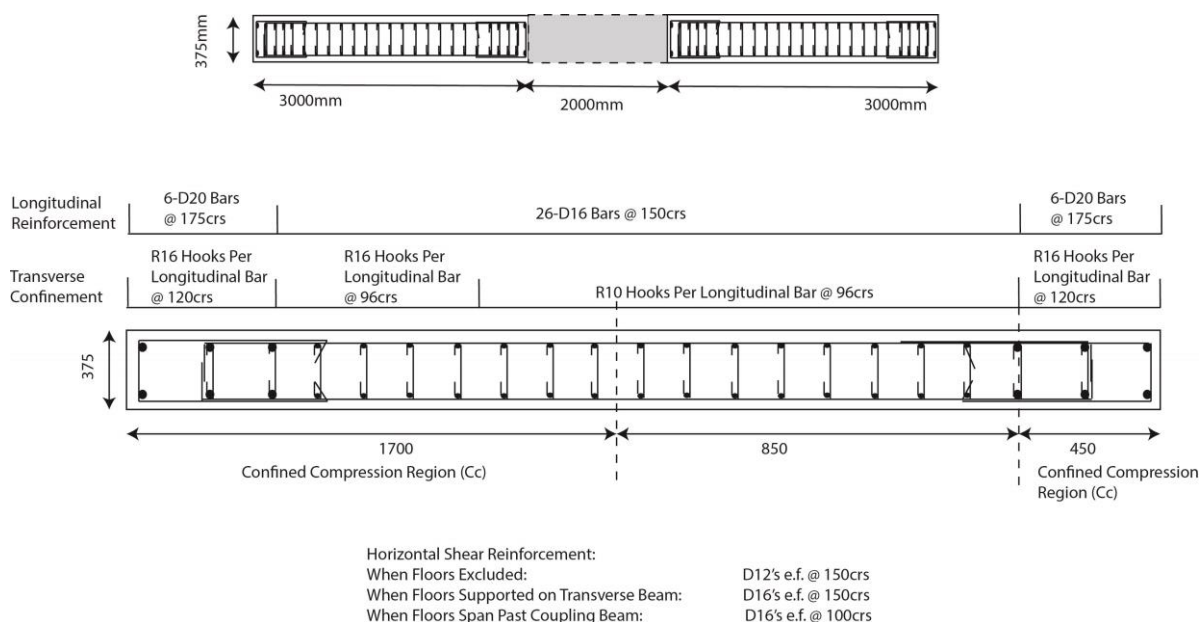


Figure 7-4: Coupled Wall 3 (CW 3) wall pier design

Table 7-2: Floor arrangements considered in coupled wall design and analysis

1. NO FLOOR	Floor assumed isolated from coupled wall
2. FUSED FLOOR	Floor assumed to be 300 Hollowcore floor, spanning parallel to coupling beam, supported on a transverse beam at coupled wall (see arrangement 2, Chapter 4). Equivalent tie capacity = 820 kN, effective width 3.2 m.
3. NON-FUSED FLOOR	Floor assumed to be 300 Hollowcore floor, spanning parallel to coupling beam, spanning past coupling beam (see arrangement 3, Chapter 4). Equivalent tie capacity = 1467 kN, effective width = 2 m.

7.1.3 Modelling inputs

Material properties for design purposes were based upon lower characteristic design strengths. However for the purposes of analysis, average material properties were used, because the intention of the analysis was to understand how a realistic coupled wall building would perform with respect to its design intent. In this way, the analysis included the effect of material strengths exceeding their design values, as would have occurred in construction practice. The average strength properties, as presented in Table 7-3, were based upon the material testing undertaken in a series of experiments (MacPherson

2005; Peng et al. 2008). Note that although the strength properties varied dependent upon the bar size, for the analyses each grade of steel was assumed to have identical properties.

Table 7-3: Material properties assumed in design and analysis (strain units presented in milli-strain)

	Design assumed		Average used in analysis			
	f_y (MPa)	ϵ_y	f_y (MPa)	f_u (MPa)	ϵ_y	ϵ_u
G300 Steel	300	1.5	325	450	1.6	200
G500 Steel	500	2.5	540	660	2.6	115
Concrete	$f'_c = 30$ MPa		$f'_c = 36$ MPa			

The coupled wall designs outlined above were input into VecTor2 software, as shown in Figure 7-1. The method of force application, as per the findings of Chapter 6, was to apply force based (equivalent static) cyclic pushover forces to the wall models. Displacement based loading was not able to be used for this modelling as enforcement of a wall pier displacement prevented coupling beam elongation from occurring, as discussed in Chapter 6. To make allowance for coupling beam elongation, the two wall piers in each model were loaded equally (with force based loading) and allowed to deform independently. Force was applied up to approximately 75% of the nominal coupled wall design capacity, and then incrementally increased until numerical instability was reached at or near peak wall capacity. Although this method only allowed analysis up to peak wall capacity, as discussed in more detail in Chapter 6, it was found in the model calibration process to be the most accurate method of assessing coupled walls. As per Chapter 6, a low stiffness spring was used near the top of the wall to provide positive stiffness near peak strength to ensure numerical stability of the wall at high levels of drift. Floors were input into the two-dimensional coupled wall models according to the process outlined in Chapter 6. Each coupled wall was modelled three times, with each of the three floor types outlined above. Consideration of the three types of floors involved using an equivalent floor tie to represent the different strength of each floor being considered in restraining coupling beam elongation. These equivalent floor ties were based upon the modelling presented in Chapters 3-5. The constitutive models found from the model calibration process were applied in VecTor2 (see Chapter 6 for more information), as presented in Appendix E. A similar analysis was undertaken of coupled walls in VecTor2 by Mohr (2007) to assess performance based design methods for coupled walls. Axial restraint was not directly considered in that study.

7.2 Base wall model results

A summary of the model results for the base model is presented in this section. Comparisons to each of the coupled wall variations are presented subsequently in section 7.3.

A series of visual outputs for the base model, shown in Figure 7-2, is presented in Figure 7-5 with varying floor arrangements. Analysis of deflected shapes indicated that the desired coupled wall

mechanism was formed when the floor and wall were isolated, as shown in Figure 7-5 (a). The coupling beams exhibited inelastic shear deformation, in conjunction with wall pier flexural plastic hinges. In contrast, when floors were included as presented in Figure 7-5 (b) and (c), the deflected shapes showed that the coupling beams largely remained elastic, with a higher proportion of the deformation attributed to plastic hinges at the base of the wall piers. These models which included floors were observed to have resulted in the tension pier being fully stressed in tension, rather than deforming in combined tension and bending. As a result, the coupled walls which included floor interaction each tended to behave more like a single cantilever wall, and the assumed coupled wall inelastic mechanism could not form. This single cantilever behaviour occurred because the cumulative coupling beam strengths, when floors contributed, were greater than the wall pier tension capacity, so that the wall tension pier was uplifted before the coupling beams could yield. In this way the tension wall acted as a 'fuse' to limit the total demand that could be imparted on the compression wall, by yielding before the coupling beams reached full strength. Despite the change in deformation mechanism, the base model shear design was found to be adequate because yielding of the tension wall pier prevented excessive shear demand being imposed on the walls.

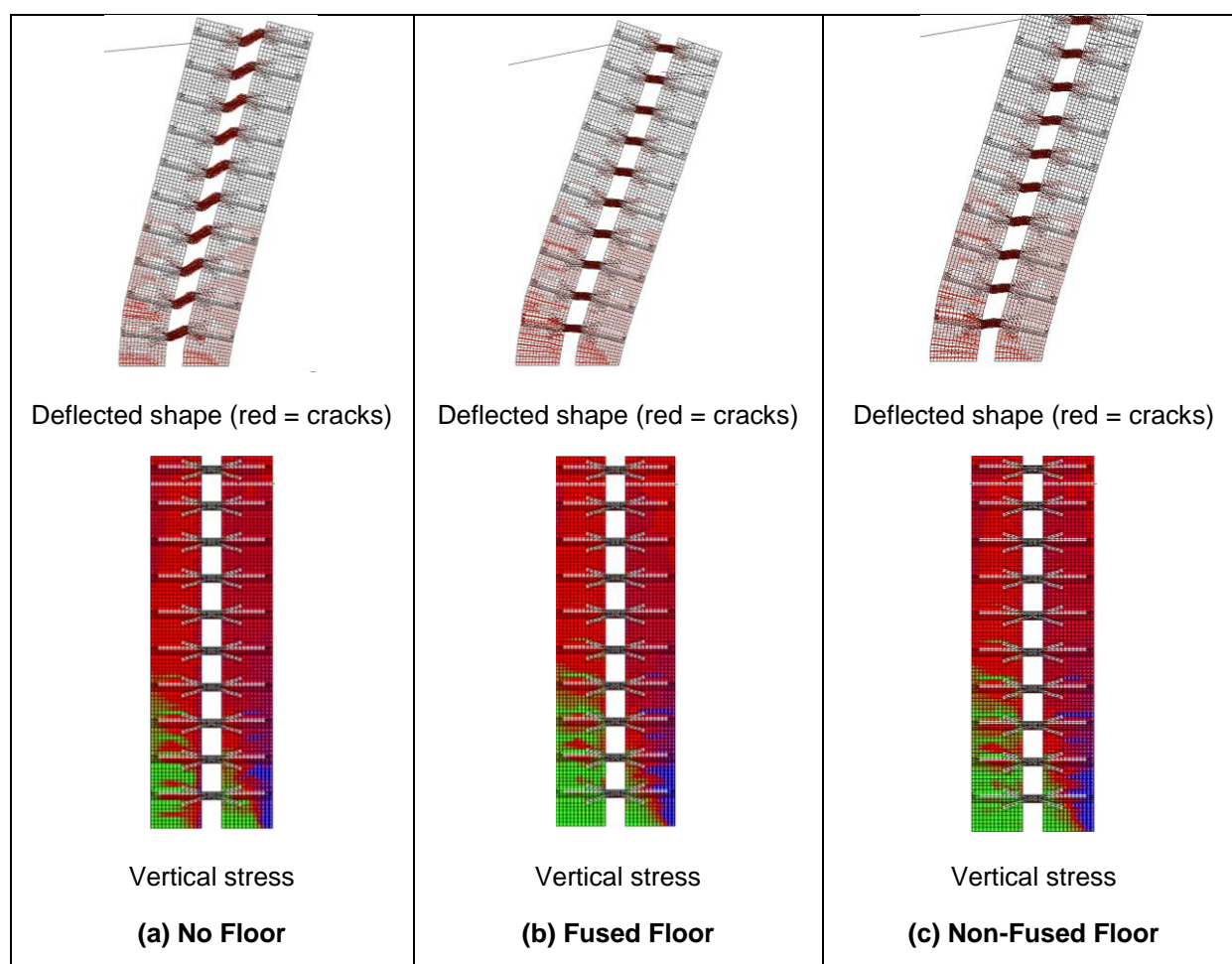


Figure 7-5: Base model visual results at peak wall demand, with different floors considered. Green represents high tension stress, red and blue represent compression stress.

Comparison of the modelled hysteretic behaviour up to peak applied force is presented in Figure 7-6 (a)-(c). The inclusion of floors can be seen to have increased the coupled wall strength significantly.

However comparison to predicted overstrength capacities indicated that NZS 3101:2006 (2014 Amdt) provided reasonable correlation to the measured wall capacity. Where floors were excluded from the model, a slightly (15%) unconservative overstrength was observed because coupling beam axial forces were not considered in NZS 3101:2006 when floors were excluded. However with floors included, NZS 3101:2006 (2014 Amdt) provided good prediction of the overstrength base shear. Inclusion of a floor system was also observed to have resulted in a much more pinched hysteretic response, with lower energy dissipation.

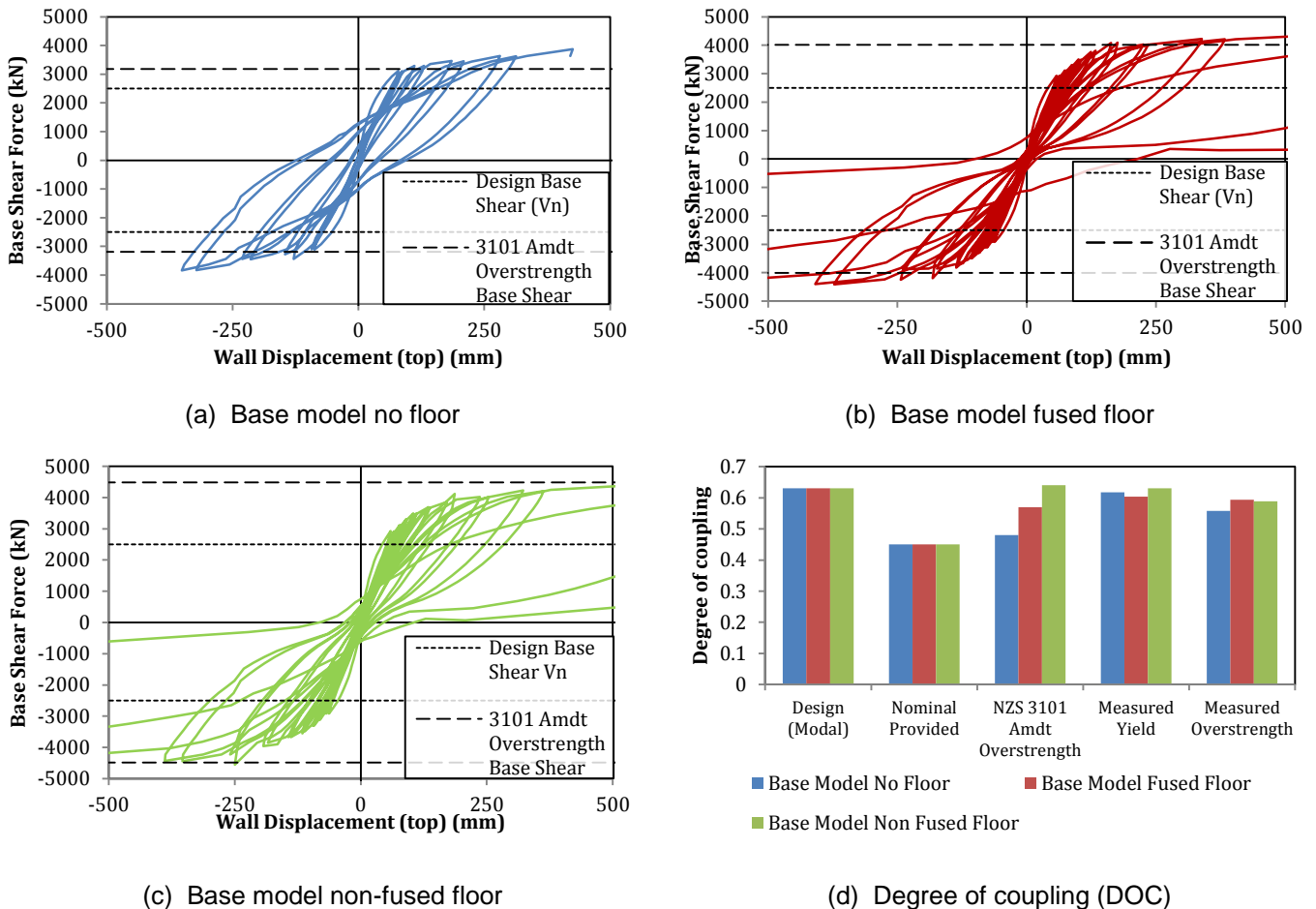


Figure 7-6: Base model global response results

The degree of coupling (DOC) was defined as the proportion of the total overturning moment M_{OT} resisted by coupling action:

$$DOC = \frac{\sum V_{CB}L}{M_{OT}} \quad (7-1)$$

The coupling action contribution was provided by the axial force induced in the wall piers, multiplied by the wall pier lever arm, L , between centroids of the wall piers. Wall pier axial force were provided by the cumulative coupling beam shear force $\sum V_{CB}$. The degree of coupling provided a measure of the lateral force resistance of a coupled wall. A low degree of coupling indicated that force was resisted by flexure in the wall piers and axial force (induced by coupling beam shear) in the wall piers, as intended in conventional coupled wall design. A high degree of coupling meant the coupled wall tended to

behave similar to a single cantilever wall with penetrations, with the majority of lateral force resistance provided by axial forces in the wall piers. As presented in Figure 7-6 (d), the initial DOC based on modal analysis was high as the coupling beam stiffness attracted large shear demand. To meet minimum wall reinforcement requirements, the wall piers were stronger than the modal analyses predictions, which gave a lower nominally provided DOC than that predicted based on the modal analyses. Due to the floor contribution to coupling beam overstrength capacity, the predicted overstrength DOC was a function of the floor interaction.

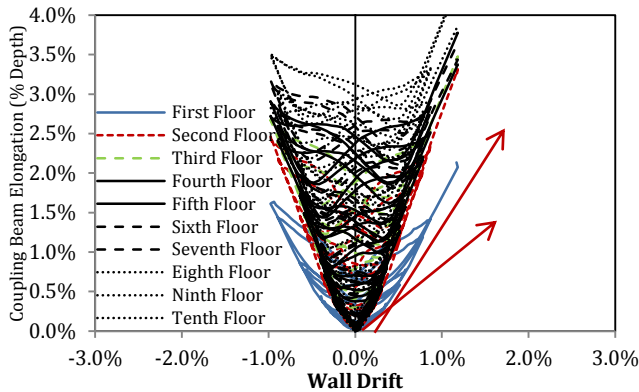
Comparison to the DOC's determined from the model results indicated that the measured DOC's were relatively constant across the three floor types, due to the tension wall capacity limiting the extent of coupling beam strength (V_{CB}) increase. The calculated DOC's were also observed to have reduced slightly as the walls were loaded to overstrength. This reduction in DOC as the walls were pushed towards overstrength was the result of the wall piers gaining strength due to strain hardening, while the coupling beam capacities remained approximately constant.

7.2.1 Coupling beam performance

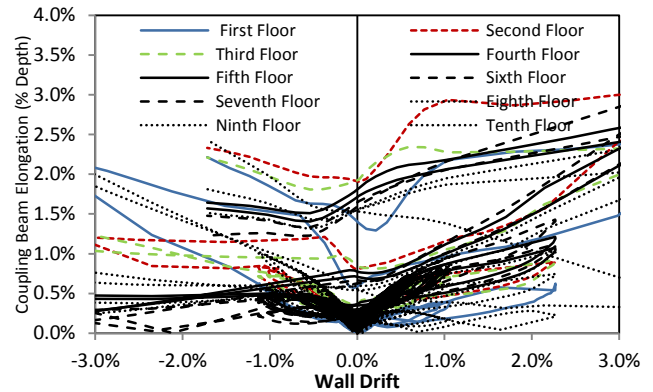
Base model results specific to coupling beam performance are presented in Figure 7-7. The coupling beams were observed to have elongated by pushing the wall piers apart, as presented in Figure 7-7 (a) and (b). However the inclusion of floors in the base model was found to have significantly reduced the coupling beam elongation in two ways. Firstly, the floors were observed to have acted as ties between wall piers to prevent them from moving apart. Secondly the floors increased the capacity of the coupling beams because they acted as effective flanges, in addition to inducing axial compressive forces to restrain elongation. Due to the increased coupling beam capacity, the coupled wall began to behave more like a single cantilever wall, with a higher proportion of the overall coupled wall deformation being concentrated into plastic hinges at the base of the wall piers. As a result, the coupling beams were subjected to a lower plastic strain demand and therefore their tendency to elongate was reduced by the interaction with a floor system.

A further pattern noted in the coupling beam elongation results was that when floors were isolated from the coupled wall, see Figure 7-7 (a), the elongation for all coupling beams above level one was approximately constant. However due to high resistance of the wall piers to being pushed apart near the base, the first level coupling beam elongation was restrained to approximately half of the upper level magnitudes. The rate of development of this elongation at level one was also observed to have increased, as indicated by the arrows in Figure 7-7 (a). This change in elongation rate corresponded to approximately 0.2% wall drift, which aligned with the first longitudinal wall reinforcement yield. This finding indicated that the first level coupling beam did not elongate appreciably until after the wall piers began to yield because the level one coupling beam was unable to yield until after formation of plastic hinges at the base of the wall piers. Consequently, only recoverable geometric elongation in the elastic range was observed in this coupling beam prior to wall pier plastic hinge formation. However after the wall piers developed plastic hinges, the restraint applied to the level one coupling beam was relaxed.

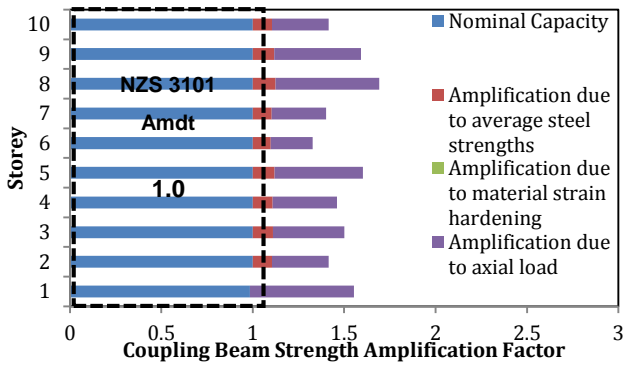
Consequently the level one coupling beam was able to yield and so exhibited more rapid inelastic elongation development.



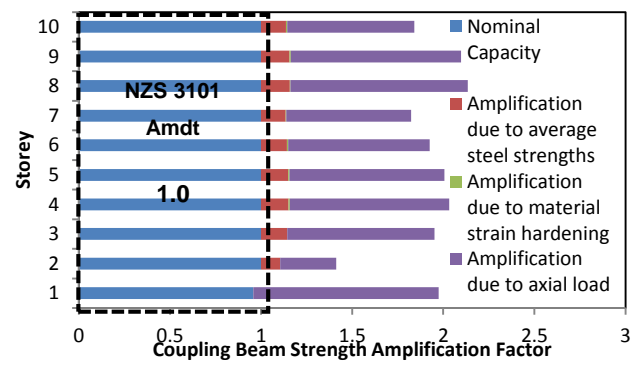
(a) Coupling beam elongation



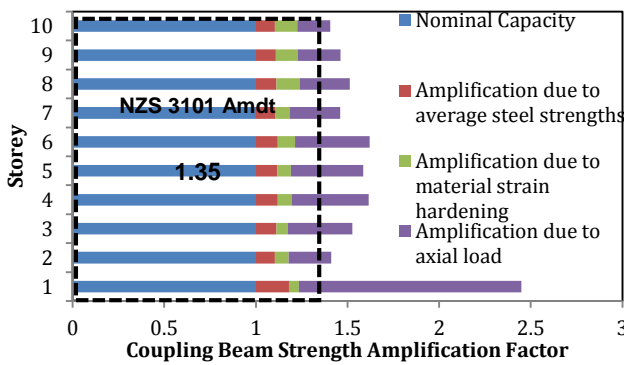
(b) Coupling beam elongation



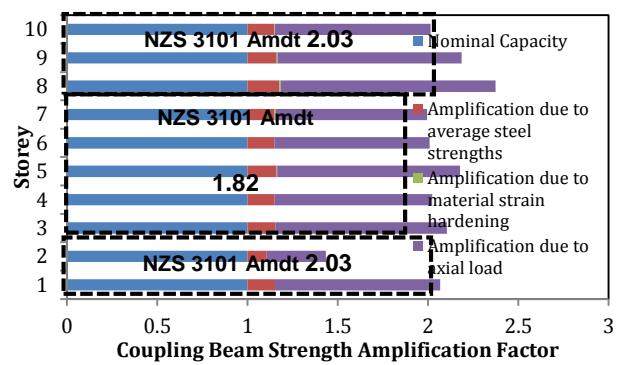
(c) Coupling beam strengths at wall yield



(d) Coupling beam strengths at wall yield



(e) Coupling beam strengths at peak wall capacity



(f) Coupling beam strengths at peak wall capacity

No Floor Model

Fused Floor Model

Figure 7-7: Base model coupling beam results (Plots a, c, e, shown on the left, relate to the coupled wall model without floors. Plots b, d, f, shown on the right, relate to the coupled wall model which included a fused floor)

The coupling beam strengths determined from the model results are compared to their nominal design strengths in Figure 7-7 (c) to (f), to assess the extent to which the coupling beam strengths were amplified by axial restraint effects. Coupling beam strength amplifications were broken down into

contributions from average material strengths (as compared to lower characteristic), strain hardening, and axial forces induced by coupling beam restraint. Comparison was made to strength predictions based upon NZS 3101:2006 (2014 Amdt). Note that the provisions of NZS 3101:2006 (2014 Amdt) included the effect of floor axial restraint on coupling beam overstrength. However no provision for the axial restraint provided by wall piers was included. Material overstrength factors of 1.35 were also included for both Grade 300 and Grade 500 reinforcement.

The nominal strength comparisons, shown in Figure 7-7 (c) and (d), showed that coupling beam strengths at the onset of yield in the coupled wall were underestimated by existing design methods. The reason for this underestimation was observed to have partly resulted from material properties exceeding lower characteristic values. However the primary reason for the strength underestimate was that existing design procedures did not consider the contribution of axial restraint compressive forces in the nominal coupling beam capacity. NZS 3101:2006 (2014 Amdt) assumed that axial restraint only became significant in the coupling beams at overstrength. However the majority of the coupling beam axial restraint force was found to have developed at nominal wall capacity, which gave rise to larger than predicted nominal capacities. As the axial restraint was activated at or near nominal capacity, little extra coupling beam strength was gained as the wall was pushed to overstrength. Consequently the nominal capacity of the overall coupled wall, and of individual coupling beams, was under-predicted when using existing design procedures.

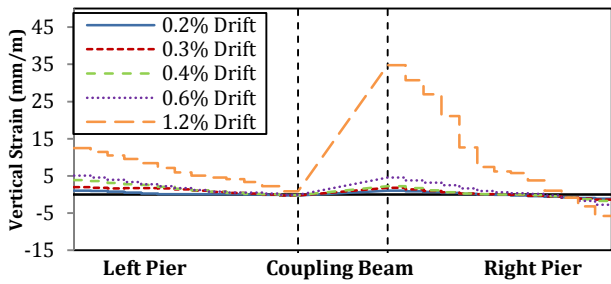
NZS 3101:2006 (2014 Amdt) provisions for coupling beam overstrength capacity were compared to the modelled coupling beam overstrengths (taken at peak wall demand) in Figure 7-7 (e) and (f). When floors were included in the model, the NZS 3101:2006 (2014 Amdt) provisions for coupling beam overstrength provided good correlation to the measured coupling beam overstrength capacities. However when floors were excluded from the model, axial restraint was not included in the overstrength provisions of NZS 3101:2006 (2014 Amdt) and consequently the coupling beam overstrength capacities were under-predicted.

A final observation related to the performance of the coupling beams in the base model was that as the coupled wall was pushed towards overstrength, the level one coupling beam tended to jack the base of the walls apart, and therefore a larger axial force was induced in the level one coupling beam. As seen in Figure 7-7 (e), the increase in level one coupling beam axial force was associated with a reduction in the axial forces of the upper coupling beams. Consequently these upper level coupling beams elongated more under a relaxed axial restraint force and activated a higher strain hardening component.

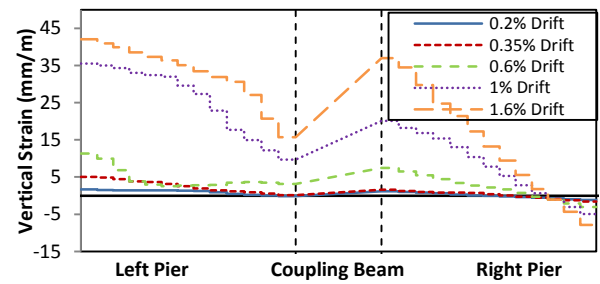
7.2.2 Wall pier performance

A comparison of wall pier vertical stress and strain measurements for the base model is presented in Figure 7-8. When floors were not included, as per Figure 7-8 (a) and (c), the stress and strain profile indicated that flexure occurred in both wall piers. In contrast, analysis of Figure 7-8 (b) and (d), for the case where a floor was included, demonstrated that the tension wall was stressed entirely in tension, and began to uplift as the coupled wall responded analogously to a single cantilever wall. Results

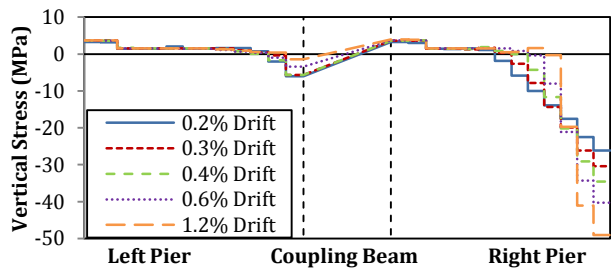
presented in Figure 7-8 (c) and (d) showed that the compressive wall stress demands did not increase significantly, despite this change in deformation behaviour. Demands on the compression wall were not increased because the tension wall yielded and limited the axial compressive force induced. However, as shown in Figure 7-9, tension strains at the base of the walls were observed to have increased markedly with floors included, as the tension wall was yielded in tension before the coupling beams yielded. These tension strains were measured in the heavily reinforced boundary elements at the edges of the wall piers. In addition, larger tension wall crack widths reduced the shear capacity of the tension wall, which reduced the tension walls shear resistance.



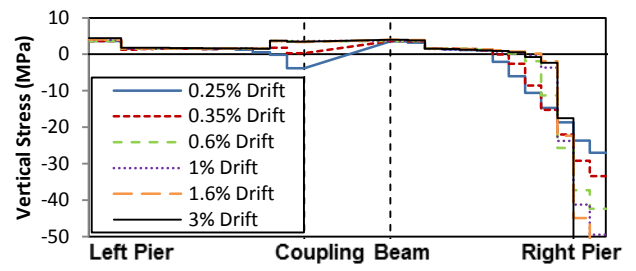
(a) No floor model - Wall pier vertical strain



(b) Fused floor model - Wall pier vertical strain

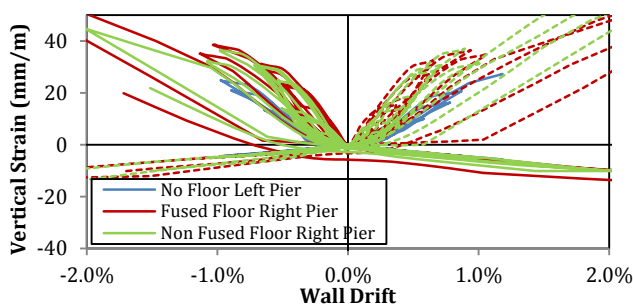


(c) No floor model - Wall pier vertical stress

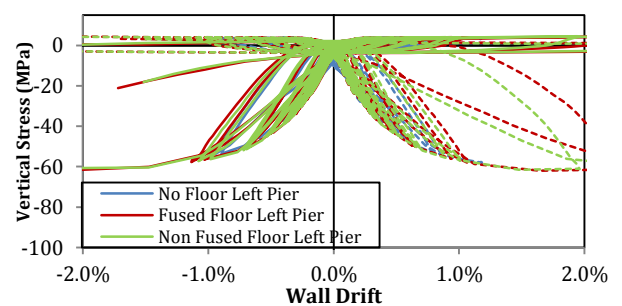


(d) Fused floor model - Wall pier vertical stress

Figure 7-8: Base model wall pier vertical stress and strain measurements taken at base of wall



(a) Wall boundary element strain

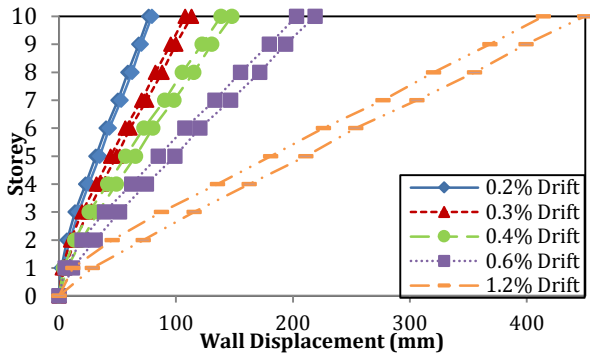


(b) Wall boundary element stress

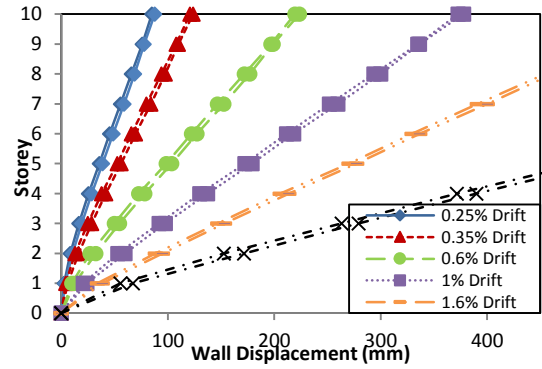
Figure 7-9: Base model external boundary element stress and strain taken at base of wall (compression stress and strain negative, dashed lines represent opposite wall pier)

Presented in Figure 7-10 is a series of wall deformation plots for the base model including and excluding floors. Analysis of wall pier displacements, shown in Figure 7-10 (b), indicated that the fused floor was observed to exhibit increased interstorey drift towards the top of the wall which is more typical of a typical cantilever wall deflected shape than of a coupled wall deflected shape. In contrast, the no floor

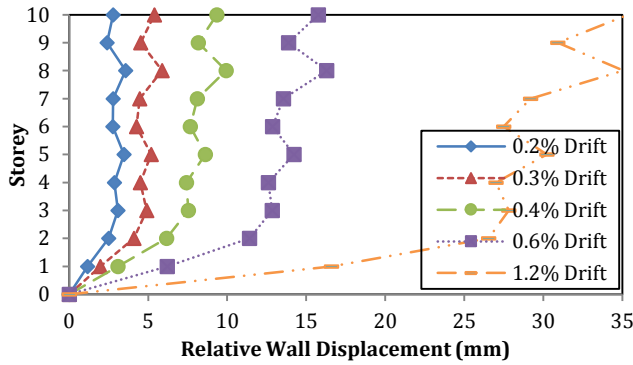
model, shown in Figure 7-10 (a) tended to deform more like a coupled wall was designed to deform, with peak interstorey drift near mid-wall height. These deflected shapes reflected the change in mechanism which occurred due to floor inclusion. Shown in Figure 7-10 (c) and (d) are the wall pier relative displacements, taken as the difference in wall pier deformations. Comparison of these plots showed that relative wall pier displacements were much larger when no floors were included than with floors included. These floors acted to tie the wall piers together and constrained the walls to displace together by restricting coupling beam elongation.



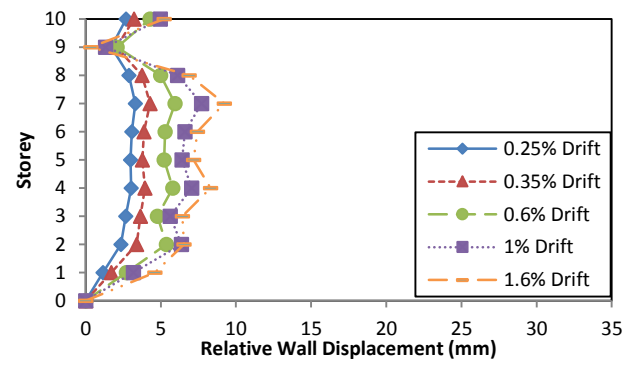
(a) No floor model – Wall pier displacements (Left pier shown on left, right pier shown on right)



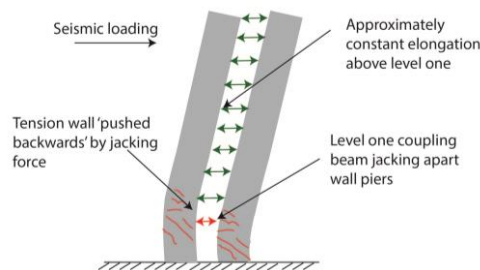
(b) Fused floor model – Wall pier displacements (Left pier shown on left, right pier shown on right)



(c) No floor model – Pier relative displacement



(d) Fused floor model – Pier relative displacement



(e) Coupled wall relative deformation due to jacking effect of level one coupling beam

Figure 7-10: Base model wall pier displacements (Drifts taken at top of wall)

As shown in Figure 7-10 (c) and (d), the relative wall displacement developed predominantly in the lower storey (or two storey's for larger drift levels), above which the wall piers remained approximately parallel. This deformation pattern was found to result from the first floor coupling beam jacking the wall

piers apart, which increased the level one coupling beam axial compressive force, as shown in Figure 7-10 (e). Relative deformation induced by jacking of the level one coupling beam caused the walls to deform outwards and relax the axial restraint applied by the walls to the upper coupling beams so that the walls remained approximately parallel in the upper storeys. This was particularly true when floors were included in the model as the floors acted as ties to constrain the wall piers to deform together.

Shear stress demands observed at the base of the wall piers are presented in Figure 7-11 for the model excluding floors. The tension wall (left) resisted a negligibly small proportion of the base shear, which was redistributed to the compression wall. Based upon the shear stresses presented in Figure 7-11, the jacking apart of the wall piers by the first level coupling beam was not opposed by an additional shear demand in the tension wall. An important implication of this finding was that the walls were not observed to have activated shear stresses in opposing directions. Therefore the jacking effects at the first floor level did not directly increase the total coupled wall shear demand, by pushing the walls apart. Instead the jacking apart of the wall piers tended to enhance the proportion of base shear redistributed to the compression wall. Shear design of coupled wall piers has traditionally apportioned shear between wall piers based upon their overstrength moment capacity. Provided the wall pier axial forces were based upon the actual amplified coupling beam capacities presented above, the existing approach to the distribution of shear between wall piers was therefore found to be adequate.

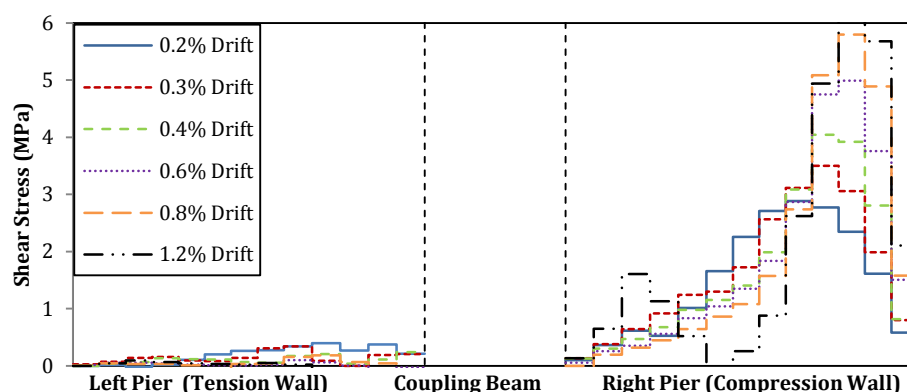


Figure 7-11: Shear stress demand (based on total wall section area) at base of wall piers for base model no floors. Drifts taken at top of walls.

As previously discussed, the jacking effect of the first floor coupling beam tended to redistribute coupling beam axial compressive forces towards level one. As a result, the attraction of more compressive axial force to the level one coupling beam caused the lateral force that was applied to the compression wall to have a lower force centroid. Hence a higher shear demand was induced for the same total coupled wall bending moment. To account for the lowering of the lateral force centroid in capacity design, a higher value for the dynamic amplification factor (ω_v), which accounts for a similar issue due to higher mode effects, could be used in NZS 3101:2006. However the effect of the lower shear force centroid appeared to be relatively small based on this study where the shear design was found to be adequate.

The base model results are discussed further in section 7.3 where they are compared to a series of coupled wall models based upon different designs.

7.3 Wall model variations

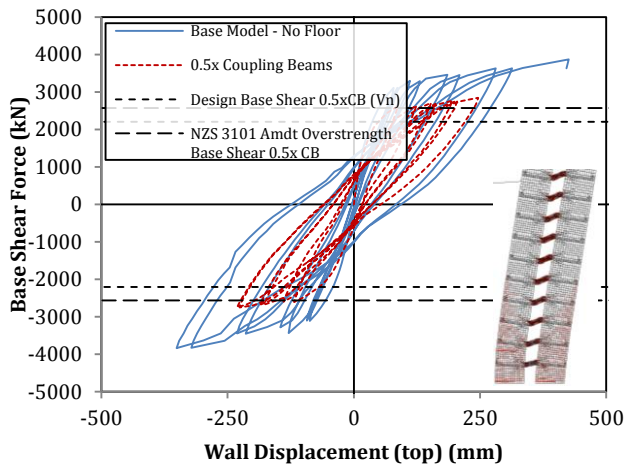
As previously discussed, a series of alternative coupled walls was designed. Each coupled wall design, as discussed below, was analysed in VecTor2 software with each of the three floor arrangements considered. A summary of the results for each coupled wall is presented below, with comparisons made between the different model's behaviour.

7.3.1 Base model with coupling beam variations (1b. 0.5x Base and 1c. 1.5x Base)

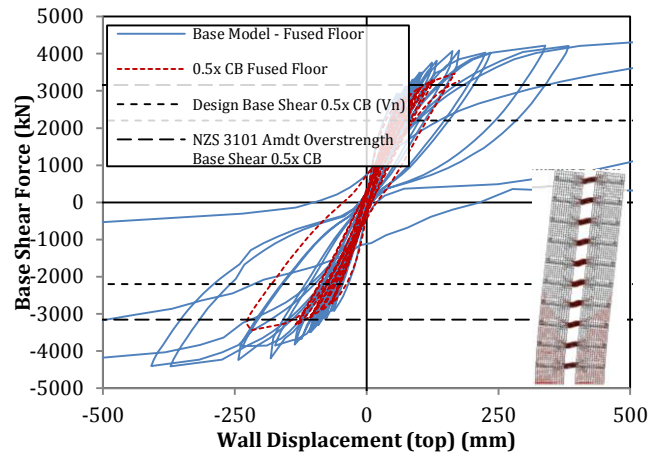
Presented in Figure 7-12 are the modelling results for models 1b. and 1c. (see Table 7-1) which related to the base model with coupling beam design strengths varied. By adjusting the coupling beam capacity but retaining the same walls as for the base model, these models were run in order to assess the effect of coupling beam strength on wall performance. A model with 50% increased coupling beam strength (1c. 1.5x Base) and a model with 50% decreased coupling beam strength (1b. 0.5x Base) as compared to the base model were considered. These models represented a designer's freedom to choose the degree of coupling.

Presented in Figure 7-12 (a) – (c) are the results for when the coupling beam design was weakened by 50% from the base model (1b. 0.5x Base). Comparison to the base model in all floor cases showed a lower base shear capacity, which was within 10% of the design overstrength from NZS 3101:2006 (2014 Amdt). Similar to the base model results, the nominal wall capacity was underestimated for all floor types, with particular severity when floors were included. However analysis of the deflected shapes indicated that weakening the coupling beams allowed the coupled wall deformation mechanism intended by design to form for the full range of floors, in contrast to the base model.

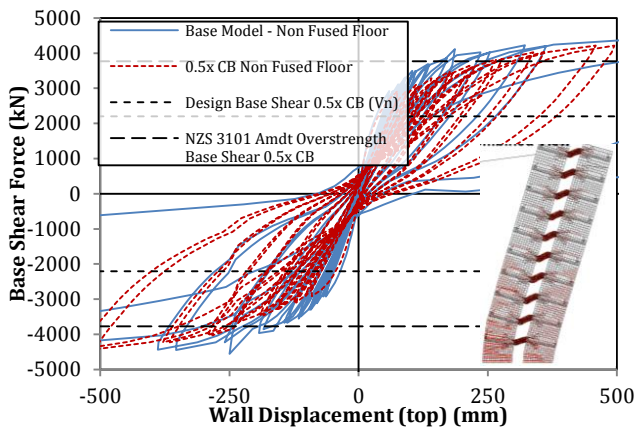
Comparable capacities were observed between the base model (in Figure 7-6 (c)) and the weakened coupling beam model (0.5x Base in Figure 7-12 (c)) when the highest strength (non-fused) floors were included. However the deformation pattern was significantly different, as the base model deformed as a single cantilever due to the tension wall having fully yielded. In contrast, weakening the coupling beams allowed the coupled wall mechanism assumed in design to form for the 0.5x Base model, even when floor interaction was considered. As a result, the 0.5x Base model provided improved energy dissipation and lower wall pier damage whilst sustaining a similar overstrength capacity. This comparison indicated that providing lower coupling beam strength meant that the tension wall pier was more likely to possess sufficient capacity to enforce full coupling beam yield. In this way, a higher level of energy dissipation and a reduction of wall damage was achieved, with little strength reduction, by weakening the coupling beams.



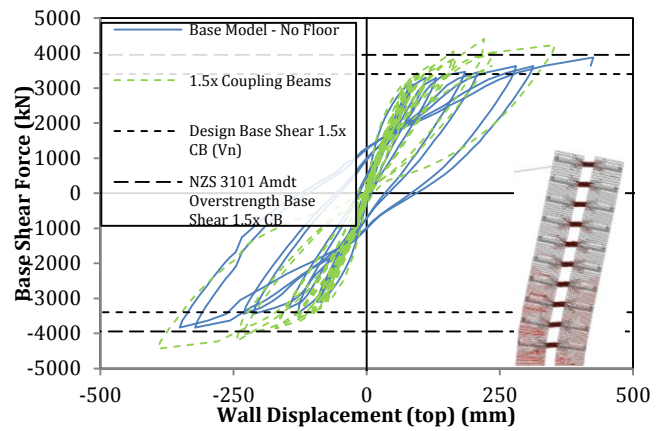
(a) Base 0.5x No floor model



(b) Base 0.5x Fused floor model



(c) Base 0.5x Non-fused floor model



(d) Base 1.5x No floor model

Figure 7-12: Base model and coupling beam variations (0.5x and 1.5x) global modelled responses

Analysis of Figure 7-12 (d) indicated that even without floors included, when the coupling beam strength was increased by 50% (Base 1.5x), the coupled wall inelastic deformation mechanism did not occur, and the tension wall fully yielded before the coupling beams yielded. As a result, the coupled wall behaved as single cantilever wall. Additionally the nominal and overstrength capacity were well predicted as yield of the tension wall prevented the coupling beams from activating their full capacities. However the change in deformation mechanism resulted in a reduction of energy dissipation and more heavily damaged wall piers. This result indicated that if the coupling beams were designed to be too strong, the desired mechanism could not form. Note that the models for 1.5x Base which included floors are not shown because they displayed behaviour similar to the single cantilever wall behaviour previously discussed.

When the coupled wall behaved as a single cantilever wall, due to the tension wall pier yielding instead of the coupling beams yielding, the level of pinching in the hysteresis plots was high. Based on these observations, it was found that as the tension wall was subjected to increasing demands, due to increasing coupling beam capacities, the level of pinching increased. As a result, walls designed with higher coupling beam capacities, tended to result in lower energy dissipation. This finding indicated

that as the amplified coupling beam capacities increased such that the tension wall capacity was approached, the lower the energy that was dissipated. Therefore to avoid this pinching, the coupling beam design capacity could have been reduced to ensure that even when amplified, the coupling beams yielded and the coupled wall mechanism formed.

7.3.1.1 Wall pier performance

The wall displacement in each pier at first floor level is presented in Figure 7-13 for the base model with coupling beam variations. Where the ductile coupled wall mechanism formed (base and 0.5x base models), the relative displacement between the wall piers was found to have increased with applied drift, as the wall piers were jacked apart by coupling beam elongation. As shown in the top right quadrant of Figure 7-13, the tension wall (solid line) was observed to have lagged behind the compression wall (dashed line) in terms of displacement. However the compression wall displacements were consistent between models. Therefore this lag effect was due to the tension wall being 'pushed backwards' in the opposite sense to the seismic demand by the level one coupling beam rather than the compression wall displacement being increased. Minimal relative wall pier displacements were observed for the 1.5x base model because the coupling beams did not elongate significantly.

A residual relative displacement was also observed between the wall piers, as the coupling beam elongation was not recovered during unloading. Consequently the wall piers were displaced outwards at zero applied drift. This residual relative displacement was the result of accumulated plastic shear strain near the base of the walls. The slip associated with this residual shear strain relaxed any axial restraint provided by the wall piers to the coupling beams during unloading and reloading. As a result, the coupling beams exhibited lower capacity upon unloading and reloading which contributed to the pinching observed.

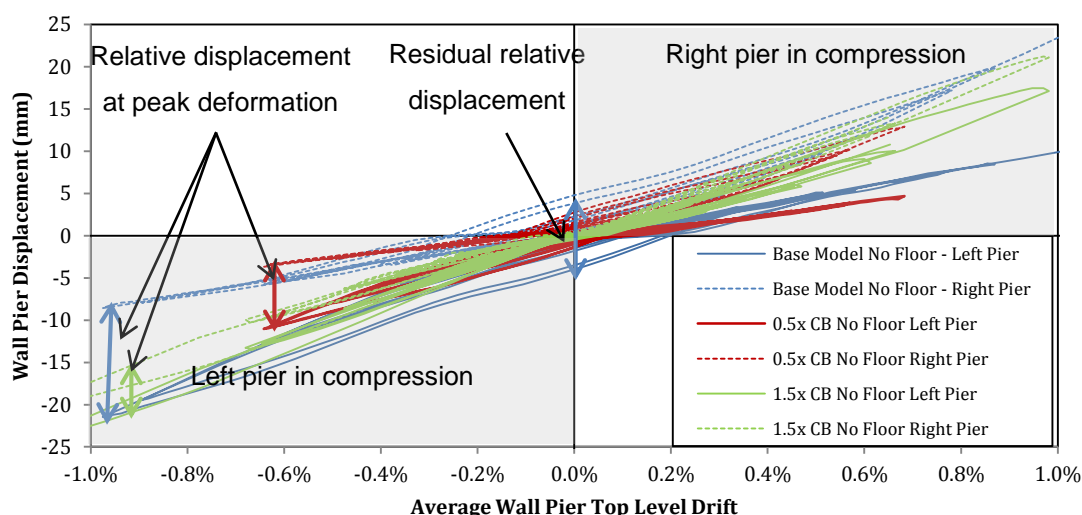


Figure 7-13: Base model no floor relative wall pier displacements at first floor level.

A comparison of stress distributions at the base of the walls is presented in Figure 7-14. A compression zone was observed in the tension wall pier when the coupling beams were weakened, as shown in

Figure 7-14 (a) and (b), which indicated that both walls were deforming according to their coupled wall design intent. The inclusion of a floor system was observed to have increased the compressive demands in the compression wall slightly, as the strength of the coupling beams was amplified. Although the increase in compressive wall demands was small, it could have a significant impact on ductility capacity as non-ductile crushing or buckling failures became more likely. Analysis of Figure 7-14 (c) indicated that when the coupling beams were strengthened, the tension wall was subjected to tension only as it uplifted and the entire coupled wall behaved as a single cantilever. A comparison of the wall extreme compression fibre strain is presented in Figure 7-15 (a), which showed that as the coupling beams strength increased the wall pier tensile strain demand increased significantly. This indicated that the coupled wall was behaving more like a single cantilever as the coupling beam strength increased.

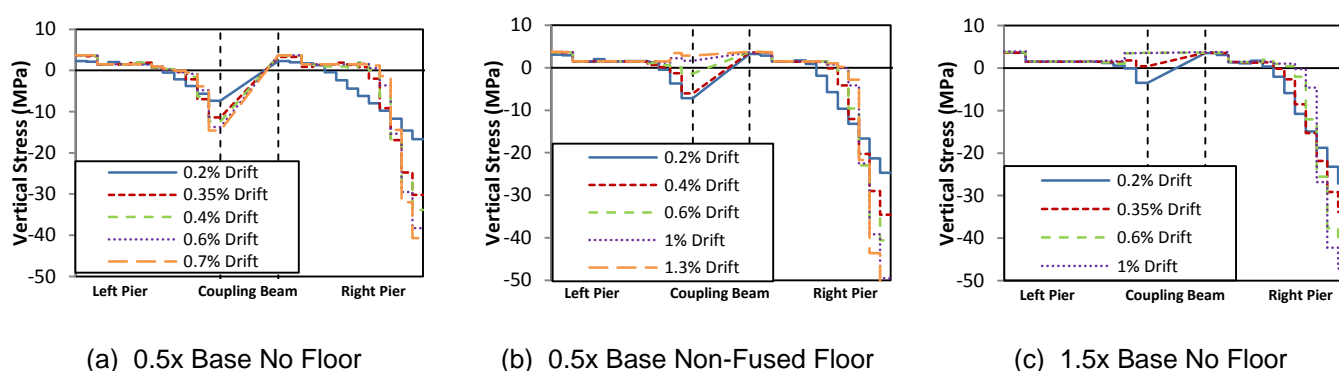


Figure 7-14: Base model coupling beam variations (1.5x and 0.5x) wall pier vertical stress (drift taken at top of wall piers)

Presented in Figure 7-15 (b) is a comparison of the degree of coupling as coupling beam strengths were varied. An important point to note is that the nominally provided degrees of coupling (DOC's) were significantly different. However the measured DOC's were approximately equal. This convergence of DOC occurred despite the deformation mechanisms and strength hierarchies differing, which suggested that regardless of the design intent, resistance to overturning moment in the coupled wall tended to distribute approximately evenly (a DOC of 0.5 indicated even distribution) between wall piers in bending, and the axial force induced by coupling action. When the nominal DOC was lower, the assumed coupled wall mechanism was able to form, which was not the case when the nominal DOC was higher. Adjustment of the nominally designed DOC therefore had a major impact on the strength hierarchy of the system. In this case, targeting a design DOC of 0.35 resulted in the intended coupled wall mechanism being able to form regardless of floor types. In contrast, this mechanism did not form when targeting a design DOC in excess of 0.55, even without floor interaction. Comparison to the base model design DOC, presented in Figure 7-6, indicated that a design DOC of 0.45 allowed the ductile mechanism to form. However when floors were included, the inelastic response of the coupling beams was limited, suggesting the onset of a mechanism change. Therefore a design DOC of approximately 0.5 was found to be an indicative limit, above which a coupled wall deformation mechanism was unlikely to form to a significant degree. Above 0.5 DOC, the coupling beams were

likely to be too strong to yield significantly when axial restraint was considered, causing the coupled wall to behave as a single cantilever wall.

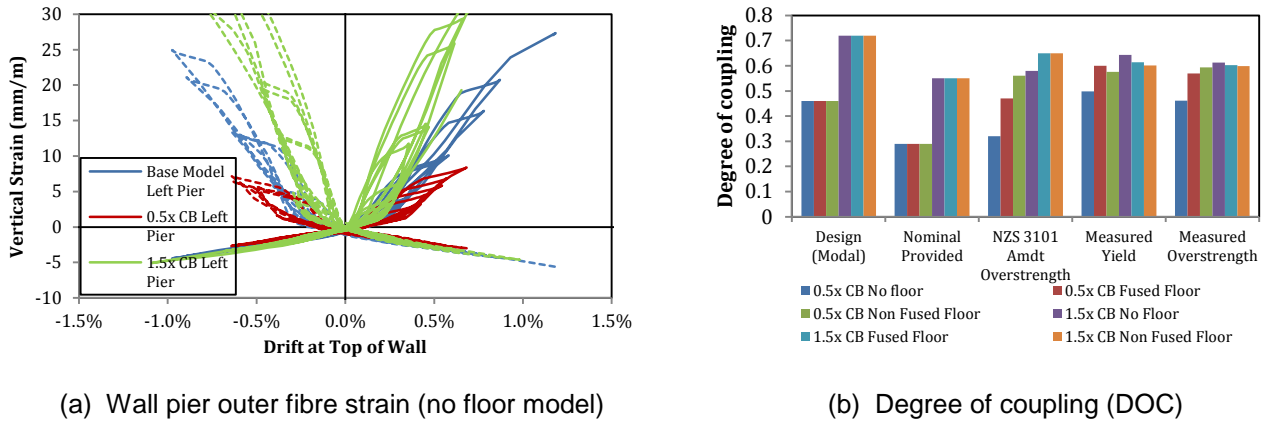


Figure 7-15: Base model coupling beam variations (1.5x and 0.5x) wall strain and degree of coupling

7.3.1.2 Coupling beam performance

A comparison of measured coupling beam elongation, as coupling beam strength was varied, is presented in Figure 7-16. As coupling beam strength was increased, the axial elongation of coupling beams was found to have reduced. The reason for this reduction was that as the coupling beam capacity was increased, a lower plastic strain demand was imposed on the coupling beams and hence a lower tendency to elongate was observed.

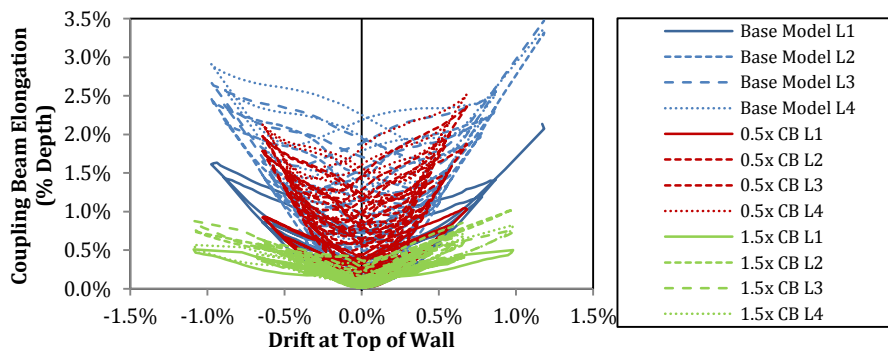


Figure 7-16: Base model coupling beam variations (1.5x and 0.5x) lower coupling beam elongations

Strength amplification factors for the coupling beams are presented in Figure 7-17, for the base models with coupling beam variations. NZS 3101:2006 (2014 Amdt) predictions of capacity when the coupling beams were strengthened (1.5x Base), presented in Figure 7-17 (c) and (f) at yield and peak demand respectively, were well correlated to measured values. Coupling beam strength amplifications in these cases were found to be relatively low because the tension wall was fully yielded which suppressed the amplification of coupling beam strengths.

When coupling beams were weakened as compared to the base model (0.5x Base), the coupling beam strength amplifications were much larger and the NZS 3101:2006 (2014 Amdt) predictions much less accurate. These amplifications were larger because when a lower degree of coupling was used, the

coupling beams were subjected to higher ductility demands. Consequently the coupling beams elongated more and hence activated larger axial restraint forces.

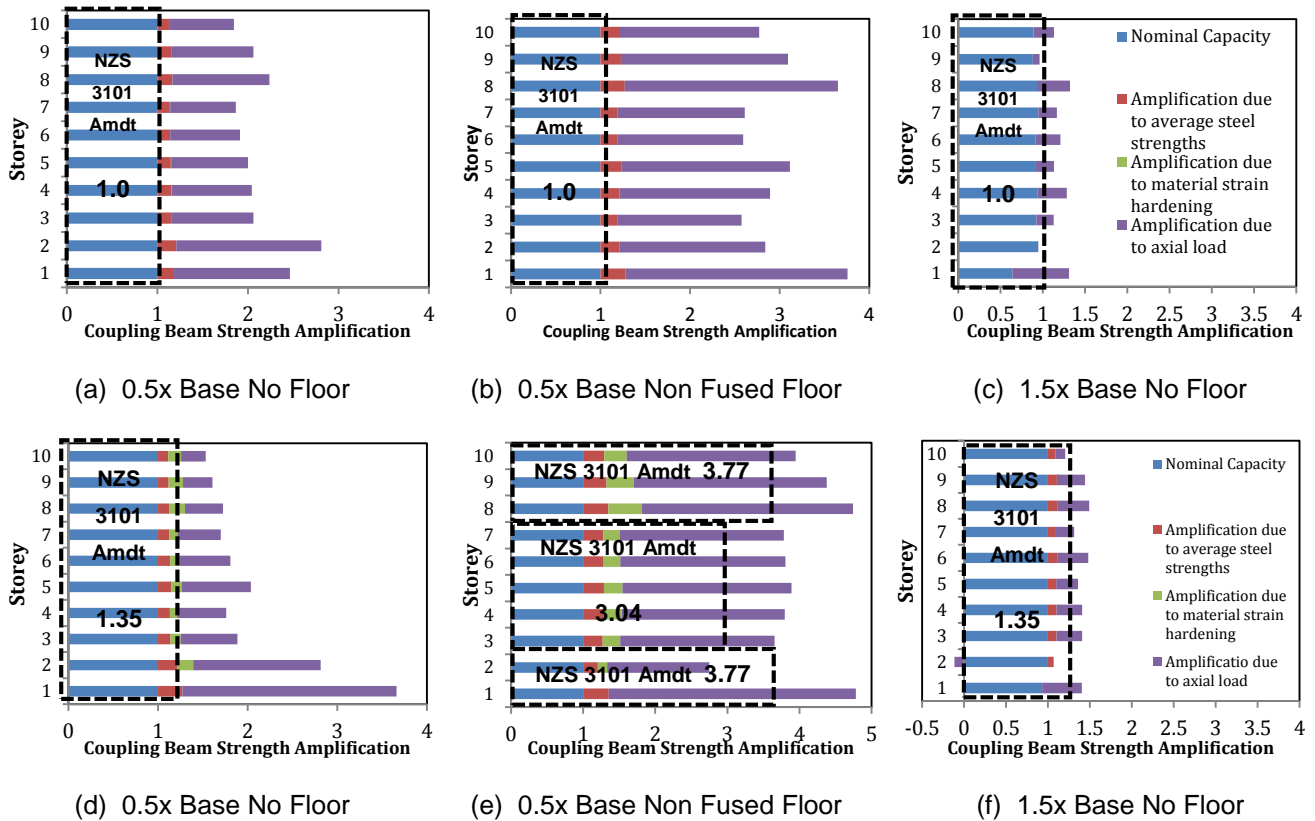


Figure 7-17: Coupling beam strength amplification factors for base model with coupling beam variations. (a)-(c) taken at wall yield, (d)-(f) taken at wall peak demand.

Enforcement of the intended coupled wall mechanism, whilst providing good energy dissipation, has been found to result in much larger strength amplifications in coupling beams. Whilst these amplifications were generally underestimated by NZS 3101:2006 (2014 Amdt), the underestimate was moderate with floors included. Assuming that the floors and coupled walls behaved independently was found to result in unconservative estimates of coupling beam capacity because axial restraint in NZS 3101:2006 (2014 Amdt) was assumed to have only developed due to floor interaction. However axial restraint was observed to be generated by the wall piers, even in absence of floor interaction. This finding suggested that the provisions of NZS 3101:2006 (2014 Amdt) did not account for a significant component of the axial restraint applied to coupling beams (from the wall piers). This effect was somewhat concealed in the models which included floors because the provisions of NZS 3101:2006 (2014 Amdt) tended to over-predict the effect of floors in the overstrength capacity of coupling beams.

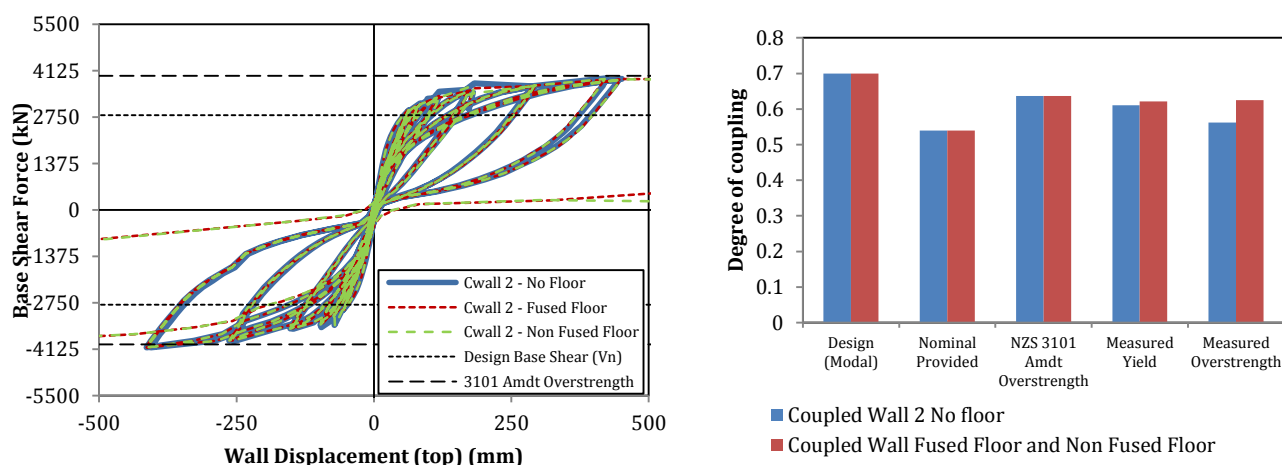
It was found to be important that a designer be aware of the magnitude of coupling beam strength amplifications when detailing a coupled wall. Whilst the overstrength capacities for the beams were reasonably well predicted by NZS 3101:2006 (2014 Amdt) requirements when floors were considered, the nominal coupling beam capacity was observed to be of the order of 2-3x design capacity when the coupled wall mechanism that was assumed in design had formed, but to be much lower when the coupled wall behaved as a single cantilever. Strength amplifications of this magnitude were found to

have a significant effect on the strength hierarchy formation. In addition, the overall coupled wall overstrengths were found to be under-predicted by up to 15%, particularly when the floor was isolated from the coupled wall. Therefore designing for a low degree of coupling provided improved coupled wall energy dissipation but tended to produce a larger nominal and overstrength capacity than would have been predicted by NZS 3101:2006.

7.3.2 Coupled wall 2 (2. CW2)

The design of coupled wall 2 (CW2) was based upon the same wall pier dimensions as the base model, but with a shorter 1 m span coupling beam, as shown in Figure 7-3. CW2 was intended to represent the geometries more typically employed in older buildings in New Zealand, which had high degrees of coupling. As anticipated, modal analysis of CW2 for design purposes showed a stiffer structure, with more shear demand in the coupling beams. More details of the CW2 design are presented in Appendix E.

Basic model results for CW2 are presented in Figure 7-18. For all floor types, the pinched hysteretic responses were essentially identical, with NZS 3101:2006 (2014 Amdt) accurately predicting the overstrength capacity. This observed accuracy was because even without floor interaction, the coupling beams were found to be too strong to yield, resulting in the tension wall pier activating fully in tension to limit the system capacity. The relatively high nominal provided degree of coupling of 0.54, presented in Figure 7-18 (b), exceeded the 0.5 indicative limit presented in section 7.3.1. As a result, the coupled wall behaved as a single cantilever due to excessive coupling beam strength. This gave a highly pinched response which was characterised by the tension pier fully yielding and limited inelastic deformation imposed on the coupling beams. This behaviour was anticipated because of the high degree of coupling, resulting from the short coupling beams.



(a) CW2 modelled hysteretic response

(b) CW2 degree of coupling

Figure 7-18: Coupled wall 2 (CW2) basic global modelling outputs

Deformation patterns of coupled wall 2 (CW2) are presented in Figure 7-19, which were in agreement with the wall behaving as a single cantilever due to cumulative coupling beam strengths exceeding the wall tension capacity. CW2 wall piers displaced almost identically due to negligible coupling beam

elongation, and the tension wall pier was observed to be fully activated in tension. Full yield of the tension wall prevented excessive demand being imposed on the compression wall. However the tension wall was subjected to large tensile strain demands as a result, which caused the pinched hysteretic responses as previously discussed. Due to the tension wall having fully yielded in tension, its shear resistance was negligible and so the base shear was redistributed almost entirely to the compression wall.

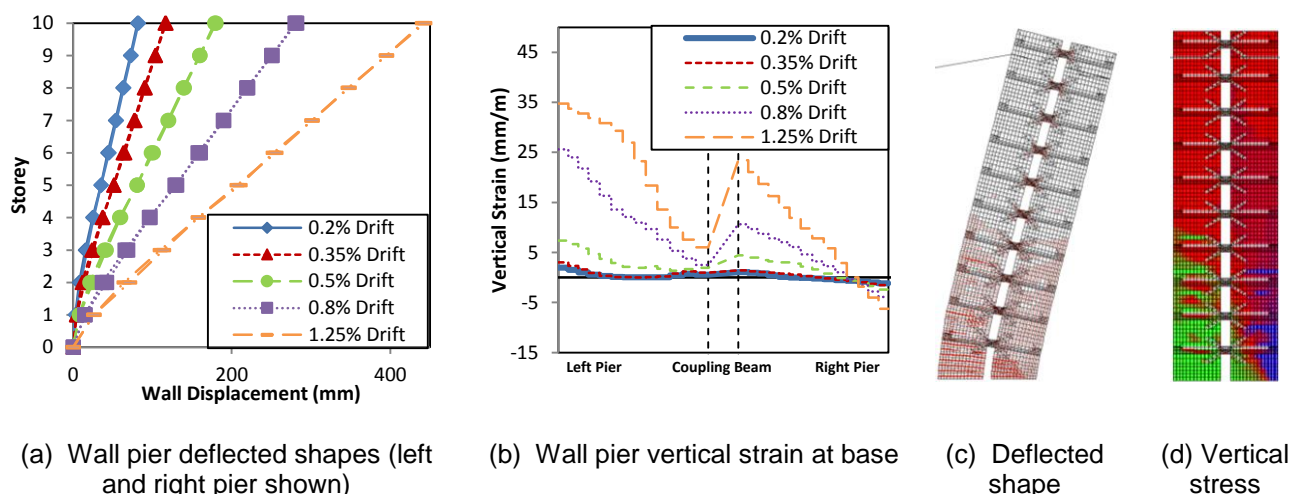


Figure 7-19: Coupled wall 2 – No floor - (CW2) wall pier results (green indicates tension stress, blue indicates compression stress in (d)). Drifts taken at top of wall piers.

Modelling results of CW2 were found to be in agreement with the findings of section 7.3.1, where targeting a high degree of coupling was found to likely prevent the formation of the coupled wall mechanism intended in design. As a consequence, the energy dissipation of CW2 was much lower, with increased wall pier damage, low coupling beam damage and an insensitivity to floor interaction because the coupling beams were already too strong to yield. Whilst CW2 did not achieve the intended deformation pattern, no catastrophic failure was observed as the tension wall acted as a fuse to limit compression wall demands. Additionally the nominal and overstrength capacities of coupling beams and the overall coupled wall were well predicted by NZS 3101:2006 (2014 Amdt). Therefore this wall provided an admissible design to resist lateral loading, provided that the designer was aware of the change in energy dissipation and shear stress distribution. In order to ensure the coupled wall mechanism formed correctly, the design strength of the coupling beams could have been reduced to achieve a lower degree of coupling.

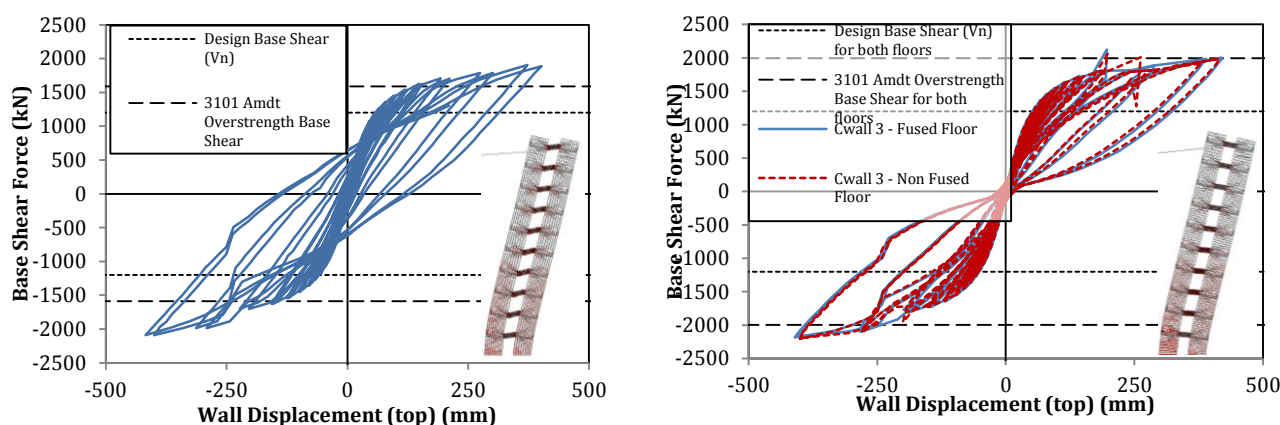
7.3.3 Coupled wall 3 (3.a CW3 and 3.b CW3 x2)

A third coupled wall design was undertaken that varied the wall pier length from the 5m base model length to 3 m, with coupling beam dimensions unchanged. Coupled wall 3 (CW3) was designed as per Figure 7-4 based upon a modal analysis. As a result of the shortened wall piers, the wall was designed as though the building had four coupled walls in each direction (rather than two for the base model) because the modal analysis results showed the building to be excessively flexible. More details of CW3 design properties are presented in Appendix E.

7.3.3.1 Coupled wall 3 (CW3)

Basic modelled results for CW3 are presented in Figure 7-20, where the hysteretic responses with and without floors are compared. Where floors were excluded, as shown in Figure 7-20 (a), the coupled wall mechanism intended in design was observed to have developed, with yielding in the coupling beams and flexure in both wall piers. As a result, the model provided good energy dissipation and the prediction of nominal capacity was reasonable. However, as discussed in section 7.3.1, because the intended coupled wall mechanism formed, global overturning overstrength predictions from NZS 3101:2006 (2014 Amdt) were found to be unconservative by approximately 15% for the no floor model. This finding was the result of a lack of consideration of coupling beam axial restraint when floors were isolated from the coupled wall and was in agreement with previous findings.

CW3 modelled results showed nearly identical responses for the two different types of floor considered. Analysis of the deflected shape and highly pinched hysteretic responses indicated that the intended coupled wall deformation mechanism was unable to form when floors were included, due to excess strength provided to the coupling beams by axial restraint. As a result, the tension wall was activated fully in tension and acted to limit compression wall demands. Consequently when floors were included in the CW3 model, the wall overstrength overturning capacity was well predicted by NZS 3101:2006 (2014 Amdt), in agreement with previous findings.



(a) CW3 No floor model hysteretic response

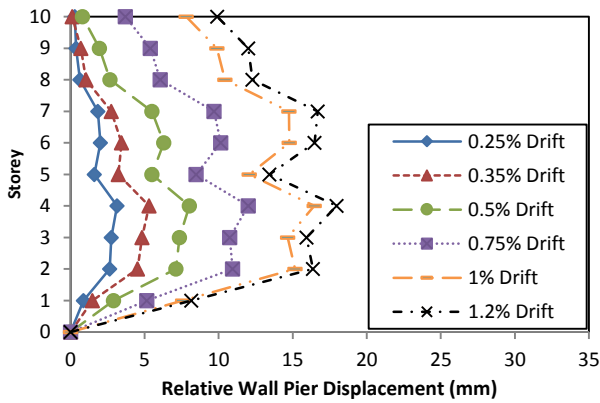
(b) CW3 Fused floor and non-fused floor model

Figure 7-20: Coupled Wall 3 (CW3) global response results

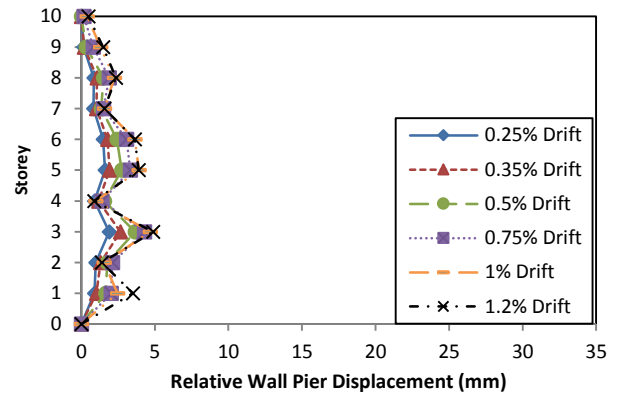
A comparison of wall deformation patterns is presented in Figure 7-21 for CW3 with and without floors. As shown in Figure 7-21 (a), when floors were excluded and the coupled wall mechanism was formed, the wall piers were jacked apart by the lower level coupling beams which induced relative wall pier displacement, as observed in previous models. However what was not observed in previous models as distinctively was that the wall piers tended to move back together towards the top of the building, suggesting that the upper level coupling beams elongated less than the coupling beams at mid-height. The convergence of the wall piers near the top was an indication that the CW3 (no floor) model was on the limit of acting as a single cantilever, as the upper level coupling beams were only just able to yield before the tension wall began to uplift. As presented in Figure 7-23 (a), the design degree of coupling

for CW3 was approximately 0.53, which was in agreement with the findings of section 7.3.1, that 0.5 formed an approximate upper limit to design degree of coupling to enforce the coupled wall mechanism. Comparison to Figure 7-21 (b) indicated that the wall pier relative displacement was small when floors were included, which confirmed the observation that coupling beams did not reach yield when floors were included because they did not elongate.

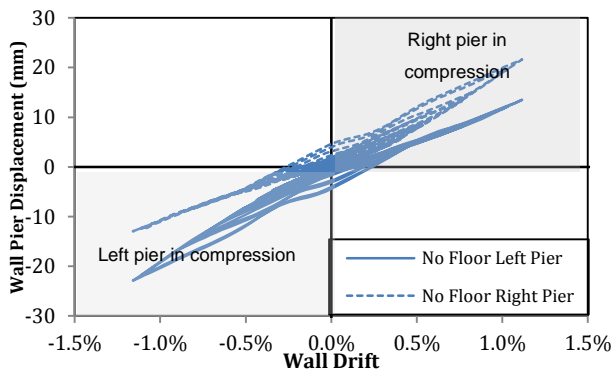
Presented in Figure 7-21 (c) and (d) is the development of first storey wall pier deformation for CW3 no-floor and fused-floor models respectively. As presented in Figure 7-21 (c), the wall piers tended to move apart at high drift levels due to jacking effects of the first floor coupling beam. As a result there was a residual deformation in the wall piers at zero applied drift due to coupling beam axial growth. This observation was in agreement with the results discussed in section 7.3.1, where it was reported that the tension wall deformation tended to lag the compression wall when the walls were proportioned to achieve the desired coupled wall mechanism. As previously discussed, the relative deformation of the wall piers was small when the wall behaved as a single cantilever, as shown in Figure 7-21 (d).



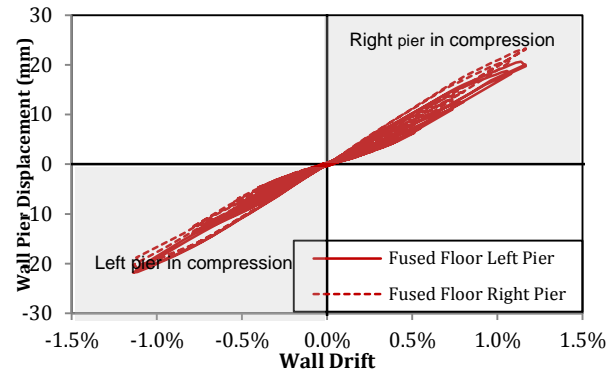
(a) No floor model relative wall displacement



(b) Fused floor model relative wall displacement



(c) First storey wall pier shear deformation (no floor model)



(d) First storey wall pier shear deformation (fused floor model)

Figure 7-21: Coupled Wall 3 (CW3) wall pier displacement results. Drifts taken at top of wall piers.

The results presented for CW3 were found to be similar to those of CW2, whereby the coupling beams were generally too strong to reach yield, particularly when floors were included in the model. For both cases, the tension wall tended to activate fully in tension and uplift before the coupling beams were able

to yield, causing the coupled walls to behave more like a single cantilever wall with penetrations. As a result the hysteretic response became severely pinched and the demands on the compression walls were limited based on the tension wall capacity. The change in behaviour was found to be the result of designing for a high degree of coupling, which did not allow enough contingency for the coupling beams to increase in strength (from their design values) before the coupled wall mechanism was invalidated due to tension wall uplift.

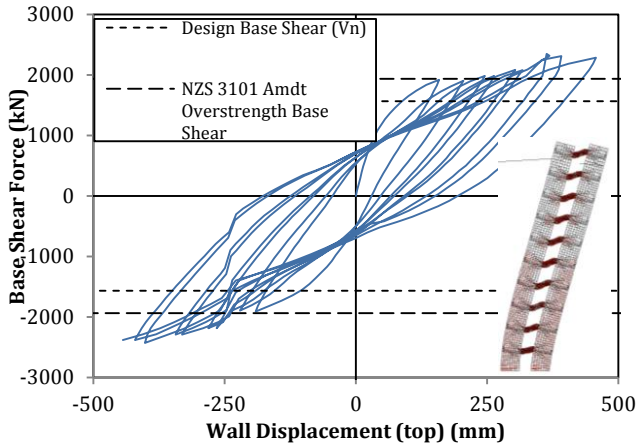
7.3.3.2 Coupled wall 3 x2 (CW3x2)

Despite the findings of CW2 and CW3 being useful for design, the question remained of what would happen if the tension wall was stronger and the full coupling beam strength amplification due to axial restraint was realised. To some extent this scenario was considered with the base 0.5x model presented in section 7.3.1, where the coupled wall strength was found to be larger than anticipated by design. However to consider the effect further, another iteration of coupled wall 3 was run, where the wall piers were assumed to be more heavily reinforced than the original CW3 design based upon modal analysis demands. Such a situation could have arisen where a designer sought to reduce the degree of coupling, to ensure the coupled wall deformed as intended, by strengthening the wall piers. CW3x2 model was run on the basis that the wall pier vertical reinforcement was doubled, with a corresponding increase in shear reinforcement based upon the overstrength capacity design. Coupling beam designs were unchanged from CW3, and the same floor variations were considered in the modelling.

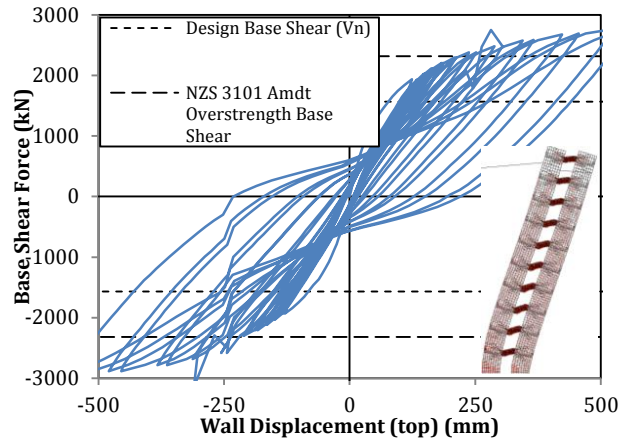
The basic modelling results for CW3x2 are presented in Figure 7-22. The intended coupled wall inelastic deformation mechanism was observed for the full variety of floors in the CW3x2 model, where the coupling beams all yielded prior to full yield of the tension wall. As per previous findings, the nominal capacity was under-predicted by design assumptions, with particular severity when floors were included. The coupled wall overstrength capacities in all CW3x2 floor cases were under-predicted by NZS 3101:2006 (2014 Amdt) by approximately 15-20%. This under-prediction was slightly more pronounced for CW3x2 than for previously discussed models. Relative wall pier displacements at level one, presented in Figure 7-22 (d) for CW3x2, were in agreement with previous findings, as the wall piers were jacked apart by the level one coupling beam.

Presented in Figure 7-23 are the degrees of coupling (DOC's) for the CW3x2 model, and the previous CW3 model for comparison. The nominally provided DOC was decreased from 0.53 in the CW3 model to 0.47 for the CW3x2 model by strengthening the wall piers. As presented above, this small change in DOC led to the coupled walls performing very differently when floors were included. By reducing the DOC, the coupled wall deformation mechanism was able to form for all floor types, providing improved energy dissipation and reduced wall pier damage. In agreement with previous findings, it was found that the DOC tended to converge to approximately the same values at yield and overstrength, despite the design intent. The presented comparison confirmed that improved performance could be achieved by targeting a lower DOC. To target a lower DOC, redistribution of design demands away from the coupling beams could be adopted while maintaining the capacity of the system.

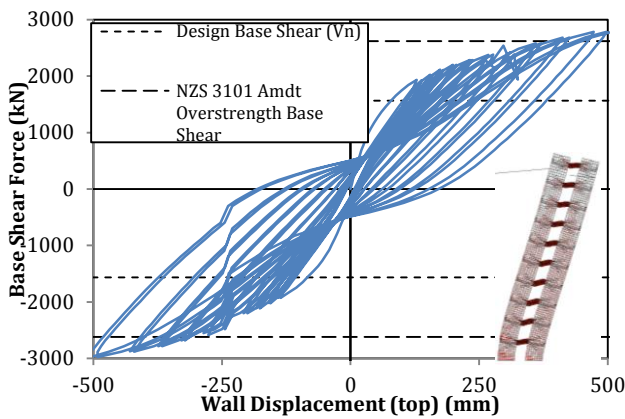
Chapter 7: Coupled Wall Modelling



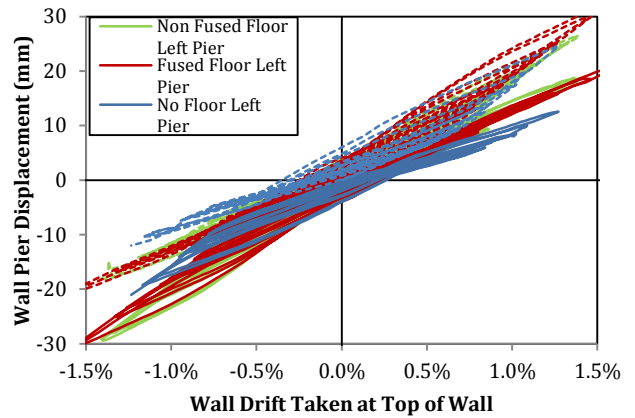
(a) CW3 x2 No floor model response



(b) CW3 x2 Fused floor model response

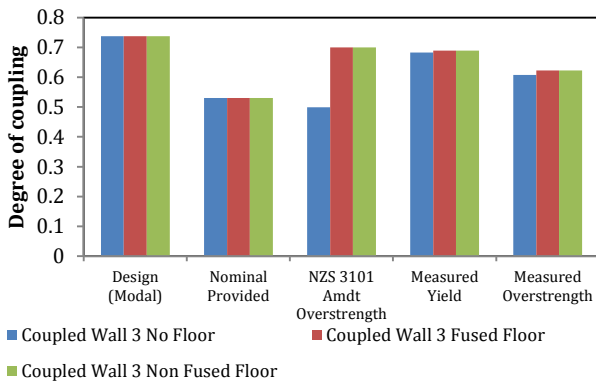


(c) CW3 x2 Non-fused floor model response

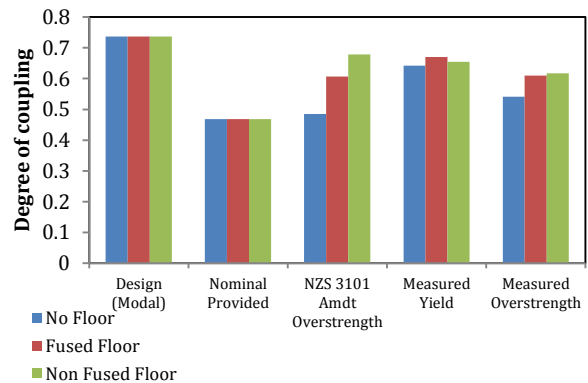


(d) CW3x2 Relative wall pier deformation at first floor level (dashed lines represent right piers)

Figure 7-22: Coupled Wall 3 x2 (CW3 x2) global coupled wall modelling results



(a) CW3 degree of coupling



(b) CW3 x2 degree of coupling

Figure 7-23: Coupled wall 3 (CW3 and CW3 x2) degree of coupling

Wall pier deformation comparisons for CW3x2 are presented in Figure 7-24, which confirmed that the level one coupling beam tended to jack the walls apart as it elongated, and that above level one the walls remained close to parallel, with similar elongation in each coupling beam. The coupling beam inelastic strains which caused the coupling beams to elongate were enforced by the wall pier curvature.

This wall curvature tended to peak at mid-wall height and as a result the coupling beam elongations were largest near the mid-wall height. A comparison of the coupling beam strengths measured in CW3x2 is presented in Figure 7-25. Similar to comparisons made previously, the nominal capacity of the coupling beams was significantly under-predicted in design due to the lack of consideration of restraint forces at nominal capacity. In addition, the difference in capacity between nominal and overstrength was found to be small which confirmed the previous findings that the coupling beams tended to activate the majority of their overstrength capacity at nominal wall capacity, with only a small increase towards overstrength.

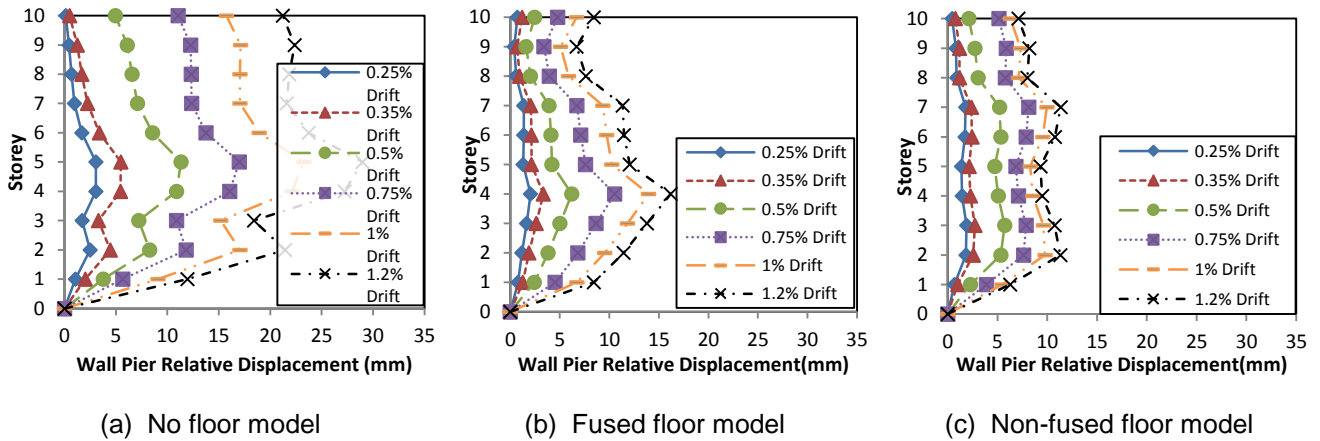


Figure 7-24: Coupled Wall 3 x2 (CW3x2) wall pier relative displacements. Drift taken at top of walls

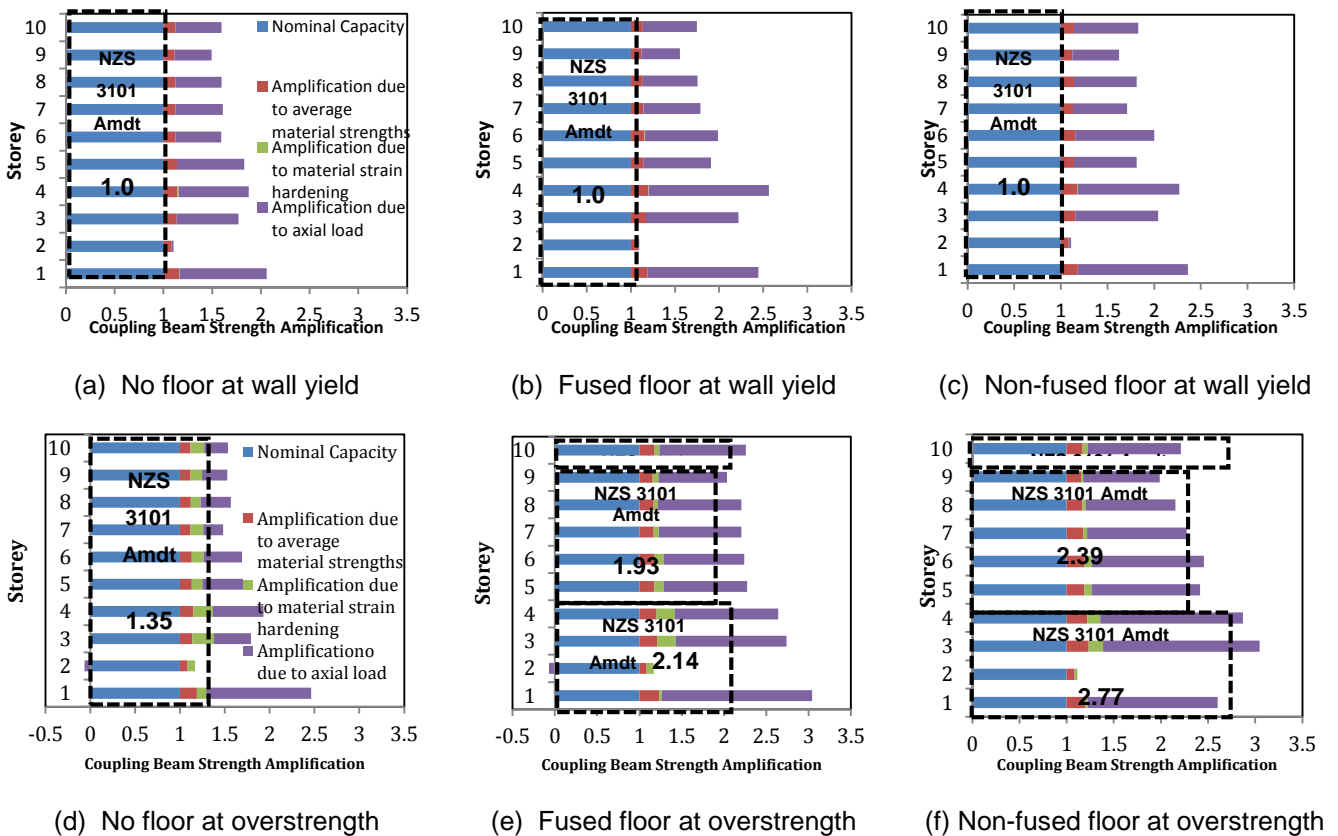
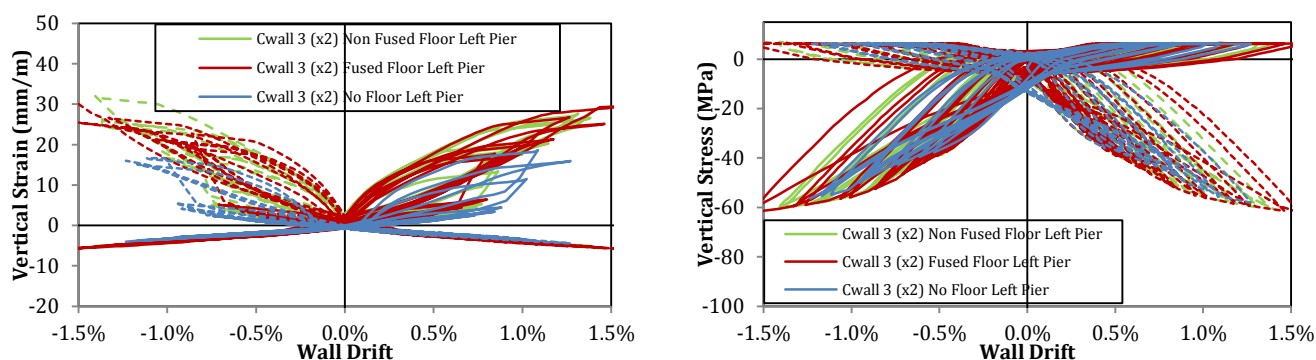


Figure 7-25: Coupled Wall 3 x2 (CW3 x2) coupling beam strength amplification factors

The magnitude of the coupling beam strength amplifications was found to be increased by the strengthening of the wall piers. As presented in section 7.3.3.1 for model CW3, when the tension wall was not strong enough to allow yielding of the coupling beams (with floors included), the coupling beam strength amplifications were limited based upon the capacity of the tension wall. In this case, NZS 3101:2006 (2014 Amdt) provided good correlation to the coupled wall overstrength capacity. However as the wall piers were strengthened for CW3x2, the tension wall pier did not suppress the coupling beam yield. Consequently, strength amplifications of the order of 2-3 were observed in the coupling beams. As a result, the overstrength capacity of the system was under-predicted by 15-20% using the NZS 3101:2006 (2014 Amdt) provisions. Therefore strengthening the wall piers provided improved energy dissipation because it enforced the coupled wall inelastic deformation mechanism to occur. However a downside of strengthening the wall piers (to prevent yield of the tension wall pier) was that the coupling beams tended to yield and elongate appreciably. This in turn activated a larger axial restraint response, which amplified the coupling beam strengths in excess of design values.

Comparison of the demands imposed on the wall pier extreme compression fibres is presented in Figure 7-26 for the CW3x2 model. The strain demand in the wall piers, shown in Figure 7-26 (a), was observed to have increased as the floor strength was increased and was particularly significant in tension (positive strain). Analysis of the boundary element stress demand, presented in Figure 7-26 (b), indicated that the compression stress demand was increased slightly for the same level of drift when floors were included. This increased compressive strain was typically not observed in previous models because yield of the tension wall tended to limit the demand induced on the compression wall. However strengthening of the wall piers allowed a larger demand to be imposed on the compression wall pier.



(a) Vertical strains (right piers shown dashed)

(b) Vertical stress (right pier shown dashed)

Figure 7-26: Coupled Wall 3 x2 (CW3 x2) strain and stress in wall pier extreme compression fibres over first storey (tension stress and strain shown positive). Drift taken at top of wall piers.

The above comparisons represented an important finding for design purposes. When the wall pier tension capacity was insufficient to resist the total coupling beam shear capacity, the coupled wall tended to behave as a single cantilever wall. In this case, the full capacities of the coupling beams were not realised, and only moderate coupling beam strengths were measured (1-1.5x nominal capacity). These coupling beam capacities were well accounted for in NZS 3101:2006 (2014 Amdt). The total coupled wall overstrength was limited in this case as a function of the wall pier tension capacity, which

tended to be well correlated to the NZS 3101:2006 (2014 Amdt) predictions. However, because the wall behaved more as a single cantilever with penetrations than a coupled wall, its energy dissipation was reduced and a higher level of tensile strain damage was observed in the tension wall.

In the alternative case, where the coupling beam strength amplifications were insufficient to cause the tension wall to fully yield, the coupling beams were able to achieve their full amplified capacities. In this scenario, the coupling beam strength amplifications were approximately 2-3, and were stronger than considered in NZS 3101:2006 (2014 Amdt), which led to an under-prediction of nominal and overstrength coupled wall capacities. This under-prediction was approximately 15%. Whilst the energy dissipation was improved and the wall pier tensile strains were reduced, the wall pier compression demands were found to be increased. Therefore it was found that a designer would need to be aware that enforcing the intended strength hierarchy in the coupled wall allowed improved energy dissipation and reduced wall pier damage. However enforcing the intended strength hierarchy also led to an under-prediction of the overstrength demands which may have had a significant impact on shear design of the wall piers.

In general the results presented above indicated that admissible coupled wall behaviour could be achieved based upon existing design approaches, even when the coupled wall did not behave in the manner that a coupled wall was traditionally assumed to behave. However the findings of the modelling also indicated that an improved understanding of coupled wall behaviour could be used to either provide an improved prediction of the behaviour which would occur with a particular design, or to use the understanding to enforce the coupled wall to behave as a traditionally assumed coupled wall. Further discussion on the implications for design is presented in section 7.4.

7.4 Discussion

The modelling results presented in the previous sections have been used to infer the behaviour of coupled walls when subjected to seismic loading. Discussion presented below addresses how the findings related to practical design, with particular attention given to determination of the type of behaviour to be expected with a particular design. In addition, discussion is provided on the specific behaviour of the wall piers and coupling beams in realistic coupled wall systems.

7.4.1 Primary findings for NZS 3101:2006

In agreement with the findings of the Canterbury Earthquakes Royal Commission (CERC), coupling beam axial restraint has been found to have a significant effect on the behaviour of seismically loaded coupled walls. In such systems, the strength of coupling beams has been found to be amplified due to axial restraint forces not considered in existing design codes. A major consequence of these coupling beam strength amplifications has been to change the coupled wall strength hierarchy and deformation mechanism. Assumed ideal behaviour of a coupled wall has traditionally involved the formation of plastic hinges at the base of wall piers and in all coupling beams. However, where the total strength of coupling beams was found to have exceeded the tension capacity of a wall pier, the tension wall pier was found to have yielded fully in tension. Yield of the wall pier was observed to have prevented the

coupling beams from yielding or supporting their full shear capacity. In this way the strength hierarchy and deformation mechanism was found to have changed, from an idealised coupled wall, to behaviour analogous to a single cantilever wall with penetrations. This change in deformation mechanism was found to have occurred due to larger than anticipated coupling beam nominal capacities, which exceeded design values. Based upon the findings presented above, it is likely that many existing coupled walls in New Zealand may not perform as intended in design. The two primary differences in behaviour between the two wall deformation mechanisms were their energy dissipation and strength capacities.

Hysteretic energy dissipation of an inelastic coupled wall system was found to be lower than anticipated, as many of the models exhibited severe pinching in their hysteretic response. This pinching was in part caused by relaxation of coupling beam axial restraint forces upon reloading, as the wall piers and floors yielded. The energy dissipation of models which behaved as a single cantilever was found to be far lower than for models behaving as coupled walls were traditionally expected to behave, due to three effects. Firstly the coupling beams did not yield, so dissipated little energy due to material strain. Secondly shear slip at the base of the tension wall upon reloading, due to the presence of tension cracks in the wall piers, caused a pinching upon reloading. Finally when the wall behaved as a single cantilever, more overturning moment was resisted in the wall pier axial force couple, rather than individual wall pier bending. Consequently the compression wall dissipated less energy because less reinforcement yielded in tension due to bending. The net effect of this behaviour was that the coupled walls which behaved as single cantilever walls were unable to dissipate energy as well as coupled walls were assumed to.

The other primary difference between walls behaving as single cantilevers versus those behaving as coupled walls were intended, was the effect on global system and local component strengths. In general, when the coupled wall behaved as a single cantilever wall (with the tension wall uplifting and preventing the coupling beams from yielding), the global coupled wall overstrength was well approximated by NZS 3101:2006 (2014 Amdt). In these cases, the local coupling beam capacities were well approximated at both nominal and overstrength. These strengths were well predicted because the tension wall acted to limit the extent of coupled wall and coupling beam strength amplification. When the coupled wall behaved as a coupled wall is intended to in design (with plastic hinges in all coupling beams and at the base of the wall piers), the strength predictions using NZS 3101:2006 (2014 Amdt) were less well correlated. Typically the overstrength capacity of the coupled wall was underestimated by 10-15% in this case. However the individual coupling beam nominal and overstrength capacities were predicted much less accurately.

As previously discussed, the effects of axial restraint on coupling beam capacity in NZS 3101:2006 (2014 Amdt) were only considered at overstrength, and only due to the restraint provided by the adjacent floor system. However as presented above, a series of models were run which showed that even without floor interaction, the coupling beam capacities were amplified by axial restraint forces which occurred due to the resistance of the wall piers to being pushed apart. These restraint forces were activated upon application of a lateral force corresponding to the nominal wall capacity and

continued to amplify the coupling beam capacity at wall overstrength. As the restraint forces in the coupling beams generated by the wall piers were not considered in NZS 3101:2006 (2014 Amdt), the nominal and overstrength capacities of the coupling beams were under-predicted by up to 2-3x when floors were assumed isolated from the coupled wall. Consequently the overstrength capacity of the coupled wall was under-predicted typically by 10-15% in these cases. The axial restraint imposed on the coupling beams was generated by an axial compressive force acting between the wall piers and this axial compressive force was partly composed of the base shear demand which was redistributed to the compression wall from the tension wall. A method estimating the maximum total axial compressive force in the coupling beams could be to assume that the full seismic demand imposed upon the tension wall was transmitted through the coupling beams in compression to the compression wall. However the floor diaphragm and collector elements in the floor provide an alternative pathway for this shear redistribution and so use of such a method was considered to be overly conservative as not all of the redistributed shear demand was expected to be transmitted through the coupling beams.

The provisions of NZS 3101:2006 (2014 Amdt) for coupling beam overstrength include an allowance for the effect of floors to restrain coupling beam elongation. Consequently the coupling beam overstrength predictions were found to be reasonably good when floors were included in the modelling. These good predictions were found to be the result of over-predicting the floor contributions to coupling beam strength and ignoring the effects of wall pier axial restraint. In this way, the errors cancelled to give a good approximation of the real behaviour. To overcome the shortcomings of the provisions in NZS 3101:2006 (2014 Amdt), it is recommended that further research be undertaken to quantify the amount of axial restraint provided by the wall piers to the coupling beams. In the event that further research leads to a codification of the restraint provided by the wall piers to a coupling beam, it is recommended that the contribution of floors to coupling beam restraint be reduced in NZS 3101:2006. This reduction is likely to be of the order of 25% based upon the coupled wall strength comparisons made above.

It is important to note that whilst the amplified coupling beam capacities resulted in a major change in wall behaviour, the coupled walls still provided admissible designs for the resistance of lateral forces. Although analysis was only undertaken up to peak wall demand, in all cases the coupled walls were found to possess displacement ductility capacities in excess of 4-5, and demonstrated suppression of undesirable failure mechanisms associated with a loss of load carrying capacity. Analysis was not undertaken beyond peak wall demand and this is an area for further research to examine. The lack of observed failures associated with a loss in load carrying capacity was an interesting finding given that the wall overstrength factors were generally underestimated by NZS 3101:2006 (2014 Amdt) by 10-15%. This finding indicated that instead of providing a prescriptive method for achieving the traditionally assumed coupled wall deformation mechanism, a more useful outcome of the research was to provide design guidance on how a coupled wall would realistically have behaved, even if that meant it did not behave as a coupled wall was traditionally assumed to.

7.4.2 Design guidance

Presented in this section is a description of how the findings presented above could be used by a designer to achieve improved performance of a coupled wall system. As outlined above, the intention was not to provide a prescriptive method to design a coupled wall to achieve certain performance criteria. Instead the recommendations were intended to provide a designer with an improved understanding of the behaviour that could be expected in a realistic coupled wall.

The most accurate and rigorous method for determining which type of behaviour would occur in a coupled wall, that is the idealised coupled wall mechanism or the single cantilever mechanism, was to compare actual coupling beam capacities to the actual wall pier resistance to uplift. In this way if the tension wall resistance to uplift (which included overcoming the applied gravity load) exceeded the cumulative coupling beam capacities, the full mechanism was able to form. However these coupling beam capacities have been found to have depended upon a range of factors including the adjacent floor type and coupling beam ductility demand. As an approximate method of assessment, an average coupling beam nominal strength amplification factor of approximately 2.0x nominal design capacity may be appropriate for an initial comparison to determine the probable coupling beam capacities when the intended deformation mechanism formed based upon the model results presented above. Use of an average value for initial design purposes would provide a reasonable approximation, provided the designer was aware that the average factor could be as high as 3.0 with strongly interacting floor systems and high coupling beam deformation demands.

The average coupling beam capacity method discussed above relied on a preliminary design already being in place. However for design purposes it would be more useful to have an understanding of the expected behaviour of a coupled wall at concept design phase. In this way, a designer would be free to adjust the design in its early stages to achieve certain performance criteria. As an approximate method for determining coupled wall behaviour at the beginning of design, (before nominal capacities were known), guidance based on design degree of coupling (DOC) was proposed. As discussed in section 7.3.1, when the design DOC was above 0.5, the walls tended to behave as a single cantilever, even when isolated from the floor system. However when the design DOC was approximately 0.35, the coupled wall mechanism was able to form, even when floors were included. At DOC of 0.45, the coupled wall mechanism formed, but consideration of floor axial restraint meant that only limited inelastic behaviour was observed in the coupling beams. Thus the relationship between deformation mechanism and DOC formed a continuum, where the inelastic behaviour in the coupling beams was reduced incrementally as DOC was increased. As a result, when the strength hierarchy was marginal, the wall behaved with components of both coupled wall and single cantilever action.

As a proxy for assessing the type of behaviour expected, the following guidance was proposed for design purposes:

- $DOC < 0.40$ Coupled wall mechanism likely to form,
- $0.40 < DOC < 0.55$ Components of both deformation types dependent upon floor arrangement, with reducing levels of inelastic behaviour in coupling beams and increasing levels of tension uplift in tension wall,
- $DOC > 0.55$ Single cantilever action likely to form.

Comparison to the ranges above could be used by a designer to either better predict the behaviour expected, or to make changes to the design in its early stages to make the desired behaviour more likely. Note that specification of a DOC was not a direct method of enforcing the intended strength hierarchy, as this was determined by a comparison between coupling beam and tension wall capacity. Thus the method provided an approximation for initial design purposes but did not replace a more rigorous strength hierarchy comparison. A similar upper limit was suggested for the DOC of coupled walls by Harries (2001) to ensure that the ductility capacity of coupling beams exceeded the ductility demand imposed on the coupling beams. Analysis by Harries (2001) showed that coupled walls with higher DOC's tended to be stiffer and so yielded at lower deformations than more flexible coupled walls with lower DOC. Consequently for the same ultimate drift, coupled walls with high DOC tended to impose larger ductility demand on the coupling beams. As the analysis conducted by Harries (2001) was based upon elastic modelling, the effects of mechanism changes due to coupling beam overstrength was not considered.

If desired, the redistribution of design demand could be used to alter the behaviour of the coupled wall being designed. By redistributing modal analysis demands, a designer may target the above range of DOC values to increase the probability that the wall would perform as a coupled wall is intended to in design. In this way the coupling beam amplifications expected would be inherently accounted for in the design demands. Redistribution of coupled wall overturning resistance away from coupling beams to wall piers was found to have provided a suitable approach to reduce the DOC of the walls analysed in section 7.3.3. As presented in section 7.3.3, redistributing demands such that the wall piers were designed for a higher demand caused the intended coupled wall deformation mechanism to form where previous results indicated that designing without redistribution did not enforce the intended strength hierarchy. This approach provided improved energy dissipation with lower wall pier damage in the model results.

The change in deformation mechanism represented a continuum between assumed coupled wall behaviour and single cantilever behaviour, hence walls tended to include components of both behaviours, particularly when close to the transition zone with marginal strength hierarchy. However discussion below is focused largely on walls whose behaviour was clearly defined to simplify the discussion. As both mechanism types have been found to provide admissible lateral force resistance for ductile structures, the discussion below is focused on the differences a designer would expect in the coupled wall properties as the mechanism changes.

7.4.3 Wall pier behaviour

Analysis of wall pier deformation behaviour has been used to develop a greater understanding of how wall piers behaved in a realistic coupled wall system. In response to coupling beam elongation, the wall piers were found to have displaced relative to each other. This relative wall pier displacement was observed to occur predominantly in the first storey and was characterised by a reduction in tension wall flexural deformation rather than an increase in compression wall flexural deformation. Elongation at level one effectively jacked the tension wall backwards, in the opposite sense to the direction of applied seismic loading, due to the low shear resistance of the tension wall. As the level one coupling beam jacked the walls apart, it was not able to yield appreciably until after the onset of yield in the wall piers, when the tension wall began to lose its shear stiffness due to partial or full uplift. This reduction in shear stiffness relaxed the restraint applied by the walls to the coupling beam, which allowed the coupling beam to yield. Flexibility in a foundation beam structure below the wall may have relaxed the level one restraint force. The study of foundation flexibility effects was outside the scope of this study and was recommended to be assessed as part of future work.

As the wall piers deformed, the curvature pattern of the coupled wall included a point of inflection above mid-wall height. As a result, coupling beam shear deformation was a maximum near the mid-wall height and reduced towards top and bottom. Axial relaxation of the wall piers with height also reduced the shear deformation in the upper level coupling beams, as the wall piers stretched or compressed in response to coupling beam shear forces. Consequently, the mid-wall height coupling beams tended to elongate the most and the wall piers tended to exhibit their highest relative displacements in this region. This pattern matched well with coupling beam strengths, which tended to peak near the mid-wall height and decrease towards the top of the walls. The inclusion of floors tended to strengthen the coupling beams and to tie the wall piers together, both of which resulted in a reduced relative displacement between the wall piers, and caused the coupled walls to behave more like a single cantilever than if the floors had been absent. Damage in the wall piers, as determined by the extent of reinforcement strain, was increased by floor interaction, because the coupled wall tended to behave more like a single cantilever wall which uplifted and so was subject to higher levels of tension strain.

An important finding of the research was the effect of coupling beam strength increases on wall pier demands. As coupling beam strengths were increased above their anticipated values (due to axial restraint) the demands in the wall piers were expected to increase correspondingly. However in many cases the full coupling beam capacities could not be realised as the tension wall fully yielded, which limited the compression wall pier demands. In these cases, where the walls behaved as a single cantilever, the wall pier axial compression demands were limited based upon the tension wall capacity which meant that they were accounted for in capacity design. In such cases, the primary considerations for design were the increased tension strain in the wall piers and the distribution of base shear resistance. As the tension wall was fully uplifted in such cases, its shear resistance was low. Therefore full redistribution of shear to the compression wall should be accounted for in the design of the compression wall, with a compressive force based upon the tension capacity of the opposite wall pier. Whilst the jacking forces in the level one coupling beam were found to result in a greater degree of

shear redistribution to the compression wall, the total shear demand at the base of the coupled wall was not observed to be increased by this jacking force because the walls did not activate shear demands in opposing directions.

In coupled walls where the tension walls did not activate as fuses, and the wall deformed as assumed in design, wall pier axial compression demands were observed to increase slightly. Due to redistribution of lateral forces applied to the wall system, the increased wall axial force that was induced by stronger than anticipated coupling beams was found to be offset somewhat by a reduction in the moment demand in the walls. Consequently the wall pier compression zones were not observed to increase markedly in this case either. Compression failures resulting in a loss of load carrying capacity were not observed in the models up to peak demand (although the behaviour beyond peak demand was unable to be analysed). Despite the tension wall retaining some ability to resist shear when the intended deformation mechanism eventuated, observations of shear distribution have shown that in excess of 90% of the base shear was resisted by the compression wall. Therefore the existing design method of proportioning shear resistance between wall piers based on wall overstrength moments was found to be appropriate due to the high moment capacity observed in compression wall piers.

The effect of interaction with surrounding gravity frames and higher mode effects on wall pier deformations and coupling beam demands was not assessed in this study. These effects were recommended to be considered as part of future research using three dimensional, non-linear time history analysis. In particular, a vertically elongating wall pier may 'pick up' a greater gravity load when the full three dimensional behaviour was considered, which may increase its overstrength capacity by activating a greater coupling beam shear capacity.

7.4.4 Coupling beam behaviour

The capacity of coupling beams in a realistic coupled wall system has been found to differ significantly from traditional design assumptions. Axial restraint of the coupling beams, provided by wall piers and floor systems, was observed to have increased coupling beam overstrength capacities by up to 2-3 times. In many cases, the coupling beam strength amplifications were found to have been sufficient to have changed the strength hierarchy of the system and cause the coupled wall to have behaved as a single cantilever wall, with the tension wall uplifting in tension.

Coupling beam axial restraint was found to have been activated when the nominal capacity of the wall was activated by a lateral force, which resulted in the coupling beams displaying strengths similar to their overstrength capacity at nominal wall capacity. The primary effect of large coupling beam nominal capacities was on the formation of the intended coupled wall mechanism, which could only form if the tension wall resistance to uplift exceeded the cumulative coupling beam shear capacity. Coupling beam strength amplifications of the order of 2-3 were observed in many cases where the coupled wall deformed as intended in design. However in walls behaving as single cantilevers, the coupling beams remained largely elastic with small elongation and axial restraint levels. Consequently the amplifications were of the order of 1.0-1.5 in such systems. On this basis, coupling beam strength amplifications could

be much lower if the tension wall could be shown to activate as a fuse and uplift prior to coupling beam yield. As the coupling beams were stronger than anticipated and subjected to axial restraint forces, at peak lateral force the strain demand in the diagonal reinforcement was low. Hence the coupling beams only began to strain harden after the overall wall began to soften, which was not captured in force based modelling.

Coupling beam resistance to applied axial forces was found to be a function of the ductility demand imposed on the coupling beams. As shown in Figure 7-27 (b), the angle of inclination of the compression struts in the concrete were found to be well matched to the diagonal reinforcement angle (as traditionally assumed) when the coupling beam ductility demand was low. However as shown in Figure 7-27 (a) and (c), the compression strut angle of inclination tended to increase as the coupling beams were highly strained in shear. As a consequence, the component of the diagonal force contributing to shear was increased. This strut angle rotation allowed heavily deformed coupling beams to resist a larger shear force for the same axial restraint force applied. The angle of inclination was found to be up to 15° larger than the diagonal reinforcement layout, which meant that for a given axial force, the additional shear force generated could be up to twice as large with a low initial strut angle (span-depth ratios >2.0). A designer should therefore be aware that the angle of inclination may increase when assessing the effect of an axial force on coupling beam shear capacity. When assessing the increase in shear capacity due to an axial force, at overstrength the angle of diagonal reinforcement plus an average increase of approximately 10° is recommended to be used. As shown in Figure 7-28, the angle rotation relied on vertical tension capacity in the coupling beam confinement reinforcement to ensure vertical equilibrium. As the vertical coupling beam reinforcement in a diagonally reinforced coupling beam was intended only for confinement purposes, no detrimental crushing effects were observed due to additional vertical demands.

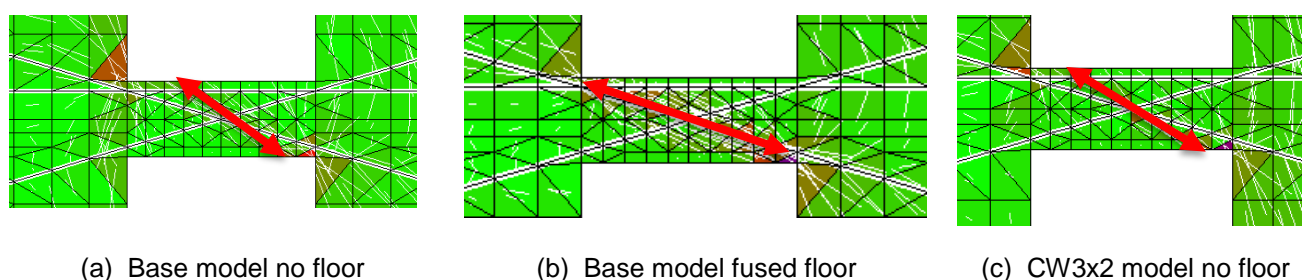


Figure 7-27: Coupling beam typical principal compression stress directions. Arrows indicate compressive stress trajectory, with higher inclination for more severely strained coupling beams.

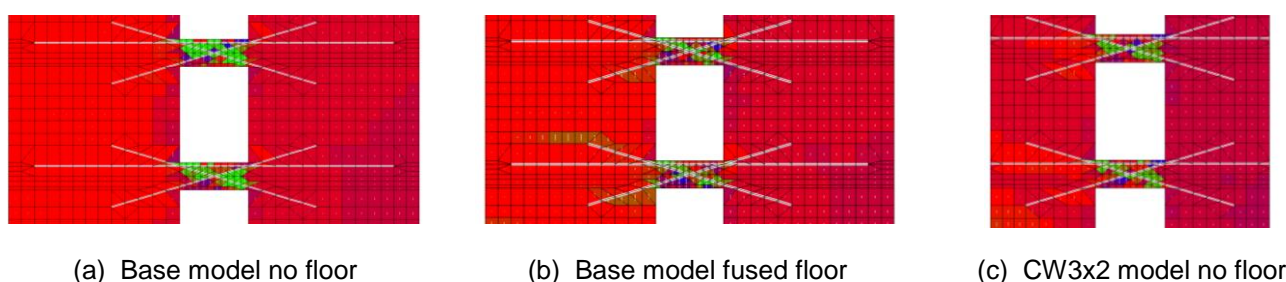


Figure 7-28: Coupling beam typical vertical stress demand in transverse reinforcement (green = tension stress, blue= compression stress, red=low/no stress)

Coupling beam performances in the models presented above were found to be good, with no sudden losses of load carrying capacity observed. Despite the consideration of large axial restraint forces, large crushing or buckling failures were not observed in the coupling beams and the coupling beams generally performed well. Consequently the NZS 3101:2006 (2014 Amdt) provisions for coupling beam reinforcement were found to be suitable to achieve good coupling beam performance. However as the modelling was only undertaken up to peak demand, shear strains were not imposed above design limitations and it was recommended that future research consider analysing the walls to failure to assess how coupling beams performed at large shear strain.

7.5 Conclusion

Analysis of a series of coupled walls has been undertaken using two-dimensional finite element software VecTor2. The coupled walls were designed to cover a wide range of possible wall layouts and considered the effect of a range of different floor arrangements on the system performance. Each wall was subjected to an inelastic cyclic pushover analysis up to peak wall demand and the behaviour of each wall was compared. The comparisons led to the following findings related to coupled wall behaviour:

- As per the findings of the Canterbury Earthquakes Royal Commission (CERC), axial restraint of coupling beams has been found to have significantly changed the behaviour of coupled wall systems. It is expected that many of the existing coupled walls in New Zealand will behave more as single cantilever walls with penetrations than as the coupled walls that they were designed to be due to a lack of consideration of this axial restraint in design.
- Axial restraint of coupling beams was found to have resulted in coupling beam strengths up to 2-3x their design capacity. Many coupled walls were observed to have behaved as single cantilever walls due to this coupling beam strength amplification. These coupled walls behaving as cantilever walls tended to exhibit reduced energy dissipation and increased inelastic strain in the wall piers when compared to walls behaving as intended in design.
- NZS 3101:2006 (2014 Amendment) makes no allowance for the coupling beam axial restraint provided by the wall piers. As a result, the coupled walls tended to resist 10-15% more lateral force at overstrength than predicted NZS 3101:2006 (2014 Amdt).
- NZS 3101:2006 (2014 Amendment) considers the effect of axial restraint due to floor interaction only. It was found that the overstrength provisions provided reasonable correlation to the coupled wall overstrength capacity. However this correlation was due to an over-estimate of the effect of floors and an underestimate of the effect of the wall piers in restraining elongation.
- The elongation of the coupling beams tended to result in base shear being fully redistributed to the compression wall.
- Wall pier demands were observed to have not increased significantly due to the increased capacity of the coupled wall when considering axial restraint of the coupling beams.

The above findings led to the following recommendations for design:

- For preliminary design purposes, the design degree of coupling (DOC) was found to provide a suitable method to more realistically target a behaviour type. In order to make the intended mechanism more likely to form, redistribution of the overturning moment was recommended by redistributing the modal analysis overturning moment away from the coupling beams to the wall piers in bending to reduce the DOC. The following DOC ranges were recommended for initial design purposes, to allow better awareness of which mechanism was likely to form:
 - $DOC < 0.40$ Coupled wall mechanism likely to form,
 - $0.40 < DOC < 0.55$ Components of both deformation types dependent upon floor arrangement, with reducing levels of inelastic behaviour in coupling beams and increasing levels of tension uplift in tension wall,
 - $DOC > 0.55$ Single cantilever action likely to form.
- When considering the effect of an axial restraint force in the coupling beam at overstrength, it is recommended that the axial force be assumed to be resisted on the same angle as the diagonal reinforcement plus 10° to account for the strut rotation which occurs at high ductility demand.
- The existing design assumption of distributing shear resistance based upon the wall pier overstrength moment was found to be adequate. Coupling beam elongation tended to increase the extent of shear redistribution so allowance should be made for the compression wall to support the full shear demand imposed upon the coupled wall when the wall behaved as a single cantilever wall.

7.5.1 Recommendations for future work

The research presented in this chapter provided significant findings for the realistic behaviour of coupled wall systems. However further work is recommended, likely using three dimensional non-linear time history analysis software, to assess the following:

- The behaviour of coupled walls when pushed to failure (post peak). In particular a study of how axial restraint changes towards the onset of failure and the ductility capacity of the coupling beams under such conditions,
- It is recommended that further research be carried out to better quantify the amount of restraint applied by wall piers to elongating coupling beams,
- The findings presented herein are based upon static loading using simplified load distribution. It is recommended that this study is extended to consider dynamic response of coupled walls using a variety of ground motions to account for higher mode effects on the deformation and yield pattern within the coupled walls.
- Three dimensional interaction of gravity frames, floors and coupled walls. In particular, how vertical elongation of a wall pier may result in additional capacity of the system,
- The effect of foundation flexibility on coupled wall behaviour should be considered by allowance of finite foundation stiffness in the modelling of coupled walls.

CHAPTER 8

8 Conclusion

Following the 2010/2011 Canterbury earthquakes, a number of coupled walls were observed to have performed undesirably with respect to their design intent. Several coupled walls were observed to have displayed higher strengths and less damage than anticipated based upon the philosophy adopted in their design. The postulated reasoning for this behaviour was that the tendency of the coupling beams to elongate was restrained by adjacent structural components, resulting in higher strength and lower damage induced in the coupling beams (Canterbury Earthquakes Royal Commission 2012). This coupling beam restraint was concluded to have been provided by interaction with floor diaphragms and the bounding wall piers.

Based upon the recommendations of the Canterbury Earthquakes Royal Commission (CERC), analysis has been undertaken in order to develop the understanding of coupled walls and to improve design provisions for such structures. Two dimensional finite element software VecTor2 was used to undertake the analysis (VecTor Analysis Group 2011). As the problem was fundamentally based upon structural interactions, the behaviour of floor diaphragms in isolation was first explored to assess how these floor diaphragms interacted with coupled wall systems. Consideration was then given to the behaviour of coupled wall systems. A series of coupled walls were designed based upon NZS 3101:2006 (2014 Amdt) with consideration given to a range of layouts and properties possible in practical design. These coupled wall configurations were then modelled, subjected to a simulated seismic demand. Floors were included in the modelling based upon the findings of the floor diaphragm analysis. Comparison was then made between the models and existing design provisions to assess how coupled walls behaved in realistic systems.

8.1 Floor diaphragm conclusions

The research into floor diaphragms has led to the following conclusions:

- 1) VecTor2 finite element software has been validated against a series of floor diaphragm experiments and found to be capable of providing a reasonable representation of floor behaviour.
- 2) Floor diaphragms have been observed to have deformed in response to the elongation of a beam plastic hinge occurring during an earthquake event. As a result of this deformation, the floor was observed to have suffered damage and to have resisted the elongation by generating an axial restraint force in the plastic hinge. The presence of

weak zones in the floor, particularly at the interface of precast floor units, has been found to dominate the behaviour of the floor diaphragm when responding to elongating plastic hinges.

- 3) The provisions of NZS 3101:2006, which placed an upper bound on the effective width of floor interacting with an elongating plastic hinge, have been confirmed to be valid. These upper bounds limited the effective width of floor (at overstrength of a beam plastic hinge) based upon either the spacing to the next plastic hinge or on the shear capacity of the link slab. As the effective width of floor determined the extent of floor activated in restraining an elongating hinge, these effective width upper bounds also placed limits on the magnitude of axial restraint force generated by the floor. The governing upper bound was found to have been dependent upon the floor arrangement considered:
 - Where precast floor units spanned perpendicular to elongation, the restraint force was limited by the topping reinforcement capacity, within an effective width of half the precast floor unit span of the elongating hinge,
 - Where precast floor units spanned parallel to elongation, and were supported on a transverse beam at the hinge location, the upper bound restraint force was determined by the reinforcement capacity across the transverse beam within an effective width of half the transverse beam span,
 - Where precast floor units spanned parallel past the elongating hinge, the activated restraint force (and effective width) was found to have been limited by the shear capacity of the link slab,
 - Where insitu mild steel reinforced floors were considered, the restraint force generated was limited by the reinforcement in the floor within an effective width of half the transverse beam span of the plastic hinge.
- 4) Floor diaphragms have been found to act as ties between coupled wall piers, to reduce the extent of coupling beam elongation and to increase the strength of coupled wall systems.

8.2 Coupled wall conclusions

Following the assessment of floor diaphragms, analysis of coupled wall systems was undertaken. Allowance was made in these models for floor diaphragm interaction based upon the findings presented above. The coupled wall analysis led to the following results:

- 1) VecTor2 finite element software has been validated as a suitable method for assessing the response of coupled walls to simulated seismic excitation. Three-dimensional effects of floor interaction were found to be adequately captured in the model by incorporating an equivalent floor tie in the two-dimensional software.

- 2) As per the findings of the Canterbury Earthquakes Royal Commission (CERC), axial restraint of coupling beams has been found to have significantly changed the behaviour of coupled wall systems. It was expected that many of the existing coupled walls in New Zealand would have behaved more as single cantilever walls with penetrations than as the coupled walls that they were designed to be due to a lack of consideration of this axial restraint in design.
- 3) Axial restraint of coupling beams was found to have resulted in coupling beam strengths up to 200-300% of their capacity assumed in design. Many coupled walls were observed to have behaved as single cantilever walls due to this coupling beam strength amplification, and tended to exhibit low energy dissipation and high damage in the wall piers.
- 4) NZS 3101:2006 (2014 Amendment) made no allowance for the coupling beam axial restraint provided by the wall piers. As a result, the coupled walls tended to be 10-15% stronger at overstrength than predicted using NZS 3101:2006 (2014 Amdt).
- 5) NZS 3101:2006 (2014 Amendment) considered the effect of axial restraint due to floor interaction only. It was found that the overstrength provisions provided reasonable correlation to the coupled wall overstrength capacity. However this was due to an overestimate of the effect of floors and an underestimate of the effect of the wall piers in restraining elongation.
- 6) The elongation of the coupling beams tended to result in base shear being fully redistributed to the compression wall.
- 7) For preliminary design purposes, the design degree of coupling (DOC) was found to provide a suitable method to realistically target a behaviour type. In order to make the intended mechanism more likely to form, redistribution of the overturning moment was recommended by redistributing the modal design demands away from the coupling beams to the wall piers in bending to reduce the DOC. The following DOC ranges were recommended for initial design purposes, to allow better awareness of which mechanism was likely to form:
 - $DOC < 0.40$ Coupled wall mechanism likely to form,
 - $0.40 < DOC < 0.55$ Components of both deformation types dependent upon floor arrangement, with reducing levels of inelastic behaviour in coupling beams and increasing levels of tension uplift in walls,
 - $DOC > 0.55$ Single cantilever action likely to form.

8.3 Recommendations for future work

Based upon the assessment of floor diaphragms and coupled walls, the following recommendations for future work were made:

- 1) Three dimensional effects in floor diaphragm axial restraint should be considered. Experimental analysis or three dimensional modelling should be undertaken to assess how the extent of floor activated in axial restraint changes due to three dimensional behaviour. In particular where a transverse beam weakness was present, the extent of floor activated to restrain axial elongation should be considered. Also the effects of deterioration of the link slab were recommended to be investigated further to ensure the transfer of diaphragm forces into the lateral loading system.
- 2) The behaviour of coupled walls when loaded beyond peak wall demand should be assessed by analysing the walls to failure.
- 3) Further research is recommended to be undertaken into the magnitude of axial restraint provided by the wall piers to elongating coupling beams in a coupled wall system.
- 4) The findings presented herein are based upon static loading using simplified load distribution. It is recommended that this study is extended to consider dynamic response of coupled walls using a variety of ground motions to account for higher mode effects on the deformation and yield pattern within the coupled walls.
- 5) Three dimensional interaction of gravity frames, floors and coupled walls should be investigated. In particular, the mechanism whereby vertical elongation of a wall pier may result in additional capacity of the system should be studied.
- 6) The effect of foundation flexibility on coupled wall behaviour should be considered by allowance of finite foundation stiffness in the modelling of coupled walls.

9 References

ACI 318-11. (2011). *Building Code Requirements for Structural Concrete (ACI318-11) and Commentary (ACI318R-11)*. American Concrete Institute, Farmington Hills, MI.

Adebar, P., Hindi, R., and Gonzalez, E. (2001). "Seismic Behaviour of a Full Scale Diagonally Reinforced Slender Coupling Beam." Department of Civil Engineering Report, University of British Columbia pp.327-337, Vancouver, BC, Canada.

Barbachyn, S. M., Kurama, Y. C., and Novak, L. C. (2012). "Analytical Evaluation of Diagonally Reinforced Concrete Coupling Beams under Lateral Loads." *ACI Struct.J.*, 109(4), 497-507.

Bower, O., and Rassati, G. (2008). "Analytical Investigation into the Effect of Axial Restraint on the Stiffness and Ductility of Diagonally Reinforced Concrete Coupling Beams." *Thesis Submitted in Partial Fulfillment of the Degree of Master of Science*, University of Cincinnati.

Canterbury Earthquakes Royal Commission. (2012). "Final Report Volumes 1-7." *Rep. No. ISBN: 978-0-478-39558-7*, New Zealand Government, Christchurch.

CCANZ. (1998). "Examples of Concrete Structural Design to New Zealand Standard 3101." *Rep. No. 1*, Cement and Concrete Association, New Zealand.

Computers and Structures Inc. (2014). "Perform 3D: Nonlinear Analysis and Performance Assessment for 3D Structures." CSI, <http://www.csiamerica.com/products/perform-3d>.

Corney, S. R., Henry, R. S., and Ingham, J. M. (2014). "Testing the support connection details of 400 hollowcore precast concrete floors under seismic action." *The New Zealand Concrete Industry Conference*, 9-11 October, Taupo, New Zealand.

Dassault Systemes. (2014). "Abaqus Finite Element Analysis Software." Version 6.14 <http://www.3ds.com/products-services/simulia/products/abaqus/>.

Fenwick, R. C., Bull, D. K., MacPherson, C. J., and Lindsay, R. A. (2006). "The Influence of Diaphragms on Strength of Beams." *NZSEE Conference*, Napier(Paper Number 21), pp12.

Fenwick, R. C., and Megget, L. M. (1993). "Elongation and load deflection characteristics of reinforced concrete members containing plastic hinges." *Bulletin of the New Zealand National Society for Earthquake Engineering*, 26(1), 28-41.

Fenwick, R. C., and Thom, C. W. (1982). "Shear deformation in reinforced concrete beams subjected to inelastic cyclic loading." *Rep. No. 279*, University of Auckland School of Engineering, Auckland.

References

- Fenwick, R. C., Bull, D. K., and Gardiner, D. (2010). "Assessment of Hollow Core Floors for Seismic Performance - University of Canterbury Research Report 2010-02." *Rep. No. 2010-02*, Christchurch.
- Fenwick, R. C., Davidson, B. J., and Lau, D. B. N. (2005). "Interaction between ductile RC perimeter frames and floor slabs containing precast units." *New Zealand Society for Earthquake Engineering Conference*, Wairakei, New Zealand, Paper No 23.
- Fenwick, R. C., and Fong, A. (1979). "The Behaviour of Reinforced Concrete Beams under Cyclic Loading." *Bulletin of NZ Society for Earthquake Engineering*, 12(2), 158-167.
- Fenwick, R. C., Tankut, A. T., and Thom, C. W. (1981). "The deformation of reinforced concrete beams subjected to inelastic cyclic loading : experimental results." *Rep. No. 268*, University of Auckland School of Engineering, Auckland.
- Fortney, P. J., Rassati, G. A., and Shahrooz, B. M. (2008). "Investigation on effect of transverse reinforcement on performance of diagonally reinforced coupling beams." *ACI Struct.J.*, 105 (6)(S72), pp781.
- Galano, L., and Vignoli, A. (2000). "Seismic behavior of short coupling beams with different reinforcement layouts." *ACI Struct.J.*, 97(S89), pp876.
- Harries, K. A. (2001). "Ductility and deformability of coupling beams in reinforced concrete coupled walls." *Earthquake Spectra*, 17(3), 457-478.
- Kwan, A., and Zhao, Z. (2002). "Cyclic behaviour of deep reinforced concrete coupling beams." *Proceedings of the ICE-Structures and Buildings*, 152(3), 283-293.
- Lau, D. B. N., Fenwick, R. C., and Davidson, B. J. (2002). "Seismic Performance of R/C Perimeter Frames with Slabs Containing Prestressed Units." *NZSEE Conference*, Napier(Paper Number 7.2), pp1-8.
- Lau, D. B. N., Davidson, B. J., and Fenwick, R. C. (2003). "Seismic Performance of R/C Perimeter Frames with Slabs Containing Prestressed Units." *2003 Pacific Conference on Earthquake Engineering*, Christchurch, New Zealand, Paper No 109.
- Lee, J., and Watanabe, F. (2003). "Predicting the longitudinal axial strain in the plastic hinge regions of reinforced concrete beams subjected to reversed cyclic loading." *Eng.Struct.*, 25(7), 927-939.
- Lehman, D., Turgeon, J., Birely, A., Hart, C., Marley, K., Kuchma, D., and Lowes, L. (2013). "Seismic Behavior of a Modern Concrete Coupled Wall." *J.Struct.Eng.*, 139(8), 1371-1381.
- Lindsay, R. A., Mander, J. B., and Bull, D. K. (2004). "Experiments on the Seismic Performance of Hollow-Core Floor Systems in Precast Concrete Buildings." *13th World Conference on Earthquake Engineering*, Vancouver, Canada, (August 1-6), Paper Number 585.

References

- MacPherson, C. J. (2005). "Seismic Performance and Forensic Analysis of Precast Concrete Hollow-Core Floor Super Assemblages." *ME Thesis, Civil Engineering*, University of Canterbury.
- MacPherson, C. J., Mander, J. B., and Bull, D. K. (2005). "Reinforced Concrete Seating Details of Hollow-Core Floor Systems." *NZSEE Conference*, (Taupo, New Zealand), Paper Number 24.
- Matthews, J. (2004). "Hollow-Core Floor Slab Performance Following a Severe Earthquake." *PhD Thesis, Civil Engineering*, University of Canterbury.
- Matthews, J. G. (2005). "Hollow-Core Floor Slab Performance Following a Severe Earthquake." *Rep. No. Commercial Report C2005-1*, Prepared for EQC - 99/411, University of Canterbury, Christchurch, New Zealand.
- McBride, A. P. (1995). "Elongation of reinforced concrete beam-column units with and without slab". Master of Engineering Dissertation. University of Auckland, Auckland.
- Mercer, S. S. (2012). "Nonlinear Shear Response of Cantilever Reinforced Concrete Shear Walls with Floor Slabs." *Thesis Submitted in Partial Fulfillment of the Requirements for the Degree of Master of Applied Science*, University of British Columbia (Vancouver)(Civil Engineering), pp186.
- Mohr, D. S. (2007). "Nonlinear Analysis and Performance Based Design Methods for Reinforced Concrete Coupled Shear Walls." *Master of Science Thesis*, University of Washington.
- Naish, D., Fry, J. A., Klemencic, R., and Wallace, J. (2009). "Experimental Evaluation and Analytical Modeling of ACI 318-05/08 Reinforced Concrete Coupling Beams Subjected to Reversed Cyclic Loading." *Report SGEL*, Vol. 6.
- NEEShub. (2014). "The George E. Brown, Jr Network for Earthquake Engineering Simulation." <https://nees.org/warehouse> (04, 2014).
- Ozselcuk, A. R. (1989). "Experimental and Analytical Studies of Coupled Wall Structures." *PhD Dissertation*, University of California(Berkeley), CA.
- Pacific Earthquake Engineering Research Centre. (2006). "OpenSees - The Open System for Earthquake Engineering Simulation." *PEERC*, <http://opensees.berkeley.edu/>.
- Paulay, T., and Binney, J. (1974). "Diagonally reinforced coupling beams of shear walls." *ACI Special Publication*, SP42.
- Paulay, T. (1971). "Coupling beams of reinforced concrete shear walls." *Journal of the Structural Division*, 97(3), 843-862.
- Paulay, T., and Priestley, M. J. N. (1992). *Seismic design of reinforced concrete and masonry buildings*. Wiley c1992, New York.

References

- Peng, B. H. H., Fenwick, R., Dhakal, R., and Bull, D. (2008). "Experimental study on the seismic performance of RC moment resisting frames with precast-prestressed floor units." *New Zealand Society for Earthquake Engineering Conference, Wairakei, New Zealand, Paper No. 37.*
- Peng, B. H. H., Dhakal, R. P., Fenwick, R. C., Carr, A. J., and Bull, D. K. (2011b). "Elongation of Plastic Hinges in Ductile RC Members: Model Verification." *Journal of Advanced Concrete Technology*, 9(3), 327-338.
- Peng, B. H. H., Dhakal, R. P., Fenwick, R. C., Carr, A. J., and Bull, D. K. (2011a). "Elongation of Plastic Hinges in Ductile RC Members: Model Development." *Journal of Advanced Concrete Technology*, 9(3), 315-326.
- Shiu, K. N., Aristizabl-Ochoa, J. D., Barney, G. B., Fiorato, A. E., and Corley, W. G. (1981). "Earthquake resistant structural walls - coupled wall tests." *Rep. No. 1 to National Science Foundation, Construction Technology Laboratories, Division of Portland Cement Association, Stokie, IL.*
- Standards New Zealand. (2014). "Amendment No.3 to Concrete Structures Standard NZS 3101:2006 (Public Comment)." *Part 1 and Part 2 (Commentary)*, Wellington(New Zealand), pp67.
- Standards New Zealand. (2006). "Concrete Structures Standard NZS3101:2006." *Part 1, Design of Concrete Structures*, pp306.
- Tassios, T. P., Moretti, M., and Bezas, A. (1996). "On the behavior and ductility of reinforced concrete coupling beams of shear walls." *ACI Struct.J.*, 93(6), 711-720.
- Turgeon, J. A. (2011). "The Seismic Performance of Coupled Reinforced Concrete Walls". Master of Science in Civil Engineering. University of Washington, Washington.
- Vecchio, F. J. (2000). "Disturbed Stress Field Model for Reinforced Concrete: Formulation." *ASCE Journal of Structural Engineering*, 126(9), 1070-1077.
- Vecchio, F. J., and Collins, M. P. (1986). "The Modified Compression Field Theory for Reinforced Concrete Elements Subject to Shear." *ACI Journal*, 83(2), 219-231.
- VecTor Analysis Group. (2011). "VecTor2 - Finite Element Analysis of Reinforced Concrete." Version 3.5 <http://www.civ.utoronto.ca/vector>.
- Wong, P. S., Vecchio, F. J., and Trommels, H. (2013). "VecTor2 & FormWorks Users Manual 2nd Edition." <http://www.civ.utoronto.ca/vector>.
- Wuu, P. (1996). "Deformations in Plastic Hinge Zone of R/C Beam in Ductile Frame Structures Subjected to Inelastic Cyclic Loading". Master of Engineering Dissertation. University of Auckland, Auckland.

Appendix A

10 Appendix A

Provided herein is a summary of the experimental research programmes undertaken on reinforced concrete coupling beams.

Table 10-1: Summary of coupling beam experimental data

Authors	Year	Objective	Specimen	Reinforcing Layout	Aspect Ratio L/D	End Restraint
Paulay and Binney	1972	Compare performance of diagonal reinforcement versus conventional reinforcement	315	Conventional	1.29	Axially Unrestrained
			316	Diagonal	1.29	
			317	Diagonal	1.29	
			395	Diagonal	1.02	
Tassios, Moretti and Bezas	1996	Compare performance of alternate 'bent up' reinforcement layout to conventional and diagonal reinforcement. Also to compare alternative dowelled reinforcement to enhance resistance to sliding shear failure.	CB1A	Conventional	1	Axially Unrestrained
			CB1B	Conventional	1.66	
			CB2A	Diagonal	1	
			CB2B	Diagonal	1.66	
			CB-3A	Rhombic	1	
			CB-3B	Rhombic	1.66	
			CB-4A	Conventional (Long Dowels)	1	
			CB-4B	Conventional (Long Dowels)	1.66	
			CB-5A	Conventional (Short Dowels)	1	
CB-5B	Conventional (Short Dowels)	1.66				
Galano and Vignoli	2000	Compare the performance of alternate reinforcement layouts and investigate the effect of different loading history. Reinforcement layouts included conventional (a), diagonal with and without confining ties (b1 and b2 respectively), and an inclined 'rhombic' configuration (c).	P01	Conventional	1.5	Axially restrained
			P02	Conventional	1.5	
			P03	Conventional	1.5	
			P04	Conventional	1.5	
			P05	Diagonal	1.5	
			P06	Diagonal	1.5	
			P07	Diagonal	1.5	
			P08	Diagonal	1.5	

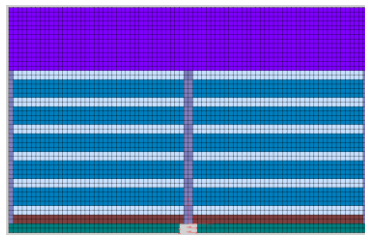
Appendix A

			P10	Diagonal (confined)	1.5	
			P11	Diagonal (confined)	1.5	
			P12	Diagonal (confined)	1.5	
			P13	Rhombic	1.5	
			P14	Rhombic	1.5	
			P15	Rhombic	1.5	
			P16	Rhombic	1.5	
Adebar et al	2001	Investigate the effect of axial restraint on a coupling beam	1	Diagonal	2.75	Axially restrained
Kwan and Zhao	2002	Investigate reinforcement layout and span/depth ratio effects. Primarily investigated conventionally reinforced beams	CCB1	Conventional	1.17	Axially unrestrained, End rotations equal
			CCB2	Conventional	1.4	
			CCB3	Conventional	1.75	
			CCB4	Conventional	2	
			CCB11	Diagonal	1.17	
			CCB12	Conventional	1.17	
Fortney, Rassati and Shahrooz	2008	Investigate effect of transverse reinforcement layout on performance of coupling beams	DCB-1	Diagonal (confined)	3	Axially unrestrained
			DCB-2		3	
Naish, Wallace, Fry and Klemencic	2009	Investigate alternate detailing options in ACI318-08. Compare full section confinement to confinement of primary diagonal bundles. Assess influence of including floor slab in experiment.	CB24F	Full section confinement	2.4	Axially unrestrained
			CB24D	Diagonal confinement	2.4	
			CB24F-RC	Full section confinement	2.4	
			CB24F-PT	Full section confinement	2.4	
			CB24F-1/2PT	Full section confinement	2.4	
			CB33F	Full section confinement	3.33	
			CD33D	Diagonal confinement	3.33	
			FB33	Full section confinement	3.33	

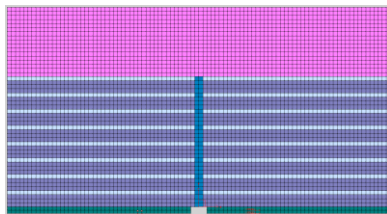
Appendix B

11 Appendix B

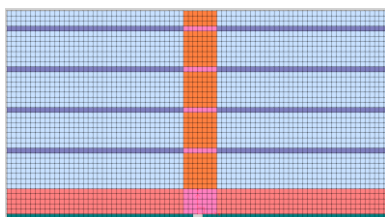
Presented in this appendix is a supplement to the computational model calibration of floor systems outlined in Chapter 3, as a more detailed summary of the iterations undertaken in order to ensure the modelling software replicated realistic floors at suitable computational expense. The general layout, and material properties used for the comparison to experimental data are presented in Figure 3-8, based upon the experimentally measured properties.



(d) Lau et al. (2002) floor model



(e) Peng et al. (2008) floor model



(f) MacPherson (2005) floor model

Steel reinforcement – Grade 430 MPa

Insitu floor concrete taken as 36MPa (Based on 30MPa targeted strength)

Steel	f_y (MPa)	f_u (MPa)	ϵ_y	ϵ_{yk}	ϵ_u
R6	444.7	557.1	0.0022	-	0.0916
R10	395.2	490.5	0.0020	0.0174	0.1355
D10	372.5	477.1	0.0019	0.0189	0.1209
D16	325.4	454.9	0.0016	0.0253	0.2084
D20	319.1	455.5	0.0016	0.0243	0.2065
HD12	541.4	668.1	0.0027	0.0191	0.1118
HD16	551.4	684.8	0.0028	0.0165	0.1158
D16*	359.4	486.2	0.0043	0.0081	0.1086
D16**	365.1	484.3	0.0033	0.0089	0.0990

* Steel bars extracted from the top of the longitudinal beam at the end of the test
 ** Steel bars extracted from the bottom of the longitudinal beam at the end of the test

Insitu floor concrete taken as 36MPa (Based on 30MPa targeted strength)

Tensile Test Strength and Strain Characteristics							
Location	Reinforcing	f_y (MPa)	f_u (MPa)	E_s (GPa)	E_{sh} (GPa)	ϵ_{sh}	ϵ_{su}
Column & Beam Longitudinal Steel	YD25	536	675	214	3.27	0.0015	0.0128
Column & Beam Transverse Steel	YR12	530	714	190	-	0.0005	0.0152
Support Connection	R16	336	469	186	4.48	0.0031	0.0200
Starter Bars and Diaphragm	D12	307	447	181	3.65	0.0029	0.0218
Drag Bars	YD20	580	724	246	3.82	0.0012	0.0156

Insitu floor concrete taken as 36MPa (Based on 30MPa targeted strength)

Material properties

Figure 11-1: General layout of VecTor2 floor models for calibration where colours represent different material properties as extracted from - (Lau et al. 2002; Peng et al. 2008; MacPherson 2005)

Mesh size was first considered as this defined the spacing increment of nodes in the numerical idealization of the floor systems. The nodes represented discrete locations in the model where the software calculated stress and strain of concrete or reinforcement elements. The mesh

size was the key parameter for ensuring suitable computational expense as it defined the number of nodes calculated at each load increment. To examine the effect of mesh size on the response of the floor, a range of the floors used in the previously discussed experiments, as shown in Figure 3-8, were analysed in VecTor2 software, as shown in Figure 11-2 to Figure 11-4.

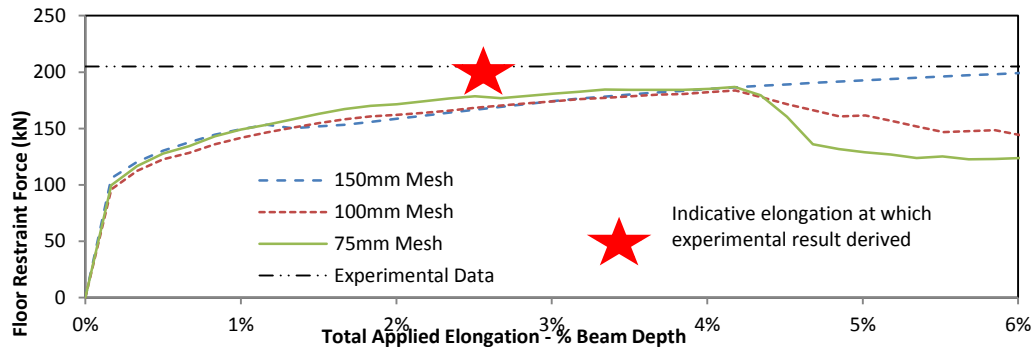


Figure 11-2: Floor elongation restraint force for Lau et al. (2002) floor with varied mesh sizes

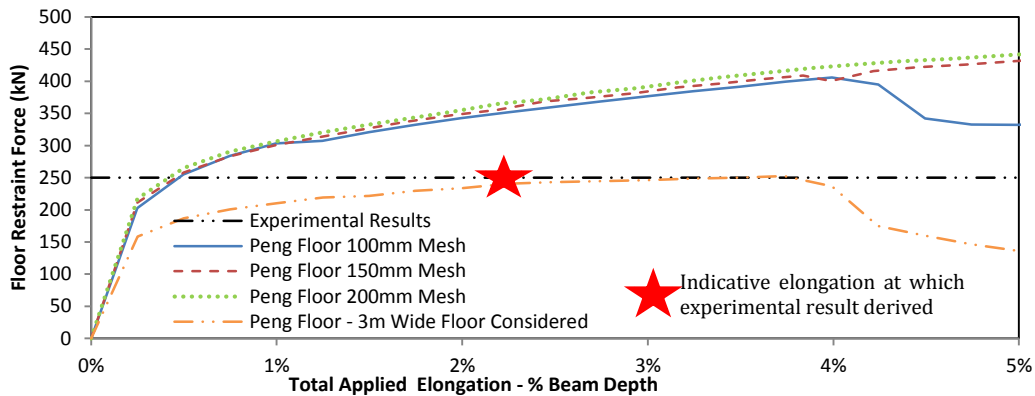


Figure 11-3: Floor elongation restraint force response for Peng et al. (2008) floor with varied mesh sizes and floor width considered

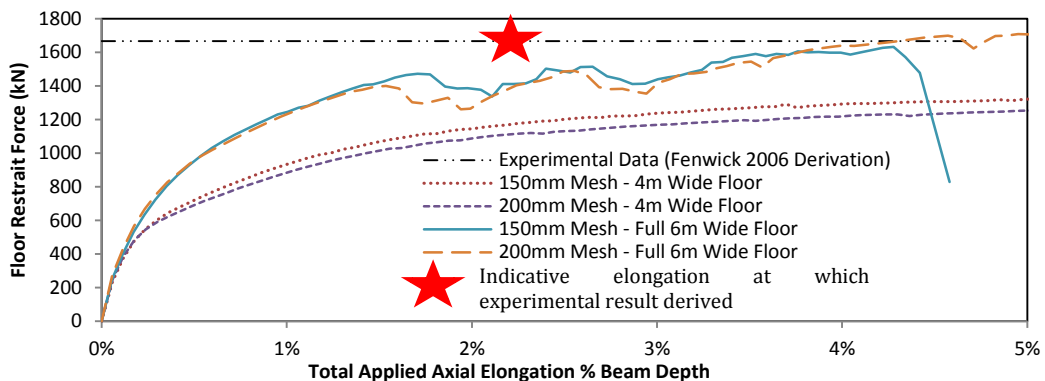


Figure 11-4: Floor elongation restraint force response for MacPherson (2005) floor with varied mesh sizes

The comparisons of varying mesh sizes showed that in general, despite the different dimensions of the floor systems considered, the floor response was relatively insensitive to the

nodal spacing used in the computational model. The floor response has been shown to be sensitive to the extent of floor considered in the model, as considering only part of the floor tended to under-predict the restraint force generated. The required mesh size was therefore determined based upon the size needed to consider the full extent of floor participating in plastic hinge restraint, as the comparisons showed that considering only part of the relatively small floors tested in the experiments, resulted in errors as compared to the full extent models.

For the simplified floor diaphragm modelling, the only applied input to the floor system was the elongation strains at the edge of the floor diaphragm. Other force inputs such as diaphragm transfer demands and out-of-plane displacement compatibility were outside the scope of the study. These applied loads were enforced using boundary conditions and applied loads, as presented in Chapter 3. However the effect of where these loads were applied was considered by adjusting the loading points. Analysis of the crack patterns observed in the Peng et al. (2008) experiment, shown in Figure 11-5, provided an indication as to how the load was transferred into the floor diaphragm in the experimental program. The crack patterns at 2% drift showed that the flexural cracking of the perimeter beam occurred over a defined plastic hinge length, rather than a single elongation gap opening up at the face of the column. As shown in Figure 11-6, the crack pattern led to two potential load/support condition layouts. Figure 11-6(a) shows an option to apply elongation at the column face only, simulating a small plastic hinge length. Figure 11-6(b) shows an option to distribute the cracking more realistically over the cracked beam length, based upon the inferred crack patterns.

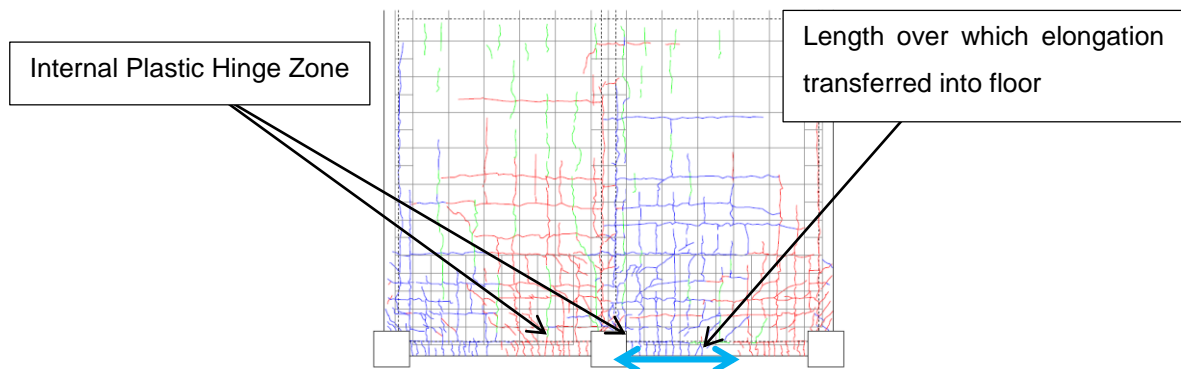


Figure 11-5: Observed crack pattern in floor plate at 2% drift Peng et al. (2008)

Models were run in order to assess the effects of load application and boundary condition supports. The crack patterns derived from the model for the Peng et al. (2008) floor are presented in Figure 11-7, showing a greater concentration of cracking at the central transverse beam when elongation was applied only at the column face. A comparison of the modelled floor restraint with the different support conditions is made in Figure 11-8 for the Peng et al. (2008) floor showing that the restraint force was slightly lower than for the case of non-distributed elongation, but effectively unchanged with respect to the centrally located supports. The distributed elongation case still over-estimated the force generated in the floor. The floor restraint response with varying support conditions for the Lau et al. (2002) floor is presented in

Figure 11-9, showing the effect of the support conditions was minimal on the predicted restraint force generated. The elongation strain capacity was increased because the distribution of cracks delayed the onset of fracture, which occurred at high levels of elongation, and was considered relatively unimportant for the analysis.

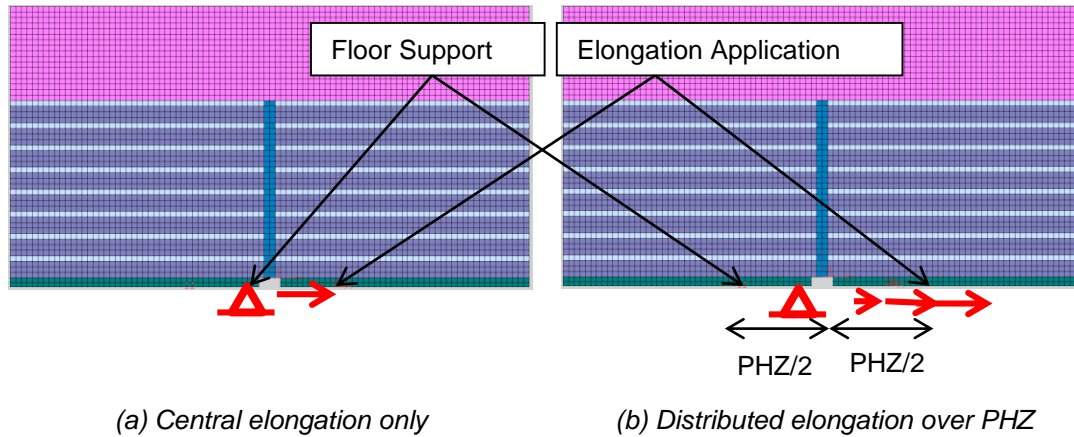


Figure 11-6: Support condition and load application for floor in-plane modelling options

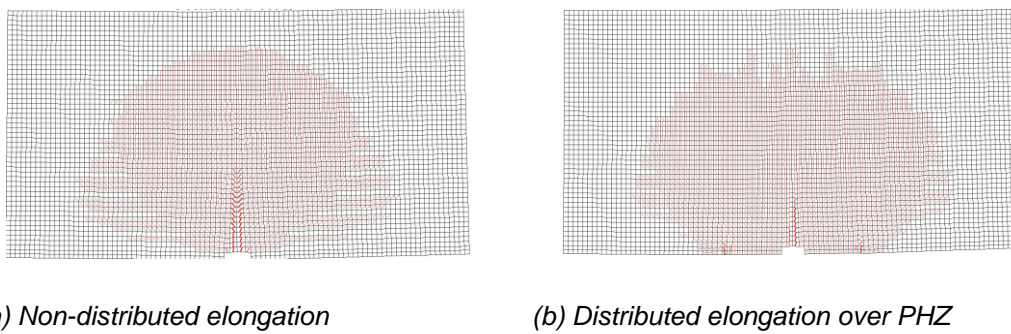


Figure 11-7: Indicative crack patterns from VecTor2 model for Peng et al. (2008) floor model at 10mm applied elongation

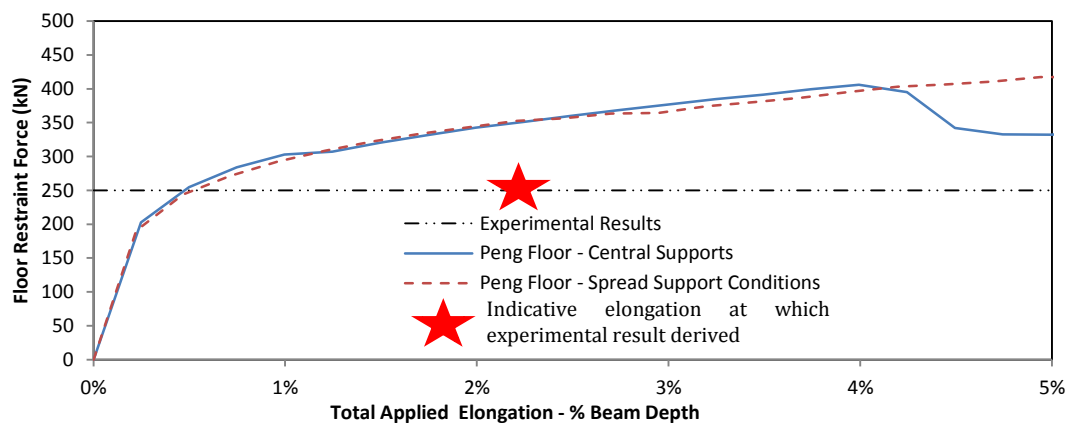


Figure 11-8: Modelled floor restraint response with support conditions varied (Peng et al. (2008) floor)

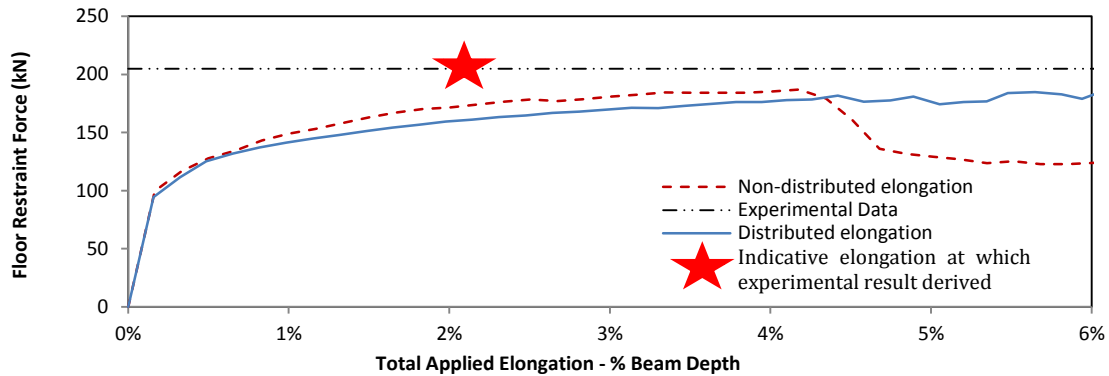


Figure 11-9: Modelled floor restraint for Lau et al. (2002) floor with varied support conditions

As shown in Figure 11-10, the applied load increment did not have a significant effect on the modelled results, and increments of 1mm were acceptable. Given that the total elongation magnitudes were small, a smaller increment was used to achieve more detailed information regarding the response.

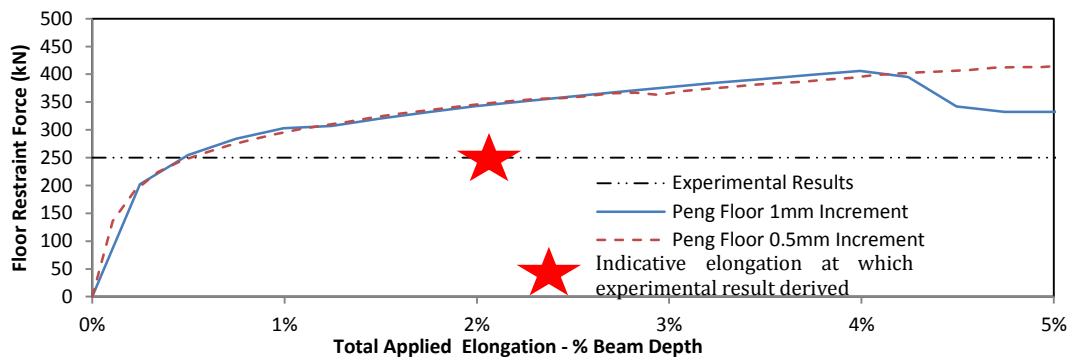


Figure 11-10: Modelled floor restraint force with load increment varied - Peng et al. (2008) (4m wide) floor

VecTor2 offered a wide range of constitutive models which could be used in the analysis, allowing the user to adjust inputs such as the stress-strain material responses, crack width checks and reinforcement bond characteristics. The full analysis options are covered in more detail in (Wong et al. 2013). VecTor2 offered two default settings – basic and advanced – which could be simply interchanged depending on the accuracy required. The basic default models are presented in Table 11-1.

Table 11-1: Basic VecTor2 constitutive models

Concrete Models		Reinforcement Models	
Compression Pre-Peak	Hognestad (Parabola)	Hysteretic Response	Baushinger (Seckin)
Compression Post Peak	Modified Park-Kent	Dowel Action	Tassios (Crack Slip)
Compression Softening	Vecchio A (ϵ_1/ϵ_2)	Buckling	Refind Dhakal-Maekawa
Confined Strength	Kupfer/Richart	Analysis Models	
Dilation	Variable - Kupfer	Strain History	Previous Considered
Cracking Criterion	Mohr-Coulomb (Stress)	Strain Rate Effects	Not Considered
Crack Stress Calculation	Basic (DSFM/MCFT)	Structural Damping	Not Considered
Crack Width Check	Agg/2.5 Max Width	Geometric Nonlinearity	Considered
Crack Slip Calculation	Walraven (Mono)	Crack Process	Uniform
Creep and Relaxation	NA		
Hysteretic Response	Nonlinear w Plastic Offsets		
Tension Stiffening	Modified Bentz 2003		
Tension Softening	Linear		
FRC Tension	SDEM Mono		

As a proxy for assessing the full effect of the constitutive models, the difference in predicted restraint forces between the basic and advanced default constitutive models are presented in Figure 11-11. As can be seen, the pre-peak responses were very similar. The advanced models predicted earlier strength loss but a lower magnitude of strength degradation once the peak floor restraint capacity was exceeded. The analysis rigour of the advanced models tended to predict a lower demand at which strength degradation began because the advanced models tended to predict softening of the concrete due to adjacent crack formation. In general, the result suggested that the constitutive models used in the analysis had a minor effect on the floor response.

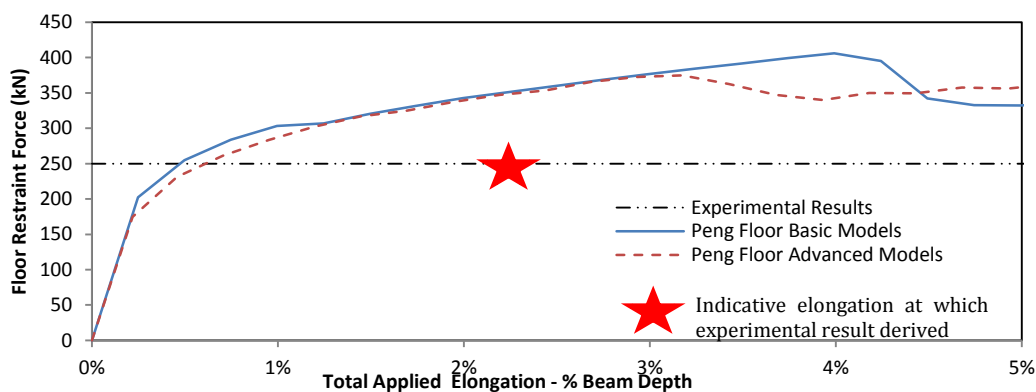


Figure 11-11: Modelled floor restraint force with constitutive models varied - Peng et al. (2008) (4m wide) floor

There were two major considerations made when considering the application of reinforcement in the computational model. The first was the choice between smeared or discrete reinforcement, particularly for the high strength pre-stress strands in the floor units, in order to simulate bond effects and to achieve greater levels of information regarding the response of

the prestress strands. In the case of the precast floors, the use of discrete reinforcement required a large number of bars spaced throughout the floor as the floor units tended to have well distributed flexural reinforcement in the direction of the unit span. The inclusion of the floor reinforcement discretely increased the bandwidth significantly and caused the VecTor2 node limit to be reached with narrow floors (only around 2m wide and 12m span), thus limiting the width of floors which could have been considered. As experiments have shown that cracked width can easily reach greater than 4m, the use of discrete reinforcement was not possible in this case. The implications of not using discrete reinforcement were that less resolution was gained on the behaviour of each strand, and the bond properties of the reinforcing bars was not accurately modelled.

The second reinforcement application consideration involved the implementation of prestress strains to the floor unit reinforcement. As the construction process involved the precast floor units being cast and prestressed before the topping was placed, the pre-compression force was not transferred into the topping concrete. The construction sequence could not be captured in VecTor2 and hence the application of prestress was resisted in compression by the topping and the floor units compositely in the model. The effect of including and excluding prestress strains on the overall response is presented in Figure 11-12 for the Peng et al. (2008) floor, showing the effect was to increase the magnitude of axial restraint force generated in the floor. The increase in the restraint force observed was due to the additional stiffness provided to the floor units by the prestress reinforcement which concentrated cracks into the transverse beam fuse. As the prestress strands in New Zealand flooring units are placed near the base of the floor units, a two-dimensional consideration of the prestress strands was deemed to result in an over-estimation of the floor unit stiffness. For simplicity it was recommended that prestress strains not be applied to the model.

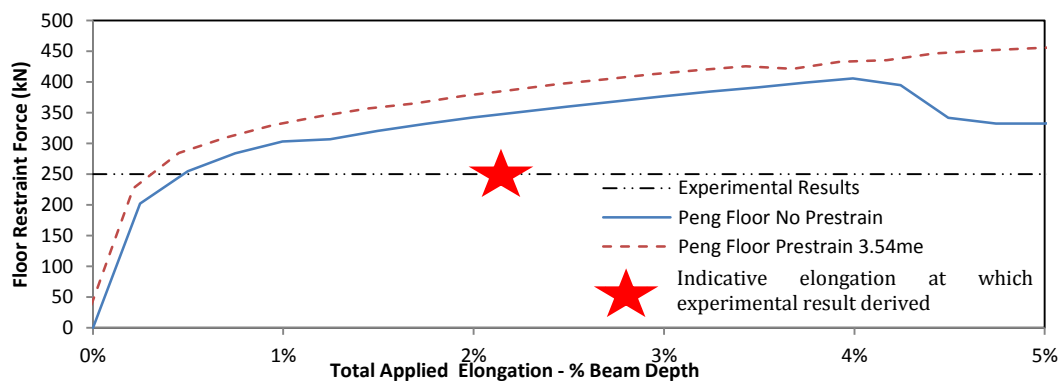


Figure 11-12: Modelled floor restraint force with strain in pre-stress strands varied – Peng et al. (2008) (4m wide) floor

The iterations undertaken in this Appendix were used as the basis for numerical convergence comparisons made in Chapter 3.

Appendix C

12 Appendix C

Presented in this appendix is a supplement to the floor parametric study presented in Chapter 4. In order to assess the effect of parametric variations in the floor arrangement and detailing, a series of base case models were first run. These base case models represented standard cases against which the effects of parametric variations could be compared. The effects of the parametric variations are compared against the base cases in Chapter 4. However the results of the initial base case modelling are presented in this appendix to supplement the comparisons made in Chapter 4. Additionally, several parametric variations which were not found to have a significant effect on the behaviour of the floor diaphragm are also presented in this appendix.

Base model results

Presented in this section is a summary of the base model results used for comparison to the parametric variations of floor detailing. The four base model layouts shown in Chapter 4 and reproduced below were modelled as per the technique presented in Chapter 3.

- Precast floor units:
 - **Arrangement 1 (A1)** - Spanning perpendicular to applied elongation,
 - **Arrangement 2 (A2)** - Spanning parallel to applied elongation, supported on a transverse beam,
 - **Arrangement 3 (A3)** - Spanning parallel to applied elongation, spanning past elongating hinge.
- **Arrangement 4 (A4)** - Cast insitu floor reinforced with mild steel.

The precast floor systems outlined below were based upon a 300 hollowcore precast flooring similar to that tested by (MacPherson 2005), without the drag bars in the topping. The precast floor units, which spanned 12m, were supported on beams at each end, with only topping spanning across the joins between units. The detailing was in line with current recommended requirements (Fenwick et al. 2010), with 2-D16 continuity bars in the filled cores at each end of each unit for continuity reinforcement. The topping comprised 75mm of insitu concrete reinforced with D12 bars at 300mm centres each way. As the tension capacity of the floor units in restraining elongation had been previously shown to be a function of the vertical load applied to the floor, an equivalent tension capacity was applied to the floor units parallel to their span. The equivalent tension capacity was based upon the floor system analysed by (Fenwick et al. 2006). More details of each of the floor arrangements are presented below, with basic model results also presented.

The general layout of arrangement 1 (precast floors spanning perpendicular to elongation) is presented in Figure 12-1. A summary of the floor properties presented in Table 12-1.

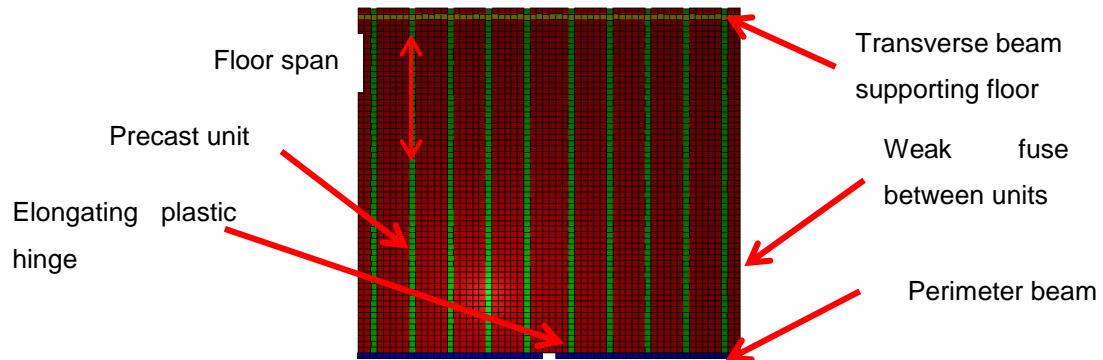
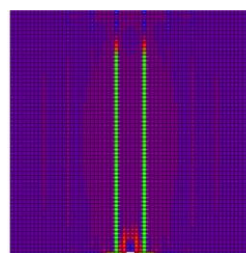


Figure 12-1: Base model layout – Arrangement 1 (Precast floor units spanning perpendicular to elongation)

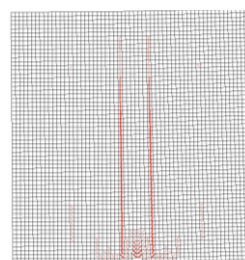
Table 12-1: Arrangement 1 (Precast units spanning perpendicular to elongation) properties

Floor span	12m	Parallel Reo (Topping)	D12's
Floor width	12m	Parallel Reo Spacing	300mm
FEM mesh size	200mm	Perpendicular Reo (Topping)	D12's
		Perpendicular Reo Spacing	300mm
Unit type	300 Hollowcore	Topping Thickness	75mm
Concrete f_c	35MPa	L1 = L2	6m
F_y (PT strands)	1860MPa	Equivalent tension capacity used	937kN/m
F_y (Mild Steel)	300MPa	<i>(Based upon Fenwick et al. (2006) floor units)</i>	

The visual model outputs are presented in Figure 12-2, showing the stress in the floor parallel to elongation and the crack pattern. The areas of high stress shown in green, indicated the joints between the floor units were subject to high tension stress and limited the response of the floor. The crack pattern shown in Figure 12-2 (b) indicated that the floor units separated over the majority of their extent with large cracks forming between the units. Little cracking was observed in the precast floor units themselves.



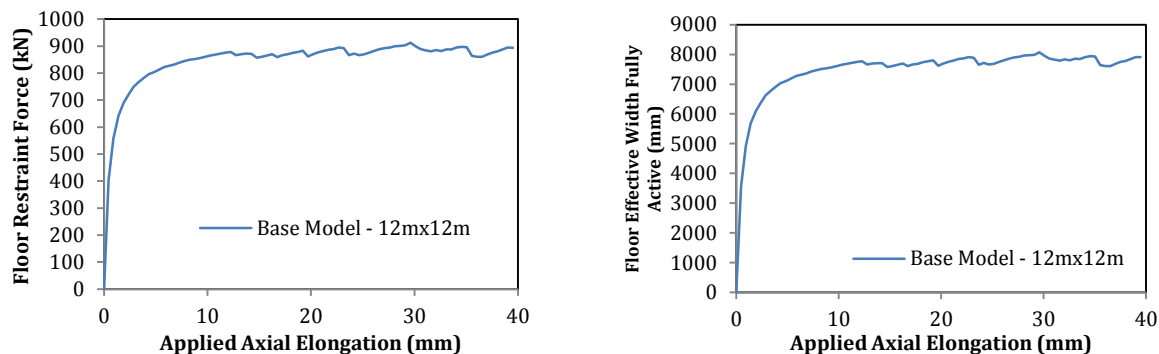
(a) Stress field parallel to elongation



(b) Crack pattern in floor

Figure 12-2: VecTor2 outputs for arrangement 1 (precast floor spanning perpendicular to elongation) - Green represents high tension, Blue represents low tension/compression

Presented in Figure 12-3 is the measured response of the floor to applied elongation strain. As shown in Figure 12-3 (b), the effective width of fully activated floor topping reinforcement was approximately 7.5m. This effective width supported the crack pattern shown in Figure 12-2 (b) whereby the floor units were seen to separate over a large proportion of the floor unit span.



(a) Floor axial restraint force generated in PHZ (b) Floor fully effective width in axial restraint

Figure 12-3: Arrangement 1 (Precast floor spanning perpendicular to elongation) basic modelling results

There were two cases to consider for precast floor systems which spanned parallel to the direction of applied axial elongation. The first was the case where the floor units were supported on a transverse beam at the elongating hinge location (arrangement 2). Arrangement 2 could occur in a moment frame situation where each column supports a transverse beam. The second was the case where the floor units spanned past the elongating hinge, supported on transverse beams located away from the hinge being considered (arrangement 3). This case could arise where the moment frame supports a transverse beam at every second column, or in a non-load bearing coupled wall situation. Based upon the calibration undertaken in Chapter 3, the behaviour of each case was expected to differ markedly. Both cases, as presented below, were based upon the 300 Hollowcore floor previously discussed.

Consideration was first given to arrangement 2, where the precast units were supported on transverse beams at the plastic hinge location. The general model layout of arrangement 2 is shown in Figure 12-4. A summary of the floor properties are presented in Table 12-2. As indicated by the purple line in Figure 12-4, the floor units were supported on a transverse beam at the internal hinge location. The floor system only included half the floor unit span each side of the elongating hinge. The reason for considering only half the floor unit span each side of the hinge was because each transverse beam would be supported on an external column in a real building. The presence of support columns in the perimeter frame would lead to an elongating plastic hinge zone associated with each transverse beam. As the modelling was based upon only a single hinge elongating at a time, the span of floor considered was based upon a tributary width approach whereby the amount of floor associated with each hinge was

assumed independent. In this way, only half the floor unit span was considered. Multiple simultaneous hinges were explored further in Chapter 5.

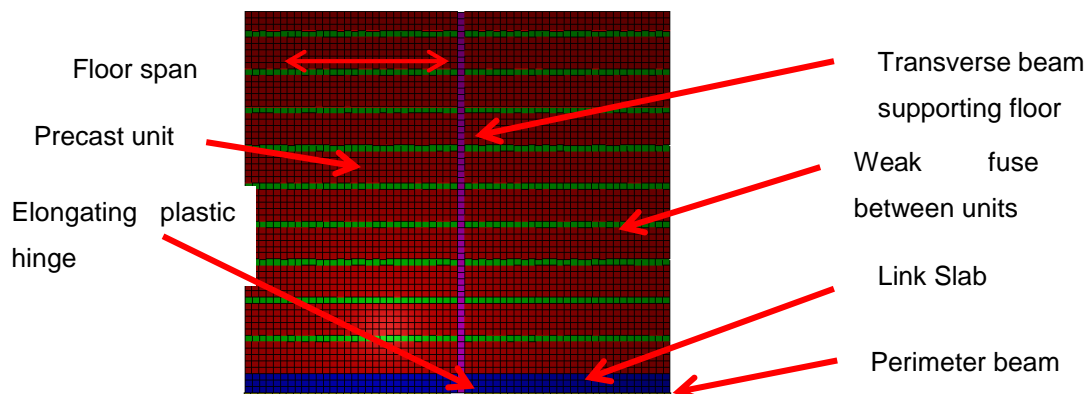
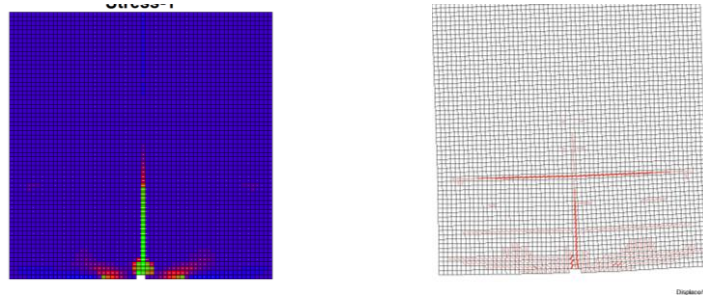


Figure 12-4: Base model layout – Arrangement 2 (Precast floor spanning parallel to elongation - supported on transverse beam)

The visual outputs from the VecTor2 model are presented in Figure 12-5. Figure 12-5 (a) shows the stress in the floor parallel to elongation, demonstrating a concentration of demand over the transverse beam. Analysis of the diagram also demonstrated that the demand in the precast floor units themselves was relatively small. Figure 12-5 (b) shows the crack pattern formed in the floor at 10mm applied elongation. The cracks can be seen to be very concentrated in the weak zones in the floor. In particular, the transverse beam fuse was observed to be subject to large cracks over a defined effective width length. Also of note was that there was significant cracking in the weak zones between the floor units, indicating the weakness between the units was also concentrating the deformation. It may also be observed that significant distributed cracking occurred in the flexible link slab connecting the perimeter beam to the floor.

Table 12-2: Arrangement 2 (Precast units spanning parallel to elongation – supported on transverse beam) - properties summary

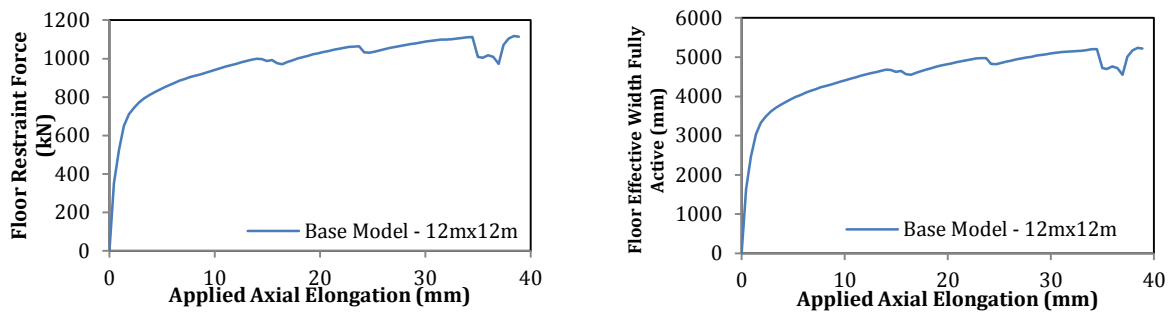
Floor span	12m (6m each side)	Parallel Reo (Topping)	D12's
Floor width	12m	Parallel Reo Spacing	300mm
FEM mesh size	200mm	Perpendicular Reo (Topping)	D12's
		Perpendicular Reo Spacing	300mm
Unit type	300 Hollowcore	Topping Thickness	75mm
Concrete f_c	35MPa	L1	0m
F_y (PT strands)	1860MPa	Equivalent tension capacity used	937kN/m
F_y (Mild Steel)	300MPa	<i>(Based upon Fenwick et al. (2006) floor units)</i>	



(a) Stress field parallel to elongation (b) Crack pattern in floor

Figure 12-5: VecTor2 outputs for arrangement 2 (precast floor spanning parallel to elongation – supported on transverse beam). Green represents high tension stress.

The basic quantitative modelling results are presented in Figure 12-6. The results showed the axial restraint force generated was in the order of 1000kN, which required the activation of 4-5m effective floor width to generate the restraint force. The response of the floor can be seen to have been initially very stiff, with the onset of yield, as indicated by the reduction in slope of the restraint force plot, occurring rapidly.



(a) Floor axial restraint force generated in PHZ (b) Floor fully effective width in axial restraint

Figure 12-6: Arrangement 2 (Precast floor spanning parallel to elongation – supported on transverse beam) - basic modelling results

The second arrangement of parallel spanning precast floors, where the floor units spanned past the elongating hinge, is presented in Figure 12-7. The general model properties are presented in Table 12-3. As indicated in Figure 12-7, the elongating hinge was located at the centre of the floor unit span, with the transverse beams located half the floor span away from the hinge. In the case of the floor units spanning past the elongating hinge, the total width of floor considered was reduced to 8m to reduce computational demands. The basis for considering a smaller floor width than the 12m considered for the previous models was that a lower width of floor was found to be engaged in this case and so considering a larger area of floor was unnecessary. The validity of considering a reduced floor width is confirmed in section 0, where different widths were considered.

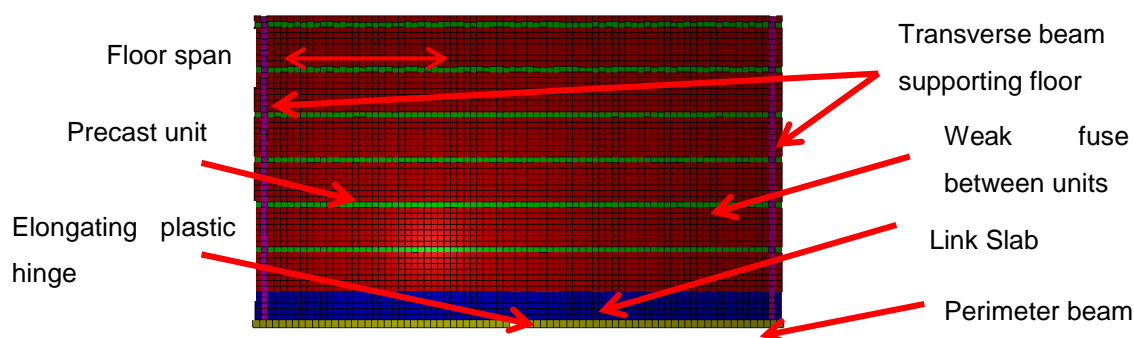


Figure 12-7: Base model layout – Arrangement 3 (Precast floor spanning parallel to elongation – spanning past hinge)

Presented in Figure 12-8 (a) is the stress field generated in the floor in the direction parallel to the applied elongation. The link slab and precast floor units were highly stressed in this case, with a relatively well distributed stress demand as compared to the previous fuse dominated cases. It may be seen that the stress in the floor spread outwards from the elongating hinge and distributed through the floor system. The crack pattern, shown in Figure 12-8 (b), indicated that there was a distributed series of cracks which propagated outwards from the hinge. In particular it was observed that the link slab near the hinge was highly damaged, but the large cracks did not spread into the precast floor units, which were subject to minor cracking only. In addition, it was observed that the joints between the units were significantly cracked, suggesting a concentration of deformation into these weak zones.

Table 12-3: Arrangement 3 (Precast units spanning parallel to elongation – spanning past hinge) - properties summary

Floor span	12m	Parallel Reo (Topping)	D12's
Floor width	8m	Parallel Reo Spacing	300mm
FEM mesh size	200mm	Perpendicular Reo (Topping)	D12's
		Perpendicular Reo Spacing	300mm
Unit type	300 Hollowcore	Topping Thickness	75mm
Concrete f_c	35MPa	L1=L2	6m
F_y (PT strands)	1860MPa	Equivalent tension capacity used	937kN/m
F_y (Mild Steel)	300MPa	<i>(Based upon Fenwick et al. (2006) floor units)</i>	

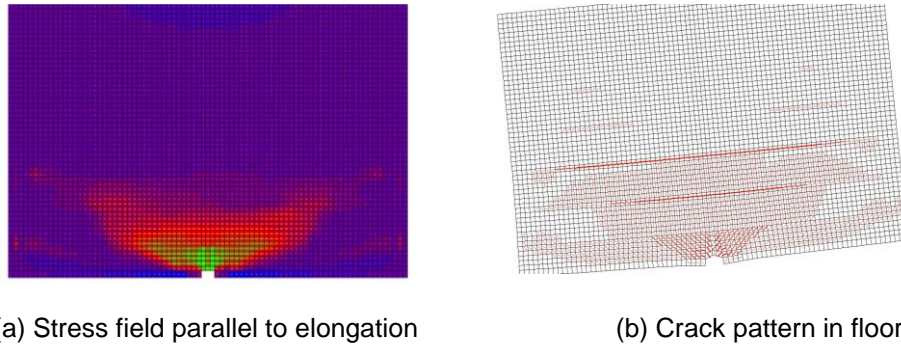
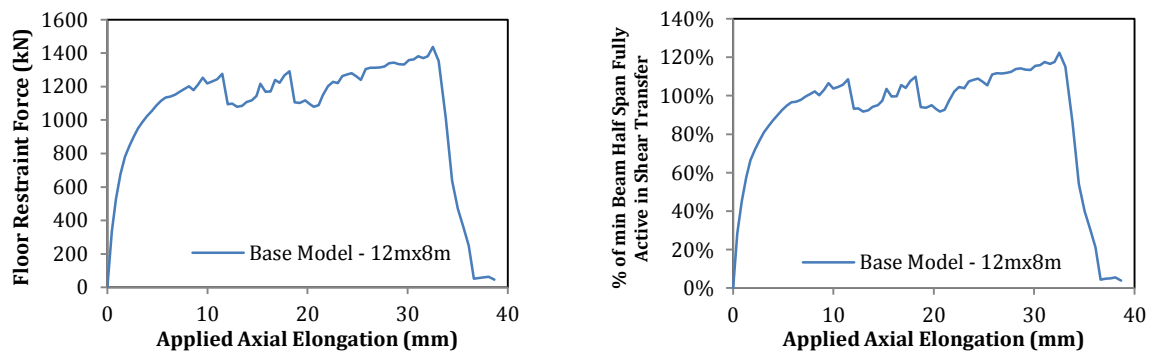


Figure 12-8: VecTor2 outputs for arrangement 3 (precast floor spanning parallel to elongation –spanning past hinge) - Green represents high tension, Blue represents low tension/compression

The basic quantitative modelling results are presented in Figure 12-9. The observed restraint force generated was of the order of 1200kN, which required the effective width activation of approximately 1200mm of floor, plus the 750mm link slab. Analysis of Figure 12-9 (b) demonstrated that the shear capacity of the link slab was fully activated in order to enforce compatibility between the floor and the perimeter frame. The full shear activation was confirmed by the variability in the axial restraint force at maximum restraint capacity. As the maximum floor restraint force was reached, significant shear deformations prevented the numerical convergence of the software as the link slab began to fail in shear. The peaks and troughs in the plots were indicative that large deformation associated with shear failure was occurring at the maximum generated restraint force.



(a) Floor axial restraint force generated in PHZ (b) Proportion of shear capacity activated at interface of beam and floor

Figure 12-9: Arrangement 3 (Precast floor spanning parallel to elongation – spanning past hinge) - basic modelling results

The final arrangement considered was based upon a cast insitu flooring system which was less common in New Zealand. The general layout of the insitu mild steel floor is presented in Figure 12-10. A summary of the properties of the model are presented in Table 12-4. No relatively weak fuses were included as the floor was cast without joints such as those seen in precast floor systems. The 150mm thick floor was reinforced with 12mm deformed bars top and bottom at 300mm centres each way.

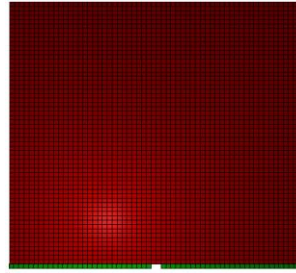
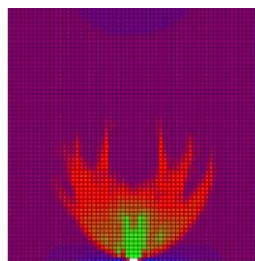


Figure 12-10: Base model layout – Arrangement 4 (Mild steel insitu floor)

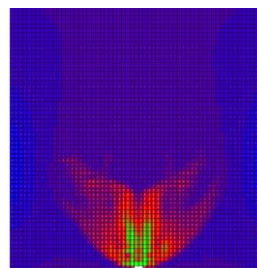
The stress fields generated in the floor reinforcement at 10mm applied elongation are presented in Figure 12-11. The stress parallel to elongation was observed to be concentrated over a defined effective width region. Similarly, the stress perpendicular to elongation indicated an effective width of floor reinforcement was activated to prevent the disconnection of the perimeter beam from the floor. The smooth shape of the stress fields was indicative of the homogeneous nature of the insitu floor, with no relatively weak zones concentrating deformation.

Table 12-4: Arrangement 4 (Cast insitu mild steel floor) properties summary

Floor span	12m	Parallel Reo	D12's Top and Bottom
Floor width	12m	Parallel Reo Spacing	300mm
FEM mesh size	200mm	Perpendicular Reo	D12's Top and Bottom
		Perpendicular Reo Spacing	300mm
Thickness	150mm		
Concrete f_c	35MPa	L1 = L2	6m



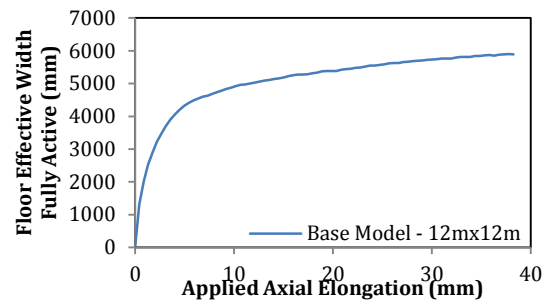
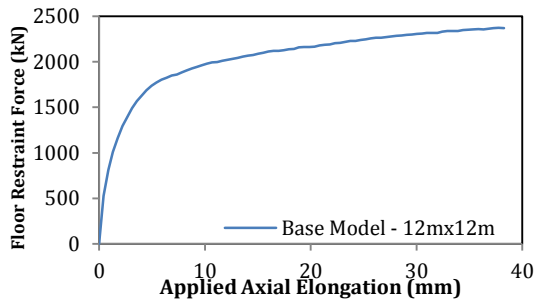
(a) Stress field parallel to elongation



(b) Stress field perpendicular to elongation

Figure 12-11: VecTor2 stress field outputs for arrangement 4 (cast insitu mild steel floor) - Green represents high tension, Blue represents low tension/compression

Presented in Figure 12-12 (a) is the total axial restraint force generated in the floor, observed to increase smoothly up to approximately 2200kN at large applied axial elongation. Presented in Figure 12-12 (b) is the width of fully effective floor, which was also observed to reach a maximum of approximately 5-6m, slightly less than half the total width of floor considered in the model.



(a) Floor axial restraint force generated in PHZ (b) Floor fully effective width in axial restraint

Figure 12-12: Arrangement 4 (Cast insitu mild steel floor) basic modelling results

A brief summary of the results from modelling the base models has been presented and has indicated that the behaviour varied significantly between the different floor arrangements. In particular the layout of weak fuses has been shown to have a significant impact on the deformation patterns in the floor and the axial restraint force generated. The results from the parametric study were compared to these base model results in Chapter 4 to assess the effects of varying floor detailing. The underlying mechanics and postulated reasoning for the observed behaviour is discussed in Chapter 5.

Supplementary parametric study results

As a supplement to the floors parametric study results presented in Chapter 4, the results of additional parameter variations are presented in this section. The results presented in this section generally indicated that the parameter being varied had a limited effect on the response of the floor to axial elongation strains. However the results were presented below for completion.

8. Floor Width

The width of floor considered in the model was varied for each of the floor arrangements to confirm that the floor extents did not influence the modelled behaviour, as shown indicatively in Figure 12-13. The floor width was defined in this case as the distance of floor extent, measured perpendicular to the applied elongation direction.

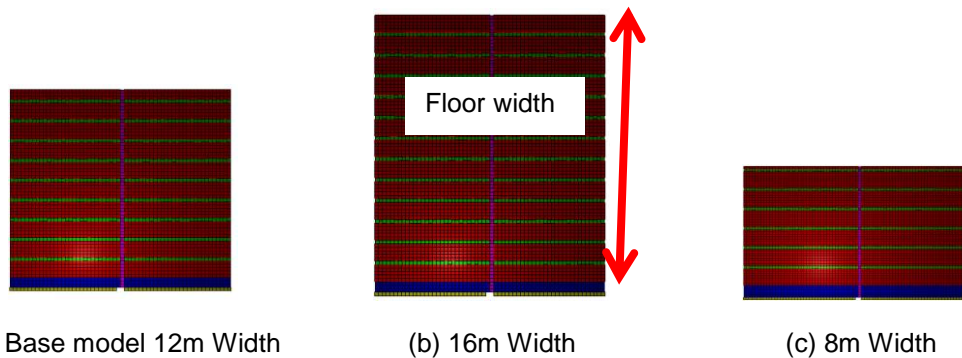


Figure 12-13: Floor width parameter variation indicative layouts for arrangement 2

A comparison of the modelled results based upon variations in the width of floor considered is presented in Figure 12-14 for the four different floor arrangements considered. For perpendicular spanning floor units (A1), the restraint force increased in proportion to the floor width considered. This result suggested the precast units tended to separate over their full length by rotating on their supports. The two cases of floor units spanning parallel to the applied elongation, arrangements 2 and 3, are shown in Figure 12-14 (b) and (c) respectively. The results for parallel spanning floors showed little variation between the modelled results for the different floor widths. Analysis of the results indicated that the modelled floor widths were sufficient to capture the large scale behaviour and was not limited by the floor width.

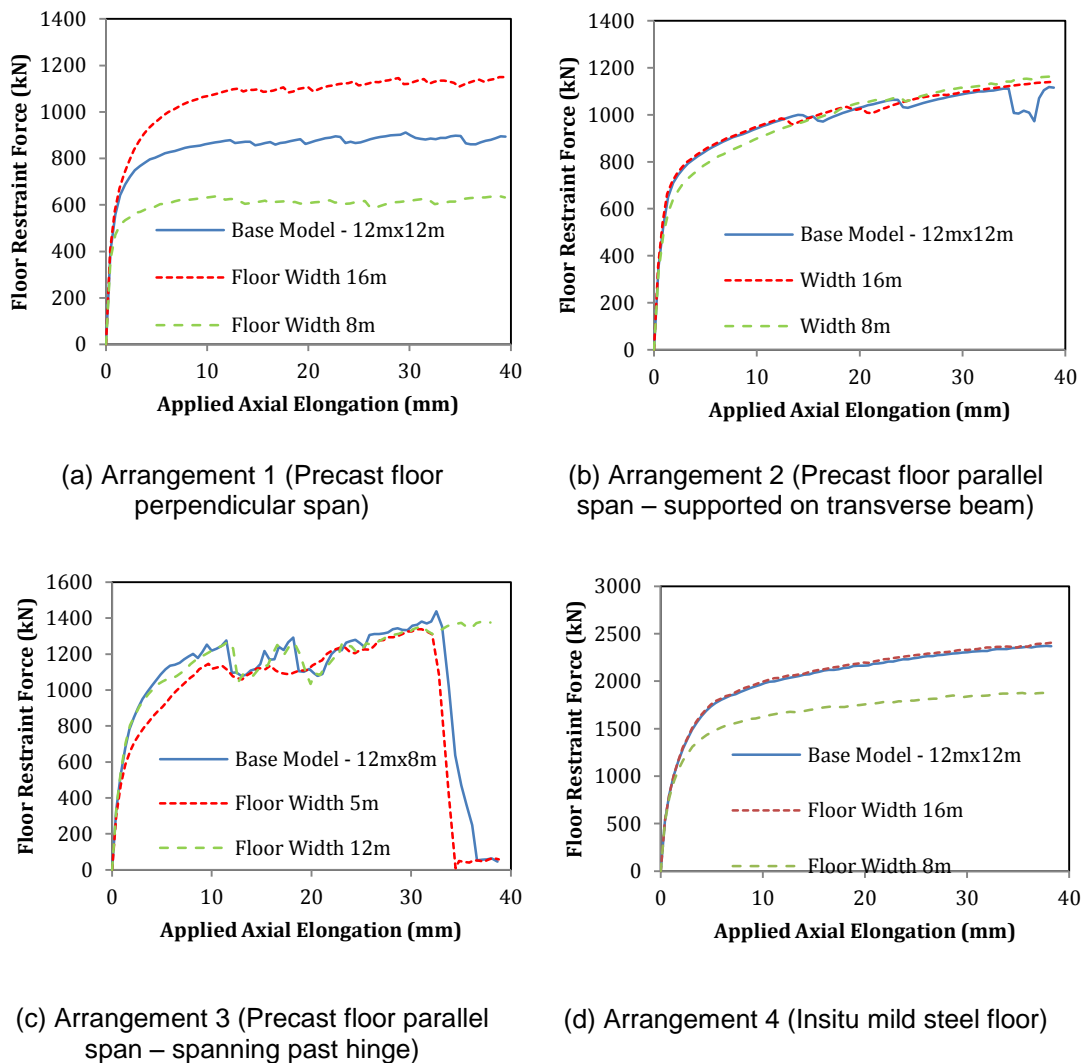


Figure 12-14: Modelled floor axial restraint response with floor widths varied

Comparisons of the widths considered in the modelling confirmed that a 12m width was suitable to capture the behaviour of the models in all cases. For arrangement 3, a smaller width of 8m was observed to be sufficient to capture the behaviour.

9. Topping Thickness

The effect of the topping thickness was explored by varying the topping between 65mm and 100mm. As shown in Figure 12-15, the effect was found to be small. The small difference was primarily due to the tension capacity of the floor concrete changing slightly. The stiffness of the response was influenced slightly because the onset of cracking took longer with thicker topping. Additionally, the thicker topping model demonstrated early strength degradation because the reinforcement was unable to generate secondary cracks as a result of the lower reinforcement ratio. The lack of secondary cracks led to strain concentration at a single crack and early fracture. However the overall effect of the topping thickness was assessed as being minor based upon this comparison.

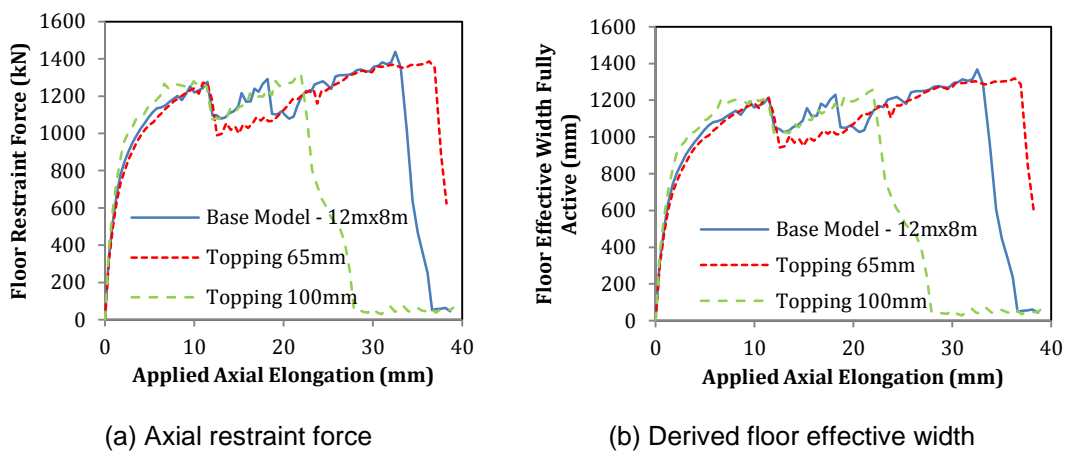


Figure 12-15: Modelled topping thickness effect for arrangement 3 (precast units spanning parallel to elongation past hinge)

10. Fuse Strain Width

The fuse strain width was an important parameter to consider for finite element modelling of floors because it defined the length over which the deformation in a fuse was averaged as a strain. This was because the element size defined the spacing of nodes in the finite element model, as presented in Figure 12-16. However, as shown in Figure 12-17, the effect of the strain width was negligible on the response of the floor. The key implication of this finding was that the response of the floor was determined only by the relative strengths between elements, rather than any effects of stiffness variations in the floor.

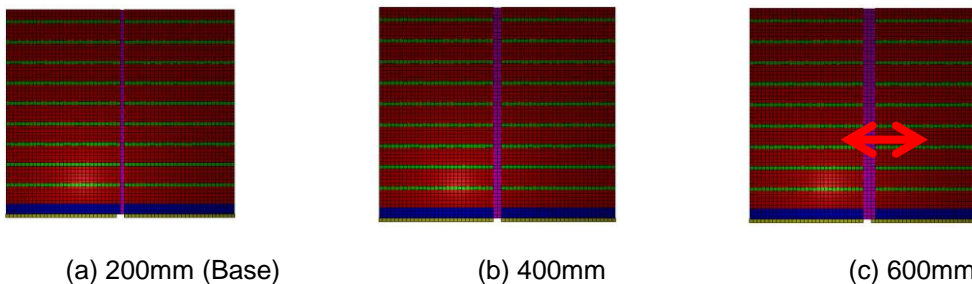


Figure 12-16: Fuse width indicative layout (arrangement 2 shown)

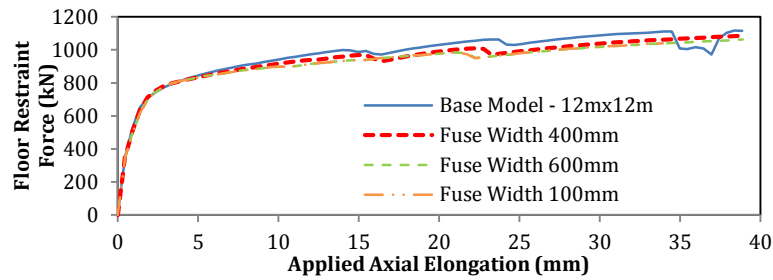


Figure 12-17: Modelled fuse strain width for arrangement 2 (precast units spanning parallel to elongation, supported on a transverse beam)

11. Link Slab Length

The effect of the link slab length was explored as per the models shown in Figure 12-18. Analysis of the results demonstrated that regardless of the link slab length, the majority of the beam span was active in restraining the axial elongation. However it may be observed that with a shorter link slab, the length of activated shear transfer, as indicated by the distribution of the high stress green area, was increased. The amount of the axial restraint force activated is presented in Figure 12-19 for arrangement 3. Analysis of the result indicated that with a shorter link slab, a slightly larger shear capacity is activated in the link slab, leading to a greater measured restraint force, although the results were all closely aligned with the anticipated 100% for this case.

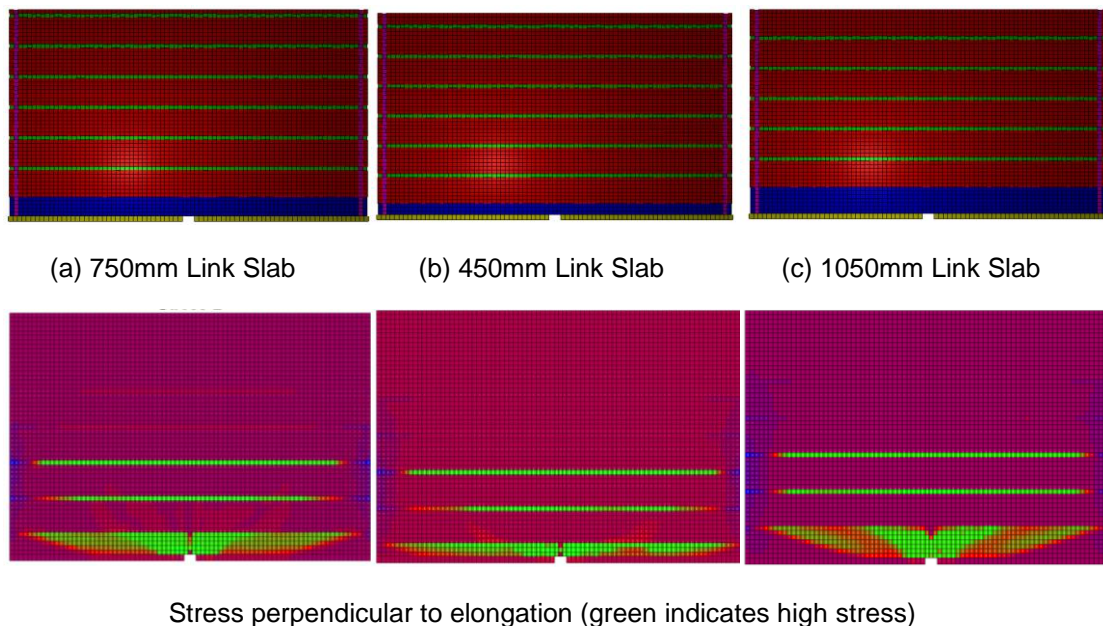


Figure 12-18: VecTor2 visualisation of link slab length effect – arrangement 3 (precast unit spanning parallel past elongating hinge)

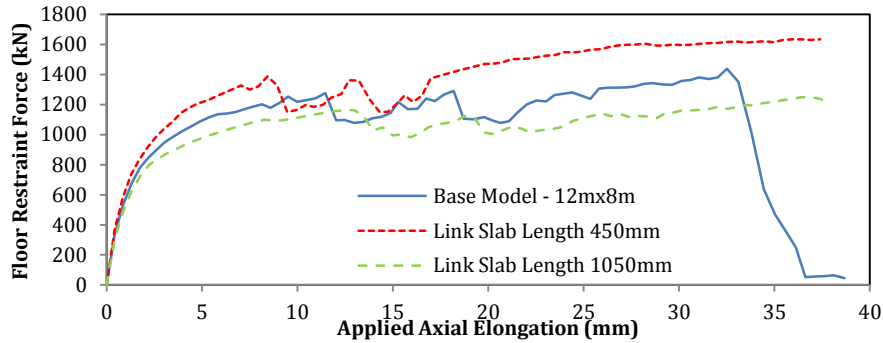


Figure 12-19: Link slab length effect on modelled axial restraint capacity activated for arrangement 3 (precast floor spanning parallel past elongating hinge)

12. Concrete Properties

The effect of the properties of concrete were also briefly considered on the response of the precast floors spanning parallel past the elongating hinge, as presented in Figure 12-20. The effect of altering the compression capacity influenced the measured behaviour only slightly, due to the software using the compressive capacity to define the concrete tension capacity. The effect of concrete properties on the floor response was therefore assessed as being relatively minor.

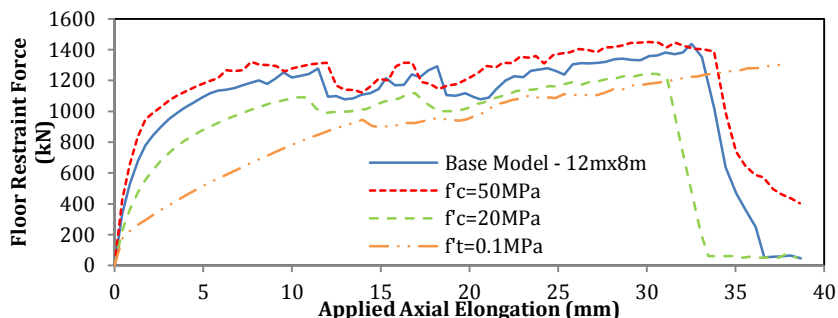


Figure 12-20: Concrete properties effect on modelled axial restraint capacity activated for arrangement 3 (precast floor spanning parallel past elongating hinge)

13. Precast Unit Depth

The effect of varying the depth of concrete considered in the modelling was considered by modelling floors with 200mm, 300mm, and 400mm deep hollowcore units. In this case, reinforcement in the units was not changed in order to isolate the effect of the concrete depth. Variations of floor unit capacity were considered separately. The results for different depths of hollowcore units are presented in Figure 12-21, indicating that the effect was negligible, and primarily the result of an increased area of concrete available to resist tension. Analysis of the result indicated that the use of two-dimensional software did not result in a loss of accuracy for different floor depths.

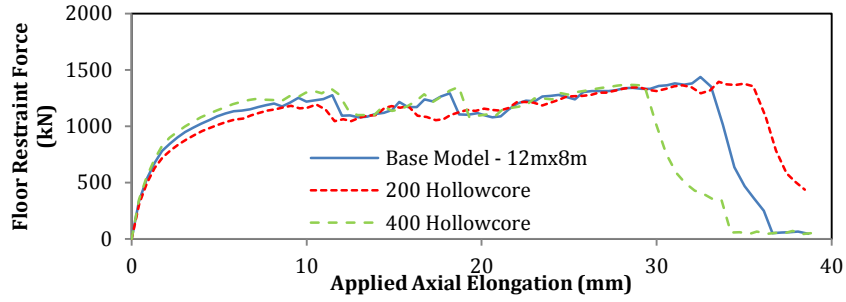
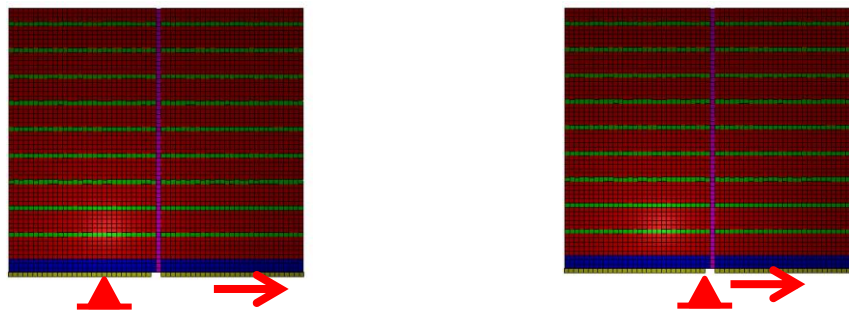


Figure 12-21: Floor unit depth effect on modelled axial restraint capacity activated for arrangement 3 (precast floor spanning parallel past elongating plastic hinge)

14. Load Application

As discussed in Chapter 3, consideration was given to spacing the load application points to the ends of the plastic hinge zone, or by applying the load at the centre, as shown in Figure 12-22. Load application was considered in order to more accurately replicate the deformation occurring at the ends of the plastic hinge zone. The effect of the support location was analysed to assess the appropriateness of the load application protocol, with the resulting floor restraint response plotted in Figure 12-23. Analysis of the results indicated that the effect of the load application point was negligible, with the floor response independent of the exact location of the load application.



(a) Load applied at end of PHZ

(b) Load applied at centre of hinge

Figure 12-22: Load application variation typical arrangement 2 shown

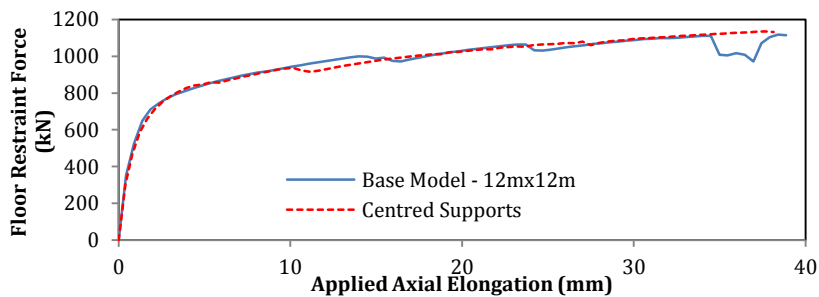


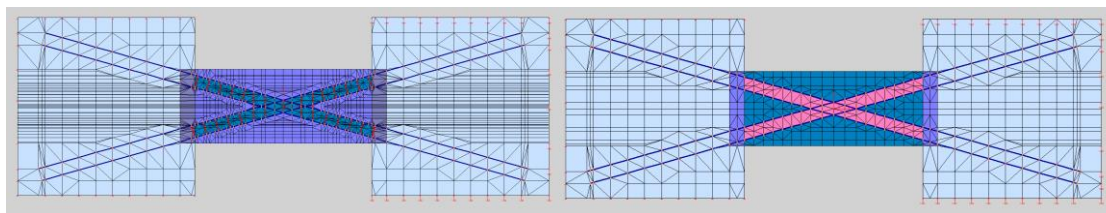
Figure 12-23: Load application effect on modelled axial restraint response for arrangement 2

Appendix D

13 Appendix D

Presented in this appendix is a supplement to the computational model calibration of coupling beams and coupled walls outlined in Chapter 6. This appendix provides a more detailed summary of the iterations undertaken in order to ensure the modelling software replicated reality at suitable computational expense.

The process undertaken to ensure numerical stability and convergence was to undertake a parametric study of variables such as mesh size and load increment to assess the effect on the model results. The optimal results were the parameters which gave the most accurate results at the lowest computational expense. In order to assess what the most accurate results were, experimental data of a Naish et al. (2009) coupling beam (CB24D) were used initially. The basic coupling beam sub-assembly idealisation in VecTor2, representing the (Naish et al. 2009) sub assembly CB24D test specimen, was used for the convergence testing as presented in Figure 13-1. A summary of the variations run for the initial convergence, and their computational efficiency are presented in Table 13-1.



(a) Discrete stirrups

(b) Smeared stirrups

Figure 13-1: Typical VecTor2 coupling beam layout (CB24D)

The two parameters which defined the computational expense of an analysis were the bandwidth and the number of load increments. Bandwidth defined the width of the main diagonal in the numerical matrix equations, thus measuring the number of equations which needed to be solved simultaneously at each load increment by the software. The number of load increments defined the number of loading stages which must be solved in the computation and was directly related to computational expense. The optimal solution achieved suitably accurate results whilst minimising the bandwidth and number of load increments required. To assess the optimal solution, a series of model iterations were undertaken on the coupling beam sub-assembly CB24D. The material properties used in the model matched that of the experiment, as presented in Chapter 6. The coupling beam models were loaded through a single cyclic load reversal, by applying shear displacement at each end of the beam, and unrestrained axially as per the experimental loading protocol. Comparisons of the results for the single cyclic loading studies are presented in Figure 13-2 to Figure 13-4.

Table 13-1: Coupling beam model convergence testing parameter variation list

#	Parameters for variation					Computational Efficiency		
	Undisturbed Region Mesh Size (mm)	Disturbed Region Mesh Size (mm)	Load Increment (mm)	Discrete (D) or Smeared (S) Stirrups	Analysis Models	# Nodes	Band-width	# Load Increment
1	100	100	1	S	Basic	660	231	241
2	100	50	1	S	Basic	851	229	241
3	100	25	1	S	Basic	1593	327	241
4	100	50	0.5	S	Basic	851	229	481
5	100	50	0.25	S	Basic	851	229	961
6	100	50	1.0	D	Basic	2155	543	241
7	100	50	0.5	S	Advance	851	229	241

The single cyclic load reversal results showed good correlation across all mesh sizes in the elastic range and the unloading portion of the response. The larger mesh sizes were observed to result in a slight 'over-shoot' effect as the coupling beam became inelastic. This resulted in a slightly larger shear capacity predicted for 100mm mesh sizes. Based on this, comparison a 50mm mesh size was found to be optimal. It was noted that the study by Mohr (2007) recommended mesh blocks sizes applied in the order of 25mm, which would have been unduly conservative for the Naish et al. (2009) coupling beam. Analysis of Figure 13-3 showed that use of 1mm load increments under-predicted the coupling beam capacity, due to rapid loading preventing stress redistribution. Consequently 0.5mm increments were found to be optimal for loading of the coupling beam. No significant accuracy difference was identified between using discrete transverse stirrups. This finding indicated that the increase in computational demand due to the use of discrete stirrups was not justified by an increase in model accuracy. Smeared stirrups were therefore deemed suitable.

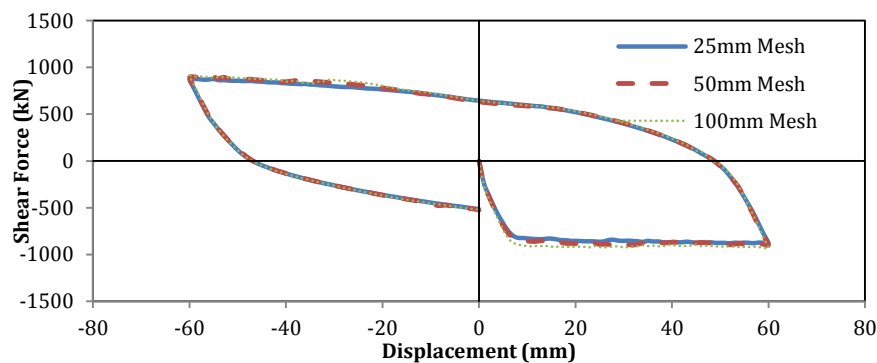


Figure 13-2: Mesh size effect on modelled global force displacement response of CB24D

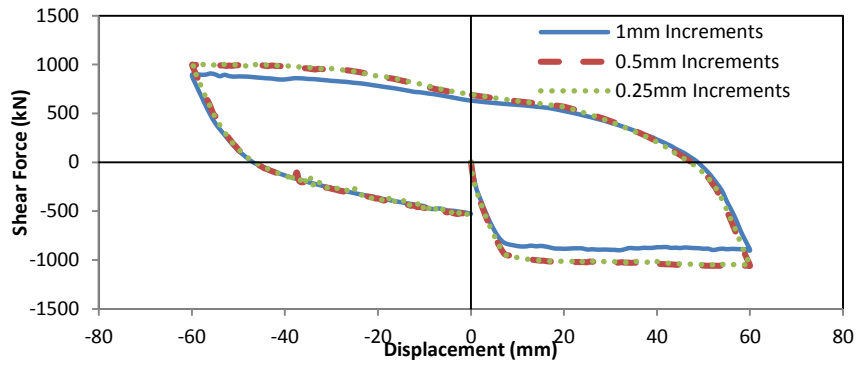


Figure 13-3: Load increment effect on modelled global force displacement response of CB24D

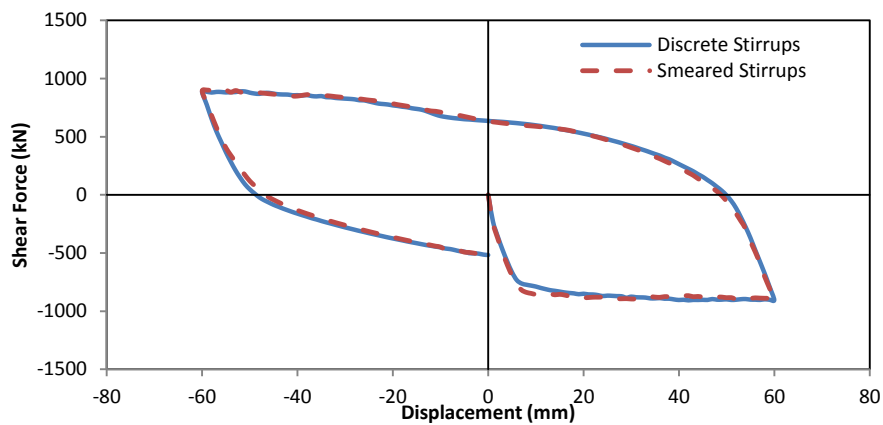


Figure 13-4: Stirrup input effect on modelled global force displacement response of CB24D

Two-dimensional cyclic loading model improvements

The model calibration process presented in this section provides a supplement to the outline presented in Chapter 6 of the two-dimensional cyclically loaded coupling beam model calibration. This calibration was undertaken by comparing the cyclically loaded coupling beam results to available experimental data. In this way the modelling technique was updated to match the experimental data from the CB24D specimen (Naish et al. 2009). As per the previous models, the coupling beam was input with dimensions and material properties which matched the experimentally measured values. Default VecTor2 constitutive models were used initially, as these were updated in Chapter 6.

The initial results of the modelling are presented in Figure 6-5. As presented in Chapter 6, there were significant initial discrepancies when comparing the model results to experimental results. These errors related to early strength degradation prediction and an over-prediction of shear capacity and coupling beam stiffness. The reasons for the inaccuracies, and a method of overcoming the inaccuracies is presented below.

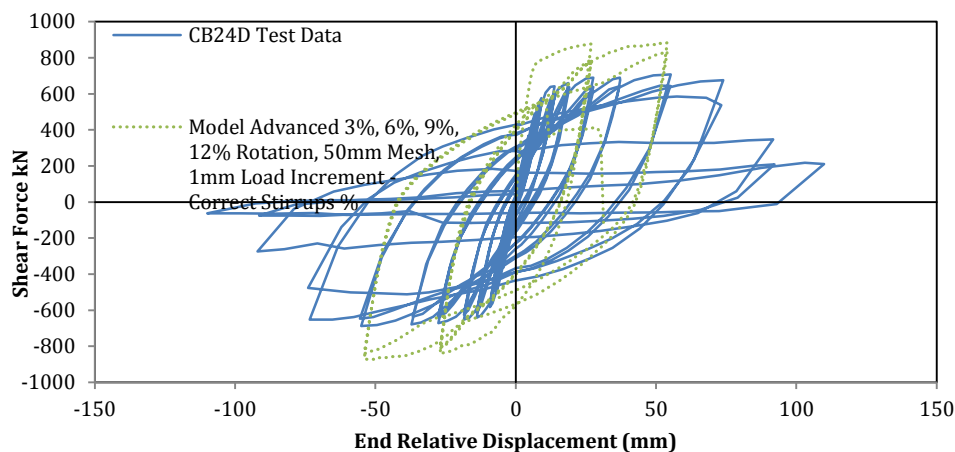


Figure 13-5: Global response of CB24D – Reproduced from Chapter 6

The modelled failure mechanism was observed to be bar fracture at lower applied chord rotation than in the experiment. The early fracture was found to be due to meshing issues within VecTor2, at the location highlighted in Figure 6-4. NZS 3101:2006 (proposed 2014 amendment) and ACI 318-11 required that longitudinal confinement reinforcement not be fully developed at the ends of the coupling beam. To account for this in VecTor2, an additional concrete element was needed as shown. However the use of such an element, when combined with diagonal reinforcement, resulted in complicated meshing around the edges of the beam. As a result, the smeared reinforcement strains were highly concentrated in this zone and early fracture was observed. Since the longitudinal reinforcement was not intended to be developed at the ends of the coupling beam, excluding these areas prevented early bar fracture without affecting the overall beam response. Comparison was also made to considering a separate and more confined concrete element between the diagonal bars as shown, to represent the well confined concrete within the diagonal. However VecTor2 was found to have accounted for the confinement of this region suitably well as the effect of including the confined region as a separate element was found to be negligible.

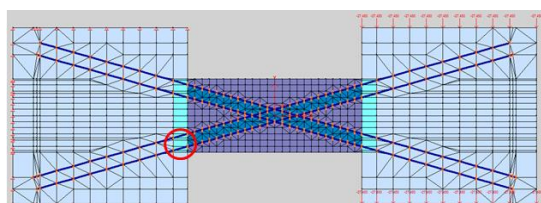


Figure 13-6: VecTor2 model of CB24D, with the end block meshing complication highlighted

The strength over-estimate was the result of the transverse reinforcement contributing unrealistically to the coupling beam shear capacity in the model. The effect of transverse reinforcement was observed experimentally by (Naish et al. 2009), who observed that adjusting the transverse reinforcement did not affect the coupling beam strength capacity, but did influence the ductility capacity by changing confinement and anti-buckling protection. However, modelling research by (Mohr 2007), showed that increasing the ratio of smeared reinforcement

in a VecTor2 model caused a notable increase in coupling beam strength. Therefore the strength increase was found to result from the transverse reinforcement unrealistically contributing to the shear capacity of the coupling beam. Reducing the transverse reinforcement to nominally low levels, for crack control only, resulted in the model strength matching the experimental strength well, as shown in Figure 13-7. However this had a detrimental effect on the confinement of the coupling beam, but was overcome by updating the constitutive models, as discussed in Chapter 6.

The stiffness over-estimate of the VecTor2 coupling beam model was analysed by means of a parametric study of the possible causes of the over-estimate, as shown in Figure 13-7. Bond and concrete stiffness were found to have a negligible effect on the modelled stiffness. However the underlying reason for the stiffness over-estimate was found to be the enforcement of perfectly rigid supports, on the end blocks representing the wall piers. Displacement of the end blocks, by supports as shown in Figure 13-8, resulted in suppression of flexural deformations which were particularly significant in the elastic range. This was because the supports enforced the wall piers to be infinitely rigid. As shown in Figure 13-7, when the supports were relocated outwards, some flexural deformations were allowed for and the stiffness was much more accurately accounted for in the model. However, as presented in Figure 13-8, the elongation was not accurately accounted for in such a model, as the coupling beam tended to deform in flexure and recover tensile strains upon reloading. It was therefore concluded that the stiffness over-prediction was the preferable error, given the importance of axial elongation for this research, so the modelling was undertaken based upon the actual support locations.

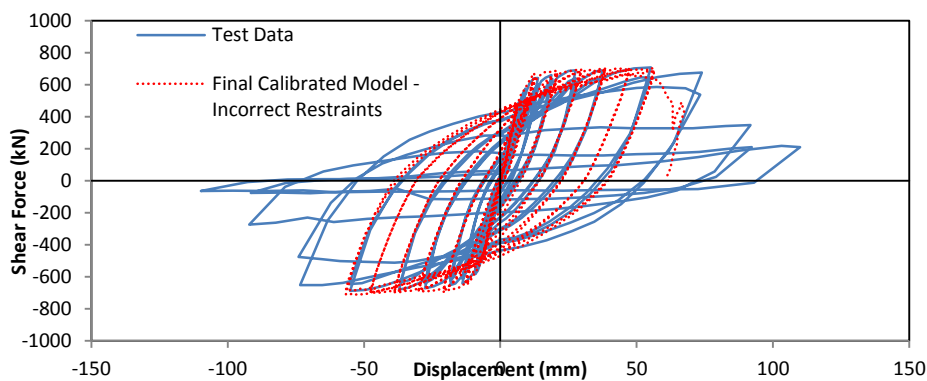


Figure 13-7: Calibrated model global response

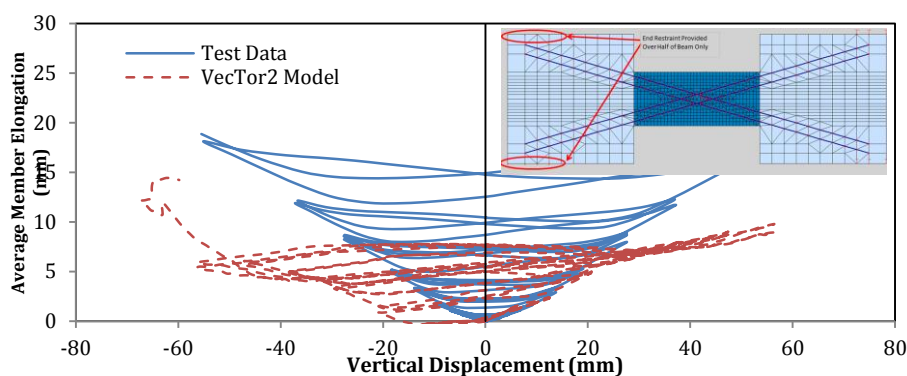


Figure 13-8: Member average axial elongation with calibrated VecTor2 model (CB24D) (relocated support conditions shown)

As discussed above, the two-dimensional models presented in Chapter 6 included only nominal transverse reinforcement and excluded the additional concrete elements. However the models also included the actual experimental support conditions to more accurately reflect coupling beam axial elongation, despite a more accurate prediction of stiffness being found when the supports were relocated.

Three-dimensional cyclic loading model improvements

Presented in this section is a supplement to the model calibration process of three-dimensional coupling beam and floor interaction presented in Chapter 6. As presented in Chapter 6, inclusion of the full floor width in a two-dimensional coupling beam model resulted in unrealistic compression failure of the coupling beam as the full floor was not always activated in axial restraint. Therefore in order to consider three dimensional behavior, the extent of floor activated to restrain a coupling beam was required to be determined.

A similar process to that outlined in Chapters 3 and 4 was used to assess the floors. As per the previous modelling, elongation strains were applied to the floors used in the experiments to assess the magnitude of axial restraint force generated. The floors were based upon the measured material and section dimensions from the experiment, and analysed according to the process outlined in Chapter 3. Based upon this process, the full floor extent was found to be activated in the CB24F-RC model (mild steel reinforced floor). However as presented in Figure 13-9, the prestressed floor of specimen CB24F-PT activated only 42% of the total tension capacity of the floor system. The lower activation may be seen by the deflected shape in Figure 13-9, which showed the outer reinforcement was not fully strained. A lower activated width was in agreement with the findings of Chapter 4, in which it was found that more heavily reinforced floors tended to activate lower effective widths in axial restraint.

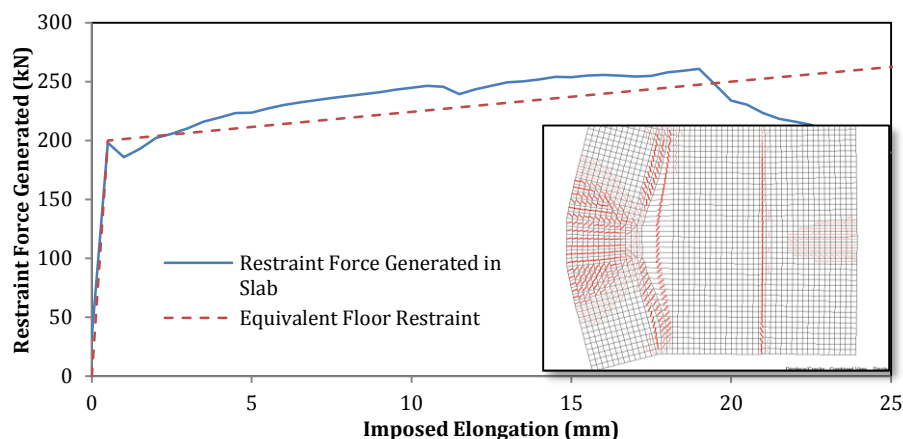


Figure 13-9: Equivalent pre-stress axial restraint force for CB24F-PT floor only (deflected shape inset)

Idealising the floors as equivalent tension ties in a two-dimensional coupling beam model was considered using two alternative approaches. The first approach involved idealising the floor reinforcement as a single reinforcement section, with the bilinear force-deformation relationship, shown in Figure 13-9, to match the modelled response of the floor. The area of reinforcement, yield capacity, ultimate capacity, initial stiffness and ultimate strain values were set in order to match the equivalent floor reinforcement tensile capacity developed from the isolated floor model. The modelled global hysteretic response, when the equivalent floor was applied to a coupling beam, is shown in Figure 13-10. The modelled response showed reasonably good correlation with the experimental data however there was an apparent loss of capacity in the model much earlier than in the experimental data. The reason for the inaccuracy in behaviour at high strain was that the equivalent floor effect idealised the floor based upon a stress-strain relationship which only considered the strain due to axial elongation. However the curvature of the coupling beam also applied strain to the equivalent floor tie in the computational model. Consequently, the equivalent floor tie was subject to a higher stress than in the isolated floor model. This higher equivalent floor tie stress induced a larger axial load in the coupling beam than was realistic. This increased axial load had two effects. Firstly it increased the nominal coupling beam shear capacity by providing an additional axial load contribution. Secondly, the larger axial load made the coupling beam more prone to compression failure at large applied chord rotation. Both of these effects were observed in Figure 13-10. This error could have been overcome by updating the equivalent tie properties at each load increment, based upon the applied drift at that load increment. However this was not feasible to undertake in VecTor2.

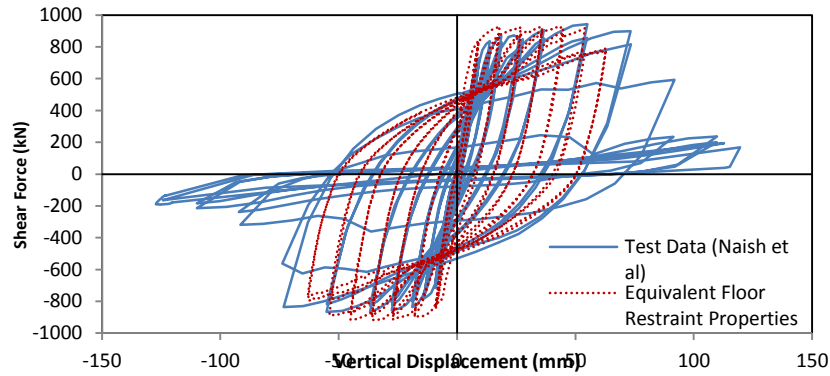


Figure 13-10: Equivalent floor tie (bilinear method) global hysteretic response of CB24F-PT

The second approach considered to idealise the floor as an equivalent tension tie was to use a single reinforcement tie, which matched the overall strength of the floor system. The equivalent floor tie was determined by modelling the floor in its own plane, as previously discussed, to determine the axial restraint force activated. In the case of the mild steel reinforced floor shown in Figure 13-11, the full floor was activated. However with the prestressed floor shown in Figure 13-9, only 42% of the total floor tension capacity was activated. The equivalent tension tie was then idealised based only upon the amount of reinforcement found to be fully activated (100% and 42% for the mild steel reinforced and prestressed floors respectively). The tie capacity was therefore matched to the tension capacity of floor reinforcement, within the effective width only. In addition to its simplicity, the primary advantage of method 2 was that the actual properties of the floor reinforcement were used such that the model better represented the experiment.

The equivalent tension tie method discussed above, was found to be the most robust method of idealising a floor in two-dimensional coupling beam modelling. Consequently the equivalent tension tie method was used for the three dimensional modelling presented in Chapter 6.

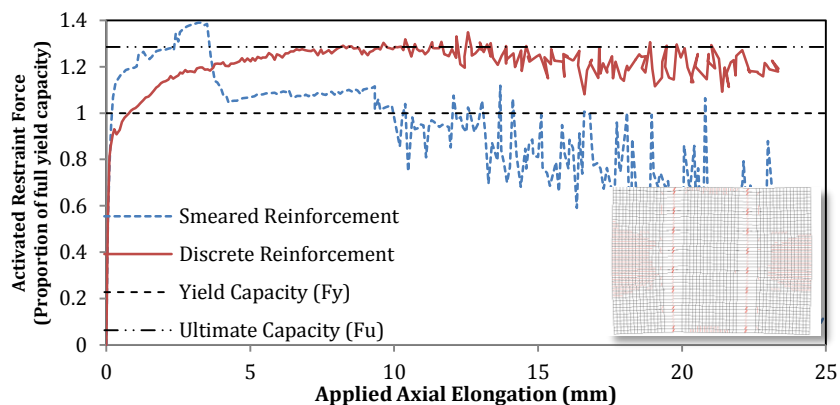


Figure 13-11: Equivalent axial restraint force for CB24F-RC mild steel reinforced floor

Appendix E

14 Appendix E

Presented in this appendix is a supplement to the computational modelling of coupled wall systems presented in Chapter 7.

A summary of the design properties for the coupled walls are presented in Table 14-2. The design properties presented were based upon modal analyses undertaken on the walls for design purposes).

Abbreviations in Table 14-2:

DOC Degree of Coupling. Refers to proportion of total overturning moment resisted by wall axial loads, where wall axial loads are provided by the summation of coupling beam shear capacity.

OS Overstrength.

Table 14-1: Constitutive models (based upon chapter 6 model calibration) used for coupled wall analysis

<u>Concrete Models</u>		<u>Reinforcement Models</u>	
Compression Pre-Peak	Popovics (NSC)	Hysteretic Response	Baushinger (Seckin)
Compression Post Peak	Popovics/Mander	Dowel Action	Tassios (Crack Slip) Refind Dhakal-
Compression Softening	Vecchio B (ϵ_1/ϵ_0)	Buckling	Maekawa
Confined Strength	Kupfer/Richart		
Dilation	Variable - Kupfer	<u>Analysis Models</u>	
Cracking Criterion	Mohr-Coulomb (Stress)	Strain History	Previous Considered
Crack Stress Calculation	Basic (DSFM/MCFT)	Strain Rate Effects	Not Considered
Crack Width Check	Omitted	Structural Damping Geometric	Not Considered
Crack Slip Calculation	Hybird 1 (Walraven)	Nonlinearity	Considered
Creep and Relaxation	NA	Crack Process	Uniform
Hysteretic Response	Nonlinear w Plastic Offsets		
Tension Stiffening	Modified Bentz 2003		
Tension Softening	Linear		
FRC Tension	SDEM Mono		

Table 14-2: Design summary of coupled wall variations

	Base	Base (0.5x)	Base (1.5x)	CWall 2	CWall 3	CWall 3 (x2)
Modal DOC	0.63	0.46	0.72	0.7	0.74	0.74
Provided DOC	0.45	0.29	0.55	0.54	0.53	0.47
Overstrength DOC (No Floor)	0.48	0.32	0.58	0.64	0.50	0.49
OS DOC (Fuse Floor)	0.57	0.47	0.65	0.64	0.7	0.61
OS DOC (Non Fuse Floor)	0.64	0.56	0.65	0.64	0.73	0.68
Modal Analysis Base Shear (kN)	1760	1760	1760	1975	846	846
Modal Analysis Fundamental Period (s)	1.5	1.5	1.5	1.3	1.6	1.6
Base Shear Capacity Provided (kN)	2499	2201	3400	2805	1201	1565
Φ_{ow} (No Floor)	1.81	1.46	1.93	2.02	1.88	2.29
Φ_{ow} (Fuse Floor)	2.11	1.79	2.24	2.02	2.36	2.74
Φ_{ow} (Non Fuse Floor)	2.34	2.14	2.54	2.02	2.50	3.10